Digital Signal Processing

Prof. Dr.-Ing. Abdelhak Zoubir

Manuscript

Revised and updated in Fall 2024

TECHNISCHE UNIVERSITÄT DARMSTADT

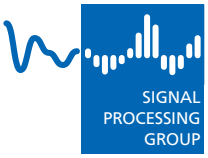

Imprint

Digital Signal Processing
Manuscript
Revised and updated in Fall 2024

Author:
Prof. Dr.-Ing. Abdelhak M. Zoubir
Technische Universität Darmstadt
Institute of Telecommunications
Signal Processing Group
Merckstr. 25
64283 Darmstadt
Germany

Contact:
E-Mail: office@spg.tu-darmstadt.de
Phone: +49 6151-16 21341
Fax: +49 6151-16 21342
Web: www.spg.tu-darmstadt.de

Preface

This draft is provided as an aid for students studying the subject Digital Signal Processing. It covers the material presented during lectures. Useful references on this subject include:

1. Böhme, J.F. *Stochastische Signale*, Teubner Studienbücher, 1998.
2. Brillinger, D.R. *Time Series, Data Analysis and Theory*, Holden Day Inc., 1981.
3. Hänsler, E. *Statistische Signale*, Springer Verlag, 3. Auflage, 2001.
4. Hayes, M.H. *Statistical Digital Signal Processing and Modeling*, John Wiley & Sons, Inc., 1996.
5. Kammeyer, K.D. & Kroschel, K. *Digitale Signalverarbeitung*, Teubner Studienbücher, 1998.
6. McClellan, J.H. & Schafer, R.W. & Yoder, M.A. *Signal Processing First*, Pearson Prentice-Hall, 2003.
7. Mitra, S.K. *Digital Signal Processing: A Computer-Based Approach*, Prentice-Hall, 1998.
8. Mulgrew, B. & Grant, P. & Thompson, J. *Digital Signal Processing - Concepts and Applications*, Palgrave Macmillan, 2003.
9. Oppenheim, A.V. & Schafer, R.W. *Discrete-Time Signal Processing*, Prentice-Hall, 1989. (also available in German)
10. Porat, B. *A Course on Digital Signal Processing*, J. Wiley & Sons Inc., 1996.
11. Priestley, M.B. *Spectral Analysis and Time Series*, Academic Press, 2001.
12. Stoica, P. & Moses, R. *Introduction to Spectral Analysis*, Prentice Hall, 1997.

Note that large parts of Chapters 4 and 5 of the manuscript have been for undergraduate students adapted from Reference 9, while large parts of Chapters 7, 9 and 10 have been adapted from Reference 1.

The References 1, 3 and 5 contain a sound treatment of statistical signal processing in German. Easy-to-read and comprehensible References 6 and 8 provide a good introduction into the field of digital signal processing.

For further treatment of spectral analysis, References 2, 4 and 10-12 are useful. Note that in the second part of the manuscript, some statements (without proof) have been adapted from Reference 2, which represents a mathematically advanced reference on time-series analysis, for undergraduate students. Furthermore, some examples have been taken from Reference 4 and 12.

Contents

1 Discrete-Time Signals and Systems

In this chapter, we briefly review basic concepts of digital signal processing which include the concept of discrete-time signals, linear and shift-invariant discrete-time systems, and the convolution.

1.1 Signals

Real-life signals can be classified into three broad groups:

1. *Analog or continuous-time* signals are continuous in both time and amplitude. Examples: speech, image, seismic and radar signals. An example of a continuous time signal is shown in Figure 1.1.

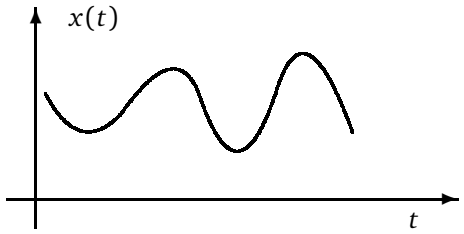

Figure 1.1.: Example of a continuous-time signal.

2. *Discrete-time* signals are discrete in time and continuous in amplitude. An example of such a signal is shown in Figure 1.2.

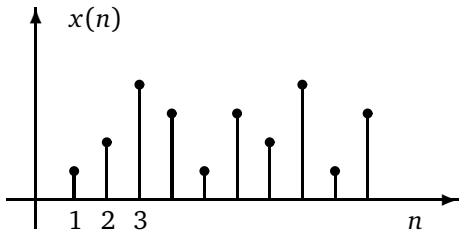

Figure 1.2.: Example of a discrete-time signal.

   A common way to generate discrete-time signals is by sampling continuous-time signals. There exist, however, signals which are intrinsically discrete in time, such as the average monthly rainfall.

3. *Digital* signals are discrete in both time and amplitude. Digital signals may be generated through amplitude quantization of discrete-time signals. The signals used by computers are digital, being discrete in both time and amplitude.

   The development of digital signal processing concepts based on digital signals requires a detailed treatment of amplitude quantization, which is extremely difficult and tedious. In addition, many useful insights are lost in such a treatment because of the mathematical complexity. For this reason, digital signal processing concepts have been developed based on discrete-time signals and continuous-time signals. Experience shows that the theories developed based on continuous-time or discrete-time signals are often applicable to digital signals. A discrete-time signal (sequence) will be denoted by functions whose arguments are integers.

For example, $x(n)$ represents a sequence which is defined for all integer values of n. If n is not integer, then $x(n)$ is not zero, but is *undefined*. The notation $x(n)$ refers to the discrete-time function x or to the value of the function x, at a specific n. Figure 1.3 gives an example of a sampled signal with sampling period T. Here we, have $x(n) = x(t)|_{t=nT}$, where n is an integer and $T > 0$.

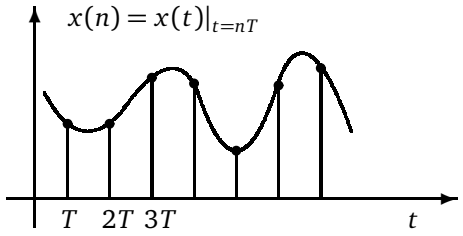

Figure 1.3.: Example of a sampled continuous-time signal.

There are some sequences which play an important role in digital signal processing, such as the unit sample sequence, the unit step sequence, exponential sequences and sinusoidal sequences. We discuss these next.

The unit sample sequence

The *unit sample sequence* is denoted by $\delta(n)$ and is defined as

$$\delta(n) = \begin{cases} 1, & n=0, \\ 0, & \text{otherwise.} \end{cases}$$

The sequence $\delta(n)$ may be regarded as an analog to the impulse function used in continuous-time system analysis. It is also known as Kronecker's delta. An important aspect is that any sequence can be represented as a linear combination of delayed Kronecker's deltas. For example, the sequence $p(n)$ in Figure 1.4 can be expressed as

$$p(n) = a_{-1}\delta(n+1) + a_1\delta(n-1) + a_3\delta(n-3)$$

where a_{-1}, a_1 and a_3 are real-valued constants.

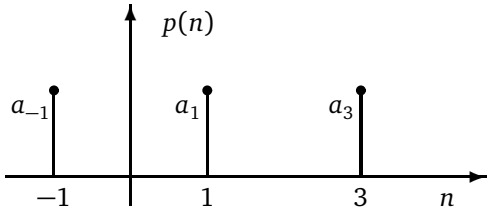

Figure 1.4.: The sequence $p(n)$.

In general, any discrete-time sequence $x(n)$ can be expressed as a sum of delayed unit sample sequences $\delta(n-k)$ which are scaled by $x(k)$, i.e.,

$$x(n) = \sum_{k=-\infty}^{\infty} x(k)\delta(n-k).$$

The unit step sequence

The *unit step sequence* denoted by $u(n)$ is defined as

$$u(n) = \begin{cases} 1, & n \geq 0, \\ 0, & \text{otherwise.} \end{cases}$$

The sequence $u(n)$ is related to $\delta(n)$ by

$$u(n) = \sum_{k=-\infty}^{n} \delta(k),$$

or alternatively

$$u(n) = \sum_{k=0}^{\infty} \delta(n-k).$$

Conversely, the unit sample sequence can be expressed as the first backward difference of the unit step sequence, i.e.,

$$\delta(n) = u(n) - u(n-1) = \sum_{k=-\infty}^{n} \delta(k) - \sum_{k=-\infty}^{n-1} \delta(k)$$

Exponential and sinusoidal sequences

Exponential and sinusoidal sequences play an important role in digital signal processing. The general form of an *exponential sequence* is

$$x(n) = A \cdot \alpha^n, \tag{1.1}$$

where A and α may be complex numbers. For a real $A > 0$ and a real $0 < \alpha < 1$, $x(n)$ is a decreasing sequence similar in appearance to Figure 1.5.

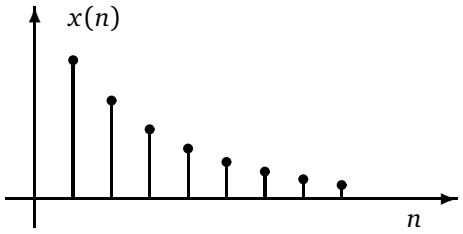

Figure 1.5.: Exponential Sequence $x(n) = A \cdot \alpha^n$ with $0 < \alpha < 1$.

For parameter $-1 < \alpha < 0$, the sequence values alternate in sign but again decrease in magnitude with increasing n, as shown in Figure 1.6. If $|\alpha| > 1$, then $x(n)$ grows in magnitude as n increases.

A *sinusoidal sequence* has the general form

$$x(n) = A \cdot \cos(\omega_o n + \phi)$$

with A and ϕ real. The sinusoidal sequence is shown in Figure 1.7 for $\omega_0 = \pi/4$ and $\phi = 3\pi/2$.

Now let A and α be complex so that $A = |A|e^{j\phi}$ and $\alpha = |\alpha|e^{j\omega_0}$, then

$$\begin{aligned} x(n) = A \cdot \alpha^n &= |A|e^{j\phi}|\alpha|^n e^{jn\omega_0} \\ &= |A| \cdot |\alpha|^n e^{j(\omega_0 n + \phi)} \\ &= |A| \cdot |\alpha|^n [\cos(\omega_0 n + \phi) + j \sin(\omega_0 n + \phi)] \end{aligned}$$

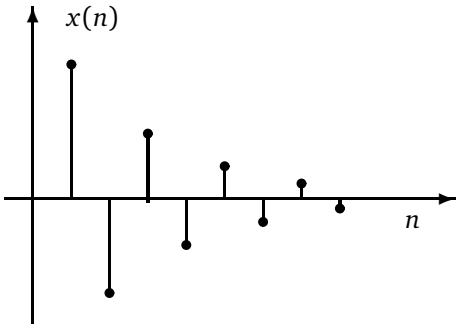

Figure 1.6.: Exponential Sequence $x(n) = A \cdot \alpha^n$ with $-1 < \alpha < 0$.

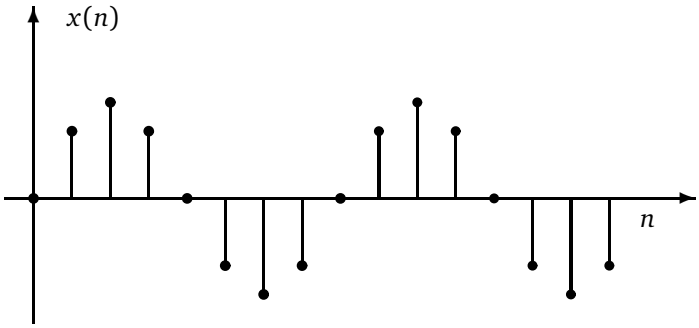

Figure 1.7.: Sinusoidal sequence.

For $|\alpha| = 1$, $x(n)$ is referred to as the complex exponential sequence, and has the form

$$x(n) = |A| \cdot e^{j(\omega_0 n + \phi)} = |A| \left[\cos(\omega_0 n + \phi) + j \sin(\omega_0 n + \phi)\right],$$

where real and imaginary parts of $e^{j\omega_0 n}$ vary sinusoidally with n.

In the continuous-time case, the quantity ω_0 is called the frequency and has the dimension radians per second. In the discrete-time case n is a dimensionless integer. Thus, the dimension of ω_0 must be radians. To maintain a closer analogy with the continuous-time case, we can specify the units of ω_0 to be radians per sample and the units of n to be samples. Following this rationale, we can define the period of a complex exponential sequence as $2\pi/\omega_0$ which has the dimension samples.

Periodic Sequences

A sequence $x(n)$ is called periodic with period N if $x(n)$ satisfies the following condition:

$$x(n) = x(n+N) \quad \forall\ n,$$

where N is a positive integer. For example, the sequence $\cos(\pi n)$ is periodic with period $2k$, $k \in \mathbb{Z}$, but the sequence $\cos(n)$ is not periodic. Note that a sinusoidal discrete-time sequence $A\cos(\omega_0 n)$ is periodic with period N if $\omega_0 N = 2\pi k, k \in \mathbb{Z}$. A similar statement holds for the complex exponential sequence $C \cdot e^{j\omega_0 n}$, i.e., periodicity with period N requires

$$e^{j\omega_0(n+N)} = e^{j\omega_0 n},$$

which is true only for

$$\omega_0 N = 2\pi k, \quad k \in \mathbb{Z}. \tag{1.2}$$

Consequently, complex exponential and sinusoidal sequences are not necessarily periodic with period $2\pi/\omega_0$. Depending on the value of ω_0, they may not be periodic at all. For example, consider $\omega_0 = 3\pi/4$, the smallest value of N for which Equation (1.2) can be satisfied with k an integer is $N = 8$ (corresponding to $k = 3$). For $\omega_0 = 1$, there are no integer values of N or k for which Equation (1.2) is satisfied.

When we combine the condition of Equation (1.2) with the observation that ω_0 and $\omega_0 + 2\pi r$, $r \in \mathbb{Z}$, are indistinguishable frequencies, then it is clear that there are only N distinguishable frequencies for which the corresponding sequences are periodic with period N. One set of frequencies is $\omega_k = 2\pi k/N$, $k = 0, 1, \ldots, N-1$. These properties of complex exponential and sinusoidal sequences are basic to both the theory and the design of computational algorithms for discrete-time Fourier analysis.

1.2 Systems

A system T that maps an input $x(n)$ to an output $y(n)$ is represented by

$$y(n) = \mathsf{T}[x(n)]$$

which is depicted in Figure 1.8.

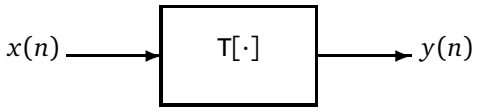

Figure 1.8.: Representation of a discrete-time system.

Example 1.2.1 *The ideal delay system is defined by $y(n) = x(n - n_d)$, $n_d \in \mathbb{Z}^+$. The system would shift the input to the right by n_d of samples corresponding to a time delay.*

This definition of a system is very broad. Without some restrictions, we cannot completely characterize a system when we know the output of a system to a certain set of inputs. Two types of restrictions greatly simplify the characterization and analysis of systems; linearity and shift invariance. Many systems can be approximated in practice by a linear and shift invariant(LSI) system. A system T is said to be linear if

$$\mathsf{T}[ax_1(n) + bx_2(n)] = ay_1(n) + by_2(n)$$

holds, where $\mathsf{T}[x_1(n)] = y_1(n)$, $\mathsf{T}[x_2(n)] = y_2(n)$, and a and b are any scalar constants. The property

$$\mathsf{T}[ax(n)] = a\mathsf{T}[x(n)]$$

is called homogeneity, and

$$\mathsf{T}[x_1(n) + x_2(n)] = \mathsf{T}[x_1(n)] + \mathsf{T}[x_2(n)]$$

is called additivity. Additivity and homogeneity are collectively known as the *Principle of Superposition*. A system is said to be shift invariant (SI) if

$$\mathsf{T}[x(n - n_0)] = y(n - n_0)$$

where $y(n) = \mathsf{T}[x(n)]$ and n_0 is any integer.

Example 1.2.2 *A system described by the relation*

$$y(n) = \sum_{k=-\infty}^{n} x(k)$$

is called an accumulator. This system is both linear and shift invariant.

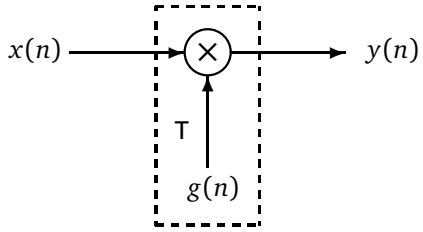

Figure 1.9.: A linear shift-variant system.

Example 1.2.3 *Consider a system as shown in Figure 1.9, which is described by*

$$y(n) = \mathsf{T}[x(n)] = x(n) \cdot g(n)$$

where $g(n)$ is an arbitrary sequence. Linearity of the system is easily verified since

$$\begin{aligned} \mathsf{T}[ax_1(n) + bx_2(n)] &= g(n)[ax_1(n) + bx_2(n)] \\ &= ag(n)x_1(n) + bg(n)x_2(n) \\ &= a\mathsf{T}[x_1(n)] + b\mathsf{T}[x_2(n)]\,. \end{aligned}$$

However, the system is shift-variant because

$$\mathsf{T}[x(n-n_0)] = x(n-n_0)g(n)$$

does not equal

$$y(n-n_0) = x(n-n_0)g(n-n_0)\,.$$

Example 1.2.4 *Consider a system described by*

$$y(n) = \mathsf{T}[x(n)] = x(n)^2\,.$$

Although this system is shift-invariant, it is non-linear. The system is non-linear because

$$\mathsf{T}[x_1(n) + x_2(n)] = [x_1(n) + x_2(n)]^2$$

does not equal

$$y_1(n) + y_2(n) = x_1(n)^2 + x_2(n)^2\,.$$

The system is shift-invariant because

$$\mathsf{T}[x(n-n_0)] = x(n-n_0)^2 = y(n-n_0)\,.$$

The unit sample response of linear systems

Consider a linear system T. Using the relationship

$$x(n) = \sum_{k=-\infty}^{\infty} x(k)\delta(n-k)$$

and the linearity property, the output $y(n)$ of a linear system T for an input $x(n)$ is given by

$$\begin{aligned} y(n) = \mathsf{T}[x(n)] &= \mathsf{T}\left[\sum_{k=-\infty}^{\infty} x(k)\delta(n-k)\right] \\ &= \sum_{k=-\infty}^{\infty} x(k)\mathsf{T}[\delta(n-k)] \end{aligned}$$

This result indicates that a linear system can be completely characterized by the response of the system to a unit sample sequence $\delta(n)$ and its delays $\delta(n-k)$. Moreover, if the system is shift-invariant, we have:

$$h(n-n_0) = \mathsf{T}[\delta(n-n_0)]$$

where $h(n) = \mathsf{T}[\delta(n)]$ is the *unit sample response* of a system T to an input $\delta(n)$.

1.3 Convolution

The input-output relation of a linear and shift-invariant (LSI) system T is given by

$$y(n) = \mathsf{T}[x(n)] = \sum_{k=-\infty}^{\infty} x(k)h(n-k)$$

This equation shows that knowledge of $h(n)$ completely characterizes the system, i.e., knowing the unit sample response, $h(n)$, of an LSI system T, allows us to completely determine the output $y(n)$ for a given input $x(n)$. This equation is referred to as *convolution* and is denoted by the convolution operator $*$. For an LSI system, we have

$$y(n) = x(n) * h(n) = \sum_{k=-\infty}^{\infty} x(k)h(n-k)$$

Two remarks on the unit sample response are:

- The unit sample response $h(n)$ loses its significance for a nonlinear or shift-variant system.
- The choice of the unit sample sequence $\delta(n)$ as an input for characterizing an LSI system is the simplest, both conceptually and in practice.

Example 1.3.1 *To compute the relationship between the input and the output with a transversal filter, $h(-k)$ is first plotted against k; $h(-k)$ is simply $h(k)$ reflected or "flipped" around $k = 0$, as shown in Figure 1.10. Replacing the argument k by $k-n$, where n is a fixed integer, leads to a shift in the origin of the sequence $h(-k)$ to $k = n$. The output sequence $y(n)$ at n is then obtained as a sum of all non-zero $x(k)h(n-k)$. See Figure 1.10.*

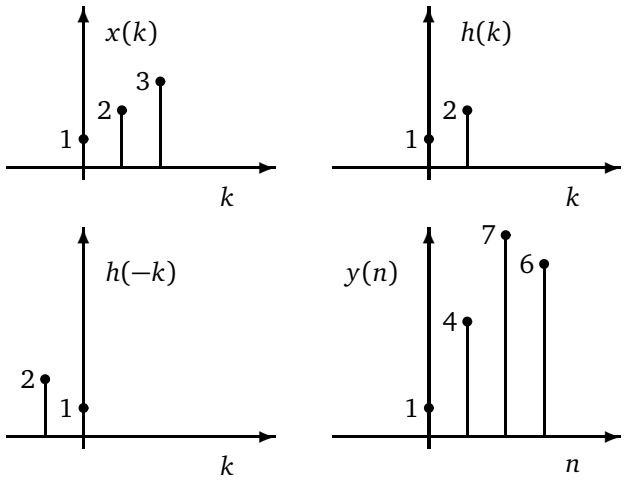

Figure 1.10.: Convolution operation.

Example 1.3.2 *A linear transversal filter is given by*

$$y(n) = \sum_{k=0}^{q} b_k x(n-k)$$

If we take $b_0 = b_1 = \cdots = b_q = 1/(q+1)$ the filter output sequence is an average of $q+1$ samples of the input sequence around the nth sample. This filter is commonly referred to as moving average filter.

1.4 Stability and Causality

To implement an LSI system in practice (realizability), we have to impose two additional constraints which are stability and causality.

Stability

A system is considered stable in the Bounded-Input Bounded-Output (BIBO) sense if and only if a bounded input always leads to a bounded output. A necessary and sufficient condition for an LSI system to be stable is that the unit sample response $h(n)$ is absolutely summable, i.e.,

$$\sum_{n=-\infty}^{\infty} |h(n)| < \infty$$

Such a sequence $h(n)$ is sometimes referred to as stable sequence. The proof of sufficiency, i.e. the system is stable if $h(n)$ is absolutely summable, is quite simple. First let $x(n)$ be bounded by M, i.e., $|x(n)| \leq M < \infty \ \forall \ n$, then using the convolution, we have

$$|y(n)| = \left| \sum_{k=-\infty}^{\infty} h(k)x(n-k) \right| \leq \sum_{k=-\infty}^{\infty} |h(k)||x(n-k)| \leq M \sum_{k=-\infty}^{\infty} |h(k)|$$

Thus given a bounded input $|x(n)| \leq M$, the output $y(n)$ is bounded if $h(n)$ is absolutely summable. Proving the other direction, i.e. $h(n)$ is absolutely summable if the system BIBO stable, is a bit more involved. For a proof, refer to e.g. Oppenheim, Schafer, 1989.

Causality

Causality is a fundamental law of physics stating that information cannot travel from the future to the past. In the context of systems, we say that a system is causal if and only if the current output $y(n)$ does not depend on any future values of the input such as $x(n+1)$, $x(n+2)$, ... Causality holds for *any* practical system regardless of linearity or shift invariance.

A necessary and sufficient condition for an LSI system to be causal is that $h(n) = 0$, for $n < 0$. The proof follows from the convolution,

$$y(n) \quad = \quad \sum_{k=-\infty}^{\infty} x(n-k)h(k).$$

To obtain y, at index n, causality implies that we cannot assume knowledge of x at index $n-k$ for $n-k > n$, or simply, for $k < 0$. Setting $h(k) = 0$ for $k < 0$ ensures this.

2 Digital Processing of Continuous-Time Signals

Discrete-time signals arise in many ways, but they most commonly occur in representations of continuous-time signals. This is partly due to the fact that the processing of continuous-time signals is often carried out on discrete-time sequences obtained by sampling continuous-time signals. It is remarkable that under reasonable constraints a continuous-time signal can be adequately represented by a sequence. In this chapter, we discuss the process of periodic sampling.

2.1 Periodic Sampling

Let $x_c(t)$, $t \in \mathbb{R}$, be a continuous-time signal and its Fourier transform be denoted by $X_c(j\Omega)$, $\Omega \in \mathbb{R}$,

$$X_c(j\Omega) = \int_{-\infty}^{+\infty} x_c(t) e^{-j\Omega t} dt\,.$$

The signal $x_c(t)$ is obtained from $X_c(j\Omega)$ by

$$x_c(t) = \frac{1}{2\pi} \int_{-\infty}^{+\infty} X_c(j\Omega) e^{+j\Omega t} d\Omega\,.$$

The typical method of obtaining a discrete-time representation of a continuous-time signal is through periodic sampling, wherein a sequence of samples $x(n)$ is obtained from the continuous-time signal $x_c(t)$ according to

$$x(n) = x_c(t)|_{t=nT} = x_c(nT), \quad n = 0, \pm 1, \pm 2, \ldots, \quad T > 0.$$

Herein, T is the sampling period, and its reciprocal, $f_s = 1/T$, is the sampling frequency, in samples per second and $\Omega_s = 2\pi f_s$ is the sampling frequency in rad/sec. This equation is the input-output relationship of an ideal A/D converter. It is generally not invertible since many continuous-time signals can produce the same output sequence of samples. This ambiguity can be removed by restricting the class of input signals to the sampler, however.

It is convenient to represent the sampling process in two stages, as shown in Figure 2.1. This consists of an impulse train modulator which is followed by conversion of the impulse train into a discrete sequence.

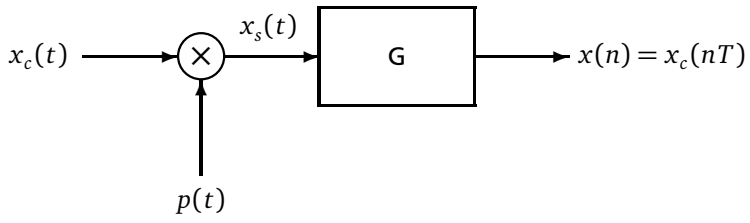

Figure 2.1.: Continuous-Time to digital converter.

The system G in Figure 2.1 represents a system that converts an impulse train into a discrete-time sequence. The modulation signal $p(t)$ is a periodic impulse train,

$$p(t) = \sum_{n=-\infty}^{\infty} \delta(t - nT)\,,$$

where $\delta(t)$ is called the Dirac delta function, defined such that

$$\int_{-\infty}^{\infty} x_c(t)\delta(t-t_0)dt = x_c(t_0) \quad \text{and} \quad \int_{-\infty}^{\infty} \delta(t)dt = 1.$$

Consequently, we have

$$x_s(t) = x_c(t)\cdot p(t) = x_c(t)\cdot \sum_{n=-\infty}^{\infty} \delta(t-nT) = \sum_{n=-\infty}^{\infty} x_c(nT)\delta(t-nT) = \sum_{n=-\infty}^{\infty} x(n)\delta(t-nT).$$

The Fourier transform of $x_s(t)$,$X_s(j\Omega)$, is obtained by convolving $X_c(j\Omega)$ and $P(j\Omega)$. The Fourier transform of a periodic impulse train is a periodic impulse train, i.e.,

$$P(j\Omega) = \frac{2\pi}{T}\sum_{k=-\infty}^{\infty} \delta(\Omega - \frac{2\pi k}{T}) = \frac{2\pi}{T}\sum_{k=-\infty}^{\infty} \delta(\Omega - k\Omega_s).$$

Since

$$X_s(j\Omega) = \frac{1}{2\pi}X_c(j\Omega) * P(j\Omega),$$

it follows that

$$X_s(j\Omega) = \frac{1}{T}\sum_{k=-\infty}^{\infty} X_c\left(j\left(\Omega - \frac{2\pi k}{T}\right)\right) = \frac{1}{T}\sum_{k=-\infty}^{\infty} X_c\left(j\Omega - kj\Omega_s\right).$$

The same result can be obtained by noting that $p(t)$ is periodic so that it can be represented as a Fourier series with coefficients $\frac{1}{T}$, i.e.,

$$p(t) = \frac{1}{T}\sum_{n=-\infty}^{\infty} e^{jn\Omega_s t}.$$

Thus

$$x_s(t) = x_c(t)p(t) = \frac{1}{T}\sum_{n=-\infty}^{\infty} x_c(t)e^{jn\Omega_s t}.$$

Taking the Fourier transform of $x_s(t)$ leads to

$$X_s(j\Omega) = \frac{1}{T}\sum_{k=-\infty}^{\infty} X_c\left(j\left(\Omega - k\Omega_s\right)\right).$$

Figure 2.2 depicts the frequency domain representation of impulse train sampling. Figure 2.2(a) represents the Fourier transform (assuming there is no phase, for convenience) of a band-limited signal where the highest non-zero frequency component in $X_c(j\Omega)$ is at Ω_B. Figure 2.2(b) shows the periodic impulse train $P(j\Omega)$, Figure 2.2(c) shows $X_s(j\Omega)$, which is the result of convolving $X_c(j\Omega)$ with $P(j\Omega)$. From Figure 2.2(c) it is evident that when

$$\Omega_s - \Omega_B > \Omega_B\,, \text{ or } \Omega_s > 2\Omega_B$$

the replica of $X_c(j\Omega)$ do not overlap, and therefore $x_c(t)$ can be recovered from $x_s(t)$ with an ideal low-pass filter with cut-off frequency of at least Ω_B but not exceeding $\Omega_S - \Omega_B$. However, in Figure 2.2(d) the replica of $X_c(j\Omega)$ overlap, and as a result the original signal cannot be recovered by ideal low-pass filtering. The reconstructed signal is related to the original continuous-time signal through a distortion referred to as *aliasing*.

If $x_c(t)$ is a band-limited signal with no components above Ω_B rad/sec, then the sampling frequency has to be equal to or greater than $2\Omega_B$ rad/sec. This is known as the Nyquist criterion and $2\Omega_B$ is known as the Nyquist frequency.

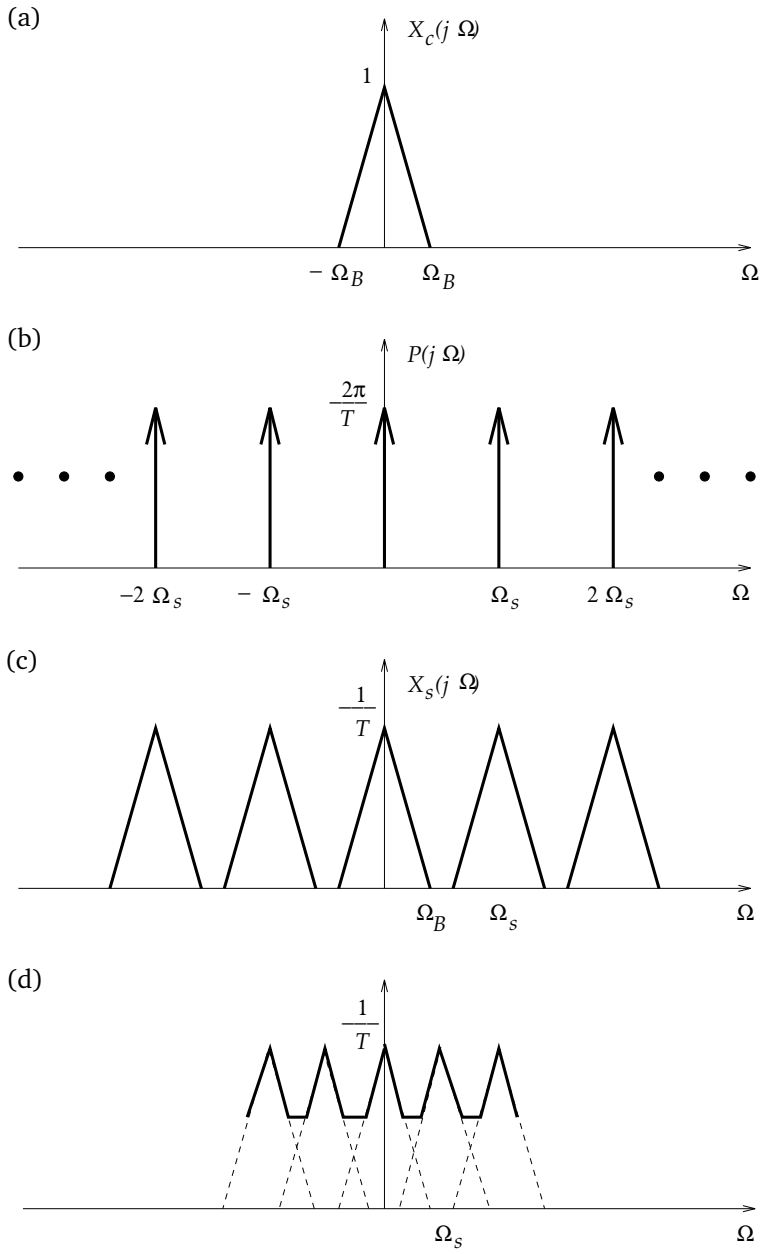

Figure 2.2.: Effect in the frequency domain of sampling in the time domain:
(a) Fourier transform of the continuous-time signal,
(b) Fourier transform of the sampling function,
(c) Fourier transform of the sampled signal with $\Omega_s > 2\Omega_B$,
(d) Fourier transform of the sampled signal with $\Omega_s < 2\Omega_B$.

2.2 Reconstruction of Band-Limited Signals

We have seen that under reasonable constraints, a continuous-time signal $x_c(t)$ can be adequately represented by a sequence $x(n)$. The constraints are a band-limited signal $x_c(t)$ with a maximum frequency Ω_B, and sampling above the Nyquist frequency $\Omega_s > 2\Omega_B$. Now assume $x(n)$ is the input to an ideal low-pass filter with frequency response $H_r(j\Omega)$ and impulse response $h_r(t)$, then the output of the filter will be

$$x_r(t) = \sum_{n=-\infty}^{\infty} x(n) h_r(t - nT)\,.$$

where T is the sampling interval. The reconstruction filter commonly has a gain of T and a cutoff frequency of $\Omega_c = \Omega_s/2 = \pi/T$. This choice is appropriate for any relationship between Ω_s and Ω_B that avoids aliasing, i.e., so long as $\Omega_s > 2\Omega_B$. The impulse response of such a filter is given by

$$h_r(t) = \frac{\sin(\pi t/T)}{\pi t/T}.$$

Consequently, the relation between $x_r(t)$ and $x(n)$ is given by

$$x_r(t) = \sum_{n=-\infty}^{\infty} x(n) \frac{\sin[\pi(t-nT)/T]}{\pi(t-nT)/T},$$

with $x_c(nT) = x(n)$.

2.3 Discrete-time Processing of Continuous-Time Signals.

A continuous-time signal $x_c(t)$ is processed by digital signal processing techniques using analog-to-digital (A/D) and digital-to-analog (D/A) converters before and after processing. This concept is illustrated in Figure 2.3. The processed continuous-time signal is denoted with $y_c(t)$. The low-pass filter limits the bandwidth of the continuous-

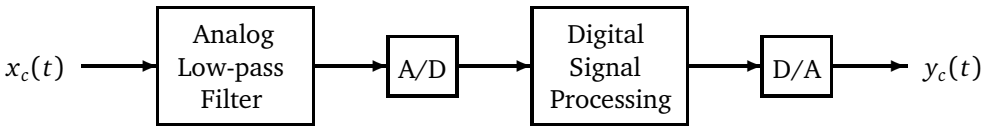

Figure 2.3.: Discrete-time processing of continuous-time signals.

time signal to reduce the effect of aliasing. The spectral characteristics (magnitude) of the low-pass filter is shown in Figure 2.4.

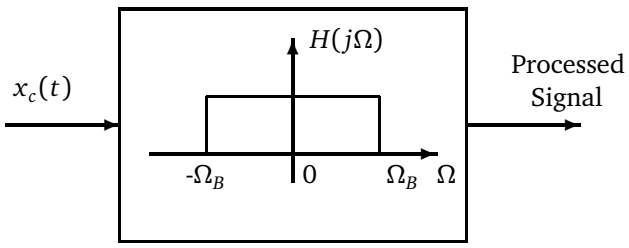

Figure 2.4.: Continuous-time low-pass filter.

Example 2.3.1 *Assume that we wanted to restore the signal $s_c(t)$ from $x_c(t) = s_c(t) + n_c(t)$, where $n_c(t)$ is background noise. The spectral characteristics of these signals are shown in Figure 2.5.*

We can perform the processing for this problem using either continuous-time or digital techniques. By using a continuous-time approach, we would filter the signal $x_c(t)$ using a continuous-time low-pass filter. Alternatively, we could adopt a digital approach, as shown in Figure 2.3. We would first low-pass filter $x_c(t)$ to prevent aliasing, and then convert the continuous-time signal into a discrete-time signal using an A/D converter. Any processing is then performed digitally on the discrete-time signal. The processed signal is then converted back to a continuous-time form using an D/A converter.

The advantages of processing signals digitally as compared with an analog approach are:

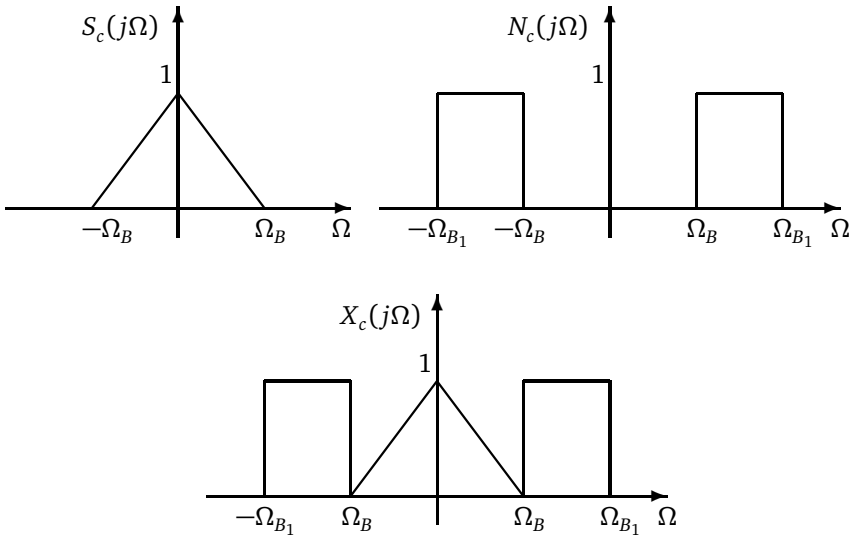

Figure 2.5.: Frequency Spectra.

1. Flexibility. If we want to change the continuous-time filter because of change in signal and noise characteristics, we would have to change the hardware components. Using the digital approach, we only need to modify the software.

2. Better control of accuracy requirements. Tolerances in continuous-time circuit components make it extremely difficult for the system designer to control the accuracy of the system.

3. The signals can be stored without deterioration or loss of signal quality.

4. Lower cost of the digital implementation.

3 Filter Design

3.1 Introduction

Filters are an important class of linear time-invariant systems. Their objective is to modify the input signal. In practice, filters are frequency selective, meaning they pass certain frequency components of the input signal and reject others. The objective of this chapter and the following ones is to introduce the concepts of frequency selective filters and the most popular filter design techniques.

The design of filters (continuous-time or digital) involves the following three steps.

1. *Filter specification:*

   This step consists of setting the required characteristics of the filter. For example, to restore a signal which has been degraded by background noise, the filter characteristics will depend on the spectral characteristics of both the signal and background noise. Typically (but not always) specifications are given in the frequency domain.

2. *Filter design:*

   Determine the unit sample response, $h(n)$ of the filter or its system function, $H(z)$ and $H(e^{j\omega})$.

3. *Filter implementation:*

   Implement a discrete time system with the given $h(n)$ or $H(z)$ or one which approaches it.

These three steps are closely related. For instance, it does not make much sense to specify a filter that cannot be designed or implemented. So, we shall consider a particular class of digital filters which possess the following practical properties:

1. $h(n)$ is real.
2. The system is causal, i.e., $h(n) = 0$ for $n < 0$.
3. The system is stable in the BIBO sense, i.e,

$$\sum_{n=0}^{\infty} |h(n)| < \infty \,.$$

In a practical setting, the desired filter is often implemented digitally on a chip and is used to filter a signal derived from a continuous-time signal by means of periodic sampling, followed by analog-to-digital conversion. For this reason, we refer to digital filters as discrete-time filters even though the underlying design techniques relate to the discrete-time nature of the signals and systems.

A basic system for discrete-time filtering of continuous-time signals is given in Figure 3.1. Assuming the input, $x_c(t)$, is band-limited and the sampling frequency is high enough to avoid aliasing, the overall system behaves as a linear time-invariant system with frequency response

$$H_{\text{eff}}(j\Omega) = \begin{cases} H(e^{j\Omega T}), & |\Omega| < \pi/T \\ 0, & |\Omega| > \pi/T \end{cases}$$

In such cases, it is straightforward to convert from specifications on the effective continuous-time filter to specifications on the discrete-time filter through the relation $\omega = \Omega T$. That is $H(e^{j\omega})$ is specified over one period by the equation

$$H(e^{j\omega}) = H_{\text{eff}}\left(j\frac{\omega}{T}\right), \quad |\omega| < \pi \,.$$

This concept will be treated in detail in Chapter 5.

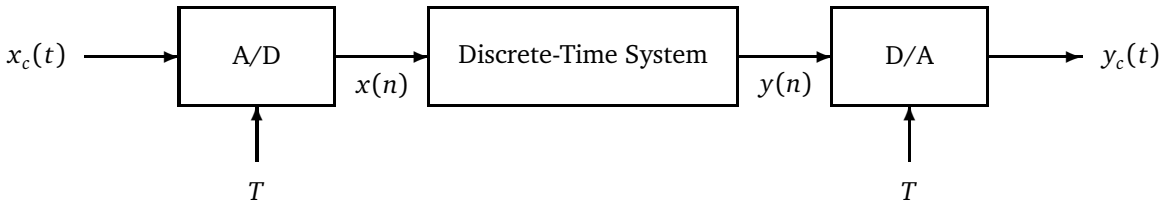

Figure 3.1.: A basic system for discrete-time filtering of a continuous-time signal.

3.2 Digital Filters

Throughout the text we will interchangeably use system and filter. Linear time-invariant discrete-time systems can be characterized by linear constant coefficient difference equations with initial rest condition of the type

$$\sum_{k=0}^{M} a_k y(n-k) = \sum_{r=0}^{N-1} b_r x(n-r), \tag{3.1}$$

where $x(n)$ and $y(n)$, $n = 0, \pm 1, \ldots$ are the input and output of the system and $\max(N-1, M)$ is the order.

The unit sample response of the system may be of either finite duration or infinite duration. It is useful to distinguish between these two classes as the properties of digital processing techniques for each differ. If the unit sample response is of finite duration, we have a *finite impulse response (FIR) filter*, and if the unit sample response is of infinite duration, we have an *infinite impulse response (IIR) filter*. If $M = 0$ so that

$$y(n) = \frac{1}{a_0} \sum_{r=0}^{N-1} b_r x(n-r), \tag{3.2}$$

then the system corresponds to an FIR filter of order $N-1$. In fact comparison with the convolution sum

$$y(n) = \sum_{k=-\infty}^{\infty} h(k) x(n-k)$$

shows that Equation (3.2) is identical to the convolution sum, hence it follows that

$$h(n) = \begin{cases} b_n/a_0, & n = 0, \ldots, N-1 \\ 0, & \text{otherwise.} \end{cases}$$

An FIR filter can be always described by a difference equation of the form (3.1) with $M = 0$. M must be greater than zero for an IIR filter.

3.3 Linear Phase Filters

Linear phase is a property of a filter's frequency response. For the sake of completeness, the definition of the frequency response in terms of the discrete-time Fourier transform is repeated here

$$H(e^{j\omega}) = \sum_{n=-\infty}^{\infty} h(n) e^{-j\omega n}$$

with its inverse transform

$$h(n) = \frac{1}{2\pi} \int_{-\pi}^{\pi} H(e^{j\omega}) e^{j\omega n} d\omega.$$

Note that ω is a continuous, normalized frequency variable. Due to its periodicity, $H(e^{j\omega})$ is often considered only for $|\omega| < \pi$.

A digital filter with unit sample response $h(n)$ is said to have linear phase if $H(e^{j\omega})$ can be expressed as

$$H(e^{j\omega}) = H_M(e^{j\omega}) e^{-j\omega\alpha} \quad |\omega| < \pi$$

where $H_M(e^{j\omega})$ is a real function of ω and α is a constant, commonly referred to as group delay.

Example 3.3.1 *The significance of a linear phase filter lies in the result that if a discrete-time signal is filtered by a linear-shift-invariant (LSI) system whose transfer function has magnitude $H_M(e^{j\omega}) = 1$ and linear phase, then the spectrum of the output is*

$$X(e^{j\omega})e^{-j\omega\alpha} \quad \bullet\!\!-\!\!\circ \quad x(n-\alpha) = y(n).$$

This relation is depicted in Figure 3.2. Simply put, a linear phase filter preserves the shape of the signal. Should the filter have the property that $|H(e^{j\omega})| = 1$, but does not have linear phase, then the shape of the signal will be distorted.

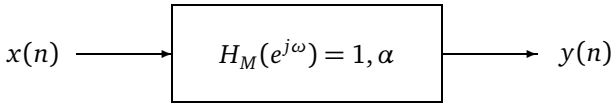

Figure 3.2.: Linear and shift-invariant filtering of $x(n)$.

We generalize the notion of linear phase to

$$H(e^{j\omega}) = H_M(e^{j\omega})e^{-j\omega\alpha+j\beta}$$

where $H_M(e^{j\omega})$ is a real function of ω, and constants α and β are group delay and initial phase, respectively. The case where $\beta = 0$ is referred to as linear phase as opposed to generalized linear phase where we have

$$\begin{aligned} H(e^{j\omega}) &= H_M(e^{j\omega})e^{j(\beta-\omega\alpha)} \\ &= H_M(e^{j\omega})\cos(\beta-\omega\alpha) + jH_M(e^{j\omega})\sin(\beta-\omega\alpha) \end{aligned}$$

or equivalentely

$$\begin{aligned} H(e^{j\omega}) &= \sum_{n=-\infty}^{\infty} h(n)e^{-j\omega n} \\ &= \sum_{n=-\infty}^{\infty} h(n)\cos(\omega n) - j\sum_{n=-\infty}^{\infty} h(n)\sin(\omega n) \end{aligned}$$

where $h(n)$ is assumed to be a real impulse response. The tangent of the phase of $H(e^{j\omega})$ can now be expressed as

$$\tan(\beta-\omega\alpha) = \frac{\sin(\beta-\omega\alpha)}{\cos(\beta-\omega\alpha)} = -\frac{\sum_{n=-\infty}^{\infty} h(n)\sin(\omega n)}{\sum_{n=-\infty}^{\infty} h(n)\cos(\omega n)}$$

Cross-multiplying and combining terms with a trigonometric identity leads to the following equation

$$\sum_{n=-\infty}^{\infty} h(n)\sin(\omega(n-\alpha)+\beta) = 0. \tag{3.3}$$

To have a linear phase, and a constant group delay, Equation (3.3) must hold for all ω. This is a necessary, but not sufficient condition on $h(n)$, α and β. For example, one can show that for $\beta = 0$ or π and $\alpha = (N-1)/2$,

$$h(2\alpha-n) = h(n) \tag{3.4}$$

satisfies Equation (3.3). Alternatively, for $\beta = \pi/2$ or $3\pi/2$,

$$h(2\alpha-n) = -h(n) \tag{3.5}$$

also satisfies Equation (3.3).

To have a causal system we also require

$$\sum_{n=0}^{\infty} h(n)\sin(\omega(n-\alpha)+\beta)=0$$

to hold for all ω. Causality and the previous conditions (3.4) and (3.5) imply that $h(n)=0, n<0$ and $n>N-1$, i.e. causal FIR filters have a generalized linear phase if they have impulse response length N and satisfy either $h(2\alpha-n)=h(n)$ or $h(2\alpha-n)=-h(n)$. Specifically if,

$$h(n)=\begin{cases} h(N-1-n), & 0\le n\le N-1,\\ 0, & \text{otherwise}, \end{cases}$$

then

$$H(e^{j\omega})=H_e(e^{j\omega})e^{-j\omega(N-1)/2},$$

where $H_e(e^{j\omega})$ is a real, even, periodic function of ω. Similarly if

$$h(n)=\begin{cases} -h(N-1-n), & 0\le n\le N-1,\\ 0, & \text{otherwise}, \end{cases}$$

then

$$H(e^{j\omega})=jH_o(e^{j\omega})e^{-j\omega(N-1)/2},$$

where $H_o(e^{j\omega})$ is a real, odd, periodic function of ω. The above two equations for $h(n)$ are sufficient, but not necessary conditions, which guarantee a causal system with generalized linear phase.

Generalized Linear Phase for FIR Filters

For now, we shall restrict our discussion to linear phase FIR filters. We classify FIR filters into four types depending on whether $h(n)$ is symmetric, i.e. $h(n)=h(N-1-n)$, or anti-symmetric, i.e. $h(n)=-h(N-1-n)$, about the point of symmetry or anti-symmetry, and whether the filter length is odd or even. The four types of FIR filters and their associated properties are discussed below and summarized in Table 3.1. Figure 3.3 shows examples of the four types of FIR filters.

1. *Type I FIR linear phase filter:*

   A type I filter has a symmetric impulse response $h(n)=h(N-1-n)$, $0\le n\le N-1$ with N an odd integer. The corresponding frequency response is

   $$H(e^{j\omega})=\sum_{n=0}^{N-1}h(n)e^{-j\omega n}=e^{-j\omega(N-1)/2}\sum_{k=0}^{(N-1)/2}a(k)\cos(\omega k),$$

   where $a(0)=h((N-1)/2)$ and $a(k)=2h((N-1)/2-k)$ for $k=1,2,\ldots,(N-1)/2$.

2. *Type II FIR linear phase filter:*

   A type II filter has a symmetric impulse response with N an even integer. The corresponding frequency response is

   $$H(e^{j\omega})=e^{-j\omega(N-1)/2}\sum_{k=1}^{N/2}b(k)\cos[\omega(k-1/2)],$$

   where $b(k)=2h(N/2-k)$ for $k=1,2,\ldots,N/2$.

3. *Type III FIR linear phase filter:*

   A type III filter has an antisymmetric impulse response $h(n) = -h(N-1-n)$, $0 \leq n \leq N-1$ with N an odd integer. The corresponding frequency response is

$$H(e^{j\omega}) = je^{-j\omega(N-1)/2} \sum_{k=1}^{(N-1)/2} c(k)\sin(\omega k),$$

   where $c(k) = 2h((N-1)/2-k)$ for $k = 1, 2, \ldots, (N-1)/2$.

4. *Type IV FIR linear phase filter:*

   A type IV filter has an antisymmetric impulse response with N an even integer. The corresponding frequency response is

$$H(e^{j\omega}) = je^{-j\omega(N-1)/2} \sum_{k=1}^{N/2} d(k)\sin[\omega(k-1/2)],$$

   where $d(k) = 2h(N/2-k)$ for $k = 1, 2, \ldots, N/2$.

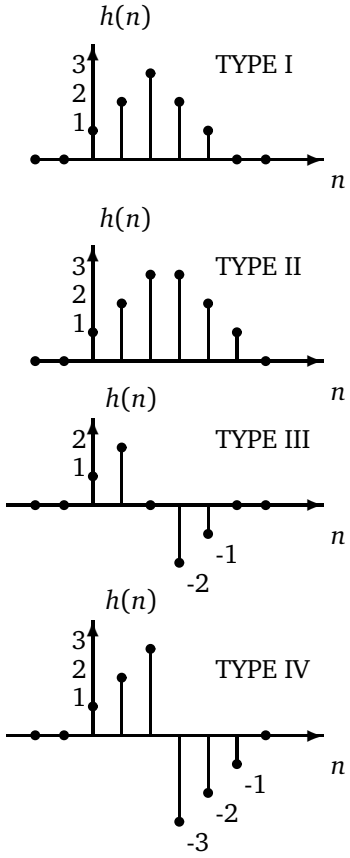

Figure 3.3.: Examples of the four types of linear phase FIR filters

Two remarks on the described filter types are:

- A filter will have no phase distortion if $H(e^{j\omega})$ is real and even since $h(n)$ will be real and even.
- Non-causal FIR filters can be made causal by an appropriate time shift so that the first non-zero value occurs at $n = 0$. The point of symmetry can therefore occur at two discrete-time points $(N-1)/2$ depending on whether N is odd or even.

Table 3.1.: The four classes of FIR filters and their associated properties, $\alpha = (N-1)/2$.

Type	Symmetry of $h(n)$	N	β	Form of $H_M(e^{j\omega})$	Constraints on $H_M(e^{j\omega}) \cdot e^{j\beta}$
I	$h(n) = h(N-1-n)$ Symmetric	Odd	0 π	$\sum_{n=0}^{(N-1)/2} a(n)\cos\omega n$	Real
II	$h(n) = h(N-1-n)$ Symmetric	Even	0 π	$\sum_{n=1}^{N/2} b(n)\cos\omega\left(n-\frac{1}{2}\right)$	Real $H_M(e^{j\pi}) = 0$
III	$h(n) = -h(N-1-n)$ Anti-Symmetric	Odd	$\frac{\pi}{2}$ $\frac{3\pi}{2}$	$\sum_{n=1}^{(N-1)/2} c(n)\sin\omega n$	Pure Imaginary $H_M(e^{j0}) = 0$ $H_M(e^{j\pi}) = 0$
IV	$h(n) = -h(N-1-n)$ Anti-Symmetric	Even	$\frac{\pi}{2}$ $\frac{3\pi}{2}$	$\sum_{n=1}^{N/2} d(n)\sin\omega\left(n-\frac{1}{2}\right)$	Pure Imaginary $H_M(e^{j0}) = 0$

Example 3.3.2 *Example of a type I FIR filter. Given a filter with unit sample response*

$$h(n) = \begin{cases} 1, & 0 \le n \le 4 \\ 0, & otherwise \end{cases},$$

we can evaluate the frequency response to be

$$H(e^{j\omega}) = \sum_{n=0}^{4} e^{-j\omega n} = \frac{1-e^{-j5\omega}}{1-e^{-j\omega}} = e^{-j2\omega}\frac{\sin(5\cdot\omega/2)}{\sin(\omega/2)}.$$

The magnitude and the phase of the frequency response of the filter are depicted in Figure 3.4

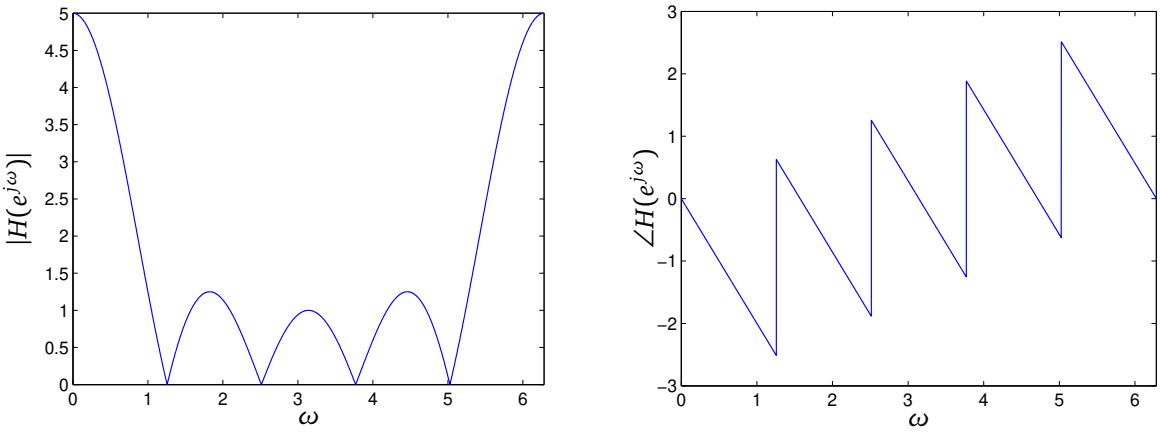

Figure 3.4.: Frequency response of type I filter of Example 3.3.2. Magnitude (left). Phase (right).

Example 3.3.3 *Example of a type II FIR filter. Consider an extension, by one sample of the impulse response of the filter in example 3.3.2. Then the frequency response of the system is given by*

$$H(e^{j\omega}) = \sum_{n=0}^{5} e^{-j\omega n} = e^{-j\omega 5/2} \frac{\sin(3\cdot\omega)}{\sin(\omega/2)},$$

whose magnitude and phase are depicted in Figure 3.5

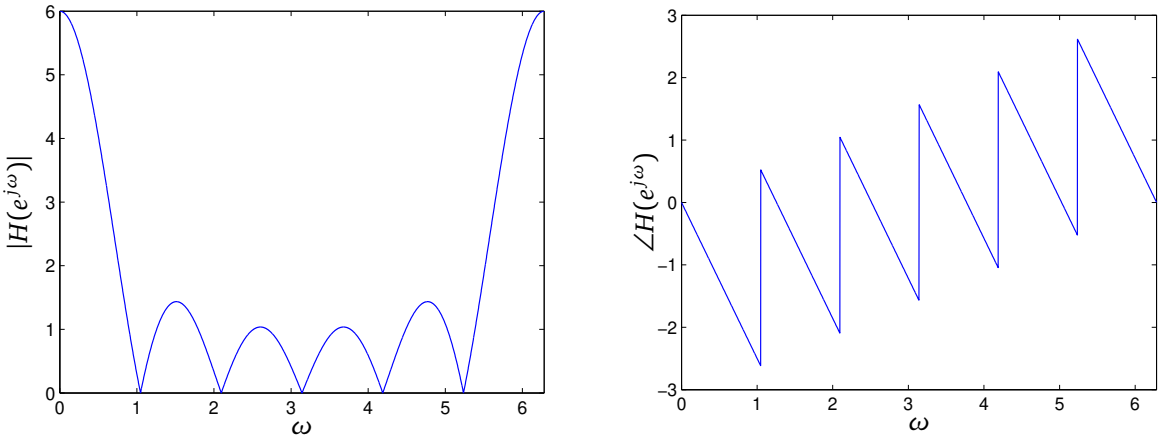

Figure 3.5.: Frequency response of type II filter of Example 3.3.3. Magnitude (left). Phase (right).

Example 3.3.4 *Example of a type III FIR filter. Consider a filter with unit impulse response*

$$h(n) = \delta(n) - \delta(n-2),$$

where $\delta(n)$ being Kronecker's delta. We can then evaluate the frequency response as

$$H(e^{j\omega}) = 1 - e^{-j2\omega} = j2\sin(\omega)e^{-j\omega} = 2e^{-j(\omega-\pi/2)}\sin(\omega).$$

The magnitude and the phase of $H(e^{j\omega})$ are depicted in Figure 3.6.

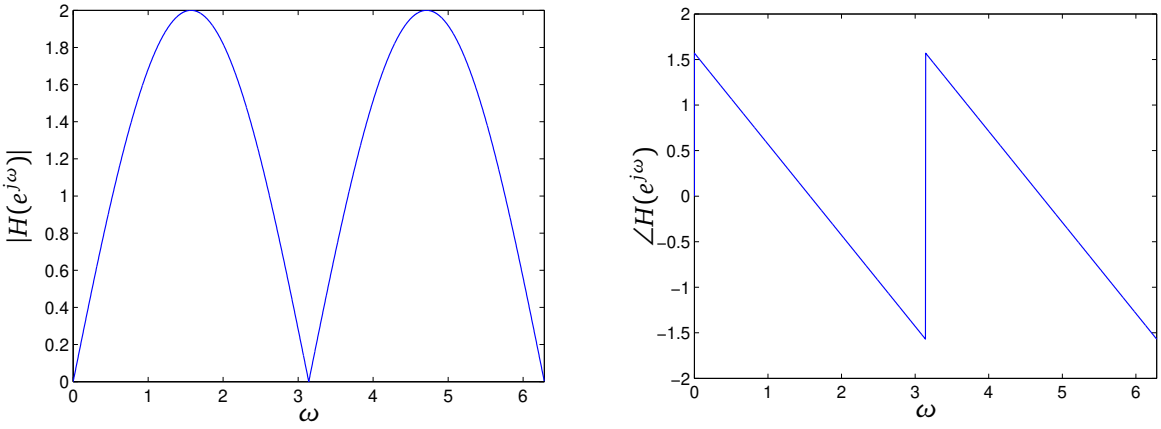

Figure 3.6.: Frequency response of type III filter of Example 3.3.4. Magnitude (left). Phase (right).

Example 3.3.5 *Example of a type IV FIR filter. Consider a filter with unit impulse response*

$$h(n) = \delta(n) - \delta(n-1).$$

We can then evaluate the frequency response as

$$H(e^{j\omega}) = 1 - e^{-j\omega} = j2\sin(\omega/2)e^{-j\omega/2} = 2e^{-j(\omega/2-\pi/2)}\sin\left(\frac{\omega}{2}\right).$$

The magnitude and the phase of $H(e^{j\omega})$ are depicted in Figure 3.7.

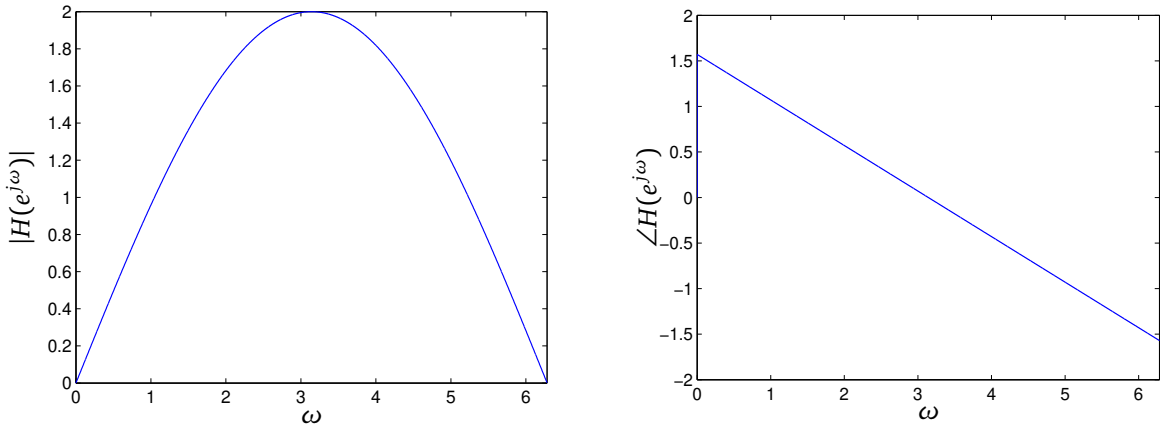

Figure 3.7.: Frequency response of type IV filter of Example 3.3.5. Magnitude (left). Phase (right).

3.4 Filter Specification

Like continuous-time filters, digital filters are specified in the frequency domain. Since $H(e^{j\omega})$ is periodic, i.e. $H(e^{j\omega}) = H(e^{j(\omega+2\pi)})$ for all ω, it is completely specified for $0 \leq \omega < 2\pi$. In addition, since $h(n)$ is assumed to be real, we have $H(e^{j\omega}) = H(e^{-j\omega})^*$. This implies that specifying $H(e^{j\omega})$ for $0 \leq \omega < \pi$ completely specifies $H(e^{j\omega})$ for all ω. To uniquely specify the complex frequency response $H(e^{j\omega})$, we actually need to specify both the magnitude and the phase of $H(e^{j\omega})$. However, since we are dealing with linear phase FIR filters, we need only to specify the magnitude. In the following we will consider filter structures having a passband and a stopband region, such as low-pass, high-pass band-pass and band-stop filters. We note that for an ideal filter, the magnitude of the frequency response is unity in the pass-band, and zero in the stop-band region. The ideal structure for the magnitude of the frequency response is given in Figure 3.8 for the low-pass, high-pass, band-pass and band-stop filter.

Example 3.4.1 *Specification of a low-pass filter. The ideal low-pass filter is composed of a pass-band and stop-band region. Ideally, $|H(e^{j\omega})|$ is unity in the passband and zero in the stopband. In practice, we also have a transition band, as a sharp transition cannot be achieved. Therefore, we supply error tolerances that require*

$$1 - \alpha_1 \leq |H(e^{j\omega})| \leq 1 + \alpha_1 \;\; \textit{for} \;\; 0 \leq \omega \leq \omega_p \,,$$

and

$$|H(e^{j\omega})| < \alpha_2 \;\; \textit{for} \; \omega_s \leq \omega \leq \pi \,.$$

Here, α_1 and α_2 are called the passband tolerance and stopband tolerance, respectively. A low-pass filter is then completely specified by four parameters α_1, α_2, ω_p and ω_s.

A similar arrangement, as for the low-pass filter from example 3.4.1, holds for high-pass, band-pass and band-stop filters. These are shown in Figure 3.9.

3.5 Properties of IIR Filters

As discussed, an IIR filter has a unit sample response of infinite duration. In general, an IIR filter with arbitrary unit sample response $h(n)$ cannot be realized, since computing each output sample requires a large amount of arithmetic operations. Therefore, we restrict ourselves to the class of filters which:

1. have a unit sample response $h(n)$ that is real, causal and stable.

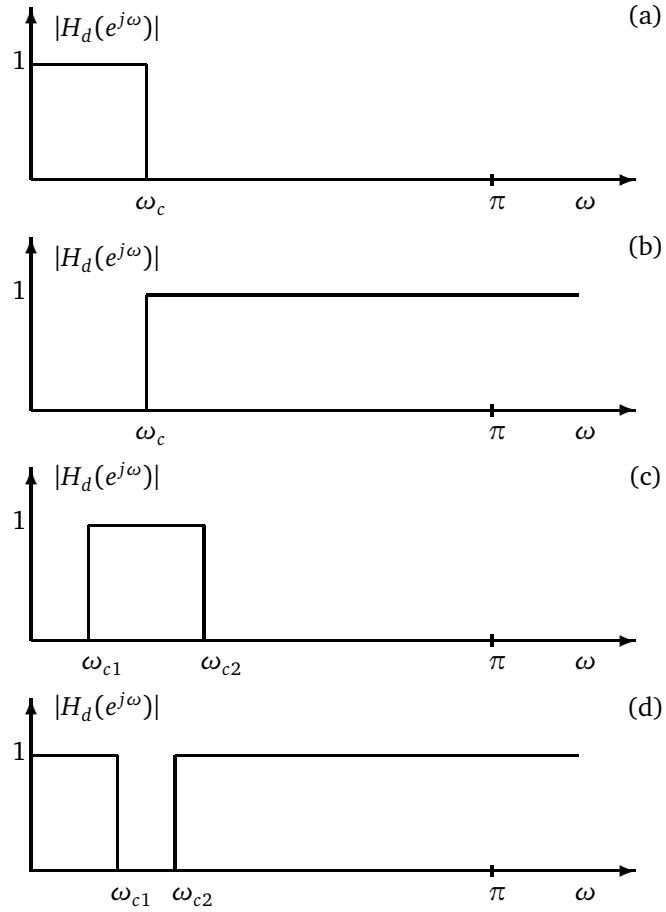

Figure 3.8.: Frequency response of ideal digital filters. (a) Low-pass (b) High-pass (c) Band-pass (d) Band-stop.

2. possess a rational z-transform with $a_0 = 1$, i.e.

$$H(z) = \frac{\sum_{r=0}^{N-1} b_r z^{-r}}{1 + \sum_{k=1}^{M} a_k z^{-k}}.$$

A causal $h(n)$ with a rational z-transform can be realized by a linear constant coefficient difference equation (LCCDE) with initial rest conditions (IRC) where the output is computed recursively, as in Equation (3.1). Thus IIR filters can be implemented efficiently.

Example 3.5.1 *Consider a causal impulse response described by*

$$h(n) = \left(\frac{1}{2}\right)^n \cdot u(n),$$

with $H(z)$ given by

$$H(z) = \frac{1}{1 - \frac{1}{2}z^{-1}}.$$

Defining $y(n)$ and $x(n)$ as the output and the input of the filter, respectively, this can be realized by

$$y(n) = \frac{1}{2}y(n-1) + x(n)$$

assuming IRC. Note that although $h(n)$ is of infinite extent, the number of arithmetic operations required per output is only one multiplication and one addition using an LCCDE formulation.

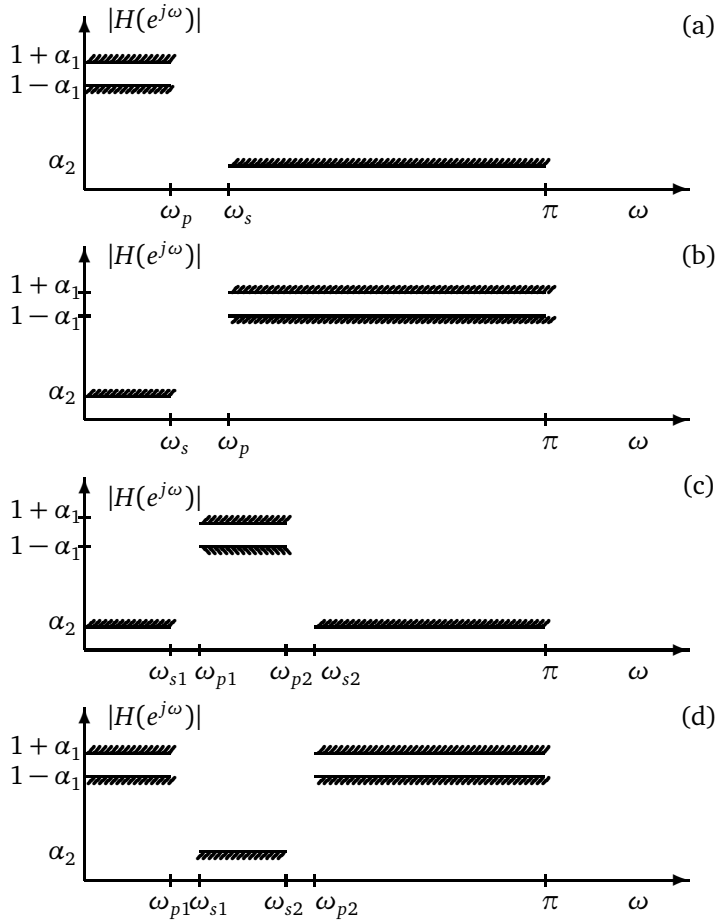

Figure 3.9.: Tolerance scheme for digital filter design. (a) Low-pass (b) High-pass (c) Band-pass (d) Band-stop.

3.6 Stability and Linear Phase

Note that an FIR filter is stable if $h(n)$ is finite for all n. Therefore, stability is not a problem in practical design or implementation of FIR filters. However, care must be taken with an IIR filter, where all the poles of $H(z)$ must lie inside the unit circle to ensure filter stability. Also, it is simple to achieve linear phase with FIR filters, to the point that we require all FIR filters to possess this property. It is much more difficult to control the phase of an IIR filter. As a result, we specify only the magnitude response for the IIR filter and accept the resulting phase characteristics. On the other hand, digital IIR filters are generally more efficient in terms of achieving a sharp transition region, since they have numerator and denominator polynomials, as opposed to FIR filters.

4 Finite Impulse Response Filter Design

4.1 Introduction

We begin with a motivating example for filter design.

Example 4.1.1 *Photoplethysmography is an optical technique for detecting blood volume changes. The Photoplethysmogram (PPG) can contribute to acquire valuable health-related information, for example, blood pressure, heart beat rate, and oxygen saturation. However, it is usually contaminated by noise. In order to remove this noise, the PPG can be processed with an FIR band-stop filter that strongly attenuates certain frequency components, but keeps the other frequency components unaltered.*

In Figure 4.1, the upper two plots show an excerpt of a PPG measured in the Signal Processing Group Biomedical Lab using a finger clip sensor and the resulting signal after band-stop filtering. The lower two plots show the magnitude of the discrete-time Fourier transform of these two signals where the DC component was removed by subtracting the sample mean. It can be seen in the time domain that there is a fast oscillation superimposed to the true PPG, resulting from the noise. This is clearly visible in the frequency domain, where we observe the 50*Hz frequency component and its harmonics that explain the fast oscillation in the time domain. An appropriately designed band-stop filter removes the electrical power noise without distorting the true PPG, which has its power distributed in the frequency range below* 50 *Hz.*

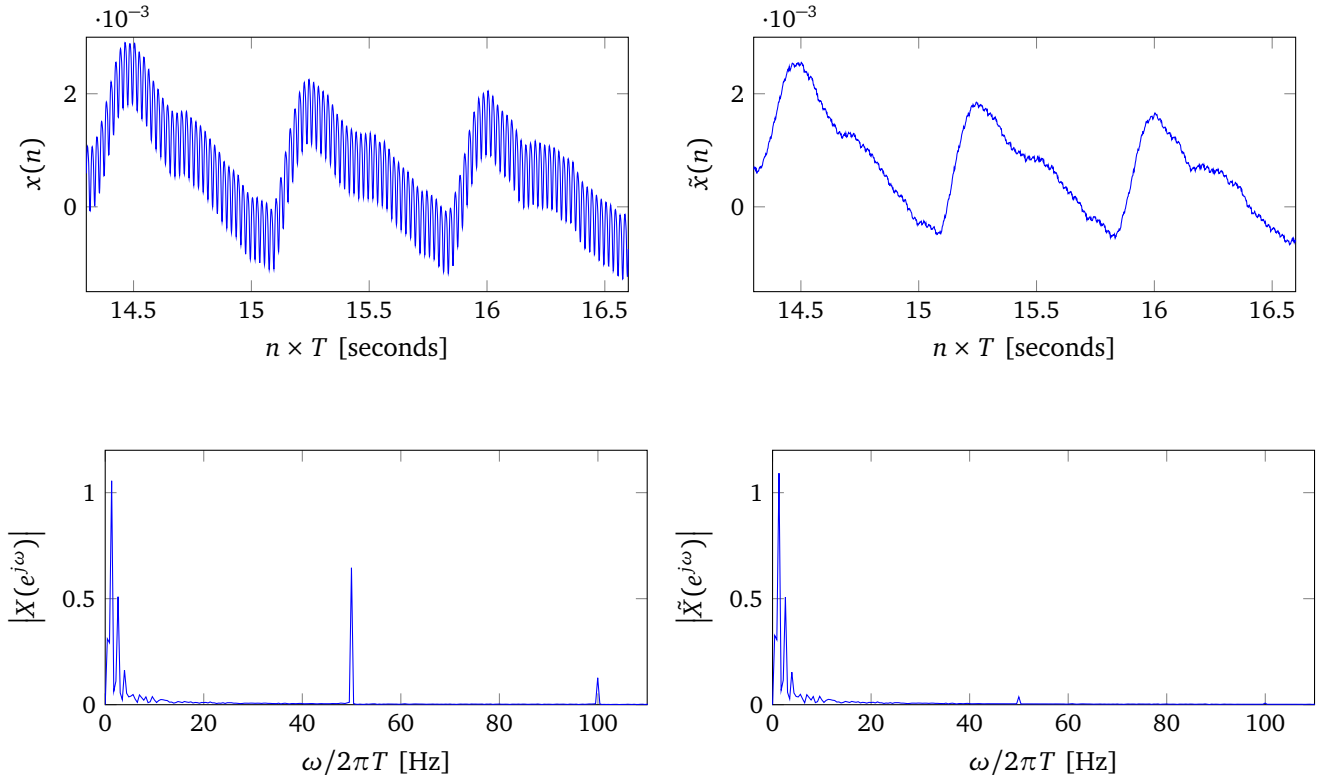

Figure 4.1.: PPG example: excerpt of the measured PPG (upper left), the resulting signal after band-stop filtering (upper right), the magnitude of the discrete-time Fourier transform of the measured PPG (lower left), and that of the filtered PPG (lower right).

The filter design problem is that of determining $h(n), H(e^{j\omega})$ or $H(z)$ to meet the design specifications. The first step is to choose the type of filter from the previously discussed four types of FIR filters. Some types of filters may not be suitable for a given design specification. For example, from Table 3.1 a Type II filter is not suitable for a high-pass filter design as it will always have $H(e^{j\omega}) = 0$ at $\omega = \pi$ since $\cos \pi(n - 1/2) = 0$. Table 4.1 shows what type of filters are not suitable for a given class of filter.

Table 4.1.: Suitability of a given class of filter for the four FIR types

Type	Low-pass	High-pass	Band-pass	Band stop
I				
II		Not suitable		Not suitable
III	Not suitable	Not suitable		Not suitable
IV	Not suitable			Not suitable

The two standard most commonly used approaches for FIR filter design are:

1. The window method.
2. The optimal filter design method.

We now discuss each of these approaches in turn.

4.2 Design of FIR Filters by Windowing

Many idealized systems are defined by piecewise-constant or piecewise-functional frequency responses with discontinuities at the boundaries between bands. As a result, they have non causal impulse responses that are infinitely long. The most straightforward approach for obtaining a causal FIR approximation to such systems is to truncate the ideal response. Let $H_d(e^{j\omega})$ be the desired frequency response of the filter. Then

$$H_d(e^{j\omega}) = \sum_{n=-\infty}^{\infty} h_d(n) e^{-j\omega n},$$

where $h_d(n)$ is the corresponding unit sample response sequence given by

$$h_d(n) = \frac{1}{2\pi} \int_{-\pi}^{\pi} H_d(e^{j\omega}) e^{j\omega n} d\omega .$$

The simplest way to obtain a causal FIR filter from $h_d(n)$ is to define a new system with unit sample response

$$h(n) = \begin{cases} h_d(n), & 0 \le n \le N-1, \\ 0, & \text{elsewhere}, \end{cases}$$

which can be re-written as

$$h(n) = h_d(n) \cdot w(n),$$

and therefore

$$H(e^{j\omega}) = \frac{1}{2\pi} \int_{-\pi}^{\pi} H_d(e^{j\theta}) \cdot W(e^{j(\omega-\theta)}) d\theta .$$

Note that $H(e^{j\omega})$ represents a smeared version of $H_d(e^{j\omega})$. This principle is visualized in Figure 4.2, where we start with the ideal frequency response $H_d(e^{j\omega})$ on top right, and calculate the corresponding ideal impulse response

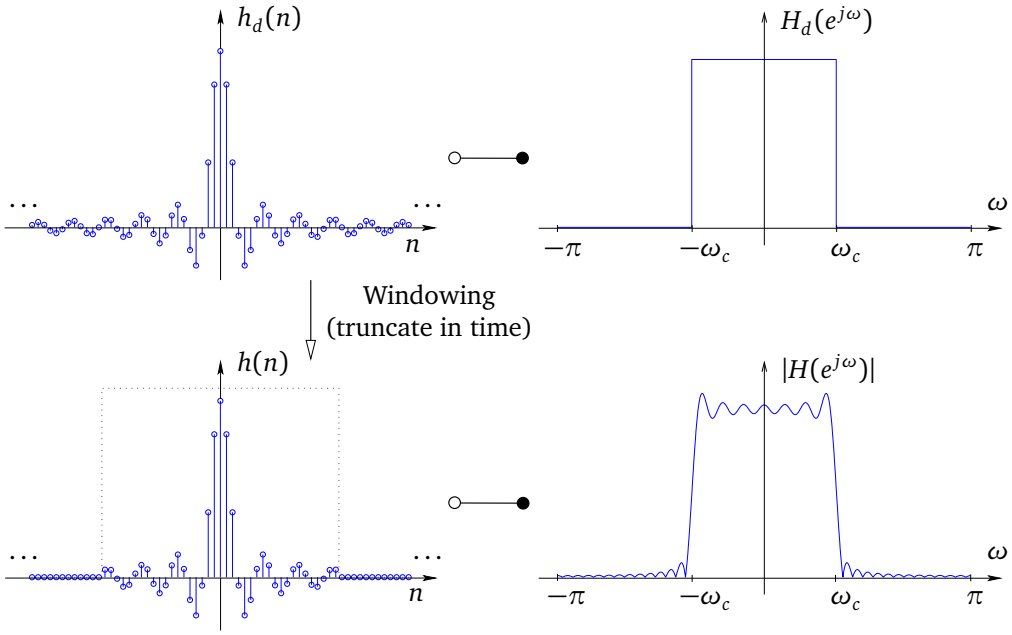

Figure 4.2.: The principle of the windowing technique.

$h_d(n)$ via inverse Fourier transform, on top left. Continuing in Figure 4.2, we then obtain the approximated impulse response $h(n)$ by truncation of $h_d(n)$, on bottom left, and finally we calculate the approximated frequency response $H(e^{j\omega})$ via Fourier transform, on bottom right.

Note also that if $h_d(n)$ is symmetric (or anti-symmetric) with respect to a certain point of symmetry (or anti-symmetry) and $w(n)$ is also symmetric with respect to the same point of symmetry, then $h_d(n) \cdot w(n)$ is the unit sample response of a linear phase filter.

Example 4.2.1 *Low-pass filter design with specifications α_1, α_2, ω_p, ω_s. We choose a Type I filter for the design. Since the desired frequency response $H_d(e^{j\omega})$ should be consistent with the filter type, as in Table 3.1, $H_d(e^{j\omega})$ is given by*

$$H_d(e^{j\omega}) = \begin{cases} e^{-j\omega\alpha}, & 0 \le |\omega| \le \omega_c\,, \\ 0, & \omega_c \le |\omega| \le \pi \end{cases}$$

where $\alpha = (N-1)/2$, $\omega_c = (\omega_p + \omega_s)/2$, and N is the filter length (odd). The inverse Fourier transform of $H_d(e^{j\omega})$ is

$$h_d(n) = \frac{\sin \omega_c(n-\alpha)}{\pi(n-\alpha)}$$

If we apply a rectangular window to $h_d(n)$, the resulting filter impulse response $h(n)$ is

$$h(n) = \begin{cases} \dfrac{\sin \omega_c(n-\alpha)}{\pi(n-\alpha)} & , \quad \text{for } 0 \le n \le N-1\,, \\ 0 & , \quad \text{otherwise}\,. \end{cases}$$

The sequence $h(n)$ is shown in Figure 4.3 for $N = 7$ and $\omega_c = \pi/2$. Note that this filter may or may not meet the design specification.

4.3 Importance of the Window Shape and Length

When multiplying the ideal impulse response with a window function in the time-domain, we have

$$h(n) = h_d(n) \cdot w(n)\,,$$

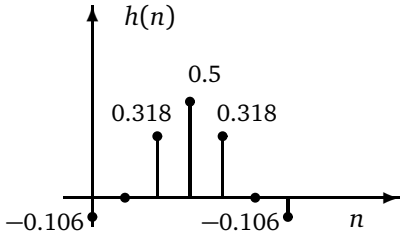

Figure 4.3.: The sequence $h(n)$ from example 4.2.1.

which corresponds to a circular convolution in the frequency domain

$$\begin{aligned} H(e^{j\omega}) &= H_d(e^{j\omega}) \circledast W(e^{j\omega}) \\ &= \frac{1}{2\pi}\int_{-\pi}^{\pi} H_d(e^{j\theta})W(e^{j(\omega-\theta)})d\theta. \end{aligned} \tag{4.1}$$

If we do not truncate at all, so that $w(n) = 1$ for all n, $W(e^{j\omega})$ is a periodic impulse train with period 2π, and therefore $H(e^{j\omega}) = H_d(e^{j\omega})$. This interpretation suggests that if $w(n)$ is chosen so that $W(e^{j\omega})$ approximates an impulse, i.e., is concentrated in a narrow band of frequencies around $\omega = 0$, then $H(e^{j\omega})$ approximates $H_d(e^{j\omega})$ very closely except where $H_d(e^{j\omega})$ changes abruptly. At the same time, we want $w(n)$ as short as possible in order to minimize computation in the implementation of the filter. These are conflicting requirements. Take, for example, the case of the rectangular window, where

$$W(e^{j\omega}) = \sum_{n=0}^{N-1} e^{-j\omega n} = \frac{1-e^{-j\omega N}}{1-e^{-j\omega}} = e^{-j\omega(N-1)/2}\frac{\sin(\omega N/2)}{\sin(\omega/2)}.$$

Note that $W(e^{j\omega})$ for the rectangular window has a generalized linear phase. The magnitude of the function $\sin(\omega N/2)/\sin(\omega/2)$ is shown in Figure 4.4 for the case $N = 8$.

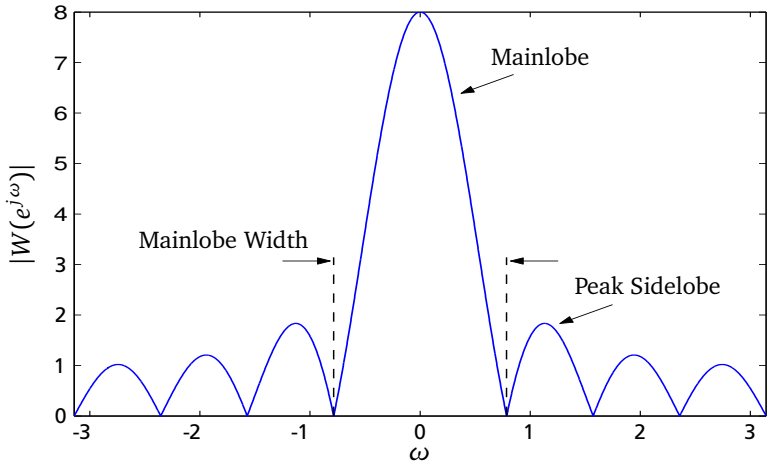

Figure 4.4.: Magnitude of the Fourier transform of a rectangular window ($N = 8$).

As N increases, the width of the "main-lobe" decreases. The main-lobe is usually defined as the region between the first zero crossing on either side of the origin, as indicated in Figure 4.4. For the rectangular window, the main-lobe width is $\Delta\omega = 4\pi/N$. However, for the rectangular window, the side lobes are large and, in fact, as N increases, the peak amplitudes of the main-lobe and the side-lobes grow in a manner such that the area under each lobe is a constant even though the width of each lobe decreases with N.

For an interpretation of the frequency domain convolution as in Equation (4.1), we consider the Fourier transform $W(e^{j(\omega-\theta)})$ sliding by a discontinuity of ideal frequency response $H_d(e^{j\omega})$ with increasing ω. The integral

$W(e^{j(\omega-\theta)})H_d(e^{j\omega})$ will oscillate as each side-lobe of $W(e^{j(\omega-\theta)})$ moves past the discontinuity of $H_d(e^{j\omega})$. A graphical visualization is left to the reader; the result of the convolution between $H_d(e^{j\omega})$ and $W(e^{j\omega})$, for a rectangular window of length $N = 39$, is depicted as an example in the bottom right plot in Figure 4.2.

We can modify this effect by tapering the window smoothly to zero at each end so that the height of the side-lobes are diminished; however this is achieved at the expense of a wider main-lobe and thus a wider transition at the discontinuity.

Commonly used windows

Five common windows are used in practice: the rectangular, Bartlett, Hanning, Hamming and Blackman window. The formula for these windows are given below.

- *Rectangular:*

$$w(n) = \begin{cases} 1, & 0 \le n \le N-1\,, \\ 0, & \text{elsewhere.} \end{cases}$$

- *Bartlett:*

$$w(n) = \begin{cases} \dfrac{2n}{N-1}, & 0 \le n \le \dfrac{N-1}{2}\,, \\ 2 - \dfrac{2n}{N-1}, & \dfrac{N-1}{2} < n \le N-1\,. \end{cases}$$

- *Hanning:*

$$w(n) = \frac{1}{2}\left[1 - \cos(\frac{2\pi n}{N-1})\right],\ 0 \le n \le N-1\,.$$

- *Hamming:*

$$w(n) = 0.54 - 0.46\cos\left(\frac{2\pi n}{N-1}\right),\ 0 \le n \le N-1\,.$$

- *Blackman:*

$$w(n) = 0.42 - 0.5\cos\left(\frac{2\pi n}{N-1}\right) + 0.08\cos\left(\frac{4\pi n}{N-1}\right),\ 0 \le n \le N-1\,.$$

Figure 4.5 compares these window functions for $N = 128$. A good choice of the window corresponds to choosing a window with small main-lobe width and small side-lobe amplitude. Clearly, the shape of a window affects both main-lobe and side-lobe behavior.

Figure 4.6 shows the magnitude of a Rectangular, Bartlett, Hamming and Blackman window in the frequency domain for $N = 33$. For comparison, Figure 4.7 shows the magnitude of the Hamming window in the frequency domain for $N = 65$ and 129, respectively. It can be observed that the main-lobe behavior is affected primarily by window length.

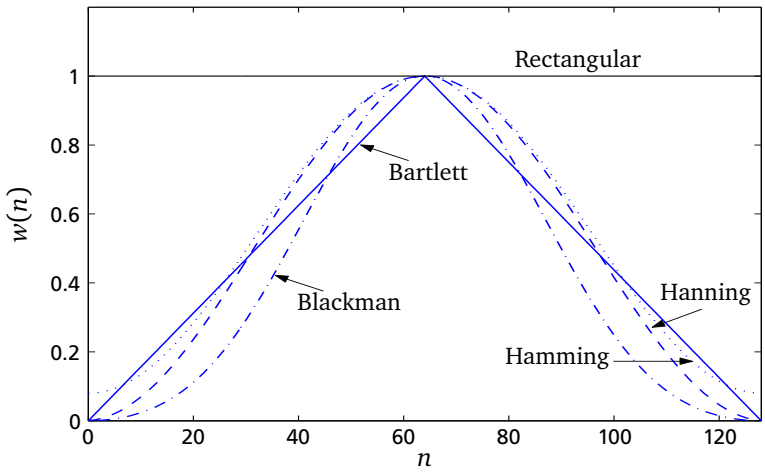

Figure 4.5.: Commonly used windows for FIR filter design ($N = 128$).

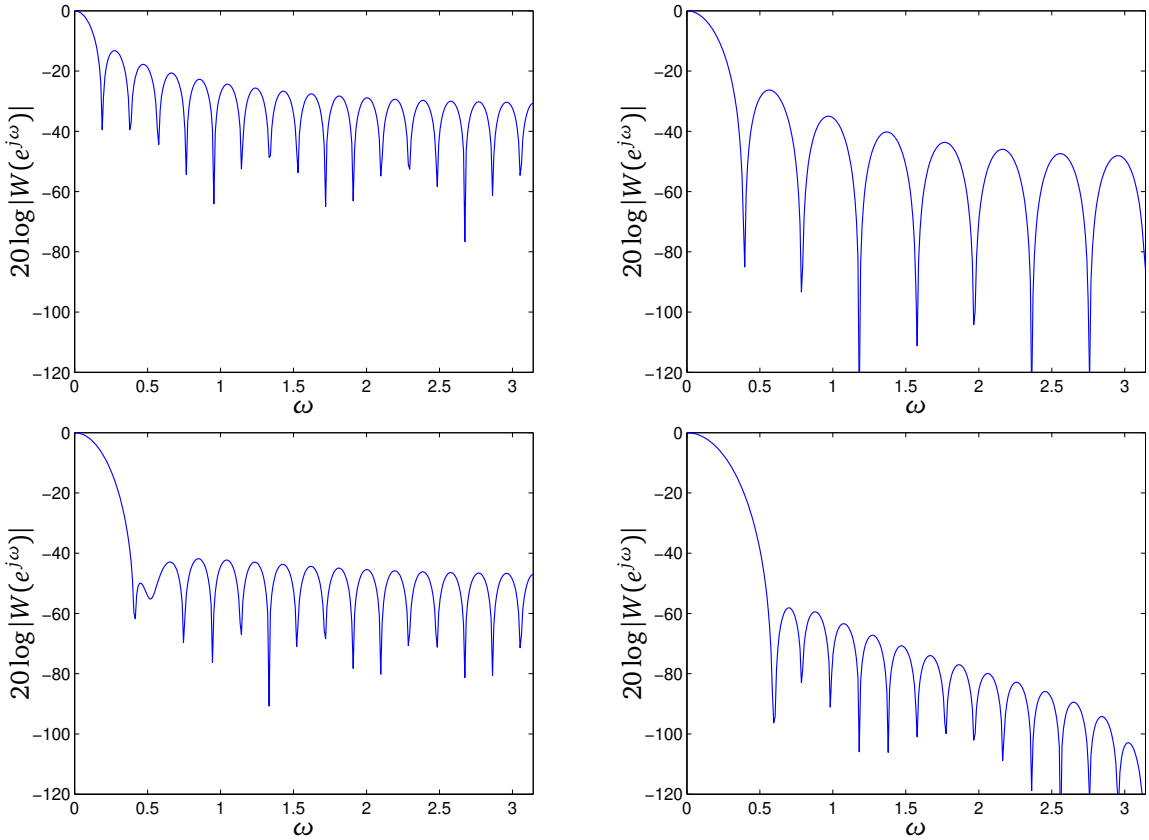

Figure 4.6.: Discrete-time Fourier transform magnitude of Rectangular, Bartlett, Hamming and Blackman window (from top left to bottom right) of length $N = 33$.

Choice of the window function

In the preceding section, we presented the windowing principle with an interpretation, and several window functions. Now the question arises how to choose the window function properly. The effect of the shape and size of the window can be summarized as follows:

1. The window shape controls the peak sidelobe as well as the mainlobe width
2. The window length controls main-lobe behavior only.

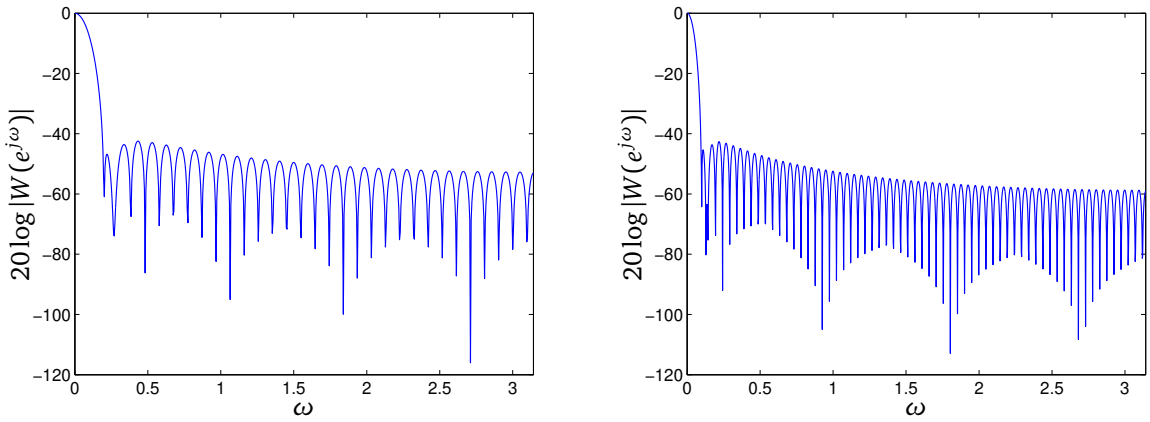

Figure 4.7.: Discrete-time Fourier transform magnitude of Hamming window for $N = 65$ (left) and $N = 129$ (right).

Since the sidelobe behavior and therefore pass-band and stop-band tolerances are affected only by the shape of the window, the pass-band and stop-band requirements dictate which window is to be chosen. The window size is then determined from the transition width requirements.

Let us focus on the window shape first. In general, we want to design the window function such that the difference between the actual frequency response $H(e^{j\omega})$ and the ideal frequency response $H_d(e^{j\omega})$ is small over the entire spectrum. It should therefore fulfill

$$\max_{\omega\in(-\pi,\pi]} |H_d(e^{j\omega}) - H(e^{j\omega})| \leq \alpha, \tag{4.2}$$

where α determines the maximally allowed deviation from the ideal specifications. The term on the left hand side of (4.2) usually is very hard to evaluate. However, a result from approximation theory can be used to upper bound it. More precisely, when approximating an ideal low pass filter with cutoff frequency ω_c, it can be shown that for each window shape there exists a constant γ such that

$$\max_{\omega\in(-\pi,\pi]} |H_d(e^{j\omega}) - H(e^{j\omega})| \leq \gamma \cdot \Delta H_d(e^{j\omega_c}),$$

where $\Delta H_d(e^{j\omega_c})$ is the size of the jump at the discontinuity ω_c, i.e.,

$$\Delta H_d(e^{j\omega_c}) = \lim_{\varepsilon\to 0} |H_d(e^{j(\omega_c+\varepsilon)}) - H_d(e^{j(\omega_c-\varepsilon)})|.$$

The constant γ is called the peak approximation error (PAE) and is an important characteristic of a window function. It has been calculated for all commonly used window shapes. Examples can be found in the last column of Table 4.2, where the values are given in dB for numerical convenience. As mentioned above, the level of the first sidelobe, which is given in the first column of Table 4.2, is closely related to the PAE. We will not discuss its influence on $H(e^{j\omega})$ in detail, though.

In conclusion, we can guarantee that a low pass filter designed by the windowing method fulfills the specifications, if

$$\gamma \cdot \Delta H_d(e^{j\omega_c}) \leq \min(\alpha_1, \alpha_2),$$

where α_1 and α_2 are the passband and stopband tolerances (compare Fig. 3.9 in Chapter 3). For different filter types, such as high pass, band pass, and band stop, the corresponding results can be obtained by expressing them as a superposition of low pass filters (see tutorials).

From the requirements on the PAE, we obtain the feasible window shapes. What is left to determine, is the length N of the window, which only influences its main-lobe width $\Delta\omega_m$. Since the width of the transition band approximately corresponds to the main-lobe width, the filter length has to be chosen so as to fulfill $\Delta\omega_m < \omega_p - \omega_s$. The second column of Table 4.2 contains approximations for the main-lobe width of commonly used filter types and can be used to determine the required filter length. The usage of Table 4.2 is addressed in the following example.

Table 4.2.: Properties of different windows.

Window Type	Peak Amplitude of Sidelobe SLL in dB	Approximate Width of Mainlobe $\Delta\omega_m$ in rad	Peak Approximation Error $20\log_{10}\gamma$
Rectangular	-13	$4\pi/N$	-21
Bartlett	-25	$8\pi/(N-1)$	-25
Hanning	-31	$8\pi/(N-1)$	-44
Hamming	-41	$8\pi/(N-1)$	-53
Blackman	-57	$12\pi/(N-1)$	-74

Example 4.3.1 *Filter design problem. We wish to design a low-pass filter with a required stop-band attenuation of at least* $-50dB$. *Which filter is most appropriate?*

The PAE, as shown in the third column of Table 4.2, contains information on the best stop-band attenuation or pass-band ripple we can expect from a given window shape. Therefore, we can see that the rectangular, Bartlett and Hanning windows will not meet the specifications. The Hamming window may just meet the requirements, but the Blackman window will clearly be the most appropriate one.

From the second column of Table 4.2 the length of the window required can be derived. The distance between the peak ripples on either side of discontinuity is approximately equal to the main-lobe width $\Delta\omega_m$. *The transition width* $\Delta\omega = \omega_s - \omega_p$ *is therefore somewhat less than the main-lobe width. For example, for the Blackman window,* N *can be determined from the relationship* $12\pi/(N-1) \simeq \Delta\omega$. *Therefore* $N \approx 12\pi/\Delta\omega + 1$ *samples.*

4.4 Kaiser Window Filter Design

We can quantify the trade-off between main-lobe width and side-lobe area by seeking the window function that is maximally concentrated around $\omega = 0$ in the frequency domain. Kaiser proposed the window function

$$w(n) = \begin{cases} \dfrac{I_0[\beta(1-[(n-\alpha)/\alpha]^2)^{1/2}]}{I_0(\beta)}, & 0 \le n \le N-1, \\ 0, & \text{elsewhere}, \end{cases}$$

where $\alpha = (N-1)/2$, and $I_0(\cdot)$ is the zeroth-order modified Bessel function of the first kind. In contrast to the previously discussed windows, this one has two parameters; the length N, and a shape parameter β. By varying N and β we can trade side-lobe amplitude for main-lobe width. Figure 4.8 shows Kaiser windows for several values of β. Figure 4.9 shows the trade-off that can be achieved for several values of β and N.

From Figure 4.9 we infer that, if β is increased, i.e. if the window is tapered more, the side-lobes of the Fourier transform become smaller, but the main-lobe becomes wider. Alternatively, we can hold β constant and increase N, causing the main-lobe to decrease in width without affecting the amplitude of the side-lobes.

Kaiser obtained formulae that permitted the filter designer to estimate the values of N and β which were needed to meet a given filter specification. Consider a frequency selective filter with the specifications shown in Figure 3.9(a). Kaiser found that over a usefully wide range of conditions α_1 is determined by the choice of β. Given α_1, the passband cutoff frequency ω_p of the low-pass filter is defined to be the highest frequency such that $|H(e^{j\omega})| \ge 1-\alpha_1$. The stop-band cutoff frequency ω_s is defined to be the lowest frequency such that $|H(e^{j\omega})| \le \alpha_2$. The transition region width is therefore

$$\Delta\omega = \omega_s - \omega_p$$

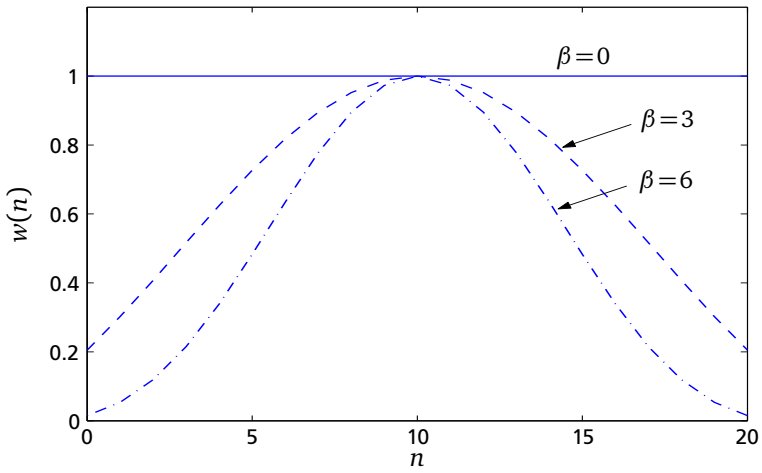

Figure 4.8.: Kaiser windows for $N = 20$, $\beta = 0$, 3 and 6.

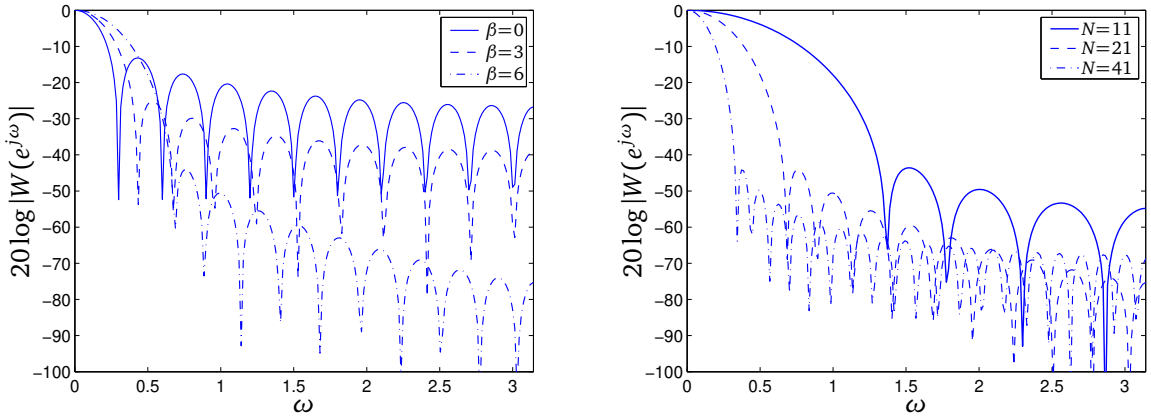

Figure 4.9.: Fourier transform magnitude of Kaiser windows for several values of β, N. (left) $N = 21$, $\beta = 0$, 3 and 6. (right) $\beta = 6$, $N = 11$, 21 and 41.

for the low-pass filter approximation. Defining the negative peak approximation error

$$A = -20\log_{10}\min(\alpha_1, \alpha_2),$$

Kaiser determined empirically that in order to achieve a specified value of A, we require that

$$\beta = \begin{cases} 0.1102(A-8.7), & A > 50, \\ 0.5842(A-21)^{0.4} + 0.07886(A-21), & 21 \le A \le 50, \\ 0, & A < 21. \end{cases}$$

To achieve prescribed values of A and $\Delta\omega$, N must satisfy

$$N = \left\lceil \frac{A-8}{2.285\Delta\omega} + 1 \right\rceil.$$

where $\lceil \cdot \rceil$ means rounding up towards the next integer. Generally, with these design equations, no iterations or "trial and check" procedure is required.

Example 4.4.1 *Given the specifications of a low-pass filter $\omega_p = 0.4\pi$, $\omega_s = 0.6\pi$, $\alpha_1 = \alpha_2 = 0.001$ and $\Delta\omega = 0.2\pi$, find the unit sample response. Using the Kaiser design equations, we find*

$$A = -20\log_{10}\alpha_1 = 60$$

and

$$\beta = 5.653, \quad N = 38\,.$$

The designed filter is

$$h(n) = \begin{cases} \dfrac{\sin \omega_c(n-\alpha)}{\pi(n-\alpha)} \cdot \dfrac{I_0[\beta(1-[(n-\alpha)/\alpha]^2)^{1/2}]}{I_0(\beta)}, & 0 \le n \le N-1, \\ 0, & \textit{elsewhere} \end{cases}$$

where $\alpha = (N-1)/2 = 37/2 = 18.5$ *and* $\omega_c = (\omega_s + \omega_p)/2$. *Since* N *is an even integer, the resulting linear phase system would be of type II. Figure 4.10 shows* $h(n)$ *and* $H(e^{j\omega})$.

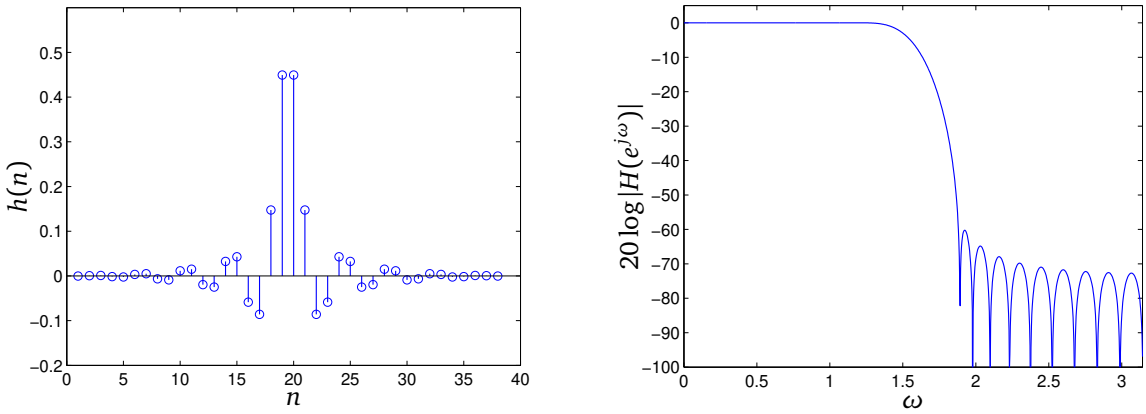

Figure 4.10.: Response functions. Impulse response (left). Log magnitude (right).

Example 4.4.2 *Design of a high-pass filter. In the following, we consider a high-pass filter with specifications* $\omega_s = 0.35\pi$, $\omega_p = 0.5\pi$ *and* $\alpha_1 = 0.021$. *Again using the formulae proposed by Kaiser, we get* $\beta = 2.6$ *and* $N = 25$. *Figure 4.11 shows* $h(n)$ *and* $H(e^{j\omega})$. *The resulting peak error is* $0.0213 > \alpha_1 = \alpha_2 = 0.021$ *as specified. Thus we increase* N *by 26. In this case the filter would be of type II and is not appropriate for designing a high-pass. Therefore we use* $N = 27$, *which exceeds the required specifications.*

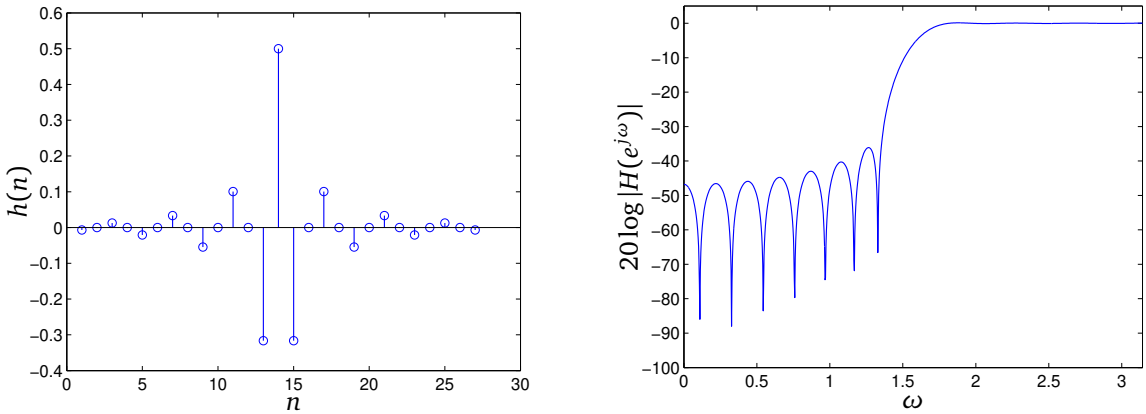

Figure 4.11.: Kaiser window estimate. Impulse response (left). Log magnitude (right).

The design of FIR filters by windowing is straightforward to apply and it is quite general even though it has a number of limitations. However, we often wish to design a filter that is the "best" that can be achieved for a given value of N. We describe two methods that attempt to improve upon the windowing method by introducing a new criterion of optimality.

4.5 Optimal Filter Design.

As seen, the design of a filter with the window method is straightforward and easy to handle but it is not optimal in the sense of minimizing the maximum error. Through the Fourier approximation, any filter design which uses windowing attempts to minimize the integrated error

$$\epsilon^2 = \frac{1}{2\pi}\int_{-\pi}^{\pi} \left|H_d(e^{j\omega}) - H(e^{j\omega})\right|^2 d\omega.$$

In many applications, we get a better result by minimizing the maximum error. Using the windowing method and Fourier approximation, we always get the Gibbs phenomenon which implies that the maximum error will be at discontinuities of $H_d(e^{j\omega})$. Better results can be achieved if the approximation error is spaced equally over the whole frequency band. In the following section, only type I linear phase FIR filters are taken into account but the implementation of other linear phase FIR filters is straightforward. Take a non-causal FIR filter having a symmetric impulse response, i.e. $h(n) = h(-n)$. The corresponding frequency response is

$$\begin{aligned} H(e^{j\omega}) &= \sum_{n=-L}^{L} h(n)e^{-j\omega n} = h(0) + \sum_{n=1}^{L} 2h(n)\cos(\omega n) \\ &= \sum_{n=0}^{L} a(n)\cos(\omega n) \\ &= \sum_{n=0}^{L} \breve{a}(n)\cos(\omega)^n \end{aligned}$$

which is real and even. The filter's specification tolerances are as defined as

$$1-\alpha_1 \le |H(e^{j\omega})| \le 1+\alpha_1 \quad \text{for} \quad 0 \le \omega \le \omega_p\,,$$

and

$$-\alpha_2 \le |H(e^{j\omega})| \le \alpha_2 \quad \text{for} \; \omega_s \le \omega \le \pi\,.$$

To design the filter, the Parks-McClellan algorithm formulates the problem as one of polynomial approximation which can be solved by the Chebyshev approximation over disjoint sets of frequencies ($F = \{0 \le \omega \le \omega_p,\ \omega_s \le \omega \le \pi\}$). The approximation error function, $E(\omega)$, is defined as

$$E(\omega) \hat{=} W(\omega)\left[H_d(e^{j\omega}) - H(e^{j\omega})\right]. \tag{4.3}$$

$E(\omega)$ measures the error between the optimum and attained frequency response, which is weighted by $W(\omega)$ where

$$W(\omega) = \begin{cases} \frac{\alpha_2}{\alpha_1} & : \quad 0 \le \omega \le \omega_p \\ 1 & : \quad \omega_s \le \omega \le \pi \end{cases}.$$

The optimal $H(e^{j\omega})$ minimizes the maximum weighted error which means that we have to search for an $H(e^{j\omega})$ that fulfills

$$\min_{\breve{a}(n)\,:\,0\le n\le L}\left(\max_{\omega\in F}|E(\omega)|\right) = \min_{\breve{a}(n)\,:\,0\le n\le L}\left(\max_{\omega\in F}\left|W(\omega)\left[H_d(e^{j\omega}) - H(e^{j\omega})\right]\right|\right).$$

Theorem 4.5.1 (Alternation Theorem) *With a closed disjoint subset F on the real axis, a necessary and sufficient condition for*

$$H(e^{j\omega}) = \sum_{n=0}^{L} \breve{a}(n)\cos(\omega)^n$$

to be the unique, best weighted Chebyshev approximation of $H_d(e^{j\omega})$ in F is that the error function $E(\omega)$ has at least $L+2$ alternating frequencies in F. This means that there must exist at least $L+2$ frequencies ω_i in F such that $\omega_0 < \omega_1 < \cdots < \omega_{L+1}$ with $E(\omega_i) = -E(\omega_{i+1})$ and

$$|E(\omega_i)| = \max_{\omega\in F}|E(\omega)| \qquad i = 0,\ldots,L+1.$$

The maximum of the alternating frequencies can be found from the derivative of $E(\omega)$. If we calculate the derivative of $E(\omega)$ and take into account that $H_d(e^{j\omega})$ is constant in F, we get for the maximal frequencies

$$\begin{aligned}\frac{dE(\omega)}{d\omega} &= \frac{d}{d\omega}\left\{W(\omega)\left[H_d(e^{j\omega})-H(e^{j\omega})\right]\right\} \\ &= -\frac{dH(e^{j\omega})}{d\omega}W(\omega) \\ &= W(\omega)\sin(\omega)\sum_{n=1}^{L} n\check{a}(n)\cos(\omega)^{n-1} \stackrel{!}{=} 0.\end{aligned} \tag{4.4}$$

This means that there are at most $L+1$ maxima belonging to the polynomial structure and to the frequencies at $\omega = 0$ and $\omega = \pi$. Two more maxima will occur at $\omega = \omega_p$ and $\omega = \omega_s$ because of the discontinuity and the inability to approximate this. As it can be seen in Equation (4.4), the error function $E(\omega)$ and the approximation function $H(e^{j\omega})$ possess maxima at the same frequencies ω_i. Thus from Theorem 4.5.1 we can write the error $E(\omega)$ at the ω_i, $i = 0 \ldots L+1$, as

$$E(\omega_i) = W(\omega_i)\left[H_d(e^{j\omega_i})-H(e^{j\omega_i})\right] = (-1)^i\rho \qquad i = 0 \ldots L+1$$

and can express the ideal frequency response as

$$H_d(e^{j\omega_i}) = H(e^{j\omega_i}) + \frac{(-1)^i\rho}{W(\omega_i)} = \sum_{n=0}^{L} a(n)\cos(\omega_i n) + \frac{(-1)^i\rho}{W(\omega_i)}$$

or

$$\begin{bmatrix} 1 & \cos(\omega_0) & \cdots & \cos(L\omega_0) & \frac{1}{W(\omega_0)} \\ \vdots & \vdots & \ddots & \vdots & \vdots \\ 1 & \cos(\omega_{L+1}) & \cdots & \cos(L\omega_{L+1}) & \frac{(-1)^{L+1}}{W(\omega_{L+1})} \end{bmatrix} \begin{bmatrix} a_0 \\ \vdots \\ a_L \\ \rho \end{bmatrix} = \begin{bmatrix} H_d(e^{j\omega_0}) \\ \vdots \\ H_d(e^{j\omega_{L+1}}) \end{bmatrix}.$$

To solve these equations for the parameter a_n, we use an algorithm called "Remez" which was developed by Rabiner *et. al.* in 1975. After an initial guess of $L+2$ extremal frequencies of $H(e^{j\omega})$, we can compute ρ according to

$$\rho = \frac{\gamma_0 H_d(e^{j\omega_0}) + \ldots + \gamma_{L+1}H_d(e^{j\omega_{L+1}})}{\frac{\gamma_0}{W(e^{j\omega_0})} + \ldots + \frac{(-1)^{L+1}\gamma_{L+1}}{W(e^{j\omega_{L+1}})}} \tag{4.5}$$

with

$$\gamma_k = \prod_{n=0,\ n\neq k}^{L+1} \frac{1}{\cos(\omega_k)-\cos(\omega_n)}.$$

Since $E(\omega)$ has the same extremal frequencies as $H(e^{j\omega})$, we can write

$$\hat{H}(e^{j\omega_i}) = H_d(e^{j\omega_i}) - \frac{(-1)^i\rho}{W(\omega_i)}.$$

Using Lagrange interpolation, it follows that

$$H(e^{j\omega}) = \frac{\sum_{k=0}^{L} \hat{H}(e^{j\omega_i})\frac{\beta_k}{\cos(\omega)-\cos(\omega_k)}}{\sum_{k=0}^{L} \frac{\beta_k}{\cos(\omega)-\cos(\omega_k)}}$$

with

$$\beta_k = \prod_{n=0,\ n\neq k}^{L} \frac{1}{\cos(\omega_k) - \cos(\omega_n)}.$$

With $H(e^{j\omega})$ it is possible to calculate the error $E(\omega)$ according to Equation (4.3). After calculating $E(\omega)$, $L+2$ extremal frequencies belonging to the largest alternating peaks can be selected and the algorithm can start again by using Equation (4.5). The Algorithm is summarized in Figure 4.12. By using the Remez algorithm we are able to find the δ that defines the upper bound of $|E(\omega)|$, which is the optimum solution for the Chebyshev approximation. After the algorithm converges, the filter coefficients $h(n)$ can be calculated by taking $L+1$ frequencies from $H(e^{j\omega})$ with

$$h(n) = \frac{1}{L+1} \sum_{n=0}^{L} H(e^{\omega_n}) e^{j2\pi kn/(L+1)}.$$

Property of Optimal Filters

The error between the desired and attained filter frequency response achieves a minimum and maximum consecutively at a finite number of frequencies in the frequency range of interest (passband and stopband regions), called alternation frequencies. The minimum number of alternating frequencies for a Type I optimum filter is $(N+3)/2$ with $L = (N-1)/2$. Because of this characteristic, optimal filters are called *equi-ripple* filters. Two remarks are:

- Designing an optimal filter requires much more computation than the windowing method.
- The length of the filter designed by the window method is 20% to 50% longer than the length of the optimal filter.
- Optimal filter design is the most widely used FIR filter design method. In ©MATLAB the function that performs optimum filter design is called “firpm”.

4.6 Implementation of FIR Filters

Here we discuss the implementation of a discrete time system with unit sample response $h(n)$, where $h(n)$ may be a filter. The input-output relationship is given by the convolution sum

$$y(n) = \sum_{k=-\infty}^{\infty} h(k)x(n-k) = \sum_{k=0}^{N-1} h(k)x(n-k),$$

i.e., the output $y(n)$ represents a sum of weighted and delayed versions of the input $x(n)$. The signal flow graph for a single delay element is shown in Figure 4.13.

The convolution sum can be represented as in Figure 4.14.

The computational efficiency of the algorithm in Figure 4.14 may be improved by exploiting the symmetry (or anti-symmetry) of $h(n)$. For type I Filters, we have $h(n) = h(N-1-n)$ and N is odd. This leads to

$$\begin{aligned} y(n) &= \sum_{k=0}^{N-1} h(k) \cdot x(n-k) \\ &= \sum_{k=0}^{\alpha-1} h(k) \cdot x(n-k) + h(\alpha)x(n-\alpha) + \sum_{k=\alpha+1}^{N-1} h(k) \cdot x(n-k) \end{aligned}$$

with $\alpha = (N-1)/2$, and therewith

$$y(n) = \sum_{k=0}^{\alpha-1} h(k)[x(n-k) + x(n-(N-1-k))] + h(\alpha)x(n-\alpha)$$

This realization is shown by the flow graph in Figure 4.15. This method reduces the number of multiplications by 50% without affecting the number of additions or storage elements required.

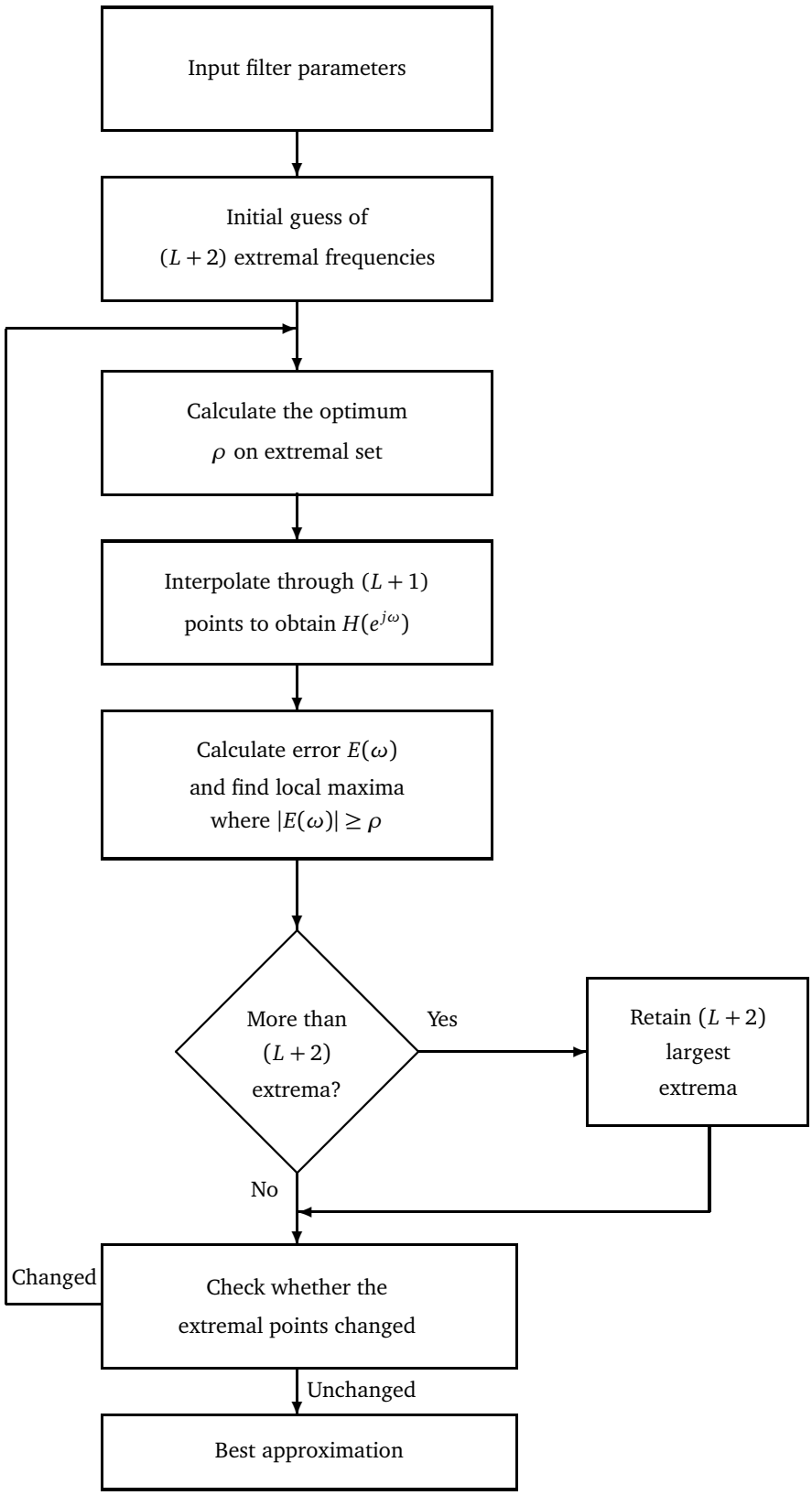

Figure 4.12.: Flowchart of Parks-McClellan algorithm.

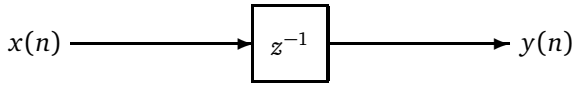

Figure 4.13.: Signal flow graph for a delay element.

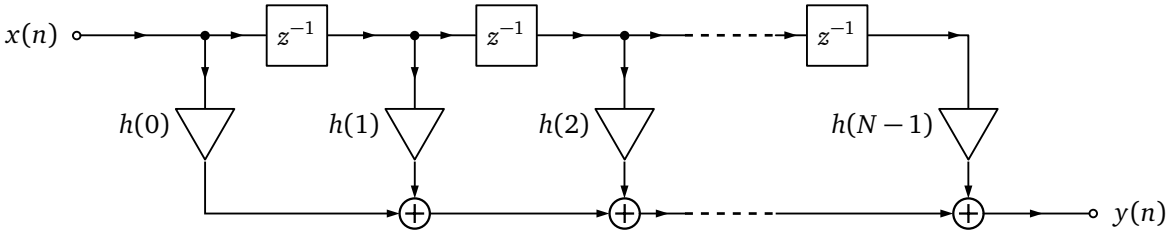

Figure 4.14.: Signal Flow graph representing the convolution sum.

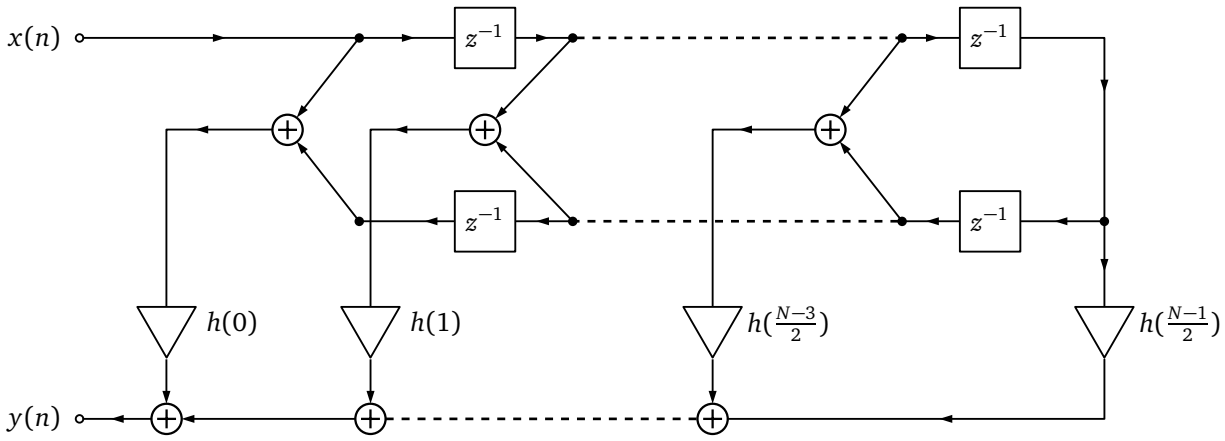

Figure 4.15.: Efficient signal flow graph for the realization of a type I FIR filter.

5 Design of Infinite Impulse Response Filters

5.1 Introduction

When designing IIR filters one must determine a rational $H(z)$ which meets a given magnitude specification. The two different approaches are :

1. Design a digital filter from an analog or continuous-time filter.
2. Design the filter directly.

Only the first approach is considered here since it is much more useful in general. Given the specification of a discrete-time filter, the design of digital filters using continuous-time prototypes consists of the following three steps:

Step 1 : Translation of the filter specifications from discrete-time to continuous-time.

Step 2 : Determination of the continuous-time filter transfer function $H_c(s)$.

Step 3 : Transformation of $H_c(s)$ to a discrete-time filter system function $H(z)$.

The three steps are summarized in Figure 5.1.

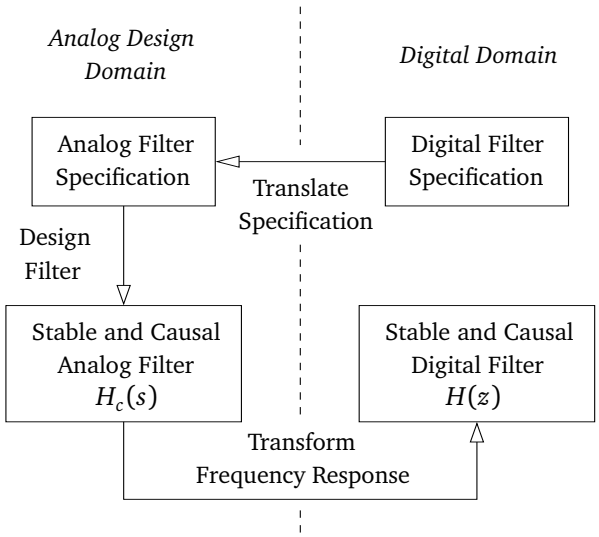

Figure 5.1.: Principle of IIR filter design using analog prototypes.

Note that Step 1 depends on Step 3 since translation of the digital filter specification to a continuous-time filter specification depends on how the continuous-time filter is transformed back to the digital domain. Further, it is desirable for Step 3 to always transform a causal and stable $H_c(s)$ to a causal and stable $H(z)$, and also that the transformation results in a digital filter with a rational $H(z)$ when the continuous-time filter has a rational $H_c(s)$. The continuous-time filter frequency response $H_c(j\Omega) = H_c(s = j\Omega)$ should map the digital filter frequency response $H(e^{j\omega}) = H(z = e^{j\omega})$. Typically Butterworth, Chebyshev and elliptic filters are used as continuous-time prototypes.

The *impulse invariance method* and *bilinear transformation* are two approaches that satisfy all the above properties, and are often used in designing IIR filters. We discuss their implementation in the following sections.

5.2 Impulse Invariance Method

In the impulse invariance method, we obtain the unit sample response of the digital filter by sampling the impulse response of the continuous-time filter. The principle of impulse invariance is depicted in Figure 5.2; the three steps are as follows:

1. From $H_c(s)$ and $H_c(j\Omega)$, we determine $h_c(t)$.
2. The sequence $h(n)$ is obtained by $h(n) = T_d \cdot h_c(nT_d)$, where T_d is the design sampling interval which does not need to be the same as the sampling period T associated with A/D and D/A conversion.
3. $H(z)$ is obtained from $h(n)$.

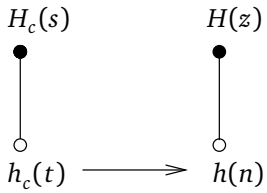

Figure 5.2.: Obtaining the digital filter from the continuous-time filter.

Example 5.2.1 *A continuous-time filter is described by*

$$H_c(s) = \frac{1}{s - s_c}.$$

The inverse Laplace transform is

$$h_c(t) = e^{s_c t} \cdot u(t).$$

Therefore, assuming $T_d = 1$,

$$h(n) = h_c(t)|_{t=nT_d} = e^{s_c n} \cdot u(n)$$

which leads to

$$H(z) = \frac{1}{1 - e^{s_c} z^{-1}}$$

In general, to transform $H_c(s)$ to $H(z)$, $H_c(s)$ is first expressed as a linear combination of system functions of the form $1/(s - s_c)$, which is then transformed to give $H(z)$, i.e. perform a partial fraction expansion and transform each component. If $H_c(s)$ has multiple poles at $s = s_c$, $H_c(s)$ would have a component of the form $1/(s - s_c)^p$ with $p > 1$. Its z-transform can be obtained by following the same steps as the above example.

In previous chapters, especially Section 2.1, we have seen that the Fourier transform of sampled continuous-time signals is of the form

$$H(e^{j\omega}) = \sum_{k=-\infty}^{\infty} H_c\left(j\frac{\omega}{T_d} + j\frac{2\pi}{T_d}k\right). \tag{5.1}$$

So, $H(e^{j\omega})$ is not simply related to $H_c(j\Omega)$ because of aliasing. If there were no aliasing effect,

$$H(e^{j\omega}) = H_c\left(j\frac{\omega}{T_d}\right) \quad \text{for } -\pi \le \omega \le \pi, \tag{5.2}$$

and the shape of $H(e^{j\omega})$ would be the same as $H_c(j\Omega)$. Note that in practice $H_c(j\Omega)$ is not band limited and therefore aliasing is present which involves some difficulty in the design. In practice, we suppose that the relation $H(e^{j\omega}) = H_c(j\omega/T_d)$ holds over $[-\pi, \pi)$ and we carry out the remaining steps, instead of using Equation (5.1).

Note that the discrete-time frequency ω is related to the continuous-time frequency Ω by $\omega = \Omega T_d$. Because of the approximation, the resulting filter may not satisfy the digital filter specifications and some iterations may be needed. Also due to aliasing, it is difficult to design band-stop or high-pass filters that have no significant aliasing.

In the impulse invariance design procedure, we transform the continuous-time filter specifications through the use of Equation (5.2) to the discrete-time filter specifications. We illustrate this in the following example.

Example 5.2.2 *Assume that we have the low-pass filter specifications as shown in Figure 5.3 with* $\alpha_1 = 0.10875$, $\alpha_2 = 0.17783$, $\omega_p = 0.2\pi$, $T_d = 1$ *and* $\omega_s = 0.3\pi$. *In this case the passband is between* $1 - \alpha_1$ *and* 1 *rather than between* $1 - \alpha_1$ *and* $1 + \alpha_1$. *Historically, most continuous-time filter approximation methods were developed for the design of passive systems, i.e. systems with a gain less than* 1. *Therefore, the design specifications for continuous time filters have typically been formulated so that the passband is less than or equal to* 1.

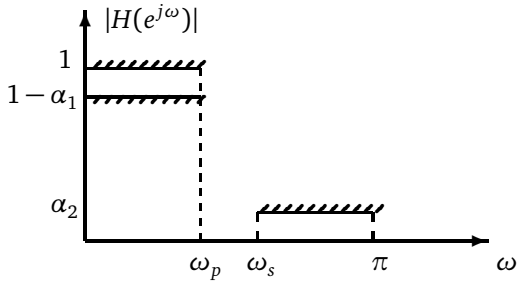

Figure 5.3.: IIR low-pass filter specifications.

We will design a filter by applying the impulse invariance method to an appropriate Butterworth continuous-time filter. A Butterworth low-pass filter is defined by its magnitude-squared function

$$|H_c(j\Omega)|^2 = \frac{1}{1 + (\Omega/\Omega_c)^{2N}} \tag{5.3}$$

where N *is an integer corresponding to the order of the filter. The magnitude response of a Butterworth filter of* N*th order is maximally flat in the passband, i.e., the first* $(2N-1)$ *derivatives of the magnitude-squared function are zero at* $\Omega = 0$. *An example of this characteristic is shown in Figure 5.4 for* $N = 2$, 4 *and* 8.

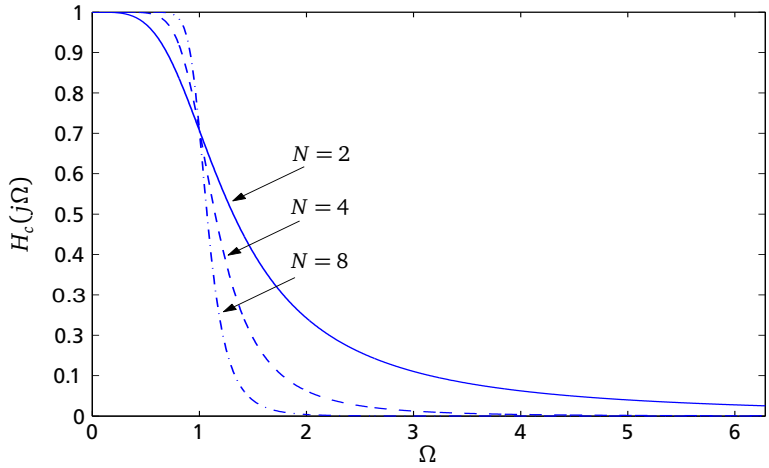

Figure 5.4.: Magnitude transfer function $H_c(j\Omega)$ of a Butterworth filter.

The first step is to transform the discrete-time specifications to continuous-time filter specifications. Assuming that the aliasing involved in the transformation from $H_c(j\Omega)$ *to* $H(e^{j\omega})$ *will be negligible, we obtain the specification on* $H_c(j\Omega)$ *by applying the relation* $\Omega = \omega/T_d$ *to obtain the continuous-time filter specifications shown in Figure 5.5.*

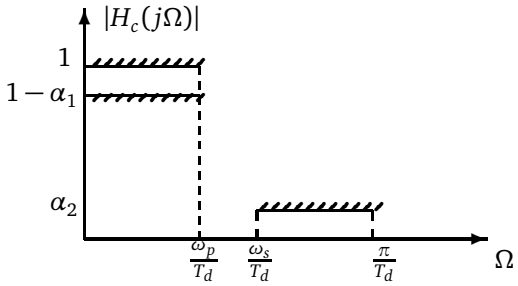

Figure 5.5.: Translated filter specifications for Example 5.2.2.

The desired continuous-time Butterworth filter should satisfy the following specifications,

$$1-\alpha_1 = 0.89125 \le |H_c(j\Omega)| \le 1\,, \quad 0 \le |\Omega| \le 0.2\pi\,,$$

and

$$|H_c(j\Omega)| \le 0.17783 = \alpha_2\,, \quad 0.3\pi \le |\Omega| \le \pi\,.$$

which are the so-called design equations. Because $|H_c(j\Omega)|$ is a monotonic function of Ω, the specifications will be satisfied if

$$|H_c(j0.2\pi)| \ge 0.89125$$

and

$$|H_c(j0.3\pi)| \le 0.17783$$

Now, we determine N and Ω_c, which are parameters of $|H_c(j\Omega)|^2$, as defined in Equation (5.3). To meet the specifications, we have

$$1+\left(\frac{0.2\pi}{\Omega_c}\right)^{2N} = \left(\frac{1}{0.89125}\right)^2 \tag{5.4}$$

and

$$1+\left(\frac{0.3\pi}{\Omega_c}\right)^{2N} = \left(\frac{1}{0.17783}\right)^2 \tag{5.5}$$

which can be solved for N as

$$N = \frac{\log\left(\frac{1}{0.89125^2}-1\right)-\log\left(\frac{1}{0.17783^2}-1\right)}{2\left(\log 0.2\pi - \log 0.3\pi\right)} = 5.8858.$$

Since N must be an integer, we choose $N = 6$. Substituting this N into Equation (5.4) we obtain $\Omega_c = 0.7032$. With these values, the pass-band specification will be met exactly and the stop-band specifications will be exceeded, reducing the potential of aliasing. With order $N = 6$, the $2N = 12$ poles of

$$H_c(s)H_c(-s) = 1/[1+(s/j\Omega_c)^{2N}]$$

are uniformly distributed around a circle of radius $\Omega_c = 0.7032$. We can determine the poles on the left half of the s-plane as

$$s_k = \Omega_c e^{j\frac{\pi}{2N}(2k+N+1)}, \quad k = 0,\ldots,N-1$$

which gives three pole pairs with coordinates

$$\begin{aligned} s_{0/5} &= -0.182 \pm j0.679 \\ s_{1/4} &= -0.497 \pm j0.497 \\ s_{2/3} &= -0.679 \pm j0.182 \end{aligned}$$

so that we can construct $H_c(s)$ using

$$H_c(s) = \frac{\Omega_c^N}{\prod_{k=0}^{N-1}(s - s_k)}$$

which gives

$$H_c(s) = \frac{0.12093}{(s^2 + 0.364s + 0.4942)(s^2 + 0.994s + 0.494)(s^2 + 1.358s + 0.4542)}.$$

Expressing $H_c(s)$ in a partial fraction expansion, we can transform $1/(s - s_k)$ into $1/(1 - e^{s_k} z^{-1})$. Note that generally, this step is non-trivial, and may need numerical programming in practice. For the sake of completeness, we present the final result

$$H(z) = \frac{0.2871 - 0.4466z^{-1}}{1 - 1.2971z^{-1} + 0.6949z^{-2}} + \frac{-2.1428 + 1.1455z^{-1}}{1 - 1.0691z^{-1} + 0.3699z^{-2}} + \frac{1.8557 - 0.6303z^{-1}}{1 - 0.9972z^{-1} + 0.2570z^{-2}}.$$

5.3 Bilinear Transformation

The other main approach to the design problem is the bilinear transformation. With this approach, $H(z)$ is obtained directly from the continuous-time frequency response $H_c(s)$ by replacing s by

$$s = \frac{2}{T_d}\left[\frac{1 - z^{-1}}{1 + z^{-1}}\right]$$

so that

$$H(z) = H_c\left[\frac{2}{T_d}\left(\frac{1 - z^{-1}}{1 + z^{-1}}\right)\right].$$

A sample on the unit circle, $z = e^{j\omega}$, corresponds to the point

$$s = \frac{2}{T_d} \cdot \frac{1 - e^{-j\omega}}{1 + e^{-j\omega}} = j\frac{2}{T_d}\tan\left(\frac{\omega}{2}\right).$$

The bilinear transformation transforms the imaginary axis of the s-plane to the unit circle in the z-plane, as shown in Figure 5.6.

The inverse transform is given by

$$z = \frac{\frac{2}{T_d} + s}{\frac{2}{T_d} - s} = \frac{1 + (T_d/2)s}{1 - (T_d/2)s} = \frac{1 + \sigma T_d/2 + j\Omega T_d/2}{1 - \sigma T_d/2 - j\Omega T_d/2}.$$

The region $\mathrm{Re}\{s\} < 0$ is transformed to $|z| < 1$, i.e. the left-hand half plane $\mathrm{Re}\{s\} < 0$ of the s-plane is mapped inside the unit circle. This means the bilinear transformation will preserve the stability of systems.

In the definition of the transformation, $2/T_d$ is a scaling factor. It controls the deformation of the frequency axis when we use the bilinear transformation to obtain a digital transfer function $H(z)$ from the continuous-time transfer function $H_c(s)$. From $s = j2/T_d \tan(\omega/2) = \sigma + j\Omega$, it follows that

$$\Omega = \frac{2}{T_d}\tan\left(\frac{\omega}{2}\right) \text{ and } \sigma = 0.$$

For low frequencies, the deformation between Ω and ω is very small,i.e. for small ω, we can assume $\Omega \approx \omega/2$. This was the criterion for choosing $2/T_d$ as a scaling factor. This is shown in Figure 5.7. The choice of another criterion will yield another scaling factor.

Some remarks on the bilinear transformation are:

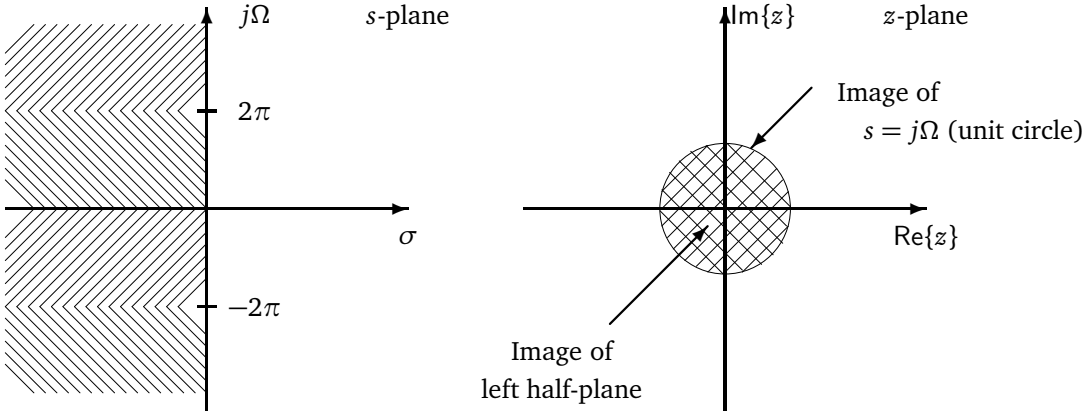

Figure 5.6.: Mapping of the s-plane onto the z-plane using the bilinear transformation.

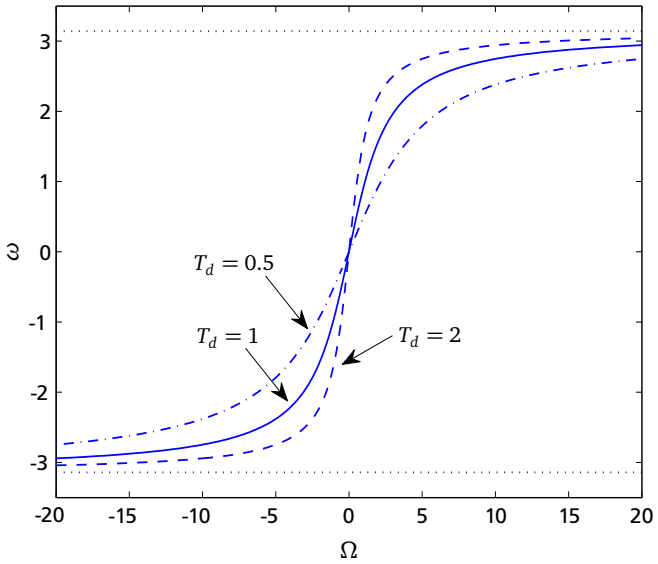

Figure 5.7.: Frequency mapping by bilinear transformation.

- This transformation is the most used in practice. It calculates digital filters from known continuous-time filter responses.
- The detailed shape of $H_c(j\Omega)$ is not preserved, by taking into account the frequency deformation,

$$\Omega = \frac{2}{T_d} \tan\left(\frac{\omega}{2}\right).$$

- The delay time is also modified

$$\tau_d = \tau_c \left\{1 + \left(\frac{\omega_c T_d}{2}\right)\right\}.$$

  If the continuous-time filter has a constant delay time, the resulting digital filter will not have this property.
- To design a digital filter using this method one must first transform the discrete time filter specifications to the continuous time specifications, design a continuous-time filter with these new requirements and then apply the bilinear transformation.

Example 5.3.1 *Consider the discrete-time filter specifications of Example 5.2.2, where we illustrated the impulse invariance technique for the design of a discrete-time filter. In carrying out the design using the bilinear transformation, the critical frequencies of the discrete-time filter must be pre-warped to the corresponding continuous-time frequencies using* $\Omega = (2/T_d)\tan(\omega/2)$ *so that the frequency distortion inherent in bilinear transformation will map them back to the correct discrete-time critical frequencies. For this specific filter, with* $|H_c(j\Omega)|$ *representing the magnitude response function of the continuous-time filter, we require that*

$$0.89125 \le |H_c(j\Omega)| \le 1, \qquad 0 \le |\Omega| \le \frac{2}{T_d}\tan\left(\frac{0.2\pi}{2}\right),$$

$$|H_c(j\Omega)| \le 0.17783, \qquad \frac{2}{T_d}\tan\left(\frac{0.3\pi}{2}\right) \le |\Omega| \le \infty.$$

For convenience we choose $T_d = 1$. *Also, as with Example 5.2.2, since a continuous-time Butterworth filter has monotonic magnitude response, we can equivalently require that*

$$|H_c(j2\tan(0.1\pi))| \ge 0.89125$$

and

$$|H_c(j2\tan(0.15\pi))| \le 0.17783.$$

We again consider a Butterworth filter whose magnitude-squared frequency response is given by

$$|H_c(j\Omega)|^2 = \frac{1}{1+(\Omega/\Omega_c)^{2N}}.$$

To meet the specifications, we have

$$1+\left(\frac{2\tan(0.1\pi)}{\Omega_c}\right)^{2N} = \left(\frac{1}{0.89125}\right)^2 \tag{5.6}$$

and

$$1+\left(\frac{2\tan(0.15\pi)}{\Omega_c}\right)^{2N} = \left(\frac{1}{0.17783}\right)^2 \tag{5.7}$$

which can be solved for N as

$$N = \frac{\log\left(\frac{1}{0.17783^2}-1\right)-\log\left(\frac{1}{0.89125^2}-1\right)}{2\log(\tan 0.15\pi)-2\log(\tan 0.1\pi)} = 5.30466.$$

Since N must be an integer, we choose $N = 6$. *Substituting this N into Equation (5.7) we obtain* $\Omega_c = 0.76622$. *For this value of* Ω_c, *the passband specifications are exceeded and stop band specifications are met exactly. This is reasonable for the bilinear transformation since we do not have to be concerned with aliasing. That is, with proper pre-warping, we can be certain that the resulting discrete-time filter will meet the specifications exactly at the desired stopband edge.*

In the s-plane, the 12 poles of the magnitude-squared function are uniformly distributed in angle on a circle of radius $\Omega_c = 0.7662$. *This is according to Example 5.2.2. The system function of the continuous-time filter obtained by selecting the left half-plane poles is*

$$H_c(s) = \frac{0.20238}{(s^2+0.3966s+0.5871)(s^2+1.0836s+0.5871)(s^2+1.4802s+0.5871)}.$$

We then obtain the system function $H(z)$ *for the discrete-time filter by applying the bilinear transformation to* $H_c(s)$ *with* $T_d = 1$, *which gives*

$$H(z) = \frac{0.0007378(1+z^{-1})^6}{(1-1.268z^{-1}+0.7051z^{-2})(1-1.0106z^{-1}+0.3583z^{-2})(1-0.9044z^{-1}+0.2155z^{-2})}.$$

Since the bilinear transformation maps the entire $j\Omega$-axis of the s-plane onto the unit circle, the magnitude response of the discrete-time filter falls off much more rapidly than the original continuous-time filter, i.e. the entire imaginary axis of the s-plane is compressed onto the unit circle. Hence, the behavior of $H(e^{j\omega})$ at $\omega = \pi$ corresponds to the behavior of $H_c(j\Omega)$ at $\Omega = \infty$. Therefore, the discrete-time filter will have a sixth-order zero at $z = -1$ since the continuous-time Butterworth filter has a sixth-order zero at $s = \infty$.

Note that as with impulse invariance, the parameter T_d is of no consequence in the design procedure since we assume that the design problem always begins with discrete-time filters specifications. When these specifications are mapped to continuous-time specifications and then the continuous-time filter is mapped back to a discrete-time filter, the effect of T_d is cancelled. Although we retained the parameter T_d in our discussion, in specific problems any convenient value of T_d can be chosen.

5.4 Implementation of IIR Filters

An IIR filter has an infinite extent and cannot be implemented by direct convolution in practice. For this reason, we require the IIR filter to have a rational z-transform, as we have seen that this can be realized by a difference equation.

Direct Form I

The difference equation that describes the system is given by

$$y(n) = -\sum_{k=1}^{M} a_k y(n-k) + \sum_{r=0}^{N-1} b_r x(n-r)$$

This can be realized in a straightforward manner as depicted in Figure 5.8 which represents the pair $v(n) = \sum_{r=0}^{N-1} b_r x(n-r)$ and $y(n) = -\sum_{k=1}^{M} a_k y(n-k) + v(n)$ for $(N-1) = M$. This representation can be viewed as an implementation of $H(z)$ through the decomposition

$$H(z) = H_2(z)H_1(z) = \left(\frac{1}{1 + \sum_{k=1}^{M} a_k z^{-k}} \right) \left(\sum_{r=0}^{N-1} b_r z^{-r} \right).$$

Direct Form II

The previous system can also be viewed as a cascade of two systems whose system functions are given by $H_1(z)$ and $H_2(z)$. Since

$$H_1(z)H_2(z) = H(z) = H_2(z)H_1(z),$$

we can change the order of $H_1(z)$ and $H_2(z)$ without affecting the overall system function. This is because the delay elements are redundant and can be combined. We then obtain the direct form II structure. The advantage of the second form lies in the reduction in the number of storage elements required, while the number of arithmetic operations required is constant. The flow graph of direct form II structure is depicted in Figure 5.9

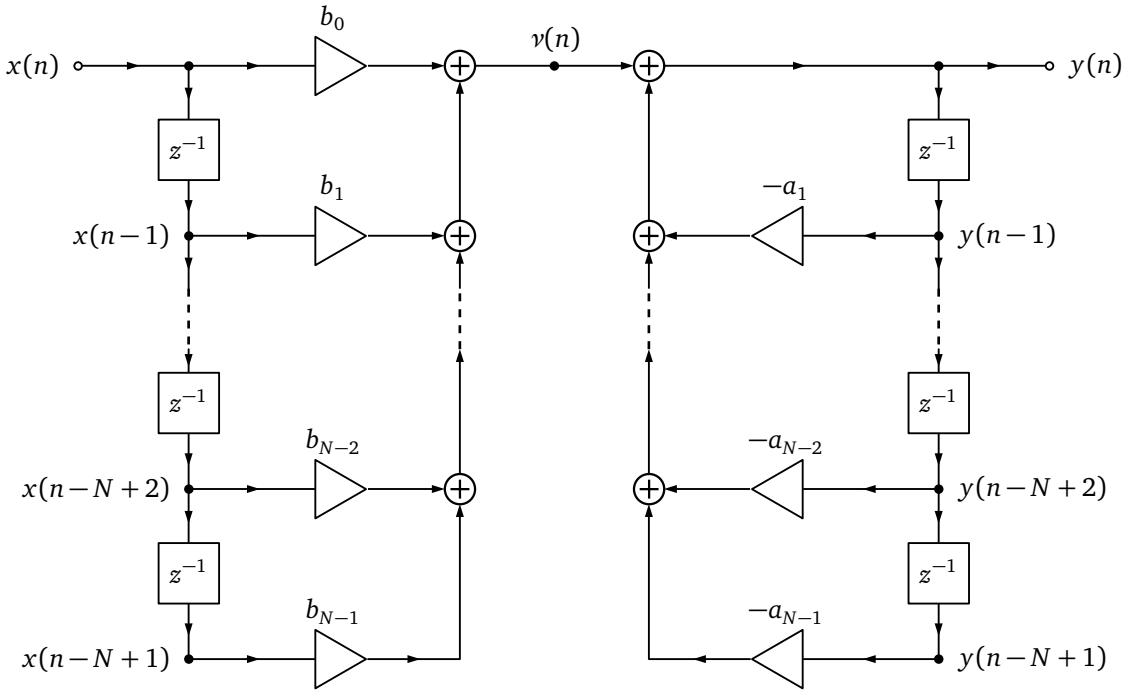

Figure 5.8.: Signal flow graph of direct form I structure for an $(N-1)$th-order system.

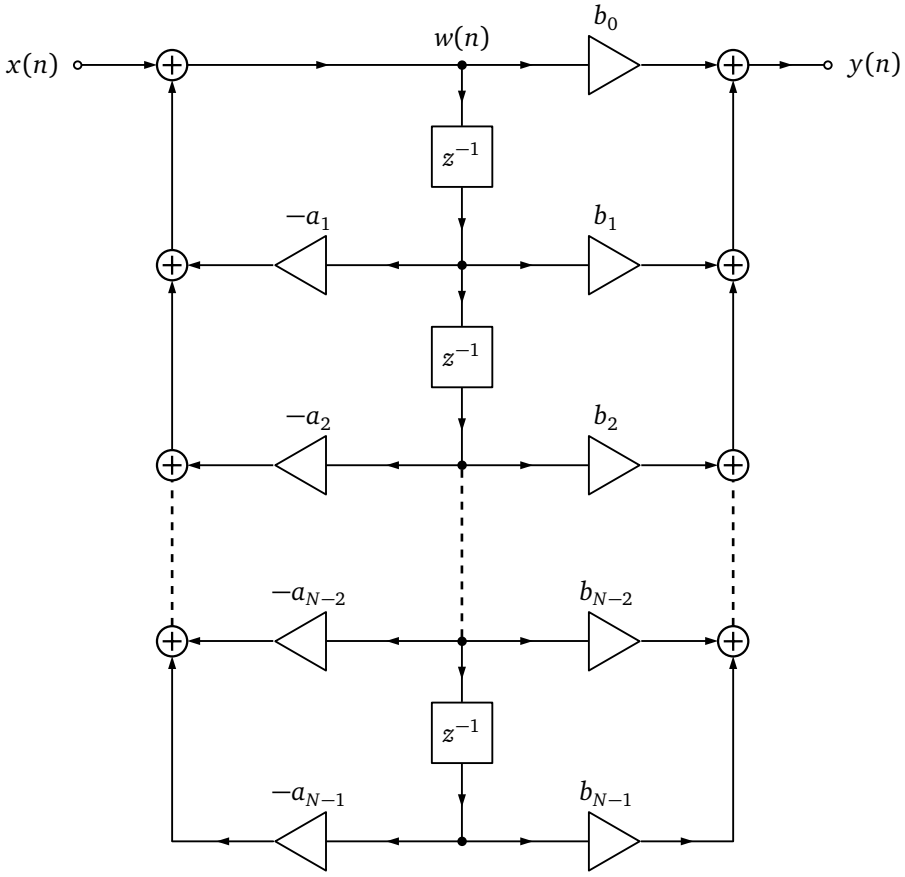

Figure 5.9.: Signal flow graph of direct form II structure for an $(N-1)$th-order system.

The rational system function

$$H(z) = \frac{\sum_{r=0}^{N-1} b_r z^{-r}}{1 + \sum_{k=1}^{M} a_k z^{-k}}$$

can be expressed in the general form,

$$H(z) = \prod_k H_k(z)$$

where $H_k(z)$ is given by :

$$H_k(z) = \frac{\beta_{0k} + \beta_{1k} z^{-1} + \beta_{2k} z^{-2}}{1 + \alpha_{1k} z^{-1} + \alpha_{2k} z^{-2}}$$

The constants β_{0k}, β_{1k}, β_{2k}, α_{1k} and α_{2k} are real, since $h(n)$ is real. The previous equations have shown that $H(z)$ can be represented by a cascade of second order sections $H_k(z)$. The cascade form is less sensitive to coefficient quantization. If we change the branch transmittance in the two direct forms, the poles and zeroes of the system function will be affected. In the cascade form, however, the change in one transmittance branch will affect the poles or zeroes only in the second order section where the branch transmittance is affected. Figure 5.10 gives the cascade structure for a 4th-order system with a direct form II realization of each second-order subsystem.

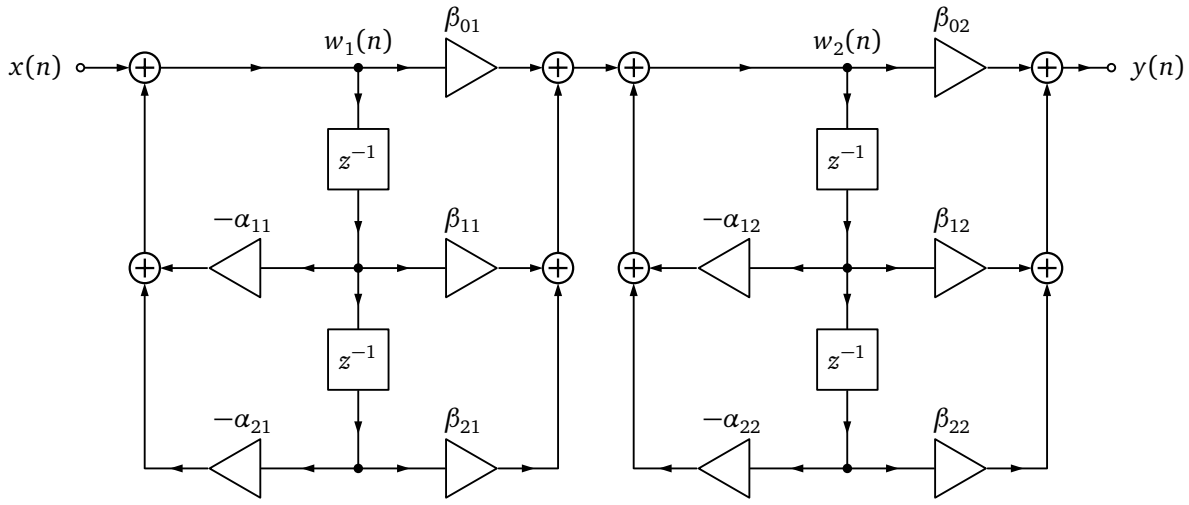

Figure 5.10.: Cascade structure for a 4th-order system with a direct form II realization of second-order sections.

5.5 A Comparison of FIR and IIR Digital Filters

After having discussed a wide range of methods for the design of both infinite and finite duration impulse response filters several questions naturally arise: What type of system is best, IIR or FIR? Which methods yields the best results? The answer is neither. We have discussed a wide range of methods for both IIR and FIR filter because no single type of filter nor single design method is best for all circumstances.

The choice between an FIR filter and an IIR filter depends upon the relative weight that one attaches to the advantages and disadvantages of each type of filter. For example, IIR filters have the advantage that a variety of frequency selective filters can be designed using closed-form design formulae. That is, once the problem has been defined in terms of appropriate specifications for a given kind of filter (e.g., Butterworth, Chebyshev, or elliptic),

then the coefficients (or poles and zeros) of the desired digital filter are obtained by straightforward substitution into a set of design equations. This kind of simplicity in the design procedure is attractive if only a few filters are to be designed or if limited computational facilities are available.

In the case of FIR filters, closed-form design equations do not exist. While the window method can be applied in a straightforward manner, some iteration may be necessary to meet a prescribed specification. Most of the other FIR design methods are iterative procedures which require relatively powerful computational facilities for their implementation. In contrast, it is often possible to design frequency selective IIR digital filters using only a hand calculator and tables of continuous-time filter design parameters. A drawback of IIR filters is that the closed-form IIR designs are preliminary limited to low-pass, band-pass, high-pass filters, etc. Furthermore, these designs generally disregard the phase response of the filter. For example, with a relatively simple computational procedure we, may obtain excellent amplitude response characteristics with an elliptic low-pass filter while the phase response will be nonlinear, especially at the band edge.

In contrast, FIR filters can have precise linear phase. Also, the window method and most algorithmic methods afford the possibility of approximating more arbitrary frequency response characteristics with little more difficulty than is encountered in the design of low-pass filters. Also, it appears that the design problem for FIR filters is much more under control than the IIR design problem because there is an optimality theorem for FIR filters that is meaningful in a wide range of practical situations.

Finally, there are questions of economics in implementing a digital filter. Concerns of this type are usually measured in terms of hardware complexity or computational speed. Both these factors are strongly related to the filter order required to meet a given specification. Putting aside phase considerations, a given amplitude response specification will, in general, be met most efficiently with an IIR filter. However, in many cases, the linear phase available with an FIR filter may be well worth the extra cost.

Thus a multitude of tradeoffs must be considered in designing a digital filter. Clearly, the final choice will most often be made in terms of engineering judgement on such questions as the formulation of specifications, the method of implementation, and computational facilities available for carrying out the design.

6 Random Variables and Stochastic Processes

This chapter provides a short introduction into the field of random variables and stochastic processes, which is fundamental for development of non-parametric and parametric spectrum estimation. For a more comprehensive treatment, we refer to the manuscript of the lecture *Stochastic Signals and Systems* and references therein.

6.1 Random Variables

A random variable is a number $X(\zeta)$ assigned to every outcome $\zeta \in \mathscr{S}$ of an experiment. This could be the gain in a game of chance, the voltage of a random source, the cost of a random component, or any other numerical quantity that is of interest when performing a random experiment.

Given $\zeta \in \mathscr{S}$, the mapping $\zeta \to X(\zeta) \in \mathbb{R}$ is a random variable, if for all $x \in \mathbb{R}$ the set $\{\zeta : X(\zeta) \leq x\}$ is also an event. This event has probability

$$\mathsf{P}(\{X \leq x\}) = \mathsf{P}(\{\zeta : X(\zeta) \leq x\})$$

Distribution Functions

We have seen that the probability $\mathsf{P}(\{X \leq x\})$ is a function of x. The mapping $x \in \mathbb{R} \to F_X(x) = \mathsf{P}(\{X \leq x\})$ is called the *probability distribution function* of the random variable X. Sometimes, the probability distribution function is also referred to as cumulative distribution function (cdf).

The probability distribution function has the following properties

1) $F_X(x)$ is bounded between 0 and 1, especially

$$\begin{aligned} \lim_{x\to\infty} F_X(x) &= 1 \\ \lim_{x\to-\infty} F_X(x) &= 0 \end{aligned}$$

2) $F_X(x)$ is continuous from the right, i.e.

$$\lim_{\epsilon\to 0} F_X(x+\epsilon) = F_X(x), \quad \epsilon > 0$$

3) If $x_1 < x_2$, then $F_X(x_1) \leq F_X(x_2)$, i.e., $F_X(x)$ is a non-decreasing function of x and

$$\mathsf{P}(\{x_1 < X \leq x_2\}) = F_X(x_2) - F_X(x_1) \geq 0$$

4) The *probability density function* (pdf) is defined as

$$f_X(x) = \frac{dF_X(x)}{dx}$$

and, if it exists, has the property $f_X(x) \geq 0$. To find $F_X(x)$, we can integrate $f_X(x)$,

$$\mathsf{P}(\{X \leq x\}) = F_X(x) = \int_{-\infty}^{x} f_X(u)du$$

and because $F_X(\infty) = 1$, we have

$$\int_{-\infty}^{\infty} f_X(x)dx = 1.$$

Further, we have

$$\mathsf{P}(\{x_1 < X \leq x_2\}) = F_X(x_2) - F_X(x_1) = \int_{x_1}^{x_2} f_X(x)dx.$$

5) For a continuous variable X, $\mathsf{P}(\{x_1 < X < x_2\}) = \mathsf{P}(\{x_1 < X \leq x_2\})$ because

$$\mathsf{P}(\{x\}) = \mathsf{P}((-\infty, x]) - \mathsf{P}((-\infty, x)) = F_X(x) - F_X(x-0) = 0$$

In the following, some examples of probability distribution functions of continuous random variables are given.

Example 6.1.1 *Uniform Distribution: A random variable X is said to be uniformly distributed on $[a, b)$ if it admits the probability density function*

$$f_X(x) = \frac{1}{b-a}\left[u(x-a) - u(x-b)\right], \quad a < b$$

where $u(x)$ is the unit step function, given by

$$u(x) = \begin{cases} 1, & x \geq 0 \\ 0, & x < 0. \end{cases}$$

Note that for this relation we often use the short notation $X \sim \mathcal{U}[a, b)$. The corresponding probability distribution function is given by

$$F_X(x) = \int_{-\infty}^{x} f_X(u)du = \frac{1}{b-a}\left[(x-a)u(x-a) - (x-b)u(x-b)\right]$$

Both, the probability distribution function $F_X(x)$ and the probability density function $f_X(x)$ of the uniform distribution are displayed in Figure 6.1.

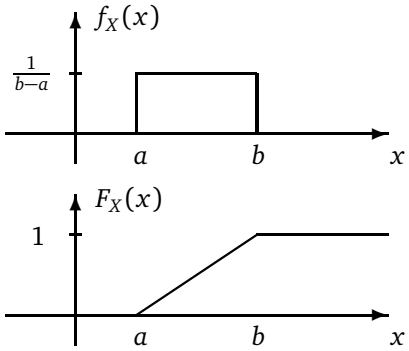

Figure 6.1.: Probability density and distribution function of the uniform distribution.

Example 6.1.2 *Normal Distribution: A random variable X is normally, or Gaussian, distributed with mean μ and variance σ^2, if*

$$f_X(x) = \frac{1}{\sigma\sqrt{2\pi}} \exp\left\{-\frac{(x-\mu)^2}{2\sigma^2}\right\}, \quad \sigma > 0, \quad -\infty < \mu < \infty$$

Note that for this relation we often use the short notation $X \sim \mathcal{N}(\mu, \sigma^2)$. The probability density function of a normal random variable is displayed in Figure 6.2 for various μ and σ.

A closed-form expression for the normal distribution function $F_X(x)$ does not exist. For $\mu = 0$ and $\sigma^2 = 1$, X is said to be standard normally distributed, and its distribution function is denoted by $\Phi_X(x)$, i.e., we have

$$F_X(x) = \Phi_X\left(\frac{x-\mu}{\sigma}\right)$$

Often we define the following as the error-function $\mathrm{erf}(x) = \Phi_X(x) - 0.5$, though there are other definitions in the literature. Numerical values for $\mathrm{erf}(x)$ are given in Table 6.1.

$$\mathrm{erf}(x) = \frac{1}{\sqrt{2\pi}} \int_0^x \exp\left\{-u^2/2\right\} du = \Phi_X(x) - \frac{1}{2}$$

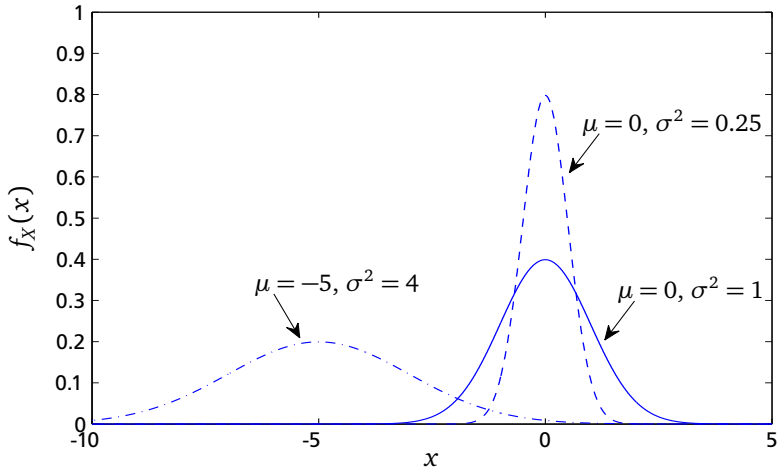

Figure 6.2.: Probability density function of a normal distribution for various μ and σ values.

Say for instance, a random variable is given by $X \sim \mathcal{N}(1000, 50^2)$ and we are interested in the probability that X is between 900 and 1050. Clearly, we have

$$P(\{900 < X \leq 1050\}) = F_X(1050) - F_X(900) = \Phi_X\left(\frac{1050-1000}{50}\right) - \Phi_X\left(\frac{900-1000}{50}\right)$$

Using the numerical values of $\mathrm{erf}(x)$ *from Table 6.1 and the relation $\Phi_X(-x) = 1 - \Phi_X(x)$, we conclude that*

$$P(\{900 < X \leq 1050\}) = \Phi_X(1) + \Phi_X(2) - 1 = 0.819.$$

Example 6.1.3 *Exponential Distribution: A random variable X is said to be exponentially distributed with parameter λ, if it admits the probability density function*

$$f_X(x) = \lambda \exp\{-\lambda x\}\, u(x), \quad \lambda > 0$$

and distribution function

$$F_X(x) = (1 - \exp\{-\lambda x\})\, u(x)\,.$$

The exponential distribution is useful in many engineering applications, e.g., to describe the life-time X of electronic devices such as a transistor. The breakdown rate of a transistor can be defined by

$$\lim_{\Delta \to 0} \frac{1}{\Delta} \frac{\mathsf{P}\{x < X \leq x + \Delta\}}{\mathsf{P}\{x < X\}}, \quad \Delta > 0\,,$$

and is given by

$$\frac{f_X(x)}{1 - F_X(x)} = \lambda$$

Example 6.1.4 *Chi-Square Distribution: Let Y_k, $k = 1, \ldots, \nu$ be independent and standard normally distributed random variables, i.e. $Y_k \sim \mathcal{N}(0,1)$. Then the random variable $X = Y_1^2 + Y_2^2 + \ldots + Y_\nu^2$ is χ^2 distributed with ν degrees of freedom. The probability density function of a χ^2 random variable is displayed in Figure 6.3 for various ν values.*

The probability density function is given by

$$f_X(x) = \frac{x^{\nu/2-1}}{2^{\nu/2}\Gamma(\nu/2)} e^{-x/2} u(x)\,,$$

where $\Gamma(x)$ is the gamma function,

$$\Gamma(x) = \int_0^\infty \xi^{x-1} e^{-\xi} d\xi\,.$$

For later reference, the mean of X is $\mu_X = \nu$, and the variance is $\sigma_X^2 = 2\nu$.

Table 6.1.: Numerical values for $\mathrm{erf}(x)$ function.

x	$\mathrm{erf}(x)$	x	$\mathrm{erf}(x)$	x	$\mathrm{erf}(x)$	x	$\mathrm{erf}(x)$
0.05	0.01994	0.80	0.28814	1.55	0.43943	2.30	0.48928
0.10	0.03983	0.85	0.30234	1.60	0.44520	2.35	0.49061
0.15	0.05962	0.90	0.31594	1.65	0.45053	2.40	0.49180
0.20	0.07926	0.95	0.32894	1.70	0.45543	2.45	0.49286
0.25	0.09871	1.00	0.34134	1.75	0.45994	2.50	0.49379
0.30	0.11791	1.05	0.35314	1.80	0.46407	2.55	0.49461
0.35	0.13683	1.10	0.36433	1.85	0.46784	2.60	0.49534
0.40	0.15542	1.15	0.37493	1.90	0.47128	2.65	0.49597
0.45	0.17364	1.20	0.38493	1.95	0.47441	2.70	0.49653
0.50	0.19146	1.25	0.39495	2.00	0.47726	2.75	0.49702
0.55	0.20884	1.30	0.40320	2.05	0.47982	2.80	0.49744
0.60	0.22575	1.35	0.41149	2.10	0.48214	2.85	0.49781
0.65	0.24215	1.40	0.41924	2.15	0.48422	2.90	0.48813
0.70	0.25804	1.45	0.42647	2.20	0.48610	2.95	0.49841
0.75	0.27337	1.50	0.43319	2.25	0.48778	3.00	0.49865

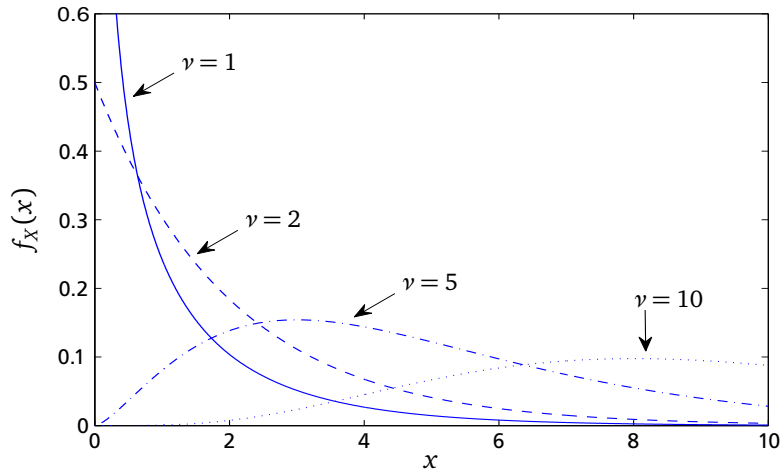

Figure 6.3.: Probability density function of a χ^2_ν distribution with $\nu = 1, 2, 5$ and 10.

Multiple Random Variables

The probability of two events $A = \{X_1 \leq x_1\}$ and $B = \{X_2 \leq x_2\}$ has already been defined as a function of x_1 and y_1, respectively called probability distribution functions

$$\begin{aligned} F_{X_1}(x_1) &= \mathsf{P}(\{X_1 \leq x_1\}) \\ F_{X_2}(x_2) &= \mathsf{P}(\{X_2 \leq x_2\}) \end{aligned}$$

We must introduce a new concept for the probability of the joint event $\{X_1 \leq x_1, X_2 \leq x_2\} = \{(X_1, X_2) \in D\}$, where x_1 and x_2 are two arbitrary real numbers and D is the quadrant shown in Figure 6.4.

The joint distribution $F_{X_1X_2}(x_1, x_2)$ of two random variables X_1 and X_2 is the probability of the joint event $\{X_1 \leq x_1, X_2 \leq x_2\}$,

$$F_{X_1X_2}(x_1, x_2) = \mathsf{P}(\{X_1 \leq x_1, X_2 \leq x_2\}).$$

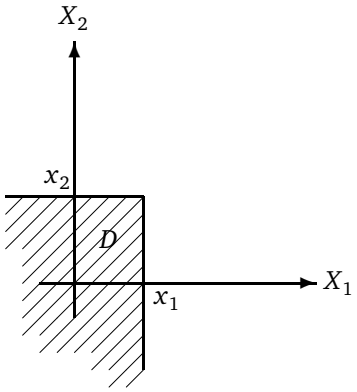

Figure 6.4.: The quadrant D of two arbitrary real numbers x and y.

The concept of joint distribution functions of random variables can be extended to the order n. Assume n random variables $X_1,\ldots,X_n$. The joint distribution function is the probability of the joint event $\{X_1 \leq x_1,\ldots,X_n \leq x_n\}$, and is denoted by

$$F_{X_1\ldots X_n}(x_1,\ldots,x_n) = \mathsf{P}(\{X_1 \leq x_1,\ldots,X_n \leq x_n\})$$

For now, we want to focus on the joint distribution of two random variables, i.e. $n = 2$, which are the so-called bivariate random variables. For a comprehensive treatment of the joint distribution of n random variables, we refer to the literature.

Bivariate distributions

The bivariate probability distribution function $F_{X_1X_2}(x_1,x_2)$ has the following properties:

1) $F_{X_1X_2}(x_1,x_2)$ is bounded between 0 and 1, especially

$$\begin{aligned} \lim_{x_1\to\infty,x_2\to\infty} F_{X_1X_2}(x_1,x_2) &= 1 \\ \lim_{x_1\to-\infty} F_{X_1X_2}(x_1,x_2) = \lim_{x_2\to-\infty} F_{X_1X_2}(x_1,x_2) &= 0 \end{aligned}$$

which holds true since $\{X_1 = -\infty, X_2 \leq x_2\} \subset \{X_1 = -\infty\}$ and $\{X_1 \leq x_1, X_2 = -\infty\} \subset \{X_2 = -\infty\}$.

2) $F_{X_1X_2}(x_1,x_2)$ is continuous from the right in each component when the other component is fixed, i.e.

$$\lim_{\epsilon\to 0} F_{X_1X_2}(x_1+\epsilon,x_2) = \lim_{\epsilon\to 0} F_{X_1X_2}(x_1,x_2+\epsilon) = F_{X_1X_2}(x_1,x_2), \quad \epsilon > 0$$

3) The event $\{x_{11} < X_1 \leq x_{12}, X_2 \leq x_2\}$ consists of all points (X_1,X_2) in the vertical half-strip D_1, as shown in Figure 6.5. Similarly, the event $\{X_1 \leq x_1, x_{21} < X_2 \leq x_{22}\}$ consists of all points (X_1,X_2) in the horizontal half-strip D_2, as shown in Figure 6.5. Thus, we have

$$\begin{aligned} \mathsf{P}(\{x_{11} < X_1 \leq x_{12}, X_2 \leq x_2\}) &= F_{X_1X_2}(x_{12},x_2) - F_{X_1X_2}(x_{11},x_2) \\ \mathsf{P}(\{X_1 < x_1, x_{21} < X_2 \leq x_{22}\}) &= F_{X_1X_2}(x_1,x_{22}) - F_{X_1X_2}(x_1,x_{21}) \end{aligned}$$

4) The event $\{x_{11} < X_1 \leq x_{12}, x_{21} < X_2 \leq x_{22}\}$ consists of all points (X_1,X_2) in the rectangle D_3, as indicated in Figure 6.6. Therefore we have,

$$\begin{aligned} &\mathsf{P}(\{x_{11} < X_1 \leq x_{12}, x_{21} < X_2 \leq x_{22}\}) = \\ &\quad F_{X_1X_2}(x_{12},x_{22}) - F_{X_1X_2}(x_{11},x_{22}) - F_{X_1X_2}(x_{12},x_{21}) + F_{X_1X_2}(x_{11},x_{21}) > 0 \end{aligned}$$

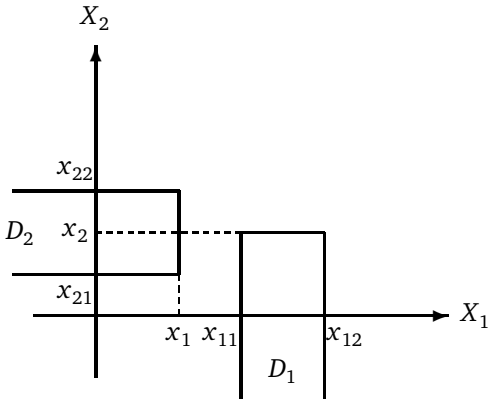

Figure 6.5.: Two half-strips D_1 and D_2 of a bivariate random variable (X_1, X_2).

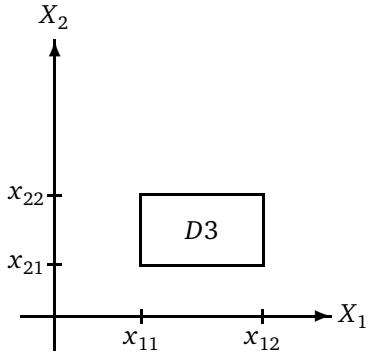

Figure 6.6.: Rectangle D_3 of a bivariate random variable (X_1, X_2).

5) The joint probability density function of X_1 and X_2 is defined as

$$f_{X_1X_2}(x_1, x_2) = \frac{\partial^2 F_{X_1X_2}(x_1, x_2)}{\partial x_1 \, \partial x_2}$$

and if it exists has the property $f_{X_1X_2}(x_1, x_2) \geq 0$. To find $F_{X_1X_2}(x_1, x_2)$, we can integrate $f_{X_1X_2}(x_1, x_2)$,

$$F_{X_1X_2}(x_1, x_2) = \int_{-\infty}^{x_1} \int_{-\infty}^{x_2} f_{X_1X_2}(u_1, u_2) du_1 du_2$$

and because $F_{X_1X_2}(\infty, \infty) = 1$, we have

$$\int_{-\infty}^{\infty} \int_{-\infty}^{\infty} f_{X_1X_2}(x_1, x_2) dx_1 dx_2 = 1.$$

The probability of the event $\{x_{11} < X_1 \leq x_{12}, x_{21} < X_2 \leq x_{22}\}$, i.e. are all points in the rectangle D_3 in Figure 6.6, can be also calculated using

$$\mathsf{P}(\{x_{11} < X_1 \leq x_{12}, x_{21} < X_2 \leq x_{22}\}) = \int_{x_{11}}^{x_{12}} \int_{x_{21}}^{x_{22}} f_{X_1X_2}(x_1, x_2) dx_1 dx_2.$$

6) In the study of multiple random variables, the statistics of each component are called *marginal statistics*. The marginal probability distribution functions can be expressed in terms of the joint probability distribution function

$$\begin{aligned} F_{X_1}(x_1) &= \lim_{x_2 \to \infty} F_{X_1X_2}(x_1, x_2) \\ F_{X_2}(x_2) &= \lim_{x_1 \to \infty} F_{X_1X_2}(x_1, x_2). \end{aligned}$$

Similarly, the marginal probability density function can be expressed in terms of the joint probability density functions,

$$f_{X_1}(x_1) = \int_{-\infty}^{\infty} f_{X_1X_2}(x_1, x_2)dx_2 \quad \text{and} \quad f_{X_2}(x_2) = \int_{-\infty}^{\infty} f_{X_1X_2}(x_1, x_2)dx_1.$$

Example 6.1.5 *The bivariate normal distribution: A bivariate random variable (X_1, X_2) is bivariate normal distributed if the bivariate probability density function is*

$$f_{X_1X_1}(x_1, x_2) = \frac{1}{2\pi\sigma_{X_1}\sigma_{X_2}\sqrt{1-\rho^2}} \times \exp\left\{-\frac{1}{2(1-\rho^2)}\left[\left(\frac{x_1-\mu_{X_1}}{\sigma_{X_1}}\right)^2 - 2\rho\frac{(x_1-\mu_{X_1})(x_2-\mu_{X_2})}{\sigma_{X_1}\sigma_{X_2}} + \left(\frac{x_2-\mu_{X_2}}{\sigma_{X_2}}\right)^2\right]\right\}$$

where μ_{X_1} and μ_{X_2} are respectively the means of X_1 and X_2, $\sigma^2_{X_1} > 0$ and $\sigma^2_{X_2} > 0$ the corresponding variances. Parameter ρ is the correlation coefficient and satisfies $-1 < \rho < 1$. The marginal distributions are $\mathcal{N}(\mu_{X_1}, \sigma^2_{X_1})$ and $\mathcal{N}(\mu_{X_2}, \sigma^2_{X_2})$. If X_1 and X_2 are independent then $\rho = 0$, and clearly $f_{X_1X_2}(x_1, x_2) = f_{X_1}(x_1)f_{X_2}(x_2)$.

6.2 Operations on Random Variables

The concept of a random variable was previously introduced as a means of providing a symmetric definition of events defined on a sample space. It formed a mathematical model for describing characteristics of some real-world random variables, which are mostly based on a single concept – expectation.

Expectation

The mathematical expectation of a random variable X, denoted $\mathsf{E}[X]$, may be read "the expected value of X" or "the mean value of X" is defined as

$$\mathsf{E}[X] = \int_{-\infty}^{\infty} x \cdot f_X(x)dx$$

where $f_X(x)$ is the probability density function of X. If X happens to be discrete, then we have a probability mass function, however, this will not be treated in the manuscript.

Example 6.2.1 *Mean of a uniform distribution: If X is uniformly distributed on the interval $[a, b)$, then*

$$f_X(x) = \frac{1}{b-a}[u(x-a) - u(x-b)], \quad a < b,$$

and the mean is obtained simply by

$$\begin{aligned} \mathsf{E}[X] &= \frac{1}{b-a}\int_a^b x dx \\ &= \frac{1}{b-a}\frac{b^2-a^2}{2} \\ &= \frac{1}{b-a}\frac{(b+a)(b-a)}{2} \\ &= \frac{a+b}{2}, \end{aligned}$$

which can be verified graphically, e.g. see Figure 6.1.

Example 6.2.2 *Mean of a normal distribution: If $X \sim \mathcal{N}(\mu, \sigma^2)$, then*

$$f_X(x) = \frac{1}{\sigma\sqrt{2\pi}} \cdot \exp\left\{-\frac{(x-\mu)^2}{2\sigma^2}\right\},$$

and the mean is obtained by using integration over changed variable $u = (x-\mu)/\sigma$:

$$\begin{aligned}
\mathsf{E}[X] &= \frac{1}{\sigma\sqrt{2\pi}} \int_{-\infty}^{\infty} x \cdot \exp\left\{-\frac{(x-\mu)^2}{2\sigma^2}\right\} dx \\
&= \frac{1}{\sigma\sqrt{2\pi}} \int_{-\infty}^{\infty} (\sigma u + \mu) \cdot \exp\left\{-u^2/2\right\} \sigma\, du \\
&= \frac{1}{\sqrt{2\pi}} \left[\sigma \int_{-\infty}^{\infty} u \cdot \exp\left\{-u^2/2\right\} du + \mu \int_{-\infty}^{\infty} \exp\left\{-u^2/2\right\} du\right] \\
&= \frac{1}{\sqrt{2\pi}} \left[\sigma \cdot 0 + \mu\sqrt{2\pi}\right] = \mu\,.
\end{aligned}$$

Example 6.2.3 *Mean of an exponential distribution: If X is exponentially distributed, then*

$$f_X(x) = \lambda \exp\{-\lambda x\}\, u(x)\,,$$

and the mean can be obtained using integration by parts:

$$\begin{aligned}
\mathsf{E}[X] &= \int_0^{\infty} x \cdot \lambda \exp\{-\lambda x\}\, dx \\
&= -x \cdot \exp\{-\lambda x\}\big|_0^{\infty} - \int_0^{\infty} (-\exp\{-\lambda x\})\, dx \\
&= -\frac{1}{\lambda} \exp\{-\lambda x\}\big|_0^{\infty} = -\left(0 - \frac{1}{\lambda}\right) = \frac{1}{\lambda}
\end{aligned}$$

Note that, as in the case of Examples 6.2.1 and 6.2.2, if a random variable's density is symmetrical about a line $x = a$, then $\mathsf{E}[X] = a$, i.e.

$$\mathsf{E}[X] = a, \quad \text{if } f_X(x+a) = f_X(-x+a)$$

Expected Value of a Function of Random Variables

Suppose that we are interested in the mean of the random variable $Y = g(X)$

$$\mathsf{E}[Y] = \int_{-\infty}^{\infty} y \cdot f_Y(y) dy$$

and we are given $f_X(x)$. Then,

$$\mathsf{E}[Y] = \mathsf{E}[g(X)] = \int_{-\infty}^{\infty} g(x) \cdot f_X(x) dx$$

Note that it is not necessary to calculate the density $f_Y(y)$ explicitly to determine $\mathsf{E}[Y]$.

Example 6.2.4 *The average power in a 1 Ω resistor can be found as*

$$\mathsf{E}[V^2] = \int_{-\infty}^{\infty} v^2 \cdot f_V(v) dv$$

where V and $f_V(v)$ are respectively the random voltage and its probability density function.

In particular, if we apply the transformation $g(\cdot)$ to the random variable X, defined as

$$g(X) = X^n, \quad n = 0, 1, 2, \ldots,$$

the expectation of $g(X)$ is known as the nth order moment of X and denoted by μ_n:

$$\mu_n = \mathsf{E}[X^n] = \int_{-\infty}^{\infty} x^n \cdot f_X(x) dx\,.$$

Sometimes, it is also of importance to use central moments of X around the mean. These are defined as

$$\mu_n' = \mathsf{E}[(X - \mathsf{E}[X])^n] = \int_{-\infty}^{\infty} (x - \mathsf{E}[X])^n \cdot f_X(x) dx\,, \quad n = 0, 1, 2 \ldots$$

Clearly the first order central moment is zero.

The Variance

The variance of a random variable X is by definition

$$\sigma^2 = \int_{-\infty}^{\infty} (x - \mathsf{E}[X])^2 \cdot f_X(x) dx.$$

Note that this is equivalent with the second order central moment μ_2', which has been defined above. The positive constant σ, is called the standard deviation of X. From the definition it follows that σ^2 is the mean of the random variable $(X - \mathsf{E}[X])^2$. Thus,

$$\begin{aligned}
\sigma^2 &= \mathsf{E}[(X - \mathsf{E}[X])^2] = \mathsf{E}[X^2 - 2X \cdot (\mathsf{E}[X]) + (\mathsf{E}[X])^2] \\
&= \mathsf{E}[X^2] - 2\mathsf{E}[X\mathsf{E}[X]] + (\mathsf{E}[X])^2 \\
&= \mathsf{E}[X^2] - 2(\mathsf{E}[X])^2 + (\mathsf{E}[X])^2 \\
&= \mathsf{E}[X^2] - (\mathsf{E}[X])^2 \\
&= \mathsf{E}[X^2] - \mu_1^2
\end{aligned}$$

Example 6.2.5 *The variance of a uniform distribution: similarly to Example 6.2.1, and using the definition of the variance, we first determine*

$$\begin{aligned}
\mathsf{E}[X^2] &= \frac{1}{b-a} \int_a^b x^2 dx \\
&= \frac{1}{b-a} \frac{b^3 - a^3}{3} \\
&= \frac{1}{b-a} \frac{(b-a)(b+a)^2}{3} = \frac{(a+b)^2}{3}
\end{aligned}$$

The variance of a uniform random variable is then given by

$$\mathsf{E}[(X - \mathsf{E}[X])^2] = \mathsf{E}[X^2] - (\mathsf{E}[X])^2 = \frac{(a+b)^2}{3} - \frac{(a+b)^2}{4} = \frac{(a+b)^2}{12}$$

Example 6.2.6 *The variance of a normal distribution: we can determine the variance of a normal random variable by considering*

$$\int_{-\infty}^{\infty} \exp\left\{-\frac{1}{2}\frac{(x-\mu)^2}{\sigma^2}\right\} dx = \sigma\sqrt{2\pi}$$

Differentiating with respect to σ, we obtain

$$\int_{-\infty}^{\infty} \frac{(x-\mu)^2}{\sigma^3} \exp\left\{-\frac{1}{2}\frac{(x-\mu)^2}{\sigma^2}\right\} dx = \sqrt{2\pi}$$

Multiplying both sides by $\sigma^2/\sqrt{2\pi}$, we conclude that

$$\mathsf{E}[(X-\mu)^2] = \mathsf{E}[(X - \mathsf{E}[X])^2] = \sigma^2.$$

Example 6.2.7 *The variance of an exponential distribution: similarly to Example 6.2.3, and using the definition of the variance, we first determine*

$$\begin{aligned} \mathsf{E}[X^2] &= \int_0^\infty x^2 \cdot \lambda \exp\{-\lambda x\}\, dx \\ &= -x^2 \cdot \exp\{-\lambda x\}\big|_0^\infty + 2\int_0^\infty x \cdot \exp\{-\lambda x\}\, dx \\ &= \frac{2}{\lambda}\mathsf{E}[X] = \frac{2}{\lambda^2} \end{aligned}$$

The variance of an exponential random variable is then given by

$$\mathsf{E}[(X-\mu)^2] = \mathsf{E}[X^2] - (\mathsf{E}[X])^2 = \frac{2}{\lambda^2} - \frac{1}{\lambda^2} = \frac{1}{\lambda^2}$$

Transformation of a Random Variable

In practice, one may wish to transform one random variable X into a new random variable Y by means of a transformation

$$Y = g(X),$$

where the probability density function $f_X(x)$ or distribution function $F_X(x)$ of X is known. The problem is to find the probability density function of $f_Y(y)$ or distribution function $F_Y(y)$ of Y. Let us assume that $g(\cdot)$ is continuous and differentiable at all values of x for which $f_X(x) \neq 0$. Furthermore, we assume that $g(\cdot)$ is monotone for which the inverse $g^{-1}(\cdot)$ exists. Then:

$$F_Y(y) = \mathsf{P}(\{Y \leq y\}) = \mathsf{P}(\{g(X) \leq y\}) = \mathsf{P}\left(\{X \leq g^{-1}(y)\}\right) = \int_{-\infty}^{g^{-1}(y)} f_X(x)dx$$

holds. The density function of $Y = g(X)$ is obtained via differentiation which leads to

$$f_Y(y) = f_X\left(g^{-1}(y)\right) \cdot \left|\frac{dg^{-1}(y)}{dy}\right|$$

Example 6.2.8 *The cumulative distribution function and probability density function of a linearly transformed random variable: Let*

$$Y = aX + b.$$

To find the probability density function of Y knowing $F_X(x)$ or $f_X(x)$, we calculate

$$\begin{aligned} F_Y(y) &= \mathsf{P}(\{Y \leq y\}) = \mathsf{P}(\{aX + b \leq y\}) \\ &= P\left(\left\{X \leq \frac{y-b}{a}\right\}\right),\ a > 0 \\ &= F_X\left(\frac{y-b}{a}\right), \end{aligned}$$

and

$$F_Y(y) = 1 - F_X\left(\frac{y-b}{a}\right),\ a < 0$$

By differentiating $F_Y(y)$, we obtain the probability density function

$$f_Y(y) = \frac{1}{|a|} \cdot f_X\left(\frac{y-b}{a}\right)$$

Example 6.2.9 *The cumulative distribution function and probability density function of a squared random variable: Let*

$$Y = X^2$$

To find the probability density function of Y knowing $F_X(x)$ or $f_X(x)$, we calculate

$$F_Y(y) = \mathsf{P}\big(\{X^2 \le y\}\big) = \begin{cases} 0, & y < 0 \\ \mathsf{P}(\{-\sqrt{y} \le X \le \sqrt{y}\}), & y \ge 0 \end{cases}$$

which yields

$$F_Y(y) = F_X(\sqrt{y}) - F_X(-\sqrt{y})$$

By differentiating $F_Y(y)$, we obtain the probability density function

$$f_Y(y) = \begin{cases} 0, & y < 0 \\ \dfrac{f_X(\sqrt{y}) + f_X(-\sqrt{y})}{2\sqrt{y}}, & y > 0 \end{cases}$$

$F_Y(y)$ is non-differentiable at $y = 0$. We may choose arbitrarily $f_Y(y) = 0$ at $y = 0$.

6.3 The Covariance

The covariance describes the relation or dependence between two random variables. If the statistical properties of the two random variables X_1 and X_2 are described by their joint probability density function $f_{X_1X_2}(x_1, x_2)$, then we have

$$\mathsf{E}[g(X_1, X_2)] = \int_{-\infty}^{\infty}\int_{-\infty}^{\infty} g(x_1, x_2) \cdot f_{X_1X_2}(x_1, x_2) dx_1 dx_2$$

For $g(X_1, X_2) = X_1^n X_2^k$

$$\mu_{nk} = \mathsf{E}\big[X_1^n X_2^k\big] = \int_{-\infty}^{\infty}\int_{-\infty}^{\infty} x_1^n x_2^k f_{X_1X_2}(x_1, x_2) dx_1\, dx_2, \quad n, k = 0, 1, 2, \ldots$$

are called the joint moments of X_1 and X_2. Clearly $\mu_{0k} = \mathsf{E}[X_2^k]$, while $\mu_{n0} = \mathsf{E}[X_1^n]$. The second order moment $\mathsf{E}[X_1X_2]$ of X_1 and X_2 is denoted by $r_{X_1X_2}$,

$$r_{X_1X_2} = \mathsf{E}[X_1X_2] = \int_{-\infty}^{\infty}\int_{-\infty}^{\infty} x_1 x_2 f_{X_1X_2}(x_1, x_2) dx_1 dx_2$$

Note that in the engineering literature $r_{X_1X_2}$ is often called correlation. We reserve this term to describe the normalized covariance as it is common in the statistical literature.

If $r_{X_1X_2} = \mathsf{E}[X_1X_2] = \mathsf{E}[X_1] \cdot \mathsf{E}[X_2]$, then X_1 and X_2 are uncorrelated. If $r_{X_1X_2} = 0$, then X_1 and X_2 are orthogonal. Furthermore, the joint central moments are defined by

$$\begin{aligned} \mu'_{nk} &= \mathsf{E}\big[(X_1 - \mathsf{E}[X_1])^n (X_2 - \mathsf{E}[X_2])^k)\big] \\ &= \int_{-\infty}^{\infty}\int_{-\infty}^{\infty} (x_1 - \mathsf{E}[X_1])^n (x_2 - \mathsf{E}[X_2])^k f_{X_1X_2}(x_1, x_2) dx_1 dx_2,\ n, k = 0, 1, 2, \ldots \end{aligned}$$

The second order central moments $\mu'_{20} = \sigma^2_{X_1}$ and $\mu'_{02} = \sigma^2_{X_2}$ are the variances of X_1 and X_2, respectively. The joint central moment μ'_{11} is called covariance of X_1 and X_2 and denoted by $c_{X_1X_2}$

$$\begin{aligned} c_{X_1X_2} &= \mathsf{E}[(X_1 - \mathsf{E}[X_1])(X_2 - \mathsf{E}[X_2])] \\ &= \int_{-\infty}^{\infty}\int_{-\infty}^{\infty} (x_1 - \mathsf{E}[X_1])(x_2 - \mathsf{E}[X_2]) \cdot f_{X_1X_2}(x_1, x_2) dx_1 dx_2 \end{aligned}$$

Clearly

$$c_{X_1X_2} = r_{X_1X_2} - \mathsf{E}[X_1]\mathsf{E}[X_2].$$

If two random variables are independent, i.e. $f_{X_1X_2}(x_1, x_2) = f_{X_1}(x_1)f_{X_2}(x_2)$, they are also uncorrelated and we have $c_{X_1X_2} = 0$. The converse however is not always true, except for the Gaussian case. The normalized second order moment

$$\rho = \frac{\mu'_{11}}{\sqrt{\mu'_{20}\mu'_{02}}} = \frac{c_{X_1X_2}}{\sigma_{X_1}\sigma_{X_2}}$$

is known as the correlation coefficient of X_1 and X_2. It can be shown that

$$-1 \leq \rho \leq 1$$

In the following example, we will show that two uncorrelated random variables are not necessarily independent.

Example 6.3.1 *Say U is uniformly distributed on $[-\pi, \pi)$. Random variables X_1 and X_2 are given by*

$$X_1 = \cos(U) \quad \text{and} \quad X_2 = \sin(U)$$

Since $X_1^2 + X_2^2 = 1$, variables X_1 and X_2 are not independent. Furthermore,

$$\begin{aligned} c_{X_1X_2} &= \mathsf{E}\left[(X_1 - \mathsf{E}[X_1])(X_2 - \mathsf{E}[X_2])\right] \\ &= \mathsf{E}[X_1X_2] = \mathsf{E}[\cos(U)\sin(U)] \\ &= \tfrac{1}{2}\mathsf{E}[\sin(2U)] = 0. \end{aligned}$$

Thus X_1 and X_2 are uncorrelated but not independent.

Example 6.3.2 *Let X_i, $i = 1, \ldots, N$ be random variables and α_i, $i = 1, \ldots, N$ be scalar values. We calculate the mean and the variance of*

$$Y = \sum_{i=1}^{N} \alpha_i X_i$$

given the means and variances (and covariances) of X_i.

$$\mathsf{E}[Y] = \sum_{i=1}^{N} \alpha_i \mathsf{E}[X_i]$$

$$\sigma_Y^2 = \mathsf{E}\left[(Y - \mathsf{E}[Y])^2\right] = \sum_{i=1}^{N}\sum_{j=1}^{N} \alpha_i\alpha_j c_{X_iX_j}$$

For the special case $c_{X_iX_j} = 0$, $i \neq j$

$$\sigma_Y^2 = \sum_{i=1}^{N} \alpha_i^2 \sigma_{X_i}^2.$$

6.4 Stochastic Processes

In contrast to random variables, random processes describe signals with random properties. Generally, random processes cannot be reliably predicted after a finite observation time. Therefore, we try to find models which describe a class of possible outcomes rather than the signals observed at the moment.

Stochastic processes, or *random processes*, naturally arise in many engineering applications. For example, the voltage waveform of a noise source is a continuous-time random process. The monthly rainfall or the daily stock market index are examples of discrete-time random processes. However, random sequences are most commonly encountered when sampling continuous-time processes, as discussed in the preceding chapter. The remainder of the manuscript focuses solely on discrete-time random processes. However the results presented herein apply in a similar fashion to the continuous-time case.

Definition 6.4.1 *A real random process is an indexed set of real functions of time that has certain statistical properties. We characterize a real random process by a set of real functions and associated probability description.*

We denote a random process by $X(n) = X(n,\zeta)$, $n \in \mathbb{Z}$, $\zeta \in \mathscr{S}$, where n is a discrete-time index and ζ is an event from the set of possible outcomes $\mathscr{S}$. We consider two special cases when either the event or time is fixed:

- When the event is fixed, $\zeta_i \in \mathscr{S}$, this results in a realization or so-called sample function, and is denoted by $x_i(n) = X(n,\zeta_i), n \in \mathbb{Z}$. One can think of the waveform that is obtained when the event ζ_i of the process occurs. The set of all possible waveforms is also called the *ensemble* of a random process.
- When the time is fixed, $n_j \in \mathbb{Z}$, we have $X_j = X(n_j) = X(n_j,\zeta)$ with $\zeta \in \mathscr{S}$, which is simply a random variable, and has been described in Section 6.1.

Exemplarily, we show in Figure 6.7 the ensemble of a random process $X(n) = X(n,\zeta)$. When the event $\zeta = \zeta_i$ is fixed, we have a sample function (realization) $x_i(n)$. Also illustrated by the vertical dashed lines is the case when the time $n = n_j$ is fixed and we simply have a random variable X_j.

Without loss of generality, we restrict ourselves to time indexes n_1 to n_N. To describe the random processes, we define the joint cumulative distribution function (cdf)

$$\begin{aligned} F_X(x_1,\ldots,x_N;n_1,\ldots,n_N) &= F_{X(n_1),\ldots,X(n_N)}(x_1,\ldots,x_N) \\ &= \mathsf{P}(\{X(n_1)\le x_1,\ldots,X(n_N)\le x_N\}). \end{aligned}$$

We assume that the following derivative of the cdf exists, and we define the joint probability density function (pdf) as

$$f_X(x_1,\ldots,x_N;n_1,\ldots,n_N) = \frac{\partial^N F_X(x_1,\ldots,x_N;n_1,\ldots,n_N)}{\partial x_1 \ldots \partial x_N}.$$

The defined joint cdf or pdf describe a random process completely. However, their practical application is only feasible in special cases. Therefore, it is common to assume an identical distribution $f_X(x;n)$ for all time indexes of interest $n_1,\ldots,n_N$ and thus, to describe random processes with their moments. Similarly to the definitions for random variables, the mean of process $X(n)$ is given by

$$\mu(n) = \mathsf{E}[X(n)] = \int_{-\infty}^{\infty} x \cdot f_X(x;n)dx$$

and the variance by

$$\sigma^2(n) = \mathsf{E}[X(n)^2] - \mathsf{E}[X(n)]^2 = \int_{-\infty}^{\infty} x^2 \cdot f_X(x;n)dx - \mu(n)^2.$$

Because in general, $f_X(x;n)$ depends on time index n, the mean and variance of random process $X(n)$ will also depend on time index n. While the mean function describes a deterministic component of a random process, the variance function characterizes the power of the random (or noise) component.

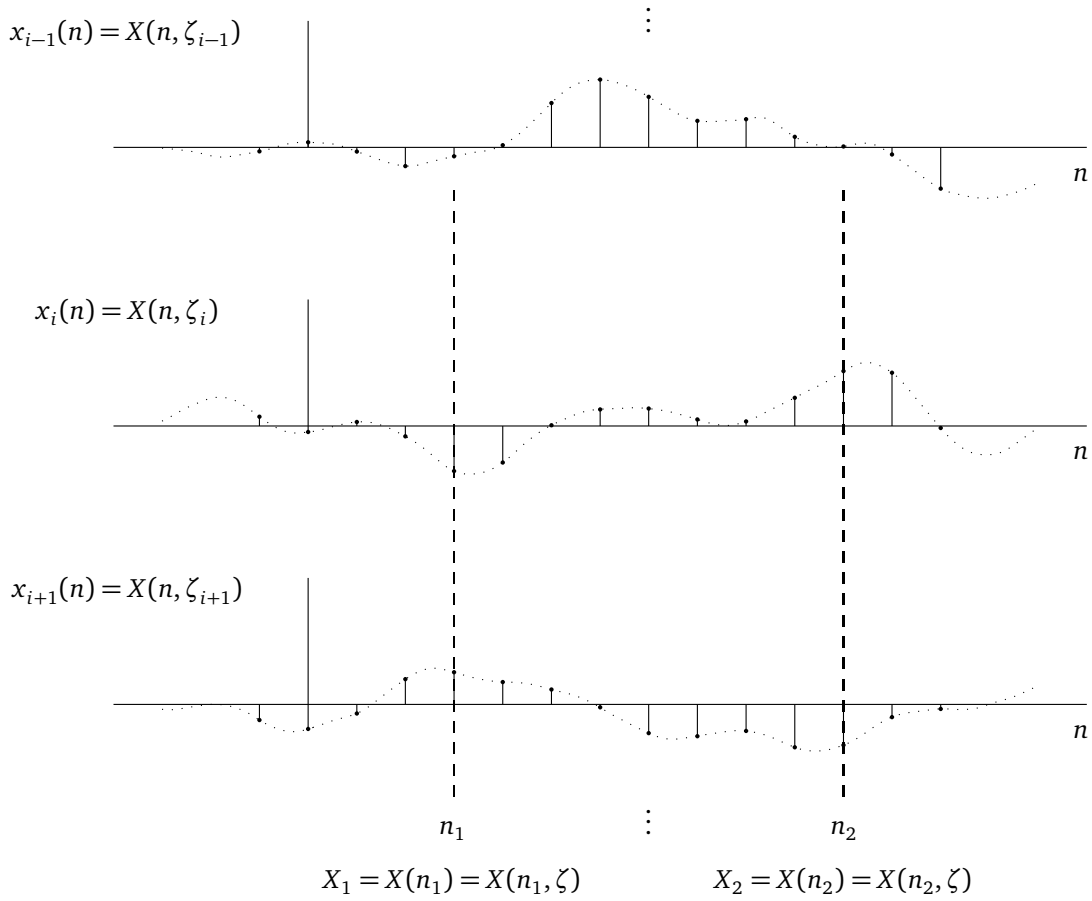

Figure 6.7.: Voltage waveforms emitted from a noise source.

Again, similarly to the definition of the second-order moment and covariance of random variables, we can define the second-order moment function (SOMF) as

$$\begin{aligned} r_{XX}(n_1, n_2) &= \mathsf{E}[X(n_1)X(n_2)] \\ &= \int_{-\infty}^{\infty}\int_{-\infty}^{\infty} x_1 x_2 f_{X_1X_2}(x_1, x_2; n_1, n_2)\, dx_1\, dx_2. \end{aligned}$$

The central SOMF is also called the *covariance function* and is defined by

$$\begin{aligned} c_{XX}(n_1, n_2) &= \mathsf{E}\left[(X(n_1) - E[X(n_1)])(X(n_2) - E[X(n_2)])\right] \\ &= \int_{-\infty}^{\infty}\int_{-\infty}^{\infty} (x_1 - \mu(n_1))(x_2 - \mu(n_2)) f_{X_1X_2}(x_1, x_2; n_1, n_2)\, dx_1\, dx_2. \end{aligned}$$

The covariance function is related to the SOMF by $c_{XX}(n_1, n_2) = r_{XX}(n_1, n_2) - \mu_X(n_1)\mu_X(n_2)$. To better understand the introduced quantities, we point out the analogy with the concept of random variables. For random variables, we have used the second-order moment or the covariance to describe the linear relation (correlation) between two random variables. For random processes, on the other hand, the SOMF and the covariance function are used to describe the linear relation between a random process at times n_1 and n_2.

Stationarity

Definition 6.4.2 *A random process $X(n)$, $n \in \mathbb{Z}$ is said to be stationary to the order N if, for any $n_1, \ldots, n_N$, and $x_1, \ldots, x_N$, and any n_0*

$$F_X(x_1, \ldots, x_N; n_1, \ldots, n_N) = F_X(x_1, \ldots, x_N; n_1 + n_0, \ldots, n_N + n_0)$$

holds, or equivalently

$$f_X(x_1,\ldots,x_N;n_1,\ldots,n_N) = f_X(x_1,\ldots,x_N;n_1+n_0,\ldots,n_N+n_0).$$

The process is said to be strictly stationary if it is stationary to the infinite order. If a process is stationary, it can be shifted in time without changing its statistical description.

Wide-Sense Stationarity

Definition 6.4.3 *A random process is* wide-sense stationary *(WSS) if the first two moments do not depend on the absolute time index n. This means that the two subsequent conditions must be satisfied*

1. $\mathrm{E}[X(n)]$ *is a constant, and*
2. $r_{XX}(n_1,n_2) = r_{XX}(\kappa)$*, where* $\kappa = n_1 - n_2$.

Often we use the notation $n_1 = n+\kappa$ and $n_2 = n$. A WSS process is said to be stationary to the second order.

Example 6.4.1 *Given the stochastic process* $X(n) = A\cos(\omega_0 n + \phi)$ *where* ω_0 *is a fixed frequency, A is a constant amplitude and* ϕ *is a uniformly distributed phase on* $[-\pi,\pi)$*. Is* $X(n)$ *WSS? First we determine the expected value of the random variable at time n*

$$\begin{aligned}\mathrm{E}[X(n)] &= \int_{-\infty}^{\infty} A\cos(\omega_0 n+\varphi) f_\phi(\varphi)\,d\varphi \\ &= \frac{A}{2\pi}\int_{-\pi}^{\pi}\cos(\omega_0 n+\varphi)\,d\varphi = 0.\end{aligned}$$

Then the SOMF is obtained as

$$\begin{aligned}r_{XX}(n_1,n_2) &= \mathrm{E}[X(n_1)X(n_2)] \\ &= \mathrm{E}[A\cos(\omega_0 n_1+\phi)A\cos(\omega_0 n_2+\phi)] \\ &= \frac{A^2}{2}\mathrm{E}[\cos(\omega_0(n_1-n_2)) + \cos(\omega_0(n_1+n_2)+2\phi)] \\ &= \frac{A^2}{2}\mathrm{E}[\cos(\omega_0(n_1-n_2))] = \frac{A^2}{2}\cos(\omega_0(n_1-n_2)).\end{aligned}$$

The expected value is independent of time and the SOMF depends only on the time difference $n_1 - n_2 = \kappa$*. Thus the process is WSS.*

Ergodicity

Ergodicity describes the relationship between statistical averages and time averages. Suppose that, for example, we wish to determine the mean $\mu(n)$ of a process $X(n)$. For this purpose, we observe a large number of samples $X(n,\zeta_i)$, $i = 1,\ldots,L$ and we use their ensemble average as the estimate for $\mu(n) = \mathrm{E}[X(n)]$, i.e.

$$\hat{\mu}(n) = \frac{1}{L}\sum_{i=1}^{L} X(n,\zeta_i)$$

Suppose, however, that we have access only to a single sample $x_i(n) = X(n,\zeta_i)$ of $X(n)$ for $0 \le n \le N-1$, where N is the size of the observation interval. The question arises whether we can use the time average

$$\overline{X(n)} = \lim_{N\to\infty}\frac{1}{N}\sum_{n=0}^{N-1} X(n,\zeta_i)$$

as the estimate for $\mu(n)$? This is, of course, impossible if $\mu(n)$ depends on n. However, if $\mu(n) = \mu$ is a constant, then under the general conditions, $\overline{X(n)}$ approaches μ.

Definition 6.4.4 *A random process is said to be ergodic if all time averages of any sample function are equal to the corresponding ensemble averages (expectation).*

Example 6.4.2 *DC and RMS values are defined in terms of time averages, but if the process is ergodic, they may be evaluated by ensemble averages. The DC value of $X(n)$ is*

$$X_{\mathrm{dc}} = \mathsf{E}[X(n)]$$

whereas the RMS value is given by

$$X_{\mathrm{rms}} = \sqrt{\mathsf{E}[X(n)^2]}.$$

If $X(n)$ is ergodic, the time average is equal to the ensemble average, that is

$$X_{\mathrm{dc}} = \lim_{N\to\infty} \frac{1}{N} \sum_{n=0}^{N-1} X(n) = \mathsf{E}[X(n)] = \int_{-\infty}^{\infty} x f_X(x;n)dx = \mu_X$$

Similarly, we have for the RMS value:

$$X_{\mathrm{rms}} = \sqrt{\lim_{N\to\infty} \frac{1}{N} \sum_{n=0}^{N-1} X(n)^2} = \sqrt{\mathsf{E}[X(n)^2]} = \sqrt{\sigma_X^2 + \mu_X^2} = \sqrt{\int_{-\infty}^{\infty} x^2 f_X(x;n)dx}$$

where μ_X and σ_X^2 are the mean and variance of $X(n)$, respectively.

If a process is ergodic, all time and ensemble averages are interchangeable. The time average is by definition independent of time. As it equals the ensemble averages, the latter are also independent of time. Thus, an ergodic process must be stationary. But not all stationary processes are ergodic.

Example 6.4.3 *Let us consider the same random process as in Example 6.4.1, $X(n) = A\cos(\omega_0 n + \phi)$. For calculating the ensemble averages (expectation), we already know that $E[X(n)] = 0$ and the SOMF is given by $r_{XX}(\kappa) = A^2/2 \cdot \cos(\omega_0\kappa)$. Therefore, for $\kappa = 0$ we get the second-order moment as $E[X(n)^2] = A^2/2$. Note that the process is stationary up to the second order as found in Example 6.4.1.*

Now, let us evaluate the corresponding time averages using a sample function of the random process. For example, the sample function $X(n, \zeta_0) = A\cos(\omega_0 n)$ occurs when $\varphi = 0$, which corresponds to one of the events. The time average for any of the sample functions can be calculated by letting φ be any value between 0 and 2π. For the time averages of the mean, we have

$$\overline{X(n)} = \lim_{N\to\infty} \frac{1}{N} \sum_{n=0}^{N-1} A\cos(\omega_0 n + \varphi) = 0$$

and for the second order moment, we have

$$\overline{X(n)^2} = \lim_{N\to\infty} \frac{1}{N} \sum_{n=0}^{N-1} [A\cos(\omega_0 n + \varphi)]^2 = \frac{A^2}{2}$$

In this example, φ disappears when the time average is calculated. We see that the time average is equal to the ensemble average for the first and second moments.

We have not yet proved that the process is *ergodic* because we have to evaluate all the orders of moments and averages. In general, it is difficult to prove that a process is ergodic. In this manuscript we will focus on stationary processes.

Properties of the SOMF

If the process $X(n)$ is said to be stationary to the second order (WSS), the SOMF is only a function of the time difference denoted by $\kappa = n_1 - n_2$, and the definition of the SOMF is reduced to

$$r_{XX}(\kappa) = \mathsf{E}\left[X(n+\kappa)X(n)\right]$$

Equivalently, the covariance function is defined by

$$c_{XX}(\kappa) = \mathsf{E}\left[(X(n+\kappa) - \mathsf{E}[X(n+\kappa)])(X(n) - \mathsf{E}[X(n)])\right] = r_{XX}(\kappa) - \mu_X^2,$$

where $\mu_X = \mathsf{E}[X(n)]$ is the constant mean of $X(n)$.

The properties of the SOMF and the covariance function are given by

1) $r_{XX}(0) = \mathsf{E}[X(n)^2] = \sigma_X^2 + \mu_X^2$ is the second order moment, and
   $c_{XX}(0) = \mathsf{E}[(X(n) - E[X(n)])^2] = \sigma_X^2$ is the variance

2) $r_{XX}(\kappa) = r_{XX}(-\kappa)$

3) $r_{XX}(0) \geq |r_{XX}(\kappa)|$

The second and the third property also hold for the covariance function $c_{XX}(\kappa)$. Proofs for the first and second properties follow from the definition, which should be verified by the reader as an exercise. The third property holds because

$$\begin{aligned} \mathsf{E}[(X(n+\kappa) \pm X(n))^2] &= \mathsf{E}[X(n+\kappa)^2] \pm 2\mathsf{E}[X(n+\kappa)X(n)] + \mathsf{E}[X(n)^2] \\ &= r_{XX}(0) \pm 2\, r_{XX}(\kappa) + r_{XX}(0) \geq 0. \end{aligned}$$

The Cross-SOMF

Definition 6.4.5 *The cross-SOMF for two real processes $X(n)$ and $Y(n)$ is defined as*

$$r_{XY}(n_1, n_2) = \mathsf{E}[X(n_1)Y(n_2)]$$

If $X(n)$ and $Y(n)$ are jointly WSS, the cross-SOMF reduces to $r_{XY}(n_1, n_2) = r_{XY}(\kappa)$ where $\kappa = n_1 - n_2$.

The cross-covariance function for two real processes $X(n)$ and $Y(n)$ is defined accordingly as

$$c_{XY}(n_1, n_2) = \mathsf{E}[(X(n_1) - \mathsf{E}[X(n_1)])(Y(n_2) - \mathsf{E}[Y(n_2)])]$$

If $X(n)$ and $Y(n)$ are jointly WSS, the cross-covariance reduces to $c_{XY}(\kappa) = r_{XY}(\kappa) - \mu_X \mu_Y$, where $\mu_X = \mathsf{E}[X(n)]$ and $\mu_Y = \mathsf{E}[Y(n)]$ are the constant means of $X(n)$ and $Y(n)$, respectively.

If the cross-covariance function of two random processes $X(n)$ and $Y(n)$ satisfies $c_{XY}(n_1, n_2) = 0$, they are said to be uncorrelated, i.e. we have $r_{XY}(n_1, n_2) = \mathsf{E}[X(n_1)]\mathsf{E}[Y(n_2)]$. If we have $r_{XY}(n_1, n_2) = 0 \;\forall\; n_1, n_2$ on the other hand, processes $X(n)$ and $Y(n)$ are said to be orthogonal.

The cross-SOMF and cross-covariance function have the following properties for jointly WSS processes

1) $r_{XY}(-\kappa) = r_{YX}(\kappa)$

2) $|r_{XY}(\kappa)| \leq \sqrt{r_{XX}(0) r_{YY}(0)}$

3) $|r_{XY}(\kappa)| \leq [r_{XX}(0) + r_{YY}(0)]/2.$

Note that the second property constitutes a tighter bound than that of the third property, because the geometric mean of two positive numbers cannot exceed the arithmetic mean, that is

$$\sqrt{r_{XX}(0)r_{YY}(0)} \leq \frac{1}{2}[r_{XX}(0)+r_{YY}(0)]$$

If the random processes $X(n)$ and $Y(n)$ are jointly ergodic, the time average may be used to replace the ensemble average.

$$r_{XY}(\kappa) = \mathsf{E}[X(n+\kappa)Y(n)] = \mathsf{E}[X(n)Y(n-\kappa)] \equiv \lim_{N\to\infty} \frac{1}{N}\sum_{n=0}^{N-1} X(n)\,Y(n-\kappa) \tag{6.1}$$

In this case, the cross-SOMFs and auto-SOMFs may be measured by using a system composed of a delay element, a multiplier and an accumulator. This is illustrated in Figure 6.8, where the block $z^{-\kappa}$ is a delay element of order κ.

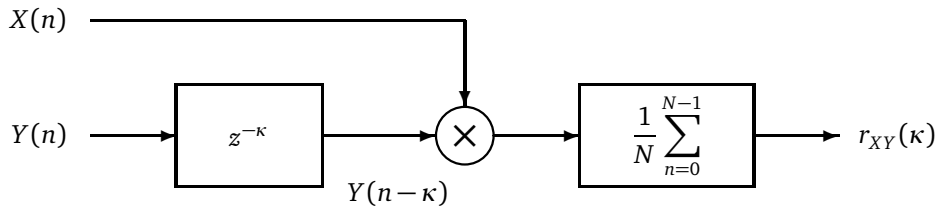

Figure 6.8.: Measurement of Cross-SOMF.

Example 6.4.4 *Here we consider a practical example, as depicted in Figure 6.9, which may occur e.g. in audio signal processing. Two spatially separated microphones record the waveform $S(n)$ from the same audio source. The microphone output signals are denoted by $X_1(n)$ and $X_2(n)$, and can be modeled as*

$$\begin{aligned} X_1(n) &= S(n)+V_1(n) \\ X_2(n) &= S(n-n_0)+V_2(n) \end{aligned}$$

where $S(n)$ is a WSS random process with zero mean and covariance function $c_{SS}(\kappa)$. The quantities $V_1(n)$ and $V_2(n)$ are independent white noise processes with zero mean and variances σ^2. We now want to determine the time-delay $n_0 \in \mathbb{Z}$, which can be used e.g. to determine the angle-of-arrival of the audio source.

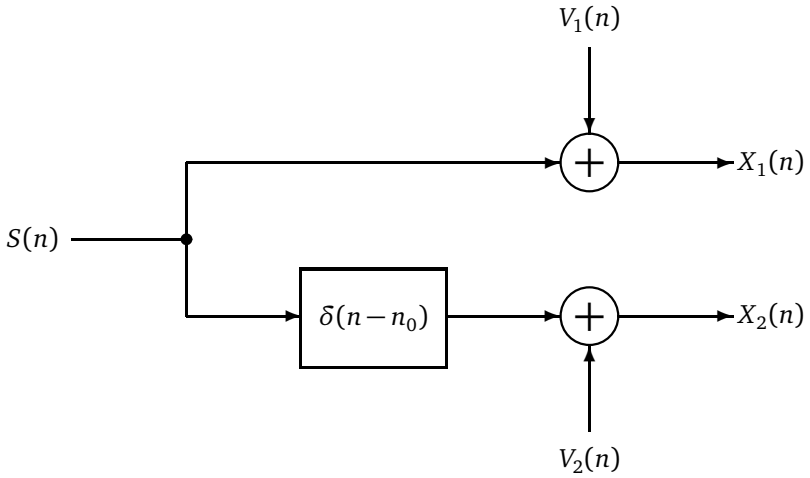

Figure 6.9.: Practical use of the cross-covariance for time-delay estimation.

This can be done by calculating the covariance function between $X_1(n)$ and $X_2(n)$, as follows

$$\begin{aligned} c_{X_1X_2}(\kappa) &= \mathsf{E}\left[(S(n+\kappa)+V_1(n+\kappa))(S(n-n_0)+V_2(n))\right] \\ &= \mathsf{E}[S(n+\kappa)S(n-n_0)]+\mathsf{E}[S(n+\kappa)V_2(n)]+\mathsf{E}[V_1(n+\kappa)S(n-n_0)]+\mathsf{E}[V_1(n+\kappa)V_2(n)] \\ &= c_{SS}(\kappa+n_0) \end{aligned}$$

where the remaining terms are zero, because $S(n)$, $V_1(n)$ and $V_2(n)$ are assumed to be mutually independent.

Consider for instance, $S(n)=\cos(\omega_0 n+\phi)$ where ω_0 is a constant and ϕ is uniformly distributed over $[0,2\pi)$. From example 6.4.1, we know that the covariance function is $c_{SS}(\kappa)=1/2\cdot\cos(\omega_0\kappa)$ which gives

$$c_{X_1X_2}(\kappa)=1/2\cos(\omega_0(\kappa+n_0))$$

A simple algorithm to determine the time-delay would be to search for the first maximum of $c_{X_1X_2}(\kappa)$.

Complex-Valued Random Processes

Definition 6.4.6 *A complex-valued random process is $Z(n)=X(n)+jY(n)$ where $X(n)$ and $Y(n)$ are real-valued random processes.*

We remark that many quantities and properties of complex-valued random processes can be inferred from real-valued random processes, when considering the real and imaginary part as separate random processes. For instance, a complex-valued random process is stationary if $X(n)$ and $Y(n)$ are jointly stationary. The mean of a complex-valued random process is defined as

$$\mathsf{E}[Z(n)]=\mathsf{E}[X(n)]+j\mathsf{E}[Y(n)].$$

Definition 6.4.7 *The SOMF for a complex-valued random process is:*

$$r_{ZZ}(n_1,n_2)=\mathsf{E}[Z(n_1)Z(n_2)^*]$$

Equivalently, the covariance function of a complex-valued random process is

$$c_{ZZ}(n_1,n_2)=\mathsf{E}\left[(Z(n_1)-\mathsf{E}[Z(n_1)])(Z(n_2)-\mathsf{E}[Z(n_2)])^*\right]=r_{ZZ}(n_1,n_2)-\mu_Z(n_1)\mu_Z(n_2)^*$$

Definition 6.4.8 *The complex-valued random process $Z(n)$ is stationary in the wide sense (WSS) if $\mathsf{E}[Z(n)]$ is a complex-valued constant and $r_{ZZ}(n_1,n_2)=r_{ZZ}(\kappa)$ where $\kappa=n_1-n_2$.*

The SOMF of a WSS complex-valued process has the symmetry property, i.e. $r_{ZZ}(-\kappa)=r_{ZZ}(\kappa)^*$, as it can be easily seen from the definition. Similarly $c_{ZZ}(-\kappa)=c_{ZZ}(\kappa)^*$.

Definition 6.4.9 *The cross-SOMF for two complex-valued random processes $Z_1(n)$ and $Z_2(n)$ is:*

$$r_{Z_1Z_2}(n_1,n_2)=\mathsf{E}\left[Z_1(n_1)Z_2(n_2)^*\right]$$

If the complex-valued random processes are jointly WSS, the cross-SOMF reduces to $r_{Z_1Z_2}(n_1,n_2)=r_{Z_1Z_2}(\kappa)$ where $\kappa=n_1-n_2$. Equivalently, the cross-covariance function of a complex-valued random process is defined as

$$c_{Z_1Z_2}(n_1,n_2)=\mathsf{E}\left[(Z_1(n_1)-\mathsf{E}[Z_1(n_1)])(Z_2(n_2)-\mathsf{E}[Z_2(n_2)])^*\right]=r_{Z_1Z_2}(n_1,n_2)-\mu_{Z_1}(n_1)\mu_{Z_2}(n_2)^*$$

and is a function of $\kappa=n_1-n_2$ only if $Z(n)$ is WSS. $Z_1(n)$ and $Z_2(n)$ are called uncorrelated if $c_{Z_1Z_2}(n_1,n_2)=0$. They are orthogonal if $r_{Z_1Z_2}(n_1,n_2)=0$.

Example 6.4.5 *A complex-valued process $Z(n)$ is comprised of a sum of M complex-valued signals*

$$Z(n) = \sum_{m=1}^{M} A_m e^{j(\omega_0 n + \Phi_m)}$$

Here ω_0 is constant, A_m is a zero-mean random amplitude of signal m with variance σ_m^2 and Φ_m is its random phase. We assume all variables A_m and Φ_m for $m = 1, \ldots, M$ to be statistically independent and the random phases uniformly distributed on $[0, 2\pi)$. Find the mean and SOMF. Is the process wide sense stationary?

The mean $\mathsf{E}[Z(n)]$ is given by

$$\begin{aligned} \mathsf{E}[Z(n)] &= \sum_{m=1}^{M} \mathsf{E}[A_m] e^{j\omega_0 n} \mathsf{E}[e^{j\Phi_m}] \\ &= \sum_{m=1}^{M} \mathsf{E}[A_m] e^{j\omega_0 n} \{\mathsf{E}[\cos(\Phi_m)] + j\mathsf{E}[\sin(\Phi_m)]\} = 0 \end{aligned}$$

Similarly, the SOMF $r_{ZZ}(n+\kappa, n) = \mathsf{E}[Z(n+\kappa)Z(n)^*]$ can be calculated to be

$$\begin{aligned} r_{ZZ}(n+\kappa, n) &= \mathsf{E}\left[\sum_{m=1}^{M} A_m e^{j\omega_0(n+\kappa)} e^{j\Phi_m} \cdot \sum_{l=1}^{M} A_l e^{-j\omega_0 n} e^{-j\Phi_l}\right] \\ &= \sum_{m=1}^{M}\sum_{l=1}^{M} \mathsf{E}[A_m A_l] \cdot e^{j\omega_0\kappa} \cdot \mathsf{E}[e^{j(\Phi_m - \Phi_l)}] \end{aligned}$$

Since

$$\mathsf{E}[e^{j(\Phi_m - \Phi_l)}] = \begin{cases} 1 & m = l \\ 0 & m \neq l \end{cases}$$

The former holds because for $m \neq l$,

$$\mathsf{E}[e^{j(\Phi_m - \Phi_l)}] = \mathsf{E}[e^{j\Phi_m}]\mathsf{E}[e^{-j\Phi_l}] = 0$$

Thus if $m = l$,

$$r_{ZZ}(n+\kappa, n) = \sum_{m=1}^{M} \mathsf{E}[A_m^2] e^{j\omega_0\kappa} = e^{j\omega_0\kappa} \sum_{m=1}^{M} \sigma_m^2$$

6.5 Power Spectral Density and Spectrum

In analogy to the Fourier analysis of deterministic discrete-time signals, we will introduce in this section a frequency domain representation of random processes. Note that the discrete-time Fourier transform (DTFT) $X(e^{j\omega})$ of some signal $x(n)$ is only defined if the sum

$$X(e^{j\omega}) = \sum_{n=-\infty}^{\infty} x(n) e^{-j\omega n}$$

converges. A sufficient condition for the sum to converge uniformly to a continuous function of ω is given if $x(n)$ is absolutely summable, i.e. we have $\sum_{n=-\infty}^{\infty} |x(n)| < \infty$.

In the case of a random process $X(n)$, which represents an ensemble of discrete-time signals, this condition is not fulfilled and consequently, the DTFT of a random process does not exist. However, a frequency domain representation, namely the power spectral density (PSD) or the spectrum of a random process can be found by taking the Fourier transform of the SOMF or the covariance function, respectively. Both, the PSD and the spectrum are important concepts for the analysis of signals in the frequency domain, in particular for spectral analysis, as discussed in the following. We begin with the definition, the so-called Wiener-Khintchine theorem, and then describe some important properties.

Theorem 6.5.1 *Wiener-Khintchine Theorem: When $X(n)$ is a wide-sense stationary process, the PSD can be obtained from the Fourier Transform of the SOMF:*

$$S_{XX}(e^{j\omega}) = \sum_{\kappa=-\infty}^{\infty} r_{XX}(\kappa)e^{-j\omega\kappa}$$

and conversely,

$$r_{XX}(\kappa) = \frac{1}{2\pi}\int_{-\pi}^{\pi} S_{XX}(e^{j\omega})e^{j\omega\kappa}d\omega$$

Equivalently, we now define the *spectrum* of a stationary random process $X(n)$ as the Fourier transform of the covariance function

$$C_{XX}(e^{j\omega}) = \sum_{\kappa=-\infty}^{\infty} c_{XX}(\kappa)e^{-j\omega\kappa}.$$

and conversely,

$$c_{XX}(\kappa) = \frac{1}{2\pi}\int_{-\pi}^{\pi} C_{XX}(e^{j\omega})e^{j\omega\kappa}\,d\omega.$$

We note that $C_{XX}(e^{j\omega})$ and $S_{XX}(e^{j\omega})$ are real, 2π periodic and non-negative. Because of the periodicity they are often considered for $\omega \in [-\pi, \pi)$ only. We will see later that when $X(n)$ is real, it is sufficient to consider them for $\omega \in [0, \pi)$. The spectrum and the PSD are related by $C_{XX}(e^{j\omega}) = S_{XX}(e^{j\omega}) - 2\pi\mu_x^2\delta(\omega)$.

Example 6.5.1 *Let us consider the same random process as in Example 6.4.1, $X(n) = A\cos(\omega_0 n + \phi)$ where A, ω_0 are constants and Φ is uniformly distributed on $[0, 2\pi)$.*

We already know that $E[X(n)] = 0$ and the SOMF is given by $r_{XX}(\kappa) = A^2/2 \cdot \cos(\omega_0\kappa)$. By taking the Fourier transform of $r_{XX}(\kappa)$, we obtain the PSD

$$S_{XX}(e^{j\omega}) = \frac{A^2}{2}\pi\{\eta(\omega - \omega_0) + \eta(\omega + \omega_0)\}$$

where

$$\eta(\omega) = \sum_{k=-\infty}^{\infty} \delta(\omega + k2\pi)$$

Note that the expression for the PSD given above is valid for $-\infty < \omega < \infty$. As mentioned in the previous section, the PSD is often only considered in the interval $\omega \in [-\pi, \pi)$. However, this must always be clear in the context.

Example 6.5.2 *Consider a different random process $Z(n)$ which is defined as the superposition of P complex exponentials,*

$$Z(n) = \sum_{i=1}^{P} A_i \exp\{j\omega_i n\}.$$

where A_i is a random amplitude of the i^{th} complex exponential with frequency ω_i. The random amplitudes A_i are uncorrelated with zero mean and variances σ_i^2,

It can be shown that the SOMF is given by

$$r_{ZZ}(\kappa) = \sum_{i=1}^{P} \sigma_i^2 \exp\{j\omega_i\kappa\}$$

and taking the Fourier transform, we obtain the PSD as

$$S_{ZZ}(e^{j\omega}) = 2\pi\sum_{i=1}^{P} \sigma_i^2\eta(\omega - \omega_i).$$

This should be verified by the reader.

Example 6.5.3 *Suppose now that we have a random process*

$$X(n) = \sum_{i=1}^{P} [A_i \cos(\omega_i n) + B_i \sin(\omega_i n)].$$

where the random amplitudes A_i and B_i are pairwise uncorrelated with zero mean and common variance σ^2.

It can be shown by the reader that the SOMF is given by

$$r_{XX}(\kappa) = \sum_{i=1}^{P} \sigma_i^2 \cos(\omega_i \kappa)$$

and therefore the PSD can be found to be

$$S_{XX} = \pi \sum_{i=1}^{P} \sigma_i^2 [\eta(\omega - \omega_i) + \eta(\omega + \omega_i)].$$

Properties of the PSD and the Spectrum

The PSD and the spectrum have a number of important properties:

1) The PSD is always real, even if $X(n)$ is complex. This can be easily shown, using $r_{XX}(\kappa)^* = r_{XX}(-\kappa)$ and a change of variable,

$$S_{XX}(e^{j\omega})^* = \sum_{\kappa=-\infty}^{\infty} r_{XX}(\kappa)^* e^{j\omega\kappa} = \sum_{\kappa'=-\infty}^{\infty} r_{XX}(\kappa') e^{-j\omega\kappa'} = S_{XX}(e^{j\omega})$$

2) $S_{XX}(e^{j\omega}) \geq 0$, even if $X(n)$ is complex-valued.

3) When $X(n)$ is real, $S_{XX}(e^{-j\omega}) = S_{XX}(e^{j\omega})$.

4) When $X(n)$ is WSS, $\frac{1}{2\pi}\int_{-\pi}^{\pi} S_{XX}(e^{j\omega}) d\omega = P_{XX}$ is the total normalized average power.

The White Noise Process

Definition 6.5.1 *A random process $X(n)$ is said to be a white noise process if the PSD is constant over all frequencies*

$$S_{XX}(e^{j\omega}) = \sigma_X^2$$

where σ_X is a positive constant.

The SOMF for a white process is obtained by taking the inverse Fourier transform of $S_{XX}(e^{j\omega})$, as follows

$$r_{XX}(\kappa) = \frac{1}{2\pi}\int_{-\pi}^{\pi} \sigma_X^2 e^{j\omega\kappa} d\omega = \sigma_X^2 \frac{\sin(\pi\kappa)}{\pi\kappa} = \sigma_X^2 \delta(\kappa), \quad \kappa \in \mathbb{Z}$$

where $\delta(\kappa)$ is Kronecker's delta given by

$$\delta(\kappa) = \begin{cases} 1, & \kappa = 0, \\ 0, & \kappa \neq 0. \end{cases}$$

Note that the term *white noise* comes from the analysis of light, where white light means that all wavelengths are present. The flat PSD of a white noise process, and the corresponding SOMF, imply that there is no correlation structure in the data. Therefore, it is an important model for random process with maximum uncertainty. Note that due to the given definition, the white noise process is zero-mean and therewith does not have a deterministic component.

Definition 6.5.2 *For two jointly stationary processes $X(n)$ and $Y(n)$ the cross-power spectral density (cross-PSD) is given by the Fourier transform of the cross-SOMF*

$$S_{XY}(e^{j\omega}) = \sum_{\kappa=-\infty}^{\infty} r_{XY}(\kappa)e^{-j\omega\kappa}$$

and conversely,

$$r_{XY}(\kappa) = \frac{1}{2\pi}\int_{-\pi}^{\pi} S_{XY}(e^{j\omega})e^{j\omega\kappa}d\omega.$$

Equivalently, we define the cross-spectrum of two jointly stationary random processes $X(n)$ and $Y(n)$ by the Fourier transform of the cross-covariance function

$$C_{XY}(e^{j\omega}) = \sum_{\kappa=-\infty}^{\infty} c_{XY}(\kappa)e^{-j\omega\kappa}$$

and conversely,

$$c_{XY}(\kappa) = \frac{1}{2\pi}\int_{-\pi}^{\pi} C_{XY}(e^{j\omega})e^{j\omega\kappa}d\omega.$$

We remark that $C_{XY}(e^{j\omega})$ and $S_{XY}(e^{j\omega})$ are complex-valued in general, and also 2π periodic. Because of the periodicity, the cross-PSD and cross-spectrum are often considered for $\omega \in [-\pi, \pi)$ only. We will see later that when $X(n)$ and $Y(n)$ are real, it is sufficient to consider them for $\omega \in [0, \pi)$.

The cross-PSD and cross-spectrum have the following properties for jointly WSS processes:

1) $S_{XY}(e^{j\omega}) = S_{YX}(e^{j\omega})^*$. In addition, if $X(n)$ and $Y(n)$ are real, then $S_{XY}(e^{j\omega}) = S_{YX}(e^{-j\omega})$. This can easily be shown using $r_{XY}(-\kappa)^* = r_{YX}(\kappa)$ and a change of variable,

$$S_{YX}(e^{j\omega}) = \sum_{\kappa=-\infty}^{\infty} r_{YX}(\kappa)e^{-j\omega\kappa} = \sum_{\kappa=-\infty}^{\infty} r_{XY}(-\kappa)^* e^{-j\omega\kappa} = \left[\sum_{\kappa'=-\infty}^{\infty} r_{XY}(\kappa')e^{-j\omega\kappa'}\right]^* = S_{XY}(e^{j\omega})^*$$

2) If $X(n)$ and $Y(n)$ are real, $S_{XY}(e^{j\omega}) = S_{XY}(e^{-j\omega})^*$. This implies that $\mathrm{Re}\{S_{XY}(e^{j\omega})\}$ is an even function of ω, and $\mathrm{Im}\{S_{XY}(e^{j\omega})\}$ is an odd function of ω.

3) If $X(n)$ and $Y(n)$ are orthogonal, $S_{XY}(e^{j\omega}) = S_{YX}(e^{j\omega}) = 0$.

Example 6.5.4 *Let us consider the same scenario as in Example 6.4.4, where $X_1(n) = S(n) + V_1(n)$ and $X_2(n) = S(n) + V_2(n)$. With $S(n)$, $V_1(n)$ and $V_2(n)$ mutually uncorrelated and $S(n) = \cos(\omega_0 n + \phi)$, we already know that the covariance function is given by*

$$c_{X_1X_2}(\kappa) = \cos(\omega_0(\kappa + n_0)).$$

Taking the Fourier transform yields the cross-spectrum

$$C_{X_1X_2}(e^{j\omega}) = \delta(\omega - \omega_0)e^{j\omega_0 n_0} + \delta(\omega + \omega_0)e^{-j\omega_0 n_0}$$

for the interval $\omega \in [-\pi, \pi)$. Therefore, we can determine the time-delay by evaluating the phase at frequency ω_0. This represents an alternative to the approach described in Example 6.4.4.

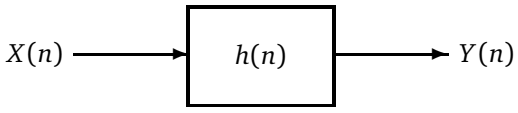

Figure 6.10.: A linear time-invariant filter.

6.6 Random Signals and Linear Systems

We are given a stationary processes $X(n)$ and a linear time-invariant (LTI) system with impulse response $h(n)$, as shown in Figure 6.10. $X(n)$ is the input and $Y(n)$ is the output of the filter. The filter is assumed to be stable in the BIBO sense, i.e. its impulse response is absolutely summable, $\sum_{n=-\infty}^{\infty} |h(n)| < \infty$.

Then for such a system, the output process $Y(n)$

$$Y(n) = \sum_{k=-\infty}^{\infty} h(k)X(n-k) = \sum_{k=-\infty}^{\infty} h(n-k)X(k)$$

exists with probability one, i.e. the process $Y_{(N)}(n) = \sum_{k=-N}^{N} h(k)X(n-k)$ converges with probability one to $Y(n)$, or $\mathsf{P}(\lim_{N\to\infty} |Y_{(N)}(n) - Y(n)| = 0) = 1$.

Consequently, if the input process $X(n)$ is stationary with $\mathsf{E}[|X(n)|] < \infty$ and the filter is stable in the BIBO sense, then the output process $Y(n)$ is also stationary. Note that if $X(n)$ is white noise with $\mathsf{E}[X(n)] = 0$ and covariance $c_{XX}(\kappa) = \sigma_X^2 \delta(\kappa)$ where σ_X^2 is the power of the noise and $\delta(n)$ is the Kronecker delta function, then $Y(n)$ is called a linear process.

Covariance Function and Spectrum of the Output

We now determine the relationship between the covariance functions and the spectra, at the input and at the output. First, let us define the zero-mean input and output processes $\tilde{X}(n) = X(n) - \mu_X$ and $\tilde{Y}(n) = Y(n) - \mu_Y$. We know that convolution is a linear operation, so we have

$$\tilde{Y}(n) = \sum_{k=-\infty}^{\infty} h(k)\tilde{X}(n-k) = \sum_{k=-\infty}^{\infty} h(n-k)\tilde{X}(k).$$

Note that in the general case, the system impulse response and the input process may be complex. The covariance function of the output $c_{YY}(\kappa) = \mathsf{E}[\tilde{Y}(n+\kappa)\tilde{Y}(n)^*]$ is determined according to

$$\begin{aligned} c_{YY}(\kappa) &= \mathsf{E}\left[\left(\sum_{k=-\infty}^{\infty} h(k)\tilde{X}(n+\kappa-k)\right)\left(\sum_{l=-\infty}^{\infty} h(l)\tilde{X}(n-l)\right)^*\right] \\ &= \sum_{k=-\infty}^{\infty}\sum_{l=-\infty}^{\infty} h(k)h(l)^*\mathsf{E}\left[\tilde{X}(n+\kappa-k)\tilde{X}(n-l)^*\right] \\ &= \sum_{k=-\infty}^{\infty}\sum_{l=-\infty}^{\infty} h(k)h(l)^* c_{XX}(\kappa-k+l) \end{aligned}$$

Taking the Fourier transform of both sides leads to

$$\begin{aligned} C_{YY}(e^{j\omega}) &= \sum_{\kappa=-\infty}^{\infty}\sum_{k=-\infty}^{\infty}\sum_{l=-\infty}^{\infty} h(k)h(l)^* c_{XX}(\kappa-k+l)e^{-j\omega\kappa} \\ &= \sum_{k=-\infty}^{\infty}\sum_{l=-\infty}^{\infty} h(k)h(l)^* \sum_{\kappa'=-\infty}^{\infty} c_{XX}(\kappa')e^{-j\omega(\kappa'+k-l)} \\ &= \sum_{k=-\infty}^{\infty} h(k)e^{-j\omega k} \sum_{l=-\infty}^{\infty} h(l)^* e^{j\omega l} \sum_{\kappa'=-\infty}^{\infty} c_{XX}(\kappa')e^{-j\omega\kappa'}. \end{aligned}$$

Here, we have changed the summations and used a change of variable $\kappa' = \kappa - k + l$. Identifying the frequency response of the filter as the Fourier transform of the respecive impulse reponse and the definition of the spectrum, the result can be summarized as

$$C_{YY}(e^{j\omega}) = H(e^{j\omega})H(e^{j\omega})^* C_{XX}(e^{j\omega}) = |H(e^{j\omega})|^2 C_{XX}(e^{j\omega})$$

Example 6.6.1 FIR filter: *Let $X(n)$ be white noise with power σ^2 and*

$$Y(n) = X(n) - X(n-1).$$

From the above, one can see that

$$h(n) = \begin{cases} 1, & n = 0 \\ -1, & n = 1 \\ 0, & \text{else} \end{cases}$$

Taking the Fourier transform leads to

$$H(e^{j\omega}) = \sum_{n=-\infty}^{\infty} h(n) e^{-j\omega n} = 1 - e^{-j\omega}$$

and thus,

$$\begin{aligned} C_{YY}(e^{j\omega}) &= |H(e^{j\omega})|^2 C_{XX}(e^{j\omega}) = |1 - e^{-j\omega}|^2 \sigma^2 \\ &= |2je^{-j\omega/2} \sin(\omega/2)|^2 \sigma^2 \\ &= 4\sin(\omega/2)^2 \sigma^2 \end{aligned}$$

Cross-Covariance Function and Cross-Spectrum

The cross-covariance function of the output $c_{YX}(\kappa) = \mathsf{E}[\tilde{Y}(n+\kappa)\tilde{X}(n)^*]$ is determined according to

$$\begin{aligned} c_{YX}(\kappa) &= \mathsf{E}\left[\left(\sum_{k=-\infty}^{\infty} h(k)\tilde{X}(n+\kappa-k)\right)\tilde{X}(n)^*\right] \\ &= \sum_k h(k)\mathsf{E}\left[\tilde{X}(n+\kappa-k)\tilde{X}(n)^*\right] \\ &= \sum_k h(k) c_{XX}(\kappa-k) \end{aligned}$$

Taking the Fourier transform of both sides leads to

$$\begin{aligned} C_{YX}(e^{j\omega}) &= \sum_{\kappa=-\infty}^{\infty} \sum_{k=-\infty}^{\infty} h(k) c_{XX}(\kappa-k) e^{-j\omega\kappa} \\ &= \sum_{\kappa'=-\infty}^{\infty} \sum_{k=-\infty}^{\infty} h(k) c_{XX}(\kappa') e^{-j\omega(\kappa'+k)} \\ &= \sum_{k=-\infty}^{\infty} h(k) e^{-j\omega k} \sum_{\kappa'=-\infty}^{\infty} c_{XX}(\kappa') e^{-j\omega\kappa'} \end{aligned}$$

Here, we have changed the summations and used a change of variable $\kappa' = \kappa - k$. Again, identifying the frequency response of the filter and the definition of the spectrum, the result can be summarized as

$$C_{YX}(e^{j\omega}) = H(e^{j\omega}) C_{XX}(e^{j\omega}).$$

Example 6.6.2 *Consider a system as depicted in Figure 6.10 where $X(n)$ is a stationary, zero-mean white noise process with variance σ_X^2. The impulse response of the system is given by*

$$h(n) = \left[\frac{1}{3}\left(\frac{1}{4}\right)^n + \frac{2}{3}\left(-\frac{1}{2}\right)^n\right]u(n)$$

where $u(n)$ is the unit step function

$$u(n) = \begin{cases} 1, & n \geq 0 \\ 0, & n < 0 \end{cases}$$

and we wish to determine $C_{YY}(e^{j\omega})$ and $C_{YX}(e^{j\omega})$.

The system transfer function is given by

$$\begin{aligned} H(e^{j\omega}) &= \frac{1/3}{1-\frac{1}{4}e^{-j\omega}} + \frac{2/3}{1+\frac{1}{2}e^{-j\omega}} \\ &= \frac{1}{1+\frac{1}{4}e^{-j\omega}-\frac{1}{8}e^{-j2\omega}} \end{aligned}$$

The spectrum and cross-spectrum are given respectively by

$$\begin{aligned} C_{YY}(e^{j\omega}) &= |H(e^{j\omega})|^2 C_{XX}(e^{j\omega}) \\ &= \frac{\sigma_X^2}{\left|1+\frac{1}{4}e^{-j\omega}-\frac{1}{8}e^{-j2\omega}\right|^2} \\ C_{YX}(e^{j\omega}) &= H(e^{j\omega})C_{XX}(e^{j\omega}) \\ &= \frac{\sigma_X^2}{1+\frac{1}{4}e^{-j\omega}-\frac{1}{8}e^{-j2\omega}} \end{aligned}$$

Interaction of Two Linear Systems

The previous result may be generalized to obtain the cross-covariance or cross-spectrum of two linear systems. Let $X_1(n)$ and $Y_1(n)$ be the input and output processes of the first system, with impulse response $h_1(n)$, and $X_2(n)$ and $Y_2(n)$ be the input and output processes of the second system with impulse response $h_2(n)$ (see Figure 6.11).

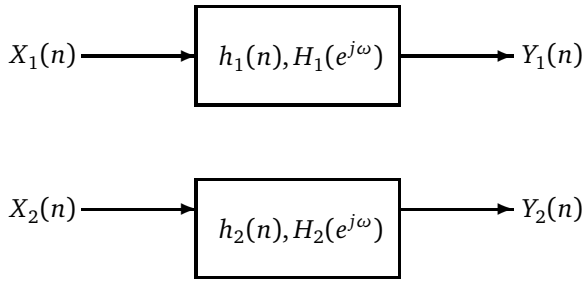

Figure 6.11.: Interaction of two linear systems

Suppose that $X_1(n)$ and $X_2(n)$ are wide-sense stationary and the systems are time-invariant and linear. Then the output cross-covariance function is:

$$c_{Y_1Y_2}(\kappa) = \sum_{k=-\infty}^{\infty}\sum_{l=-\infty}^{\infty} h_1(k)h_2(l)^* c_{X_1X_2}(\kappa - k + l)$$

Taking the Fourier transform leads to

$$C_{Y_1Y_2}(e^{j\omega}) = H_1(e^{j\omega})H_2(e^{j\omega})^* C_{X_1X_2}(e^{j\omega}).$$

Example 6.6.3 *Consider the system shown in Figure 6.11 where $X_1(n) = X_2(n) = X(n)$ is stationary, zero-mean white noise with variance σ_X^2. Let $h_1(n) = h(n)$ be the same system as discussed in Example 6.6.2 and $h_2(n)$ is given by*

$$h_2(n) = \delta(n) + \frac{1}{2}\delta(n-1) - \frac{1}{2}\delta(n-2)$$

where $\delta(n)$ is Kronecker's delta. We wish to find the cross-spectrum $C_{Y_1Y_2}(e^{j\omega})$. Using

$$H_2(e^{j\omega}) = \sum_{n=-\infty}^{\infty} h_2(n)e^{-j\omega n} = 1 + \frac{1}{2}e^{-j\omega} - \frac{1}{2}e^{-j2\omega}$$

we obtain

$$C_{Y_1Y_2}(e^{j\omega}) = H_1(e^{j\omega})H_2(e^{j\omega})^* C_{XX}(e^{j\omega}) = \frac{1 + \frac{1}{2}e^{j\omega} - \frac{1}{2}e^{j2\omega}}{1 + \frac{1}{4}e^{-j\omega} - \frac{1}{8}e^{-j2\omega}}\sigma_X^2.$$

Cascade of Linear Systems

We consider a cascade of L linear systems in serial connection, as illustrated by Figure 6.12.

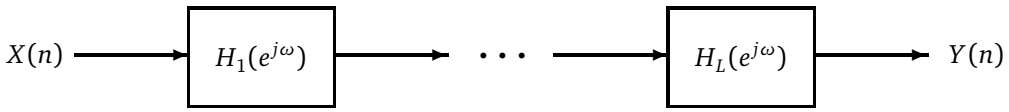

Figure 6.12.: Cascade of L linear systems.

From linear system theory, it is known that a cascade of linear systems can be equivalently represented by a system whose transfer function $H(e^{j\omega})$ is the product of the L individual system functions

$$H(e^{j\omega}) = H_1(e^{j\omega}) \cdot \ldots \cdot H_L(e^{j\omega}).$$

When a random process is the input to such a system, the spectrum of the output and cross spectrum of the output with the input are given respectively by

$$\begin{aligned} C_{YY}(e^{j\omega}) &= C_{XX}(e^{j\omega})\left|\prod_{i=1}^{L} H_i(e^{j\omega})\right|^2 = C_{XX}(e^{j\omega})\prod_{i=1}^{L}\left|H_i(e^{j\omega})\right|^2 \\ C_{YX}(e^{j\omega}) &= C_{XX}(e^{j\omega})\prod_{i=1}^{L} H_i(e^{j\omega}) \end{aligned}$$

Signal plus Noise Case

The scenario depicted in Figure 6.13 represents the case when a zero-mean signal of interest $X(n)$ is corrupted by some zero-mean additive noise process $V(n)$. Here, we do not have a filtering operation, though this case may occur before or after a filter, as e.g. in Figure 6.14. We want to treat this case separately to highlight the occurrence of cross-terms.

Assume that the processes are stationary, then the output covariance function in this case is given by

$$\begin{aligned} c_{YY}(\kappa) &= \mathsf{E}[Y(n+\kappa)Y(n)] = \mathsf{E}[(X(n+\kappa) + V(n+\kappa))(X(n) + V(n)] \\ &= \mathsf{E}[X(n+\kappa)X(n)] + \mathsf{E}[X(n+\kappa)V(n)] + \mathsf{E}[V(n+\kappa)X(n)] + \mathsf{E}[V(n+\kappa)V(n)] \\ &= c_{XX}(\kappa) + c_{XV}(\kappa) + c_{VX}(\kappa) + c_{VV}(\kappa). \end{aligned}$$

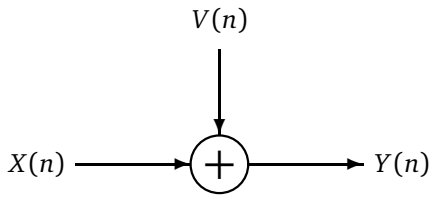

Figure 6.13.: Signal plus noise.

If $X(n)$ and $V(n)$ are uncorrelated, $c_{XV}(\kappa) = c_{VX}(\kappa) = 0 \; \forall \; \kappa \in \mathbb{Z}$. Thus, the output covariance reduces to

$$c_{YY}(\kappa) = c_{XX}(\kappa) + c_{VV}(\kappa).$$

If $V(n)$ is white noise with variance σ_V^2, we have

$$c_{YY}(\kappa) = c_{XX}(\kappa) + \sigma_V^2 \delta(\kappa).$$

The same relations hold in the spectral domain, i.e.

$$C_{YY}(e^{j\omega}) = C_{XX}(e^{j\omega}) + C_{VV}(e^{j\omega})$$

and

$$C_{YY}(e^{j\omega}) = C_{XX}(e^{j\omega}) + \sigma_V^2.$$

Linear Filter plus Noise Case

Before treating the linearly filtered process pluse noise case, we want to summarize important results for the linearly filtered process from previous sections. This is in order to use them as one of the basic components to determine output covariance and cross-covariance functions and respective output spectra and cross-spectra of more complicated systems. Therefore, let us consider again the system illustrated in Figure 6.10. The output covariance function is given by

$$c_{YY}(\kappa) = \sum_{k=-\infty}^{\infty} \sum_{l=-\infty}^{\infty} h(k) h(l)^* c_{XX}(\kappa - k + l)$$

and by taking the Fourier transform, we obtain the output spectrum

$$C_{YY}(e^{j\omega}) = H(e^{j\omega}) H(e^{j\omega})^* C_{XX}(e^{j\omega}) = |H(e^{j\omega})|^2 C_{XX}(e^{j\omega}).$$

Moreover, the cross-covariance function between output and input can be found to be

$$c_{YX}(\kappa) = \sum_{k=-\infty}^{\infty} h(k) c_{XX}(\kappa - k)$$

and by taking the Fourier transform, we obtain the output spectrum

$$C_{YX}(e^{j\omega}) = H(e^{j\omega}) C_{XX}(e^{j\omega}).$$

Now, consider the system shown in Figure 6.14. It is assumed that $X(n)$ is stationary with $\mathsf{E}[X(n)] = 0$, $V(n)$ stationary with $\mathsf{E}[V(n)] = 0$ and $c_{VX}(\kappa) = 0$ ($X(n)$ and $V(n)$ uncorrelated). It is also assumed that $h(n)$, $X(n)$ and $V(n)$ are real. The output is $Y(n) = \sum_{k=-\infty}^{\infty} h(k) X(n-k) + V(n)$

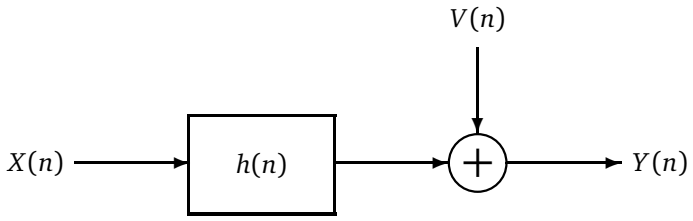

Figure 6.14.: A linear filter plus noise system.

The expected value of the output $\mathsf{E}[Y(n)]$ can be calculated as

$$\mathsf{E}[Y(n)] = \sum_{k=-\infty}^{\infty} h(k)\mathsf{E}[X(n-k)] + \mathsf{E}[V(n)] = 0$$

The covariance function of the output $c_{YY}(\kappa) = \mathsf{E}[Y(n+\kappa)Y(n)]$ is determined according to

$$\begin{aligned} c_{YY}(\kappa) &= \mathsf{E}\left[\left(\sum_{k=-\infty}^{\infty} h(k)X(n+\kappa-k) + V(n+\kappa)\right)\left(\sum_{l=-\infty}^{\infty} h(l)X(n-l) + V(n)\right)\right] \\ &= \sum_{k=-\infty}^{\infty}\sum_{l=-\infty}^{\infty} h(k)h(l)\mathsf{E}\left[X(n+\kappa-k)X(n-l)\right] \\ &+ \sum_{k=-\infty}^{\infty} h(k)\mathsf{E}\left[X(n+\kappa-k)V(n)\right] + \sum_{l=-\infty}^{\infty} h(l)\mathsf{E}\left[V(n+\kappa)X(n-l)\right] + \mathsf{E}\left[V(n+\kappa)V(n)\right] \end{aligned}$$

Since $X(n)$ and $V(n)$ are uncorrelated, we obtain

$$c_{YY}(\kappa) = \sum_{k=-\infty}^{\infty}\sum_{l=-\infty}^{\infty} h(k)h(l)c_{XX}(\kappa-k+l) + c_{VV}(\kappa)$$

and applying the Fourier transform to both sides of the above expression yields

$$C_{YY}(e^{j\omega}) = |H(e^{j\omega})|^2 C_{XX}(e^{j\omega}) + C_{VV}(e^{j\omega}).$$

Note that this result could have been obtained immediately by using the results of the signal plus noise and the linear system scenario since $V(n)$ and $X(n)$ are uncorrelated.

The cross-covariance function of the output and input $c_{YX}(\kappa) = \mathsf{E}[Y(n+\kappa)X(n)]$ is determined according to

$$\begin{aligned} c_{YX}(\kappa) &= \mathsf{E}\left[\left(\sum_{k=-\infty}^{\infty} h(k)X(n+\kappa-k) + V(n+\kappa)\right)X(n)\right] \\ &= \sum_{k=-\infty}^{\infty} h(k)\mathsf{E}\left[X(n+\kappa-k)X(n)\right] \\ &= \sum_{k=-\infty}^{\infty} h(k)c_{XX}(\kappa-k) \end{aligned}$$

Applying the Fourier transform to both sides of the above expression yields

$$C_{YX}(e^{j\omega}) = H(e^{j\omega})C_{XX}(e^{j\omega})$$

Note that when the additive noise at the output, $V(n)$ is uncorrelated with the input process $X(n)$, it has no effect on the cross-spectrum of the output and input.

Example 6.6.4 *Consider again the random process of Example 6.4.5,*

$$X(n) = \sum_{m=1}^{M} A_m e^{j(\omega_0 n + \phi_m)}$$

Here ω_0 is constant, A_m is a zero-mean random amplitude of signal m with variance σ_m^2 and Φ_m is its random phase. We assume all variables A_m and Φ_m for $m = 1, \ldots, M$ to be statistically independent and the random phases uniformly distributed on $[0, 2\pi)$.

Note that we already know from Example 6.4.5 the covariance function, which has been found to be

$$r_{XX}(\kappa) = e^{j\omega_0 \kappa} \sum_{m=1}^{M} \mathsf{E}[A_m^2]$$

Let $X(n)$ be the input to a linear, stable time-invariant system with known impulse response $h(n)$. The output of the system $Y(n)$ is buried in zero-mean noise $V(n)$, as shown in Figure 6.14. $V(n)$ has a known covariance $c_{VV}(\kappa)$ and is independent of $X(n)$. We wish to determine the cross-spectrum $C_{YX}(e^{j\omega})$ and the auto-spectrum $C_{YY}(e^{j\omega})$.

Using $C_{YX}(e^{j\omega}) = H(e^{j\omega}) C_{XX}(e^{j\omega})$, the cross-spectrum is determined as follows

$$\begin{aligned} C_{YX}(e^{j\omega}) &= H(e^{j\omega}) \left(\sum_{m=1}^{M} \sigma_m^2 \right) 2\pi \sum_{l=-\infty}^{\infty} \delta(\omega - \omega_0 + 2\pi l) \\ &= 2\pi \left(\sum_{m=1}^{M} \sigma_m^2 \right) \sum_{l=-\infty}^{\infty} H(e^{j(\omega_0 - 2\pi l)}) \delta(\omega - \omega_0 + 2\pi l), \end{aligned}$$

and using $C_{YY}(e^{j\omega}) = |H(e^{j\omega})|^2 C_{XX}(e^{j\omega}) + C_{VV}(e^{j\omega})$, the spectrum is given by

$$C_{YY}(e^{j\omega}) = 2\pi \left(\sum_{m=1}^{M} \sigma_m^2 \right) \sum_{l=-\infty}^{\infty} |H(e^{j(\omega_0 - 2\pi l)})|^2 \delta(\omega - \omega_0 + 2\pi l) + C_{VV}(e^{j\omega}).$$

7 The Finite Fourier Transform

The next chapters deal with spectrum estimation of random signals. In practice, one is always faced with finite data segments, and must estimate the spectrum based on those measurements. Therefore, we present some preliminaries on the Fourier transform of finite, discrete-time random processes, for which we introduce the term *Finite Fourier Transform*. It will become apparent that the stochastic properties of spectrum estimates, e.g. the periodogram as introduced in Section 9.2, are directly related to the properties of the Finite Fourier transform of random processes.

7.1 Definition

Let $X(0),\dots,X(N-1)$ be a model for the observations $x(0),\dots,x(N-1)$ of a stationary random process $X(n)$, $n \in \mathbb{Z}$. The function

$$X_N\left(e^{j\omega}\right) = \sum_{n=0}^{N-1} X(n) e^{-j\omega n}, \quad -\infty < \omega < \infty$$

is called the finite Fourier transform. The inverse transform is given by

$$X(n) = \frac{1}{2\pi} \int_{-\pi}^{\pi} X_N(e^{j\omega}) \mathrm{e}^{j\omega n} d\omega,$$

for $n = 0, 1, \dots, N-1$, and 0 otherwise.

Some properties of the finite Fourier transform are listed below:

1. $X_N(e^{j\omega})$ is 2π periodic, i.e. $X_N(e^{j(\omega+2\pi)}) = X_N(e^{j\omega})$.
2. If $X(n)$ is real-valued, we have $X_N(e^{-j\omega}) = X_N(e^{j\omega})^*$.
3. The finite Fourier transform is a linear operation, i.e. the finite Fourier transform of $aX(n) + bY(n)$ is $aX_N(e^{j\omega}) + bY_N(e^{j\omega})$, where a and b are non-zero constants.

Due to the fact that $X_N(e^{j\omega})$ is 2π periodic, it is often only considered for one period, i.e. $\omega \in [-\pi, \pi)$. Moreover, if $X(n)$ is real-valued, it is sufficient to consider the finite Fourier transform for $\omega \in [0, \pi)$ due to its symmetry.

The finite Fourier transform can be taken at discrete frequencies $\omega_k = 2\pi k/N$, $k = 0, \dots, N-1$ which are often called Fourier frequencies, or discrete Fourier transform (DFT) frequencies. We then have

$$X_N\left(e^{j2\pi k/N}\right) = \sum_{n=0}^{N-1} X(n) e^{-j2\pi kn/N} \quad k = 0, \dots, N-1$$

Note that this expression can be computed efficiently using the Fast Fourier Transform (FFT).

7.2 Statistical Properties

To introduce the statistical properties of the finite Fourier transform, we start with an example, where we consider the simple case of a white Gaussian process. We know from the previous chapter that for a white random process $X(n)$ with $\sigma_X^2 = 1$, the covariance function and spectrum is given by $c_{XX}(\kappa) = \delta(\kappa)$ and $C_{XX}(e^{j\omega}) = 1$, respectively.

The result of this example allows a simple interpretation, it is extended later to the general case of random process with an arbitrary $c_{XX}(\kappa)$ and $C_{XX}(e^{j\omega})$.

Example 7.2.1 *Distribution of the finite Fourier transform of a white process. Let $X(0),\ldots,X(N-1)$ be independent real random variables, each distributed as $\mathcal{N}(0,1)$. Let $N=2^r$ where $r\in\mathbb{N}$. Determine the distribution of $X_N(e^{j\omega})$ at $\omega=2\pi k/N$ for $k=0,\ldots,N/2-1$.*

In general, the finite Fourier transform is complex. Thus, we first determine the distribution of the real and imaginary part. Since the random variables $X(0),\ldots,X(N-1)$ are real-valued, we directly see from the definition that the real part and imaginary part of the finite Fourier transform can be expressed as,

$$\mathsf{Re}\left\{X_N\left(e^{j2\pi k/N}\right)\right\}=\sum_{n=0}^{N-1}X(n)\cos\left(2\pi kn/N\right)$$

and,

$$\mathsf{Im}\left\{X_N\left(e^{j2\pi k/N}\right)\right\}=-\sum_{n=0}^{N-1}X(n)\sin\left(2\pi kn/N\right).$$

The quantities $\mathsf{Re}\{X_N(e^{j2\pi k/N})\}$ and $\mathsf{Im}\{X_N(e^{j2\pi k/N})\}$ are sums of independent normal random variables and so will have a normal distribution. It remains to find the mean and variance of each quantity in order to completely specify their distributions. The expected value of the real part is given by

$$\mathsf{E}\left[\mathsf{Re}\left\{X_N\left(e^{j2\pi k/N}\right)\right\}\right]=\mathsf{E}\left[\sum_{n=0}^{N-1}X(n)\cos(2\pi kn/N)\right]=\sum_{n=0}^{N-1}\mathsf{E}\left[X(n)\right]\cos(2\pi kn/N)=0.$$

The expected value of imaginary part can also be determined to be $\mathsf{E}[\mathsf{Im}\{X_N(e^{j2\pi k/N})\}]=0$. The variance of the real part is given by

$$\begin{aligned}\mathsf{Var}\left[\mathsf{Re}\left\{X_N\left(e^{j2\pi k/N}\right)\right\}\right] &= \mathsf{E}\left[\mathsf{Re}\left\{X_N\left(e^{j2\pi k/N}\right)\right\}^2\right]-\left(\mathsf{E}\left[\mathsf{Re}\left\{X_N\left(e^{j2\pi k/N}\right)\right\}\right]\right)^2\\ &= \mathsf{E}\left[\mathsf{Re}\left\{X_N\left(e^{j2\pi k/N}\right)\right\}^2\right]\\ &= \mathsf{E}\left[\sum_{n=0}^{N-1}\sum_{m=0}^{N-1}X(n)X(m)\cos(2\pi kn/N)\cos(2\pi km/N)\right]\\ &= \sum_{n=0}^{N-1}\sum_{m=0}^{N-1}\mathsf{E}\left[X(n)X(m)\right]\cos(2\pi kn/N)\cos(2\pi km/N).\end{aligned}$$

Since $X(0),\ldots,X(N-1)$ are independent random variables, we have

$$\mathsf{E}\left[X(n)X(m)\right]=\begin{cases}1, & n=m\\ 0, & n\neq m\end{cases}$$

Using this and the trigonometric identity $\cos(\theta)^2=\frac{1}{2}(1+\cos(2\theta))$, we obtain for the variance of the real part

$$\begin{aligned}\mathsf{Var}\left[\mathsf{Re}\left\{X_N\left(e^{j\frac{2\pi k}{N}}\right)\right\}\right] &= \sum_{n=0}^{N-1}\cos(2\pi kn/N)^2\\ &= \frac{1}{2}\sum_{n=0}^{N-1}(1+\cos(4\pi kn/N))\\ &= \frac{N}{2}+\frac{1}{2}\sum_{n=0}^{N-1}\cos\left(4\pi kn/N\right).\end{aligned}$$

Let us now concentrate on the second term of the expression above,

$$\begin{aligned}
\sum_{n=0}^{N-1}\cos(4\pi kn/N) &= \frac{1}{2}\sum_{n=0}^{N-1}\left(e^{j4\pi kn/N}+e^{-j4\pi kn/N}\right)\\
&= \frac{1}{2}\left[\frac{1-e^{j4\pi k}}{1-e^{j4\pi k/N}}+\frac{1-e^{-j4\pi k}}{1-e^{-j4\pi k/N}}\right]\\
&= \frac{1}{2}\left[\frac{e^{j2\pi k}}{e^{j2\pi k/N}}\frac{\sin(2\pi k)}{\sin(2\pi k/N)}+\frac{e^{-j2\pi k}}{e^{-j2\pi k/N}}\frac{\sin(2\pi k)}{\sin(2\pi k/N)}\right]\\
&= \cos(2\pi k(1-1/N))\frac{\sin(2\pi k)}{\sin(2\pi k/N)}\\
&= \begin{cases} 0, & k=1,\ldots,N/2-1\\ N, & k=0,N/2\end{cases}
\end{aligned}$$

Note that in the last line we have used the fact that due to $N=2^r$, N is an even number. For the cases $k=0,N/2$, the limit has to be derived by applying e.g. l'Hôpital's rule. Using this result, we obtain for the distribution of the real part of the finite Fourier transform

$$\mathrm{Re}\left[X_N\left(e^{j2\pi k/N}\right)\right]\sim\mathcal{N}(0,N/2),\quad k=1,\ldots,N/2-1.$$

The distribution of the imaginary part can be found in a similar fashion,

$$\mathrm{Im}\left[X_N\left(e^{j2\pi k/N}\right)\right]\sim\mathcal{N}(0,N/2),\quad k=1,\ldots,N/2-1$$

For $k=0$ and $k=N/2$, the finite Fourier transform is purely real, and we have $\mathrm{Re}[X_N(e^{j2\pi k/N})]\sim\mathcal{N}(0,N)$.

Now we want to identify if there is some correlation between the real and the imaginary part of the finite Fourier transform. Therefore, we determine the covariance of the real and imaginary parts as

$$\begin{aligned}
\mathrm{Cov}\left[\mathrm{Re}\left\{X_N\left(e^{j2\pi k/N}\right)\right\},\mathrm{Im}\left\{X_N\left(e^{j2\pi k/N}\right)\right\}\right] &= \mathrm{E}\left[\mathrm{Re}\left\{X_N\left(e^{j2\pi k/N}\right)\right\}\mathrm{Im}\left\{X_N\left(e^{j2\pi k/N}\right)\right\}\right]\\
&= -\sum_{n=0}^{N-1}\sum_{m=0}^{N-1}\mathrm{E}[X(n)X(m)]\cos(2\pi kn/N)\sin(2\pi km/N)\\
&= -\sum_{n=0}^{N-1}\cos(2\pi kn/N)\sin(2\pi kn/N)\\
&= -\frac{1}{2}\sum_{n=0}^{N-1}\sin(4\pi kn/N)
\end{aligned}$$

Note that we have used the fact that $\mathrm{E}[\mathrm{Re}\{X_N(e^{j2\pi k/N})\}]=\mathrm{E}[\mathrm{Im}\{X_N(e^{j2\pi k/N})\}]=0$, and the trigonometric identity $\cos(\theta)\sin(\theta)=\frac{1}{2}\sin(2\theta)$. The expression above can be further simplified,

$$\begin{aligned}
\sum_{n=0}^{N-1}\sin(4\pi kn/N) &= \frac{1}{2j}\sum_{n=0}^{N-1}\left(e^{j4\pi kn/N}-e^{-j4\pi kn/N}\right)\\
&= \frac{1}{2j}\left[\frac{1-e^{j4\pi k}}{1-e^{j4\pi k/N}}-\frac{1-e^{-j4\pi k}}{1-e^{-j4\pi k/N}}\right]\\
&= \frac{1}{2j}\left[\frac{e^{j2\pi k}}{e^{j2\pi k/N}}\frac{\sin(2\pi k)}{\sin(2\pi k/N)}-\frac{e^{-j2\pi k}}{e^{-j2\pi k/N}}\frac{\sin(2\pi k)}{\sin(2\pi k/N)}\right]\\
&= \sin(2\pi k(1-1/N))\frac{\sin(2\pi k)}{\sin(2\pi k/N)}\\
&= 0,\quad k=0,\ldots,N/2
\end{aligned}$$

Therefore, the real and imaginary part of the finite Fourier transform $X_N(e^{j\omega})$ are uncorrelated for frequencies $\omega = 2\pi k/N$, $k = 0,\ldots,N/2$.

Summarizing the obtained results, we can write down the distribution of the real and imaginary part of the finite Fourier transform for a real white Gaussian process as

$$\begin{bmatrix} \mathrm{Re}\{X_N(e^{j2\pi k/N})\} \\ \mathrm{Im}\{X_N(e^{j2\pi k/N})\} \end{bmatrix} \sim \mathcal{N}\left(\begin{bmatrix} 0 \\ 0 \end{bmatrix}, \frac{N}{2} \begin{bmatrix} 1 & 0 \\ 0 & 1 \end{bmatrix} \right), \quad k = 1,\ldots,N/2-1$$

Note that we have used vector notation to highlight the independence between real and imaginary part (zero entry in the covariance matrix). For $k = 0$ and $k = N/2$, on the other hand, the finite Fourier transform is purely real and we have $\mathrm{Re}\{X_N(e^{j2\pi k/N})\} \sim \mathcal{N}(0,N)$.

In Example 7.2.1, we have introduced the distribution of the finite Fourier transform for a special case, namely for a real white Gaussian process. However, we are more interested in the result for the general case of a real stationary random process $X(n)$ with an arbitrary $\mu_X = \mathrm{E}[X(n)]$, $c_{XX}(\kappa)$ and $C_{XX}(e^{j\omega})$. We assume some mild conditions to hold (finite moments and absolutely summable cumulants of all orders, i.e. loosely speaking, the statistical dependence between $X(n)$ and $X(m)$ decreases sufficiently fast as $|n-m|$ increases). Without proof (the interested reader is referred to Brillinger, 1981) we state the asymptotic distribution of the finite Fourier transform, i.e. when $N \to \infty$

$$\begin{bmatrix} \mathrm{Re}\{X_N(e^{j\omega})\} \\ \mathrm{Im}\{X_N(e^{j\omega})\} \end{bmatrix} \sim \mathcal{N}\left(\begin{bmatrix} 0 \\ 0 \end{bmatrix}, \frac{N}{2} C_{XX}(e^{j\omega}) \begin{bmatrix} 1 & 0 \\ 0 & 1 \end{bmatrix} \right), \quad \omega \in (0,\pi).$$

For $\omega = 0$ and $\omega = \pi$, the finite Fourier transform is purely real and we have a different asymptotic distribution as $N \to \infty$, which is $\mathrm{Re}\{X_N(e^{j\omega})\} \sim \mathcal{N}(N\mu_X\delta(\omega), NC_{XX}(e^{j\omega}))$.

For fixed frequencies $0 \leq \omega_{(1)} < \omega_{(2)} < \cdots < \omega_{(M)} \leq \pi$ the random variables $X_N(e^{j\omega_{(1)}}), X_N(e^{j\omega_{(2)}}), \ldots, X_N(e^{j\omega_{(M)}})$ are asymptotically for $N \to \infty$ independently distributed. The continous frequencies can also be approximated by discrete frequencies. When we use Fourier frequencies, i.e. multiples of $2\pi/N$, the finite Fourier transform variables are orthogonal by definition.

Finally, we want to mention two important modifications of random processes, namely the division into segments and windowing. The asymptotic distribution of the finite Fourier transform for these modifications is required for the analysis of non-parametric spectrum estimators, as discussed in Chapter 9.

- Divide the random process $X(n)$, $n = 0,\ldots,N-1$ into L segments of length M with $N = ML$ (segment l is given by $X(n+(l-1)M)$, $n = 0,\ldots,M-1$). Then, the finite Fourier transform of each segment l is given by

$$X_M(e^{j\omega},l) = \sum_{n=0}^{M-1} X(n+(l-1)M)e^{-j\omega n}, \quad l = 1,\ldots,L.$$

  For large M, the asymptotic distribution of $X_M(e^{j\omega},l)$ is as the one stated above for non-segmented processes. The random variables $X_M(e^{j\omega},l)$ are for $l = 1,\ldots,L$ asymptotically as $N \to \infty$ independently distributed. In particular, we require both $N, M \to \infty$ while the number of segments $L = N/M$ is finite.

- Apply now a window $w(n) \neq 0$ for $n = 0,\ldots,N-1$ and 0 otherwise. Then, the finite Fourier transform of a windowed process is given by

$$X_{N,w}(e^{j\omega}) = \sum_{n=0}^{N-1} w(n)X(n)e^{-j\omega n}.$$

  For large N, the asymptotic distribution of $X_{N,w}(e^{j\omega})$ is similar to the one stated above for a non-windowed process, except that the variance is multiplied by the factor $\sum_{n=0}^{N-1} w(n)^2$ and the mean at $\omega = 0$ is multiplied by the factor $\sum_{n=0}^{N-1} w(n)$.

Interpretation

In this section we illustrate an engineering interpretation of the mathematical results from the previous section. Therefore, we consider a broad-band noise process with a Gaussian distributed amplitude and pass it through an ideal narrow band pass filter with transfer function

$$H(e^{j\omega}) = \begin{cases} 1, & |\omega \pm \omega_0| < \pi/N \\ 0, & \text{else} \end{cases}$$

as depicted in Figure 7.1. Considering ω at the Fourier frequencies, we have $\omega = 2\pi k/N$ for $k = 0, \ldots, N-1$.

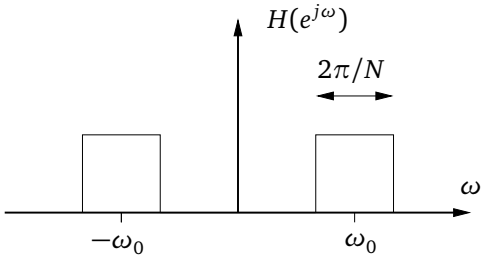

Figure 7.1.: Transfer function of an ideal band pass filter.

Consequently, the center frequency of the band pass is $\omega_0 = 2\pi k_0/N$. If $X(n)$ is filtered by the described band pass, the Fourier transform of the output signal is

$$Y_N\left(e^{j2\pi k/N}\right) \approx H\left(e^{j2\pi k/N}\right) X_N\left(e^{j2\pi k/N}\right)$$

Applying the inverse Fourier transform, we get for large N

$$Y(n) \approx \frac{1}{N} X_N\left(e^{j2\pi k_0/N}\right) e^{j2\pi k_0 n/N} + \frac{1}{N} X_N\left(e^{-j2\pi k_0/N}\right) e^{-j2\pi k_0 n/N},$$

and $Y(n)$ is approximately distributed as $\mathcal{N}(0, \frac{1}{N} C_{XX}(e^{j\omega_0}))$.

Furthermore, if we take two ideal bandpass filters of the same type as in Figure 7.1, whose frequency ranges are non-overlapping (see Figure 7.2), It is intuitive that the output of the two filters, $Y_1(n)$ and $Y_2(n)$ are then approximately independent. As we will see in Chapter 8, extending Figure 7.2 to a filter bank, provides an alternative approach to obtain the spectrum of an input process.

7.3 Relation to the Power Spectral Density

In Section 6.5, we have introduced the power spectral density (PSD) as the Fourier transform of the SOMF. The PSD is also related to the ensemble average (expectation) of the magnitude squared finite Fourier transform, in the limit when $N \to \infty$. This relation will be investigated in the following.

Calculation of the Average Power

Let $X(n, \zeta_i)$, $n \in \mathbb{Z}$, represent a sample function of a real-valued random process $X(n)$. We define a truncated version of this sample function as follows

$$x_N(n) = \begin{cases} X(n, \zeta_i), & n < N,\ N \in \mathbb{N} \\ 0, & \text{elsewhere} \end{cases}$$

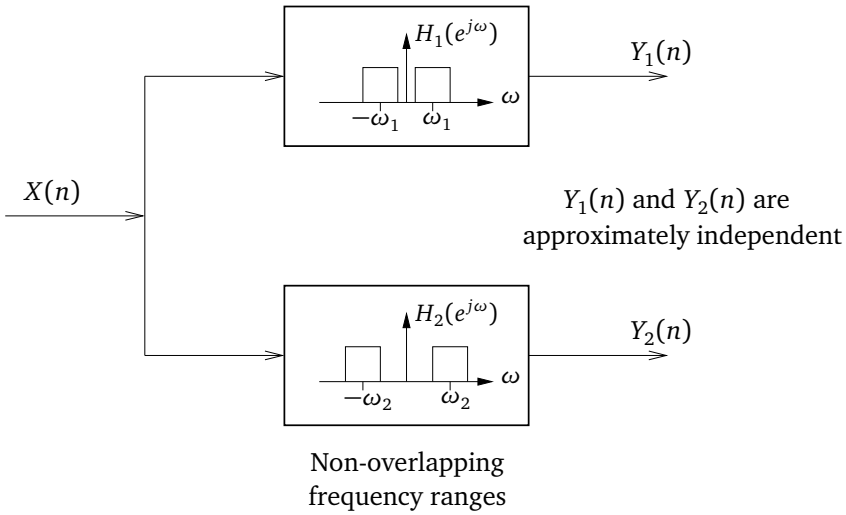

Figure 7.2.: Distinct frequencies of the finite Fourier transform.

where N is the length of the truncation (or observation) window. As long as N is finite, we assert that $x_N(n)$ will satisfy $\sum_{n=0}^{N-1} |x_N(n)| < \infty$. The finite Fourier transform of $x_N(n)$ is then given by

$$X_N(e^{j\omega}) = \sum_{n=0}^{N-1} x_N(n) e^{-j\omega n}$$

Let us calculate the normalized energy of the truncated signal as

$$E_N = \sum_{n=0}^{N-1} x_N(n)^2 = \frac{1}{2\pi} \int_{-\pi}^{\pi} \left| X_N(e^{j\omega}) \right|^2 d\omega$$

where Parseval's theorem has been used to obtain the second integral. By dividing the expression E_N by the observation time N, we obtain the average power P_N in $x_N(n)$

$$P_N = \frac{1}{N} \sum_{n=0}^{N-1} x_N(n)^2 = \frac{1}{2\pi} \int_{-\pi}^{\pi} \frac{1}{N} \left| X_N(e^{j\omega}) \right|^2 d\omega$$

We see that the average power P_N of $x_N(n)$ can be obtained by the integration of $\frac{1}{N}|X_N(e^{j\omega})|^2$. To obtain the average power for the entire sample function, we must consider the limit as $N \to \infty$. P_N provides a measure of power for a single sample function. If we want to determine the average power of the random process, we must also take the ensemble average (expected value). Thus, the average power of $X(n)$ is defined as

$$P_{XX} = \lim_{N\to\infty} \frac{1}{N} \sum_{n=0}^{N-1} \mathsf{E}[X(n)^2] = \lim_{N\to\infty} \frac{1}{2\pi} \int_{-\pi}^{\pi} \frac{1}{N} \mathsf{E}\left[|X_N(e^{j\omega})|^2 \right] d\omega$$

If $X(n)$ is WSS, $\mathsf{E}[X(n)^2]$ is a constant and $P_{XX} = \mathsf{E}[X(n)^2]$. We can also determine P_{XX} by a frequency domain integration. Let us define the PSD of $X(n)$ by

$$S_{XX}(e^{j\omega}) = \lim_{N\to\infty} \frac{1}{N} \mathsf{E}\left[|X_N(e^{j\omega})|^2 \right]$$

Then, the average power P_{XX} of a random process $X(n)$ can be calculated using

$$P_{XX} = \frac{1}{2\pi} \int_{-\pi}^{\pi} S_{XX}(e^{j\omega}) d\omega = r_{XX}(0).$$

Example 7.3.1 *Consider the random process*

$$X(n) = A\cos(\omega_0 n + \Phi)$$

where A and ω_0 are real constants and Φ is a random variable uniformly distributed on $[0, \pi/2)$. Determine P_{XX} of $X(n)$ using

$$P_{XX} = \lim_{N\to\infty} \frac{1}{N} \sum_{n=0}^{N-1} \mathsf{E}[X(n)^2].$$

The mean-squared value of $X(n)$ is

$$\begin{aligned}
\mathsf{E}[X(n)^2] &= \mathsf{E}[A^2 \cos(\omega_0 n + \Phi)^2] \\
&= \mathsf{E}[A^2 (1 + \cos(2\omega_0 n + 2\Phi))/2] \\
&= \frac{A^2}{2} + \frac{A^2}{2} \mathsf{E}[\cos(2\omega_0 n + 2\Phi)] \\
&= \frac{A^2}{2} + \frac{A^2}{2} \int_0^{\pi/2} \cos(2\omega_0 n + 2\varphi) \frac{2}{\pi} d\varphi \\
&= \frac{A^2}{2} + \frac{A^2}{2} \frac{2}{\pi} \left[\frac{\sin(2\omega_0 n + 2\varphi)}{2} \right]_0^{\pi/2} \\
&= \frac{A^2}{2} + \frac{A^2}{2} \frac{2}{\pi} \left[\frac{\sin(2\omega_0 n + \pi) - \sin(2\omega_0 n)}{2} \right] \\
&= \frac{A^2}{2} - \frac{A^2}{\pi} \sin(2\omega_0 n)
\end{aligned}$$

where we have used the fact that $\sin(\varphi + \pi) = -\sin(\varphi)$. $X(n)$ is non-stationary because $\mathsf{E}[X(n)^2]$ is a function of time. The time average of the above expression is

$$\lim_{N\to\infty} \frac{1}{N} \sum_{n=0}^{N-1} \left[\frac{A^2}{2} - \frac{A^2}{\pi} \sin(2\omega_0 n) \right] = \frac{A^2}{2}$$

The Cross-Power Spectral Density

Suppose we have observations $x_N(n)$ and $y_N(n)$ of a random process $X(n)$ and $Y(n)$, respectively. Let $X_N(e^{j\omega})$ and $Y_N(e^{j\omega})$ be their respective finite Fourier transforms, i.e.

$$X_N(e^{j\omega}) = \sum_{n=0}^{N-1} x_N(n) e^{-j\omega n}$$

and

$$Y_N(e^{j\omega}) = \sum_{n=0}^{N-1} y_N(n) e^{-j\omega n}$$

The cross-spectral density function is given as

$$S_{XY}(e^{j\omega}) = \lim_{N\to\infty} \frac{1}{N} \mathsf{E}\left[X_N(e^{j\omega}) Y_N(e^{j\omega})^* \right]$$

and thus the total average cross power is

$$P_{XY} = \frac{1}{2\pi} \int_{-\pi}^{\pi} S_{XY}(e^{j\omega}) d\omega.$$

8 Introduction to Digital Spectral Analysis

In many areas of signal processing, the signals of interest are considered to be of random nature. Even when they are not, our limited understanding of the mechanisms by which they were generated often requires to regard them as random. In the following, we briefly describe some examples.

- Communications: during the transmission of a communication signal via a cable or wireless channel, noise occurs, e.g. thermal noise or noise due to quantization errors. From the receiver's perspective, the signal has to be considered as random, as neither the original noise-free signal nor the noise is known at the receiver side.

- Computer networks: consider the traffic of some web site, i.e., the amount of data which visitors of that site send and receive. The mechanisms generating the web traffic, which are the behavior and interests of each individual person connected to the internet, are unavailable to the provider of the web site. Due to this lack of knowledge, one has to consider the web traffic to be of random nature.

- Finance: quantities such as stock prices, future investment values, etc. are often considered as, at least partially, affected by random processes. Spectral estimation is often used to analyze data and support financial theory.

- Geophysics: In geophysics physical methods are used to study both the surface of the earth and the underground. The mechanisms which generate seismic or geothermal processes (e.g. tectonic, volcanic or atmospheric sources) are in most cases unavailable and far too complicated to be examined. Thus, each measurement has to be considered as being a realization of a random process.

- Medicine: common methods to analyze brain and heart activity are the electroencephalogram (EEG) and the electrocardiogram (ECG). The biological mechanisms which generate the respective signals (e.g. interaction of neurons or reaction of a patient to outer influences) are generally unavailable and far too complex. The recording of heart beats or brain activity using electrodes, is therefore considered as a realization of a random process.

In many cases, the informational content of a time-domain representation is limited, and/or hard to interpret. A representation in the spectral domain is needed to extract important information of the process of interest. Some application examples are listed and described in the following.

- Detection of periodicities: periodicities often occur in natural signals. When purely relying on the time domain, these periodicities may not be visible, especially when their energy is relatively low compared to the contribution of other frequency bands. In the spectral domain, one is able to distinguish between different periodicities.

  For example, in seismology there are three main types of waves: P-Waves and S-Waves propagate due to particle motion in the propagation direction and perpendicular to the propagation motion, respectively. Surface waves only propagate on the earth's surface. These waves which occur with different speed can be distinguished in the spectral domain.

- Diagnosis: the spectrum gives an indication of the energy contribution at individual frequencies. A spectral representation can be used to determine which frequency bands are dominant, and which are negligible. This is useful for subsequent steps such as filtering and more generally for process understanding.

  For example, consider the mechanical engineering example of abnormal combustion in a spark ignition engine. This so called engine knock can destroy parts of the engine and disturb passengers with uncomfortable

noise. Given the recording of a combustion cycle one can use spectral techniques to detect knock. Early detection of knock is needed, e.g. for reduction of pollution. The presence of knock is characterized by energy in the frequency band between 7kHz and 35kHz, depending on the type of the engine and geometry, which can be detected in the spectrum.

- Better interpretation: Often, the important information of a signal is not visible in the time, but in the spectral domain.

  For example, when working with EEG signals one can use the spectrum to get information about the patient's condition. In the spectral domain EEG signals are divided into specific frequency bands, all of them are associated with certain conditions. When the patient is relaxed, there will be a relatively high amount of energy in the so-called alpha-band (8-13 Hz). A high amount of energy in the delta-band (0.3-3.5 Hz) on the other side means that the patient is in deep sleep. Energy in other frequency bands (gamma, beta, etc.) is associated with high concentration or even pathologies and drug effects.

- Prediction: using spectral techniques one can obtain a probabilistic model of the data. This model can be used to predict the signal's future behavior.

  For example, predictive techniques are widely used for forecasting economical and seasonal processes such as the monthly rainfall or daily temperature. Applications also include predictive coding, e.g. of speech signals where one predicts future samples based on a probabilistic model, and only transmits the prediction error, which is the difference between the original and the predicted sample, in order to save bandwidth.

In practice, one is always faced with finite measurements. Moreover, in most situations, the signal of interest cannot be measured directly as it is subject to distortions and/or additive noise. Thus, the true spectrum can never be calculated, one has to estimate it from the given finite, noisy data at hand. Spectrum estimation has been an active research area for decades. Note that the perfect spectrum estimator does not exist. A variety of estimation techniques have been proposed in the literature - all of them have their advantages and disadvantages and may be more or less suitable for one specific application.

It is the aim of the remaining part of the manuscript to give an overview of the two main branches of spectrum estimation: *non-parametric* and *parametric* spectrum estimation. Non-parametric spectrum estimation is a more general technique in which no specific data model is assumed. When no knowledge about a signal is available, these techniques should be used. On the other hand, if it is known that the signal of interest can be accurately expressed using a probabilistic model, which is the case for many natural signals such as speech, images or geophysical data, this knowledge can be included in the estimation procedure. These techniques are then referred to as parametric techniques.

8.1 The Michelson Interferometer

In spectroscopy, we wish to investigate the distribution of power in a radiation field as a function of frequency (or wavelength/wavenumber). Consider, for example, the situation shown in Figure 8.1 where a Michelson interferometer is used to measure the spectrum of a light source. Let $S(t)$ be a zero-mean stochastic stationary process which may be complex-valued. It can be seen that

$$X(t) = A(S(t-t_0) + S(t-t_0-\tau))$$

and

$$V(t) = |X(t)|^2 = A^2|S(t-t_0) + S(t-t_0-\tau)|^2 .$$

Using the notation $\tilde{t}$ for $t-t_0$, we get

$$V(t) = A^2\left[S(\tilde{t})S(\tilde{t})^* + S(\tilde{t})S(\tilde{t}-\tau)^* + S(\tilde{t}-\tau)S(\tilde{t})^* + S(\tilde{t}-\tau)S(\tilde{t}-\tau)^*\right].$$

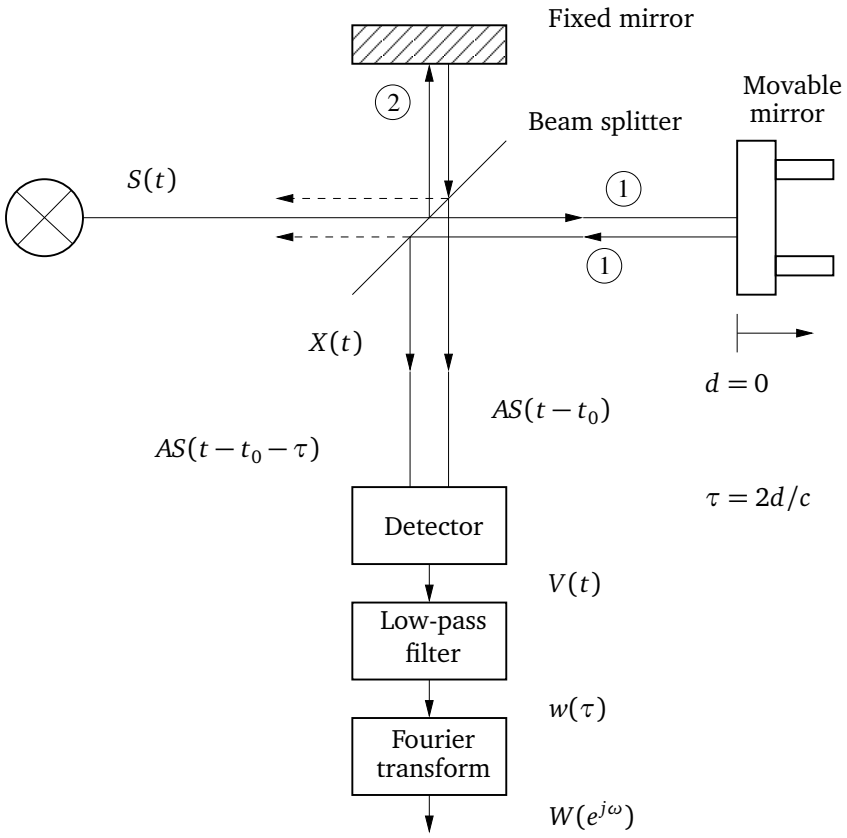

Figure 8.1.: Measuring the spectrum of a light source using a Michelson interferometer.

After low-pass filtering, we obtain (ideally)

$$\begin{aligned} w(\tau) = \mathsf{E}[V(t)] &= A^2\left[c_{SS}(0) + c_{SS}(\tau) + c_{SS}(-\tau) + c_{SS}(0)\right] \\ &= A^2\left[2c_{SS}(0) + 2\mathrm{Re}\{c_{SS}(\tau)\}\right] \end{aligned}$$

Performing a Fourier transform leads to

$$W(e^{j\omega}) = \mathscr{F}\{w(\tau)\} = A^2(2c_{SS}(0)\delta(\omega) + C_{SS}(e^{j\omega}) + C_{SS}(e^{-j\omega}))$$

Thus, the output of a Michelson interferometer is proportional to the spectrum of the light source. One of the objectives in spectroscopic interferometry is to get a good estimate of the spectrum of $S(t)$ without moving the mirror a large d.

8.2 Spectrum Estimation using Bandpass Filters

A simple device for measuring the spectrum could be as follows: A narrow band pass with variable center frequency is used to filter the signal of interest. The signal power of the band pass output gives an estimate of the spectrum in a certain frequency band.

Let $X(n)$ be a stationary stochastic process with zero-mean $\mathsf{E}[X(n)] = 0$, covariance function $c_{XX}(\kappa)$ and spectrum $C_{XX}(e^{j\omega})$. If we transform $X(n)$ by

$$Y(n) = X(n)^2$$

then

$$\mathsf{E}[Y(n)] = \mathsf{E}[X(n)^2] = c_{XX}(0) = \frac{1}{2\pi}\int_{-\pi}^{\pi} C_{XX}(e^{j\omega})d\omega$$

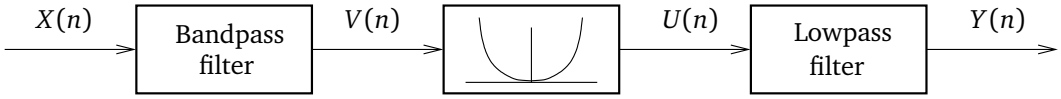

Figure 8.2.: Spectrum estimation using a bandpass filter with variable center frequency, squaring device and low-pass filter for averaging.

This motivates to estimate the spectrum as shown in Figure 8.2.

The bandpass filter has the transfer function

$$H_B(e^{j\omega}) = \begin{cases} H_B^0, & |\omega \pm \omega_0| \leq \frac{B}{2} \\ 0, & \text{otherwise}, \end{cases}$$

where magnitude H_B^0 will be specified later and ω_0 is the center frequency of the filter, as depicted in Figure 8.3.

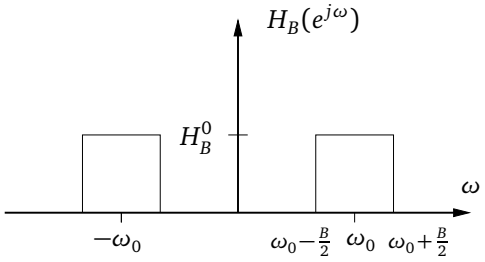

Figure 8.3.: Transfer function of an ideal band-pass filter.

To calculate the mean, we use an FIR lowpass filter with impulse response $h_L(n) = \frac{1}{N}$ for $n = 0, \ldots, N-1$ and 0 otherwise. The corresponding frequency response is given by

$$H_L(e^{j\omega}) = \frac{1}{N} \frac{\sin(\omega N/2)}{\sin(\omega/2)} e^{-j\omega(N-1)/2}$$

The spectrum of $V(n)$ is given by

$$C_{VV}(e^{j\omega}) = |H_B(e^{j\omega})|^2 C_{XX}(e^{j\omega})$$

The output process is given by

$$Y(n) = \sum_{m=0}^{N-1} \frac{1}{N} U(n-m) = \frac{1}{N} \sum_{m=0}^{N-1} V(n-m)^2$$

The mean of $Y(n)$ is given by

$$\mu_Y = \mathsf{E}[Y(n)] = \frac{1}{N} \sum_{m=0}^{N-1} \mathsf{E}[V(n-m)^2] = c_{VV}(0)$$

where $c_{VV}(0)$ can be expressed as an inverse Fourier transform at $n = 0$ as follows

$$\begin{aligned} \mu_Y &= \frac{1}{2\pi} \int_{-\pi}^{\pi} C_{VV}(e^{j\omega}) d\omega \\ &= \frac{1}{2\pi} \int_{-\pi}^{\pi} |H_B(e^{j\omega})|^2 C_{XX}(e^{j\omega}) d\omega \\ &= \frac{(H_B^0)^2}{\pi} \int_{\omega_0 - B/2}^{\omega_0 + B/2} C_{XX}(e^{j\omega}) d\omega \approx (H_B^0)^2 \frac{B}{\pi} C_{XX}(e^{j\omega_0}) \end{aligned}$$

If we choose the magnitude of the narrow band pass to be $H_B^0 = 1$, $\mu_Y = \mathsf{E}[Y(n)]$ measures the power of $X(n)$ in the frequency band $|\omega - \omega_0| \leq B/2$. On the other hand, the spectral value $C_{XX}(e^{j\omega_0})$ will be measured if we choose $H_B^0 = \sqrt{\pi/B}$, provided $B \ll \omega_0$ and $C_{XX}(e^{j\omega})$ is continuous at $\omega = \omega_0$. Note that, under the assumption that $X(n)$ is Gaussian, one can show that

$$\sigma_Y^2 \approx \frac{2\pi}{BN} C_{XX}(e^{j\omega_0})^2.$$

To measure $C_{XX}(e^{j\omega})$ in a larger frequency band, we would need a filter bank with a cascade of squarers and integrators. In some applications of acoustics, one can use such a circuit, where the center frequencies are taken to be $\omega_{k+1} = (2\omega_k)^{1/3}, k = 1, \ldots, K-1$. This is the principle of a spectral analyzer, especially when it is used for analyzing analog signals. Such a spectral analyzer yields the spectrum at frequencies $\omega_1, \ldots, \omega_k$ simultaneously. In measurement technology, one uses simpler systems that work with a band pass having variable center frequency. The signal of the system output provides an estimate of the spectrum in a certain frequency band. In that case, the accuracy of the measurement system depends on the slowness of changing the center frequency and the smoothness of the spectrum of $X(n)$.

9 Non-Parametric Spectrum Estimation

9.1 Introduction

We begin with another motivating example for spectrum estimation.

Example 9.1.1 *The sunspot number is a quantity which measures the number of sunspots and groups of sunspots present on the surface of the sun. The annual sunspot number has been collected and tabulated by researchers for around 300 years. They have found that sunspot activity is cyclical and reaches its maximum around every 9.5 to 11 years*

Figure 9.1 (left) shows an excerpt of the time-series, Figure 9.1 (right) shows $\frac{1}{N}|X_N(e^{j\omega})|^2$ *in a dB scale. Note that, according to the motivation in Section 7.3, the magnitude squared of the finite Fourier transform divided by N represents a measure for the distribution of power over frequency, and serves as an estimator for the spectrum.*

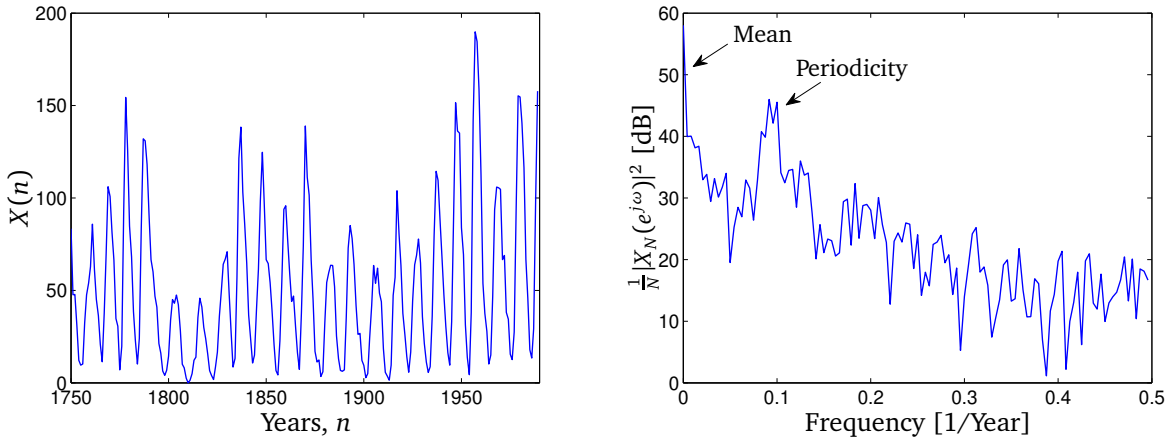

Figure 9.1.: Sunspot number example: excerpt of the time series (left) and the magnitude squared of the finite Fourier transform divided by N (right).

It can be seen in the time-series that the period of the cyclic pattern is ≈ 10 *years, and that there is a positive mean. This observation is confirmed in the spectrum estimate, where we see a strong peak at frequency* $1/10$ *years, which corresponds to the periodicity, and a strong peak at frequency* 0*, which corresponds to the mean.*

In estimation theory, we want to estimate some quantity, or parameter, based on a finite amount of data, often denoted $X(n)$, $n = 0, \ldots, N-1$. In particular, we want to estimate the spectrum at a certain frequency ω. Here, the true spectrum is denoted by $C_{XX}(e^{j\omega})$, and the estimator is denoted by $\hat{C}_{XX}(e^{j\omega})$.

Of course, a good estimator should approximate the true value as closely as possible. Commonly, the quality (or goodness) of an estimator is assessed in terms of its (asymptotic) bias and variance, or equivalently the mean squared error (MSE). For example, an estimator is called *consistent* if the MSE converges to zero as the number of samples gets very large. We will define these quantities in detail later.

To introduce the ideas of estimation and consistency, we present a simple example, in which we estimate the mean value of a random process.

Example 9.1.2 *The sample mean. Let* $X(0), \ldots, X(N-1)$ *be independent real random variables, each distributed as* $\mathcal{N}(\mu_X, \sigma_X^2)$*. Determine the bias and the variance of the sample mean estimator, which is given by*

$$\hat{\mu}_X = \frac{1}{N}\sum_{n=0}^{N-1} X(n)$$

Since the random variables are independent, the expected value can be easily calculated as

$$\mathsf{E}[\hat{\mu}_X] = \mathsf{E}\left[\frac{1}{N}\sum_{n=0}^{N-1} X(n)\right] = \frac{1}{N}\sum_{n=0}^{N-1}\mathsf{E}[X(n)] = \frac{1}{N}\sum_{n=0}^{N-1}\mu_X = \mu_X$$

The bias, which is defined as the difference between the expected value of the estimator and the true parameter, is given by $\mathsf{bias}[\hat{\mu}_X] = \mathsf{E}[\hat{\mu}_X] - \mu_X = 0$.

Further, using the identity $\mathsf{Var}[aX] = a^2\mathsf{Var}[X]$ *for any real-valued constant a, and the fact that the random variables are independent, we can calculate the variance as*

$$\mathsf{Var}[\hat{\mu}_X] = \mathsf{Var}\left[\frac{1}{N}\sum_{n=0}^{N-1} X(n)\right] = \frac{1}{N^2}\sum_{n=0}^{N-1}\mathsf{Var}[X(n)] = \frac{1}{N^2}\sum_{n=0}^{N-1}\sigma_X^2 = \frac{\sigma_X^2}{N}$$

The mean square error (MSE) is defined as $\mathsf{MSE}[\hat{\mu}_X] = \mathsf{E}[(\hat{\mu}_X - \mu_X)^2]$ *and can be rewritten in terms of the variance and bias, as follows*

$$\begin{aligned}\mathsf{MSE}[\hat{\mu}_X] &= \mathsf{E}[\hat{\mu}_X^2] - 2\mathsf{E}[\hat{\mu}_X]\mu_X + \mu_X^2 - \mathsf{E}[\hat{\mu}_X]^2 + \mathsf{E}[\hat{\mu}_X]^2 \\ &= \mathsf{E}[\hat{\mu}_X^2] - \mathsf{E}[\hat{\mu}_X]^2 + (\mathsf{E}[\hat{\mu}_X] - \mu_X)^2 \\ &= \mathsf{Var}[\hat{\mu}_X] + \mathsf{bias}[\hat{\mu}_X]^2\end{aligned}$$

Note that we have added and subtracted the term $\mathsf{E}[\hat{\mu}_X]^2$ *in the first line. Because the sample mean is an unbiased estimator, we have* $\mathsf{MSE}[\hat{\mu}_X] = \mathsf{Var}[\hat{\mu}_X]$.

An estimator is called consistent if for $N \to \infty$*, we have* $\mathsf{MSE}[\hat{\mu}_X] = 0$*. Consequently, the sample mean is a consistent estimator for the mean value* μ_X.

Consistency of Spectral Estimators

An estimator $\hat{C}_{XX}(e^{j\omega})$ of the spectrum $C_{XX}(e^{j\omega})$ is a random variable. If we could design an ideal estimator for the spectrum, we would desire it to be unbiased and the variance to be zero, i.e. $\mathsf{E}[\hat{C}_{XX}(e^{j\omega})] = C_{XX}(e^{j\omega})$ and $\mathsf{Var}[\hat{C}_{XX}(e^{j\omega})] = 0$, respectively, for all frequencies ω. Note that the pdf of this ideal estimator would be a delta function at the true value.

Because it is impossible to create an ideal estimator, we try to reach this goal asymptotically as the number N of observed samples $X(n)$, $n = 0, 1, \ldots, N-1$ tends to infinity. In this case, we require that for large N, the estimator $\hat{C}_{XX}(e^{j\omega})$ approaches the true spectrum. An estimator is called consistent if it converges in probability to the true value as N increases. A sufficient condition for consistency is that the mean square error (MSE) of the estimator converges to zero as $N \to \infty$, i.e.

$$\lim_{N\to\infty} \mathsf{E}\left[\left(\hat{C}_{XX}(e^{j\omega}) - C_{XX}(e^{j\omega})\right)^2\right] = 0.$$

As we have seen in Example 9.1.2 (relation between MSE, variance and bias), this is equivalent with

$$\lim_{N\to\infty} \mathsf{Var}\left[\hat{C}_{XX}(e^{j\omega})\right] = 0$$

and

$$\lim_{N\to\infty} \mathsf{bias}\left[\hat{C}_{XX}(e^{j\omega})\right] = 0.$$

We remark that if $\mathsf{E}[\hat{C}_{XX}(e^{j\omega})] \neq C_{XX}(e^{j\omega})$ the estimator has a bias which results in a systematic error of the method. On the other hand if $\mathsf{Var}[\hat{C}_{XX}(e^{j\omega})] \neq 0$, we get a random error, i.e. the estimates vary from data set to data set.

9.2 The Periodogram

As motivated in Example 9.1.1, the periodogram

$$I_{XX}^N(e^{j\omega}) = \frac{1}{N}\left|X_N(e^{j\omega})\right|^2 = \frac{1}{N}\left|\sum_{n=0}^{N-1} X(n)e^{-j\omega n}\right|^2$$

is a candidate estimator for the spectrum $C_{XX}(e^{j\omega})$. Note that $I_{XX}^N(e^{j\omega})$ has the same symmetry, non-negativity and periodicity properties as $C_{XX}(e^{j\omega})$. The periodogram was introduced by Schuster in 1898, as a tool for the identification of hidden periodicities. As a matter of fact, he was also experimenting with the sunspot data, as in Example 9.1.1. Indeed, in the case of

$$X(n) = \sum_{k=1}^{K} a_k \cos(\omega_k n + \phi_k), \quad n = 0, \ldots, N-1$$

and provided N is large, the periodogram $I_{XX}^N(e^{j\omega})$ for $\omega \in (0,\pi)$ has peaks at frequencies $\omega = \omega_k$, $k = 1, \ldots, K$.

Next, we want to discuss the distribution, in terms of mean and variance of the periodogram. We begin with the simple case of a white Gaussian process, as treated in Example 7.2.1. The result is extended later to the general case of a random process with an arbitrary $c_{XX}(\kappa)$ and $C_{XX}(e^{j\omega})$.

Example 9.2.1 *Distribution of the periodogram of a white process. As in Example 7.2.1, let $X(0), \ldots, X(N-1)$ be independent real random variables, each distributed as $\mathcal{N}(0,1)$. Let $N = 2^r$ where $r \in \mathbb{N}$. Determine the distribution of $I_{XX}^N(e^{j\omega})$ at $\omega = 2\pi k/N$ for $k = 0, \ldots, N/2-1$. Further, determine the mean and variance.*

We know from Example 7.2.1 that the distribution of the real and imaginary part of the finite Fourier transform for a real white Gaussian process is

$$\begin{bmatrix} \mathsf{Re}\{X_N(e^{j2\pi k/N})\} \\ \mathsf{Im}\{X_N(e^{j2\pi k/N})\} \end{bmatrix} \sim \mathcal{N}\left(\begin{bmatrix} 0 \\ 0 \end{bmatrix}, \frac{N}{2}\begin{bmatrix} 1 & 0 \\ 0 & 1 \end{bmatrix}\right), \quad k = 1, \ldots, N/2-1$$

For $k = 0$ and $k = N/2$, the finite Fourier transform is purely real and we have $\mathsf{Re}\{X_N(e^{j2\pi k/N})\} \sim \mathcal{N}(0,N)$.

We can rewrite

$$I_{XX}^N(e^{j2\pi k/N}) = \frac{1}{N}\left(\mathsf{Re}\{X_N(e^{j2\pi k/N})\}^2 + \mathsf{Im}\{X_N(e^{j2\pi k/N})\}^2\right)$$

and observe that the periodogram is the sum of the squares of two independent normal random variables. From Example 6.1.4, we know that if $Y_1, \ldots, Y_\nu$ are independent random variables, each distributed as $\mathcal{N}(0,1)$, then

$$\sum_{n=1}^{\nu} Y_n^2 \sim \chi_\nu^2$$

where χ_ν^2 is the chi-square distribution with ν degrees of freedom. Using normalized variables

$$\sqrt{\frac{2}{N}}\mathsf{Re}\{X_N(e^{j2\pi k/N})\} \sim \mathcal{N}(0,1)$$

and

$$\sqrt{\frac{2}{N}}\mathsf{Im}\{X_N(e^{j2\pi k/N})\} \sim \mathcal{N}(0,1)$$

we can conclude that

$$\frac{2}{N}\left(\mathsf{Re}\{X_N(e^{j2\pi k/N})\}^2 + \mathsf{Im}\{X_N(e^{j2\pi k/N})\}^2\right) \sim \chi_2^2$$

or $I_{XX}^N(e^{j2\pi k/N}) \sim \chi_2^2/2$ for $k = 1, \ldots, N/2-1$. For $k = 0$ and $k = N/2$, on the other hand, the finite Fourier transform is purely real with $\mathsf{Re}\{X_N(e^{j2\pi k/N})\} \sim \mathcal{N}(0,N)$. In that case, we have $I_{XX}^N(e^{j2\pi k/N}) \sim \chi_1^2$.

We also know from Example 6.1.4, that for a random variable, distributed as χ_ν^2 with ν degrees of freedom, the mean and variance are given by ν and 2ν, respectively. Therefore, the mean of the periodogram of a white Gaussian process can be found to be $\mathsf{E}[I_{XX}^N(e^{j2\pi k/N})] = 1$ for $k = 0, \ldots, N/2$. Whereas the variance $\mathsf{Var}[I_{XX}^N(e^{j2\pi k/N})]$ is 1 and 2 for $k = 1, \ldots, N/2-1$ and $k = 0, N/2$, respectively.

In Example 9.2.1, we have introduced the distribution of the periodogram for a special case, namely for a real white Gaussian process. However, we are more interested in the result for the general case of a real-valued stationary random process $X(n)$ with arbitrary mean $\mu_X = \mathsf{E}[X(n)]$, covariance function $c_{XX}(\kappa) = \mathsf{E}[\tilde{X}(n+\kappa)\tilde{X}(n)]$ with $\tilde{X}(n) = X(n) - \mu_X$, and spectrum $C_{XX}(e^{j\omega}) = \sum_{\kappa=-\infty}^{\infty} c_{XX}(\kappa)e^{-j\omega\kappa}$, which is assumed to be uniformly continuous and bounded. As stated in Section 7.2, the asymptotic distribution of the finite Fourier transform is

$$\begin{bmatrix} \mathsf{Re}\{X_N(e^{j\omega})\} \\ \mathsf{Im}\{X_N(e^{j\omega})\} \end{bmatrix} \sim \mathcal{N}\left(\begin{bmatrix} 0 \\ 0 \end{bmatrix}, \frac{N}{2} C_{XX}(e^{j\omega}) \begin{bmatrix} 1 & 0 \\ 0 & 1 \end{bmatrix} \right), \quad \omega \in (0, \pi)$$

For $\omega = 0$ and $\omega = \pi$, $X_N(e^{j\omega})$ is purely real, and we have $\mathsf{Re}\{X_N(e^{j\omega})\} \sim \mathcal{N}(N\mu_X\delta(\omega), NC_{XX}(e^{j\omega}))$. Based on the derivation in Example 9.2.1, the asymptotic distribution of the periodogram can be shown to be

$$\lim_{N\to\infty} I_{XX}^N(e^{j\omega}) \sim \frac{1}{2} C_{XX}(e^{j\omega})\chi_2^2, \quad \omega \in (0, \pi)$$

and $I_{XX}^N(e^{j\omega}) \sim C_{XX}(e^{j\omega})\chi_1^2$ for $\omega = 0$ and $\omega = \pi$, as $N \to \infty$. Consequently, the asymptotic mean and variance of the periodogram are

$$\lim_{N\to\infty} \mathsf{E}\left[I_{XX}^N(e^{j\omega})\right] = C_{XX}(e^{j\omega})$$

and

$$\lim_{N\to\infty} \mathsf{Var}\left[I_{XX}^N(e^{j\omega})\right] = C_{XX}(e^{j\omega})^2.$$

We conclude that the periodogram is asymptotically unbiased. But its variance does not decrease to zero as N tends to infinity, and so the periodogram is not a consistent estimator for the spectrum.

Example 9.2.2 *Periodogram of filtered white noise. Consider a white random process $Z(n)$ with $C_{ZZ}(e^{j\omega}) = 1$, and a recursive system $H(z) = 1/\prod_{i=1}^{6}(z - z_i)$ with complex conjugate pole pairs $z_{1/2} = 0.7e^{\pm j0.4}$, $z_{3/4} = 0.75e^{\pm j1.3}$ and $z_{5/6} = 0.9e^{\pm j1.9}$. We will see later that the output $X(n)$ to the recursive filter with a white input process is called an autoregressive (AR) process. As shown in Section 6.6, the spectrum of the output is $C_{XX}(e^{j\omega}) = |H(e^{j\omega})|^2$.*

In the left plot of Figure 9.2, we show a realization of the filtered white noise process $X(n)$. In the right plot, we show the corresponding periodogram $I_{XX}(e^{j\omega})$ and the overlaid true spectrum $C_{XX}(e^{j\omega})$.

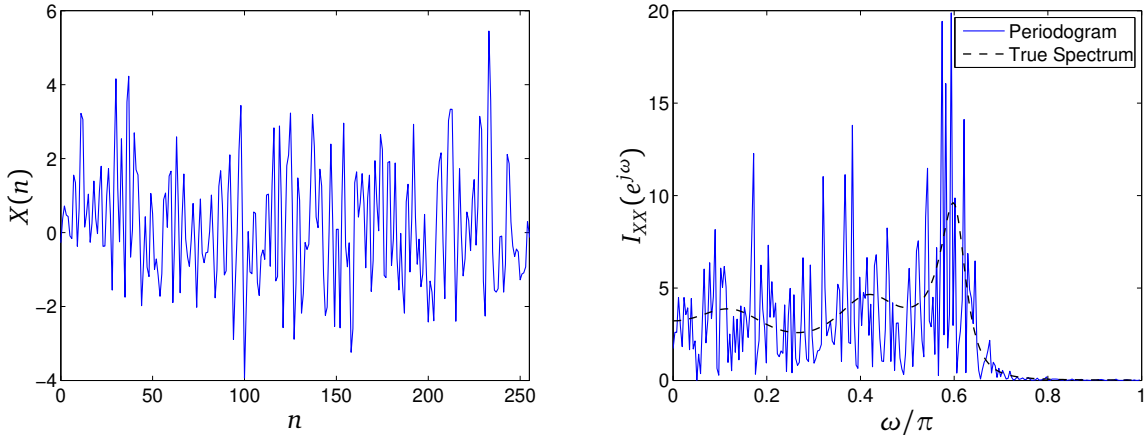

Figure 9.2.: Realization of an AR process $X(n)$ (left), corresponding periodogram estimate $I_{XX}(e^{j\omega})$ and true spectrum $C_{XX}(e^{j\omega})$ (right).

It can be observed that the variance, which corresponds to the fluctuations around the true spectrum, is quite large. Thus, the periodogram is not a suitable estimator for this estimation task.

Note that it is also possible to consider the periodogram of a windowed data sequence, with real-valued window function $w_N(n) \neq 0$, $n = 0, \ldots, N-1$. Then, we have

$$I^N_{WX,WX}(e^{j\omega}) = \frac{1}{NA}\left|\sum_{n=0}^{N-1} w_N(n)X(n)e^{-j\omega n}\right|^2$$

with normalization factor

$$A = \frac{1}{N}\sum_{n=0}^{N-1}|w_N(n)|^2.$$

Note that A is required to preserve the noise power in the spectrum estimate, this will become apparent later on. Advantages of using different window types are stated in the filter design theory part. For instance, we can enhance the dynamic range of the spectrum estimator by using a window with a reduced peak sidelobe level.

Next, we investigate the mean and the variance of the periodogram, when N is finite.

Mean of the Periodogram

Using the definition from Section 9.2 and the fact that $|X_N(e^{j\omega})|^2 = X_N(e^{j\omega})X_N(e^{j\omega})^*$, the mean of the periodogram of a stationary random process $X(n)$, $n = 0, \ldots, N-1$ can be calculated as follows

$$\begin{aligned}
\mathsf{E}\left[I^N_{XX}(e^{j\omega})\right] &= \mathsf{E}\left[\frac{1}{N}\sum_{n=0}^{N-1}X(n)e^{-j\omega n}\sum_{m=0}^{N-1}X(m)^*e^{j\omega m}\right] \\
&= \frac{1}{N}\sum_{n=0}^{N-1}\sum_{m=0}^{N-1}\mathsf{E}\left[X(n)X(m)^*\right]e^{-j\omega(n-m)} \\
&= \frac{1}{N}\sum_{n=0}^{N-1}\sum_{m=0}^{N-1}\left(c_{XX}(n-m)+\mu_X\mu_X^*\right)e^{-j\omega(n-m)} \\
&= \frac{1}{N}\sum_{n=0}^{N-1}\sum_{m=0}^{N-1}c_{XX}(n-m)e^{-j\omega(n-m)} + \frac{1}{N}\left|\Delta^N(e^{j\omega})\right|^2\mu_X\mu_X^* \\
&= \frac{1}{N}\sum_{n=0}^{N-1}\sum_{m=0}^{N-1}e^{-j\omega(n-m)}\frac{1}{2\pi}\int_{-\pi}^{\pi}C_{XX}(e^{j\lambda})e^{j\lambda(n-m)}d\lambda + \frac{1}{N}\left|\Delta^N(e^{j\omega})\right|^2\mu_X\mu_X^* \\
&= \frac{1}{2\pi}\int_{-\pi}^{\pi}C_{XX}(e^{j\lambda})\frac{1}{N}\left|\Delta^N(e^{j(\omega-\lambda)})\right|^2 d\lambda + \frac{1}{N}\left|\Delta^N(e^{j\omega})\right|^2\mu_X\mu_X^*
\end{aligned}$$

where

$$\Delta^N(e^{j\omega}) = \sum_{n=0}^{N-1}e^{-j\omega n} = e^{-j\omega(N-1)/2}\frac{\sin(\omega N/2)}{\sin(\omega/2)}$$

is the Fourier transform of a rectangular window. Thus, for a zero mean stationary process $X(n)$, the expected value of the periodogram $I^N_{XX}(e^{j\omega})$, $\mathsf{E}[I^N_{XX}(e^{j\omega})]$ is equal to the spectrum $C_{XX}(e^{j\omega})$ convolved with the magnitude squared of the Fourier transform of the rectangular window, $\frac{1}{N}|\Delta^N(e^{j\omega})|^2$. This function is shown in Figure 9.3 for $N = 20$, $N = 10$ and $N = 5$.

It can be observed from Figure 9.3 that $\frac{1}{N}|\Delta^N(e^{j\omega})|^2$ converges to a delta function $2\pi\delta(\omega)$, as N tends to infinity. This suggests that

$$\lim_{N\to\infty}\mathsf{E}\left[I^N_{XX}(e^{j\omega})\right] = C_{XX}(e^{j\omega}) + \mu_X\mu_X^* 2\pi\delta(\omega), \quad \omega \in [-\pi, \pi)$$

Therefore the periodogram estimate is asymptotically unbiased for $\omega \neq 0$. We may find an asymptotic unbiased estimator for $C_{XX}(e^{j\omega})$ for all $\omega \in [-\pi, \pi)$ by subtracting the sample mean of the data, before computing the periodogram.

When a windowed data sequence is considered, with window function $w_N(n) \neq 0$, $n = 0, \ldots, N-1$ and corresponding Fourier transform $W^N(e^{j\omega})$, the derivation of the mean of $I^N_{WX,WX}(e^{j\omega})$ is similar to the one above. In this case, we would include normalization factor A and replace the Fourier transform of the rectangular window $\Delta^N(e^{j\omega})$ by the Fourier transform of the employed window $W^N(e^{j\omega}) = \sum_{n=0}^{N-1} w_N(n)e^{-j\omega n}$.

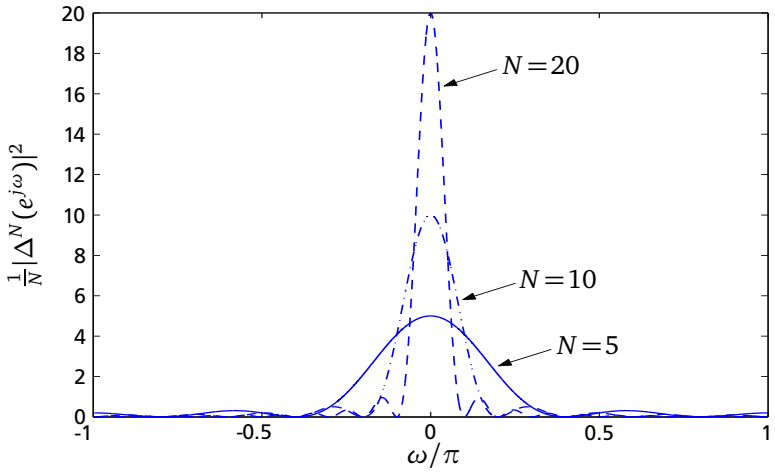

Figure 9.3.: Periodogram of the rectangular window function $\frac{1}{N}|\Delta^N(e^{j\omega})|^2$ for length $N = 20$, $N = 10$ and $N = 5$.

Variance of the Periodogram

To find the variance of the periodogram we consider the covariance function of the periodogram. For simplicity, let us assume that $X(n)$ is a real-valued white Gaussian process with variance σ^2 and $\omega, \lambda \neq 0$. Then,

$$\begin{aligned}\mathrm{Cov}\left[I_{XX}^N(e^{j\omega}), I_{XX}^N(e^{j\lambda})\right] &= \mathrm{E}\left[I_{XX}^N(e^{j\omega})I_{XX}^N(e^{j\lambda})\right] - \mathrm{E}\left[I_{XX}^N(e^{j\omega})\right]\mathrm{E}\left[I_{XX}^N(e^{j\lambda})\right] \\ &= \frac{1}{N^2}\left(\left|\Delta^N(e^{j(\omega+\lambda)})\right|^2 + \left|\Delta^N(e^{j(\omega-\lambda)})\right|^2\right)\sigma^4.\end{aligned}$$

The above result can be proven with the *formula of Isserlis*, which states that for zero-mean Gaussian random variables X_1, X_2, X_3 and X_4, we have $\mathrm{E}\left[X_1X_2X_3X_4\right] = \mathrm{E}[X_1X_2]\mathrm{E}[X_3X_4] + \mathrm{E}[X_1X_3]\mathrm{E}[X_2X_4] + \mathrm{E}[X_1X_4]\mathrm{E}[X_2X_3]$. If the process $X(n)$ is non-white and non-Gaussian, the covariance is given by (Brillinger, 1981)

$$\mathrm{Cov}\left[I_{XX}^N(e^{j\omega}), I_{XX}^N(e^{j\lambda})\right] \approx C_{XX}(e^{j\omega})^2\frac{1}{N^2}\left(\left|\Delta^N(e^{j(\omega+\lambda)})\right|^2 + \left|\Delta^N(e^{j(\omega-\lambda)})\right|^2\right),$$

which reduces the variance of the periodogram to

$$\mathrm{Var}\left[I_{XX}^N(e^{j\omega})\right] \approx C_{XX}(e^{j\omega})^2\frac{1}{N^2}\left(\left|\Delta^N(e^{j2\omega})\right|^2 + N^2\right), \quad \omega \in (0, \pi).$$

This confirms the asymptotic results. No matter how large N is, the variance of $I_{XX}^N(e^{j\omega})$ remains at the level $C_{XX}(e^{j\omega})^2$. Consequently, if an estimator with a variance smaller than this is desired, it cannot be obtained by simply increasing the sample length N.

When a windowed data sequence is considered, we proceed similarly as discussed for the mean. In this case, the variance of $I_{WX,WX}^N(e^{j\omega})$ is obtained by including the normalization factor A and replacing the term $|\Delta^N(e^{j2\omega})|^2$ with $|W^N(e^{j2\omega})|^2$.

9.3 Averaging Periodograms

We next describe two techniques for reducing the variance of the periodogram based on segmenting (and windowing) the data sequence, namely Bartlett's method and Welch's method. These techniques are based on the intuitive idea that we can reduce the variance of an estimator by averaging estimators obtained from independent measurements.

The following results are based on precise statistical assumptions imposed on the stationary process $X(n)$, which can be found in (Brillinger, 1981). Our treatment will be based on intuitive interpretations of these assumptions.

If we assume that the covariance function $c_{XX}(\kappa)$ of the process $X(n)$ is finite or can be viewed as finite with a small error and the length of $c_{XX}(\kappa)$ is much smaller than the length of the data stretch N, then we can divide the process $X(n)$ of length N into L parts with length M each, where $M \ll N$. Segment l is given by

$$X_l(n) = X(n + (l-1)M), \quad n = 0, \ldots, M-1$$

The segmentation is illustrated in Figure 9.4.

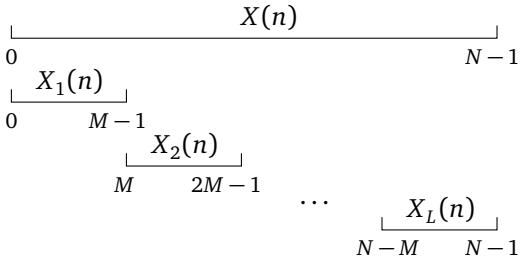

Figure 9.4.: Segmentation of $X(n)$ for periodogram averaging.

With the above assumption, the segments $X_l(n)$, $l = 1, \ldots, L$, are nearly independent, and we can calculate L nearly independent periodograms $I_{XX}^M(e^{j\omega}, l)$ as

$$I_{XX}^M(e^{j\omega}, l) = \frac{1}{M} \left| \sum_{n=0}^{M-1} X_l(n) e^{-j\omega n} \right|^2 .$$

By averaging the result, we obtain the so-called *Bartlett estimator* (named after its invention by Bartlett in 1953) as

$$\hat{C}_{XX}^B(e^{j\omega}) = \frac{1}{L} \sum_{l=1}^{L} I_{XX}^M(e^{j\omega}, l) .$$

To check the performance of the estimator we have to derive the mean and the variance. Assuming the periodograms of the segments to be nearly independent, the mean of the Bartlett estimator $\hat{C}_{XX}^B(e^{j\omega})$ can be easily obtained as

$$\mathsf{E}\left[\hat{C}_{XX}^B(e^{j\omega})\right] = \mathsf{E}\left[\frac{1}{L} \sum_{l=1}^{L} I_{XX}^M(e^{j\omega}, l)\right] = \frac{1}{L} \sum_{l=1}^{L} \mathsf{E}\left[I_{XX}^M(e^{j\omega}, l)\right] \approx \mathsf{E}\left[I_{XX}^M(e^{j\omega})\right]$$

which is the same as the mean of the periodogram of the process $X(n)$ for $n = 0, \ldots, M-1$. From Section 9.2, we know that for $M \to \infty$ the periodogram is asymptotically unbiased, and thus the Bartlett estimator is an unbiased estimator of the spectrum.

Also, the variance of the Bartlett estimator can be calculated as

$$\mathsf{Var}\left[\hat{C}_{XX}^B(e^{j\omega})\right] = \mathsf{Var}\left[\frac{1}{L} \sum_{l=1}^{L} I_{XX}^M(e^{j\omega}, l)\right] = \frac{1}{L^2} \sum_{l=1}^{L} \mathsf{Var}\left[I_{XX}^M(e^{j\omega}, l)\right] \approx \frac{1}{L} \mathsf{Var}\left[I_{XX}^M(e^{j\omega})\right]$$

which is the same as the variance of the periodogram of the process $X(n)$ for $n = 0, \ldots, M-1$ but divided by L. Therefore, asymptotically for $M \to \infty$ we obtain an estimator whose variance decreases with an increasing L

$$\lim_{M \to \infty} \mathsf{Var}\left[\hat{C}_{XX}^B(e^{j\omega})\right] \approx \frac{1}{L} C_{XX}(e^{j\omega})^2$$

Note that due to $N = ML$, not both L and M can be arbitrarily large. For the asymptotic result to be valid, we actually require N and M to be large, and L to be finite.

Based on the derivation from Example 9.2.1, and due to the fact that the sum of L independent χ^2_2 distributed variables is χ^2_{2L} distributed, the asymptotic distribution of the Bartlett estimator can be shown to be

$$\lim_{M\to\infty} \hat{C}^B_{XX}(e^{j\omega}) \sim \frac{1}{2L} C_{XX}(e^{j\omega})\chi^2_{2L}, \quad \omega \in (0,\pi)$$

and $\hat{C}^B_{XX}(e^{j\omega}) \sim \frac{1}{L} C_{XX}(e^{j\omega})\chi^2_L$ for $\omega = 0$ and $\omega = \pi$, as $M \to \infty$.

Example 9.3.1 *Bartlett estimate of filtered white noise. Consider the same process as in Example 9.2.2. For comparison, we show again the periodogram in the left plot of Figure 9.5. In the right plot, we show the corresponding Bartlett estimate $\hat{C}^B_{XX}(e^{j\omega})$ when using $L = 4$ segments, and the overlaid true spectrum $C_{XX}(e^{j\omega})$.*

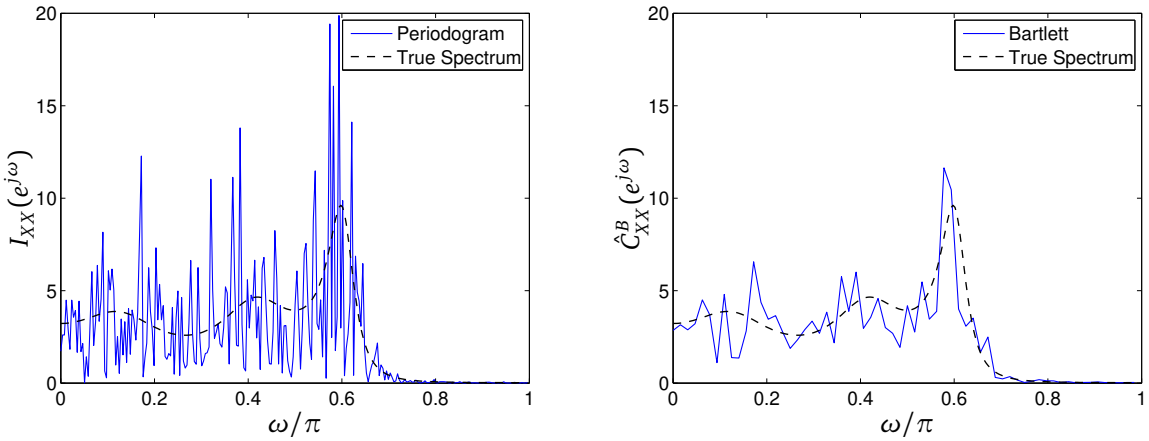

Figure 9.5.: Periodogram estimate $I_{XX}(e^{j\omega})$ (left) and Bartlett estimate $\hat{C}^B_{XX}(e^{j\omega})$ with $L = 4$ segments (right) of the data sequence from Example 9.2.2.

It can be observed that the variance, which corresponds to the fluctuations around the true spectrum, has been reduced drastically.

Welch Estimator

The idea of Bartlett's method was to reduce the variance by averaging nearly independent periodograms of data segments at a given frequency ω. Another more general method for spectrum estimation based on periodogram averaging was developed by Welch in 1967, hence called *Welch estimator*. The idea of this method is to allow the data segments to overlap. Additionally, the segments can be multiplied by a window function.

For each periodogram $l = 1,\ldots,L$ segment l is now defined as

$$X_l(n) = X(n + (l-1)D), \quad n = 0,\ldots,M-1$$

where $(l-1)D$ is the starting point of segment l. For instance, if we choose $D = M/2$ there will be $L = 2N/M - 1$ segments with an overlap of 50%. On the other hand, if we choose $D = M$, there will be $L = N/M$ segments with no overlap, as shown in Figure 9.4.

The periodograms are defined similarly as for the Bartlett estimator, except for a multiplication by a window function $w_M(n)$, i.e. we have

$$I^M_{WX,WX}(e^{j\omega}, l) = \frac{1}{MA}\left|\sum_{n=0}^{M-1} w_M(n)X_l(n)e^{-j\omega n}\right|^2$$

with normalization factor

$$A = \frac{1}{M}\sum_{n=0}^{M-1} |w_M(n)|^2.$$

By averaging the result, Welch defined his estimator as

$$\hat{C}^W_{WX,WX}(e^{j\omega}) = \frac{1}{L}\sum_{l=1}^{L} I^M_{WX,WX}(e^{j\omega}, l)$$

If we set $D = M$ and $w_M(n)$ as a rectangular window of length M, the Welch estimator is equivalent to the Bartlett estimator. Thus, Bartlett's method is a special case of Welch's method.

To check the performance of the estimator, we have to derive the mean and the variance. As for the Bartlett estimator, assuming the periodograms to be nearly independent, the mean of the Welch estimator $\hat{C}^W_{WX,WX}(e^{j\omega})$ is obtained as

$$\mathsf{E}\left[\hat{C}^W_{WX,WX}(e^{j\omega})\right] = \mathsf{E}\left[\frac{1}{L}\sum_{l=1}^{L} I^M_{WX,WX}(e^{j\omega}, l)\right] = \frac{1}{L}\sum_{l=1}^{L}\mathsf{E}\left[I^M_{WX,WX}(e^{j\omega}, l)\right] \approx \mathsf{E}\left[I^M_{WX,WX}(e^{j\omega})\right]$$

From the analysis of the mean of the periodogram of a windowed sequence (including normalization factor A and replacing $\Delta^M(e^{j\omega})$ by $W^M(e^{j\omega})$), we know that

$$\mathsf{E}\left[I^M_{WX,WX}(e^{j\omega})\right] = \frac{1}{2\pi}\int_{-\pi}^{\pi} C_{XX}(e^{j\lambda})\frac{1}{MA}\left|W^M(e^{j(\omega-\lambda)})\right|^2 d\lambda + \frac{1}{MA}\left|W^M(e^{j\omega})\right|^2 \mu_X^2$$

Using Parseval's theorem, we have

$$\frac{1}{2\pi}\int_{-\pi}^{\pi} |W^M(e^{j\lambda})|^2 d\lambda = \sum_{n=0}^{M-1} |w_M(n)|^2 = MA.$$

Assuming now that M is large, the energy of $W^M(e^{j\omega})$ is concentrated around $\omega = 0$, and we can state approximately

$$\mathsf{E}\left[I^M_{WX,WX}(e^{j\omega})\right] \approx \frac{1}{MA}C_{XX}(e^{j\omega})\frac{1}{2\pi}\int_{-\pi}^{\pi} |W^M(e^{j\lambda})|^2 d\lambda + \frac{1}{MA}\left|W^M(e^{j\omega})\right|^2 \mu_X^2 \approx C_{XX}(e^{j\omega}), \quad \omega \neq 0$$

we see that for $\omega \neq 0$ and $M \to \infty$ the windowed periodogram, and therewith the Welch estimator, is unbiased.

For $M \to \infty$, the variance of the Welch estimator for non-overlapping data segments with $D = M$ is asymptotically the same as for the Bartlett estimator (unwindowed data)

$$\lim_{M\to\infty} \mathsf{Var}\left[\hat{C}^W_{WX,WX}(e^{j\omega})\right] = \lim_{M\to\infty} \mathsf{Var}\left[\hat{C}^B_{XX}(e^{j\omega})\right] \approx \frac{1}{L}C_{XX}(e^{j\omega})^2.$$

In the case of 50% overlap, i.e. $D = M/2$ and for a Bartlett window, Welch calculated the asymptotic variance of the estimator to be

$$\lim_{M\to\infty} \mathsf{Var}\left[\hat{C}^W_{WX,WX}(e^{j\omega})\right] \approx \frac{9}{8L}C_{XX}(e^{j\omega})^2,$$

which seems higher than the variance of Bartlett's estimator. But note that when using $D = M/2$, we actually have almost twice the number of segments, in particular $L = 2N/M - 1$, and thus the variance is reduced by almost factor two. So, the advantage of using Welch's estimator with overlap is that one can use more segments for the same amount of data. This reduces the variance of the estimator while having a bias which is comparable to the one obtained by the Bartlett estimator.

Additionally, the shape of the window only affects the bias of the estimate, not the variance. So even for non-overlapping segments, the selection of suitable window functions can result in an estimator of reduced bias. These advantages make Welch's method one of the most used non-parametric spectrum estimators. The method is also implemented as the "pwelch" function in ©MATLAB.

9.4 Smoothing the Periodogram

From Section 7.2, we know that for pairwise distinct frequencies $\omega_k \neq \omega_l$, the finite Fourier transform ordinates $X_N(e^{j\omega_k})$ and $X_N(e^{j\omega_l})$ are asymptotically as $N \to \infty$ independent. This suggests that for $\omega_k \neq \omega_l$, the periodogram ordinates $I_{XX}^N(e^{j\omega_k})$ and $I_{XX}^N(e^{j\omega_l})$ are also asymptotically independent. In the following, let us restrict ourselves to discrete frequencies $\omega_k = 2\pi k/N$, $k \in \mathbb{Z}$ in the neighborhood of a value of ω at which we wish to estimate $C_{XX}(e^{j\omega})$. This motivates the estimate

$$\hat{C}_{XX}^S(e^{j\omega}) = \frac{1}{2m+1} \sum_{k=-m}^{m} I_{XX}^N(e^{j2\pi(k(\omega)+k)/N})$$

where $2\pi k(\omega)/N$ is the nearest frequency to ω, i.e. $2\pi k(\omega)/N \approx \omega$ for $N \to \infty$, at which the spectrum $C_{XX}(e^{j\omega})$ is to be estimated. Given the above property, we can expect to reduce the variance of the estimation by averaging over adjacent periodogram ordinates. Note that the principle is similar to the method of periodogram averaging where also asymptotically independent quantities are averaged to reduce the variance.

For a real-valued $X(n)$, the periodogram (and the spectrum) is symmetric and 2π periodic. Therefore, it is sufficient to consider $\omega \in [0, \pi)$, and consequently in the estimation $0 < k(\omega) + k < N/2$ must hold. When implementing the method of periodogram smoothing, one has to take into account that we have less periodogram ordinates available for averaging at the borders of the interval $[0, \pi)$, i.e. $\omega = 0$ and $\omega = \pi$.

To check the performance of the estimator, we have to derive its mean and its variance. Assuming the periodogram ordinates to be nearly independent, the mean of the smoothed periodogram estimator $\hat{C}_{XX}^S(e^{j\omega})$ is obtained as

$$\mathsf{E}\left[\hat{C}_{XX}^S(e^{j\omega})\right] = \frac{1}{2m+1} \sum_{k=-m}^{m} \mathsf{E}\left[I_{XX}^N\left(e^{j\frac{2\pi}{N}(k(\omega)+k)}\right)\right].$$

In the following calculation we will assume that $\omega = 2\pi k/N$. Using the formula for the mean of the periodogram, we obtain

$$\begin{aligned}
\mathsf{E}\left[\hat{C}_{XX}^S(e^{j\omega})\right] &= \frac{1}{2m+1} \sum_{k=-m}^{m} \frac{1}{2\pi} \int_{-\pi}^{\pi} \frac{1}{N} \left|\Delta^N(e^{j(\omega+2\pi k/N-\lambda)})\right|^2 C_{XX}(e^{j\lambda}) d\lambda + \frac{1}{N} \left|\Delta^N(e^{j\omega})\right|^2 \mu_X^2 \\
&= \frac{1}{2\pi} \int_{-\pi}^{\pi} \underbrace{\frac{1}{2m+1} \sum_{k=-m}^{m} \frac{1}{N} \left|\Delta^N(e^{j(\omega+2\pi k/N-\lambda)})\right|^2}_{A_m(e^{j(\omega-\lambda)})} C_{XX}(e^{j\lambda}) d\lambda + \frac{1}{N} \left|\Delta^N(e^{j\omega})\right|^2 \mu_X^2 \\
&= \frac{1}{2\pi} \int_{-\pi}^{\pi} A_m(e^{j(\omega-\lambda)}) C_{XX}(e^{j\lambda}) d\lambda + \frac{1}{N} \left|\Delta^N(e^{j\omega})\right|^2 \mu_X^2.
\end{aligned}$$

Thus, the expected value of the smoothed periodogram $\hat{C}_{XX}^S(e^{j\omega})$ is equal to the spectrum $C_{XX}(e^{j\omega})$ convolved with the function $A_m(e^{j\omega})$. To examine the shape of $A_m(e^{j\omega})$ for $N = 20$, this function is shown in Figure 9.6 for $m = 0$, $m = 1$ and $m = 3$. Note that $A_0(e^{j\omega})$ corresponds to $\frac{1}{N}|\Delta^N(e^{j\omega})|^2$, which is also shown in Figure 9.3. We can describe $A_m(e^{j\omega})$ as having approximately a rectangular shape.

A comparison of the mean of the periodogram and the mean of the smoothed periodogram suggests that the bias of $\hat{C}_{XX}^S(e^{j\omega})$ will generally be greater than the bias of $I_{XX}^N(e^{j\omega})$ as the integral extends over a greater range. Both will be the same if the spectrum $C_{XX}(e^{j\omega})$ is flat. Nevertheless, $\hat{C}_{XX}^S(e^{j\omega})$ is unbiased as $N \to \infty$.

The calculation of the asymptotic variance of $\hat{C}_{XX}^S(e^{j\omega})$ is similar to the calculation of the variance of the Bartlett method, and results in

$$\lim_{N\to\infty} \mathsf{Var}\left[\hat{C}_{XX}^S(e^{j\omega})\right] = \frac{1}{2m+1} \lim_{N\to\infty} \mathsf{Var}\left[I_{XX}^N(e^{j\omega})\right] = \frac{1}{2m+1} C_{XX}(e^{j\omega})^2.$$

Regarding the asymptotic distribution of the smoothed periodogram, we know from Section 9.2 that as $N \to \infty$, we have $I_{XX}^N(e^{j\omega}) \sim C_{XX}(e^{j\omega})\chi_2^2/2$ for $\omega \in (0, \pi)$. Consequently, based on the derivation from Example 9.2.1, and

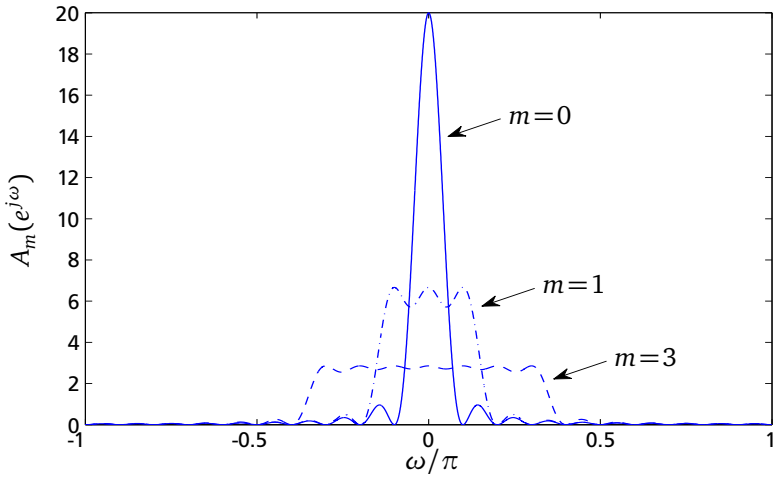

Figure 9.6.: Periodogram smoothing with $N = 20$, function $A_m(e^{j\omega})$ for $m = 0$ (which corresponds to $\frac{1}{N}|\Delta^N(e^{j\omega})|^2$), $m = 1$ and $m = 3$.

due to the fact that the sum of $2m + 1$ independent χ^2_2 distributed variables is χ^2_{4m+2} distributed, the asymptotic distribution of the smoothed periodogram estimator can be shown to be

$$\lim_{N\to\infty} \hat{C}^S_{XX}(e^{j\omega}) \sim \frac{1}{4m+2} C_{XX}(e^{j\omega}) \chi^2_{4m+2}, \quad \omega \in (0, \pi)$$

Example 9.4.1 *Smoothed periodogram of filtered white noise. Consider the same process as in Example 9.2.2. In the left and right plot of Figure 9.7, we show the smoothed periodogram estimate $\hat{C}^S_{XX}(e^{j\omega})$ when using $m = 3$ and $m = 10$, respectively. The true spectrum $C_{XX}(e^{j\omega})$ is overlaid.*

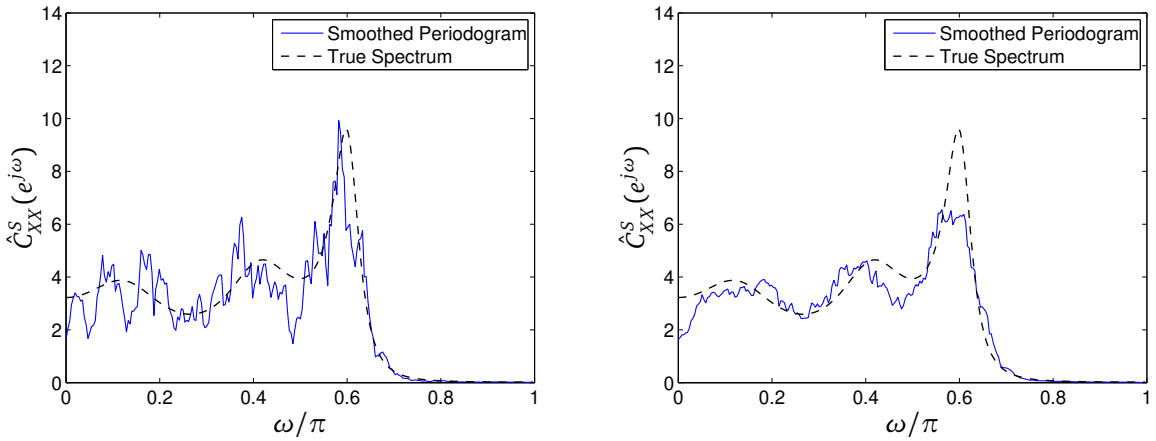

Figure 9.7.: Periodogram smoothing estimates $\hat{C}^S_{XX}(e^{j\omega})$ for $m = 3$ (left) and $m = 10$ (right) of the data sequence from Example 9.2.2.

It can be observed that the variance, which corresponds to the fluctuations around the true spectrum, is reduced as m increases. However, with an increasing m, the bias increases.

A General Class of Spectral Estimators

In section 9.4 we considered an estimator which utilized the independence property of the periodogram ordinates. The smoothed periodogram weighted equally all periodogram ordinates near ω, which, for a nearly constant spectrum is reasonable. However, if the spectrum $C_{XX}(e^{j\omega})$ varies strongly around ω, this method creates a larger

bias. In this case it is more appropriate to weight periodogram ordinates near ω more than those further away. Analogously motivated as in Section 9.4, we construct the estimator as

$$\hat{C}_{XX}^{SW}(e^{j\omega}) = \frac{1}{(2m+1)A} \sum_{k=-m}^{m} W_k I_{XX}^{N}(e^{j2\pi(k(\omega)+k)/N})$$

with normalization factor

$$A = \frac{1}{2m+1} \sum_{k=-m}^{m} W_k,$$

chosen such that the estimator is asymptotically unbiased. For $\omega = 2\pi k(\omega)/N$, the mean of the estimator $\hat{C}_{XX}^{SW}(e^{j\omega})$ is the same as for the smoothed periodogram, but the function $A_m(e^{j\omega})$ is replaced with

$$A_m^W(e^{j\omega}) = \frac{1}{(2m+1)A} \sum_{k=-m}^{m} W_k \frac{1}{N} \left|\Delta^N(e^{j(\omega+2\pi k/N-\lambda)})\right|^2$$

Indeed if we set $W_k = 1$ for $k = -m, \ldots, m$ it follows automatically that $A_m^W(e^{j\omega}) = A_m(e^{j\omega})$. In other words, periodogram smoothing is a special case of the general class of spectral estimates. With the weights W_k, we have more control over the shape of $A_m^W(e^{j\omega})$ which also leads to a better control of the bias of the estimator.

The asymptotic variance of the estimator $\hat{C}_{XX}^{SW}(e^{j\omega})$ can be shown to be

$$\lim_{N\to\infty} \mathrm{Var}\left[\hat{C}_{XX}^{SW}(e^{j\omega})\right] = \frac{1}{(2m+1)^2A^2} \sum_{k=-m}^{m} W_k^2 \lim_{N\to\infty} \mathrm{Var}\left[I_{XX}^{N}(e^{j2\pi k/N})\right] = \frac{1}{(2m+1)^2A^2} \left(\sum_{k=-m}^{m} W_k^2\right) C_{XX}(e^{j\omega})^2$$

Note that the lowest possible variance is achieved for a uniform weighting, which corresponds to the smoothed periodogram (see Section 9.4). We see that $\hat{C}_{XX}^{S}(e^{j\omega})$ has the largest bias for a fixed N but the lowest variance of the general class of spectrum estimators covered in this section.

9.5 The Log-Spectrum

Instead of estimating the spectrum directly, it is possible to estimate $10\log C_{XX}(e^{j\omega})$ from $10\log \hat{C}_{XX}(e^{j\omega})$. The log-function can be used as a variance stabilizing technique (Priestley, 2001). We then find

$$\begin{aligned} \mathrm{E}\left[10\log \hat{C}_{XX}(e^{j\omega})\right] &\approx 10\log C_{XX}(e^{j\omega}) \\ \mathrm{Var}\left[10\log \hat{C}_{XX}(e^{j\omega})\right] &\approx \frac{(10\log e)^2}{C} \end{aligned}$$

where C is a constant which controls the variance. If we use Bartlett's estimator, we have $C = L$. The above equation shows that the variance is approximately a constant and does not depend on $C_{XX}(e^{j\omega})$. This can be in particular useful for the construction of confidence intervals for the spectrum.

9.6 An Estimator Based on the Sample Covariance

We know from Section 6.5 (Wiener-Khintchine theorem) that for WSS processes, the spectrum is defined as the Fourier transform of the covariance function, i.e.

$$C_{XX}(e^{j\omega}) = \sum_{\kappa=-\infty}^{\infty} c_{XX}(\kappa) e^{-j\omega\kappa}$$

In this section, we want to present spectrum estimates which use this relation, but with an estimate of the covariance function, $\hat{c}_{XX}(\kappa)$ replacing $c_{XX}(\kappa)$.

For a WSS random process $X(n)$, with constant mean $\mu_X = \mathsf{E}[X(n)]$, the covariance function $c_{XX}(\kappa)$ is defined in Chapter 6 as

$$c_{XX}(\kappa) = \mathsf{E}\left[(X(n+\kappa)-\mu_X)(X(n)-\mu_X)^*\right].$$

Given observations of the random process $X(n)$, $n = 0,\ldots,N-1$ where N is the sample size, a natural estimate for $c_{XX}(\kappa)$ is the so-called *sample covariance function*

$$\hat{c}_{XX}(\kappa) = \frac{1}{N}\sum_{n=0}^{N-1-\kappa}(X(n+\kappa)-\bar{X})(X(n)-\bar{X})^*, \quad 0 \le \kappa \le N-1$$

where the sample mean $\bar{X} = \frac{1}{N}\sum_{n=0}^{N-1} X(n)$ is an estimate for the mean μ_X. The sample covariances for negative lags are then constructed using the symmetry property of the covariance function:

$$\hat{c}_{XX}(\kappa) = \hat{c}_{XX}(-\kappa)^*, \quad \kappa = -N+1,\ldots,0$$

It can be shown that $\hat{c}_{XX}(\kappa)$ is an asymptotically consistent estimator of the covariance function $c_{XX}(\kappa)$.

Note that for the sample covariance function, the upper limit of the sum depends on the lag index κ, because only samples $X(n)$ for $n = 0,\ldots,N-1$ are available to form the time average.

It is intuitive to suggest an estimator for $C_{XX}(e^{j\omega})$ as follows

$$\hat{C}_{XX}(e^{j\omega}) = \sum_{\kappa=-\infty}^{\infty}\hat{c}_{XX}(\kappa)e^{-j\omega\kappa} = \sum_{\kappa=-N+1}^{N-1}\hat{c}_{XX}(\kappa)e^{-j\omega\kappa}$$

In the context of spectrum analysis, this estimate is sometimes called *correlogram*. It can be shown (by the reader as an exercise) that this estimator is equivalent to the periodogram of $X(n)-\bar{X}$, $n = 0,\ldots,N-1$ which can be denoted as $I^N_{X-\bar{X},X-\bar{X}}(e^{j\omega})$, see Section 9.2. Therefore, the correlogram is not a consistent estimator for the spectrum.

Blackman-Tukey Method

In 1958, Blackman and Tukey developed a spectrum estimator, here referred to the *Blackman-Tukey method*, which is based on the sample covariance function. The basic idea of the method is to use the sample covariance function $\hat{c}_{XX}(\kappa)$ and window it with a function $w_{2M-1}(\kappa)$ of length $2M-1$ where $M \ll N$, of the following form

$$w_{2M-1}(\kappa) = \begin{cases} w_{2M-1}(-\kappa), & |\kappa| \le M-1 \\ 0, & \text{otherwise.} \end{cases}$$

This condition ensures that the Fourier transform of the window is real-valued and that the estimator $\hat{C}^{BT}_{XX}(e^{j\omega})$ will not be complex. We then get

$$\hat{C}^{BT}_{XX}(e^{j\omega}) = \sum_{\kappa=-\infty}^{\infty} w_{2M-1}(\kappa)\hat{c}_{XX}(\kappa)e^{-j\omega\kappa} = \sum_{\kappa=-M+1}^{M-1} w_{2M-1}(\kappa)\hat{c}_{XX}(\kappa)e^{-j\omega\kappa}.$$

Using the equivalence between the periodogram and the correlogram, we have

$$\hat{C}^{BT}_{XX}(e^{j\omega}) = \frac{1}{2\pi}\int_{-\pi}^{\pi} I^N_{X-\bar{X},X-\bar{X}}(e^{j\lambda})W_{2M-1}(e^{j(\omega-\lambda)})d\lambda$$

which is the convolution of the periodogram $I^N_{X-\bar{X},X-\bar{X}}(e^{j\omega})$ with the Fourier transform of the window $w_{2M-1}(\kappa)$. From this consideration, we get another constraint for the window, i.e.

$$W_{2M-1}(e^{j\omega}) \ge 0 \quad \forall\omega,$$

to ensure the estimate $\hat{C}_{XX}^{BT}(e^{j\omega})$ is non-negative for all ω.

As for the other estimators, we have to derive the mean and the variance to check the performance of $\hat{C}_{XX}^{BT}(e^{j\omega})$. The mean of $\hat{C}_{XX}^{BT}(e^{j\omega})$ can be easily calculated as

$$\mathsf{E}\left[\hat{C}_{XX}^{BT}(e^{j\omega})\right] = \frac{1}{2\pi}\int_{-\pi}^{\pi} \mathsf{E}\left[I_{X-\bar{X},X-\bar{X}}^{N}(e^{j\lambda})\right] W_{2M-1}(e^{j(\omega-\lambda)})d\lambda$$

which, according to Section 9.2, is given by

$$\mathsf{E}\left[\hat{C}_{XX}^{BT}(e^{j\omega})\right] = \frac{1}{2\pi}\int_{-\pi}^{\pi} C_{XX}(e^{j\theta})\frac{1}{2\pi}\int_{-\pi}^{\pi}\frac{1}{N}\left|\Delta^{N}(e^{j\vartheta})\right|^{2} W_{2M-1}(e^{j(\omega-\theta-\vartheta)})d\vartheta d\theta.$$

Note that this is the double convolution of the spectrum with the Fourier transform of the window $w_{2M-1}(\kappa)$ and the magnitude square Fourier transform of the rectangular observation window. We know also from Section 9.2, that $\frac{1}{N}|\Delta^{N}(e^{j\omega})|^2$ converges to a Dirac delta function on the interval $\omega = [-\pi, \pi)$. Therefore, we can reduce the mean of the estimator to a simple convolution, as follows

$$\lim_{N\to\infty} \mathsf{E}\left[\hat{C}_{XX}^{BT}(e^{j\omega})\right] = \frac{1}{2\pi}\int_{-\pi}^{\pi} C_{XX}(e^{j\lambda})W_{2M-1}(e^{j(\omega-\lambda)})d\lambda.$$

If we also assume that for large M, the energy of $W_{2M-1}(e^{j\omega})$ is concentrated around $\omega = 0$, we can conclude that the Blackman-Tukey estimator is unbiased for $N, M \to \infty$.

The asymptotic variance of the estimator can be shown to be

$$\mathsf{Var}\left[\hat{C}_{XX}^{BT}(e^{j\omega})\right] \approx C_{XX}(e^{j\omega})^2\frac{1}{N}\int_{-\pi}^{\pi} W_{2M-1}(e^{j\omega})^2 d\omega = C_{XX}(e^{j\omega})^2\frac{1}{N}\sum_{\kappa=-M+1}^{M-1} w_{2M-1}(\kappa)^2$$

where we have used Parseval's inequality. Based on this approximation the variance of the Blackman-Tukey estimator tends to zero if the window function $w_{2M-1}(\kappa)$ has finite energy. Note that the ratio between M and N determines the achieved bias-variance trade-off.

Example 9.6.1 *Correlogram and Blackman-Tukey estimate of filtered white noise. Consider the same process as in Example 9.2.2. In the left plot of Figure 9.8, we show the correlogram $\hat{C}_{XX}(e^{j\omega})$ which is equivalent with the periodogram, as depicted in Figure 9.2. In the right plot, we show the Blackman-Tukey estimate $\hat{C}_{XX}^{BT}(e^{j\omega})$ for $M = 14$. The true spectrum $C_{XX}(e^{j\omega})$ is overlaid.*

9.7 Cross-Spectrum Estimation

If $X(n)$ and $Y(n)$ are jointly stationary and real-valued, with constant means $\mu_X = \mathsf{E}[X(n)]$ and $\mu_Y = \mathsf{E}[Y(n)]$, the cross-covariance function is defined as

$$c_{YX}(\kappa) = \mathsf{E}[(Y(n+\kappa)-\mu_Y)(X(n)-\mu_X)]$$

The cross-spectrum is defined by

$$C_{YX}(e^{j\omega}) = \sum_{\kappa=-\infty}^{\infty} c_{YX}(\kappa)e^{-j\omega\kappa} = C_{XY}(e^{j\omega})^* = C_{XY}(e^{-j\omega})$$

Note that unlike the spectrum, the cross-spectrum is generally complex-valued. The objective is to estimate the cross-spectrum $C_{YX}(e^{j\omega})$ for $\omega \in [-\pi, \pi)$, given observations $X(0), \ldots, X(N-1)$ and $Y(0), \ldots, Y(N-1)$.

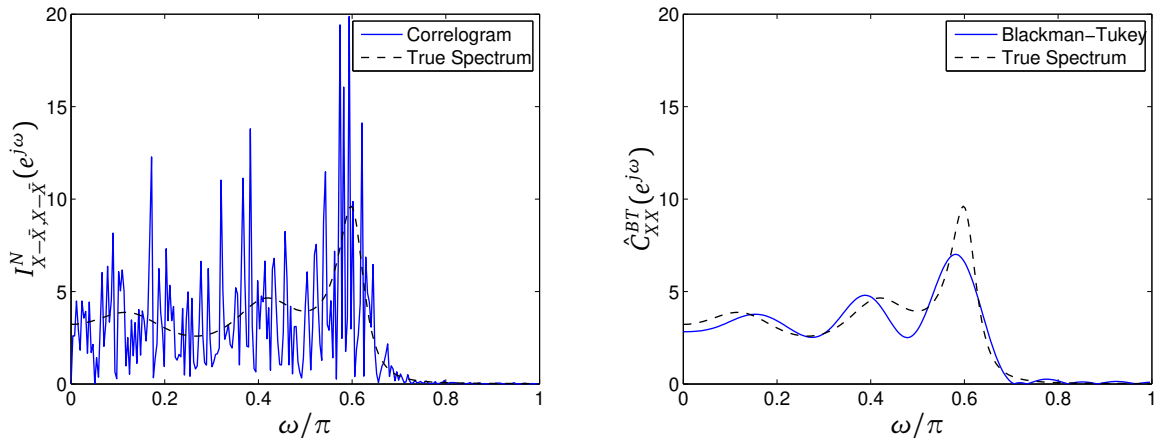

Figure 9.8.: Correlogram or periodogram (left) and Blackman-Tukey estimate with rectangular window and $M = 14$ (right) of the data sequence from Example 9.2.2.

An intuitive way is to use the cross-periodogram, which is defined as

$$I^N_{YX}(e^{j\omega}) = \frac{1}{N} Y_N(e^{j\omega}) X_N(e^{j\omega})^*$$

where the finite Fourier transforms of $X(n)$ and $Y(n)$ are given by

$$Y_N(e^{j\omega}) = \sum_{n=0}^{N-1} Y(n) e^{-j\omega n} \quad \text{and} \quad X_N(e^{j\omega}) = \sum_{n=0}^{N-1} X(n) e^{-j\omega n}$$

As for the periodogram, it can be shown that the cross-periodogram is asymptotically for large N unbiased, i.e. we have

$$\lim_{N\to\infty} \mathsf{E}\left[I^N_{YX}(e^{j\omega})\right] = C_{YX}(e^{j\omega}).$$

Also, we have $\mathsf{E}[Y_N(e^{j\omega}) X_N(e^{j\omega})] = 0$. The variance of the cross-periodogram is asymptotically

$$\lim_{N\to\infty} \mathsf{Var}\left[I^N_{YX}(e^{j\omega})\right] = C_{YY}(e^{j\omega}) C_{XX}(e^{j\omega})$$

Because of the identity

$$\left|C_{YX}(e^{j\omega})\right|^2 \le C_{YY}(e^{j\omega}) C_{XX}(e^{j\omega}),$$

the variance of $I^N_{YX}(e^{j\omega})$ is never smaller than $\left|C_{YX}(e^{j\omega})\right|^2$ for any N.

To construct estimates for $C_{YX}(e^{j\omega})$ with lower variance, we can use the same independence properties between segments, as for the Bartlett method, and calculate

$$\hat{C}^B_{YX}(e^{j\omega}) = \frac{1}{L} \sum_{l=1}^{L} \frac{1}{M} Y_M(e^{j\omega}, l) X_M(e^{j\omega}, l)^*$$

where the finite Fourier transforms of segments $l = 1, \ldots, L$ of $X(n)$ and $Y(n)$ are given by

$$Y_M(e^{j\omega}, l) = \sum_{n=0}^{M-1} Y(n + (l-1)M) e^{-j\omega n} \quad \text{and} \quad X_M(e^{j\omega}, l) = \sum_{n=0}^{M-1} X(n + (l-1)M) e^{-j\omega n}$$

Asymptotically, and for a large segment length M, we then have

$$\begin{aligned} \mathsf{E}\left[\hat{C}_{YX}(e^{j\omega})\right] &\approx C_{YX}(e^{j\omega}) \\ \mathsf{Var}\left[\hat{C}_{YX}(e^{j\omega})\right] &\approx \frac{1}{L} C_{YY}(e^{j\omega}) C_{XX}(e^{j\omega}) \end{aligned}$$

As for spectrum estimation, an alternative to cross-periodogram averaging is cross-periodogram smoothing over neighboring frequencies, which produces similar results. However, care must be taken with cross-periodogram smoothing when one is interested in the phase.

10 Parametric Spectrum Estimation

In parametric spectrum estimation, the signal of interest $X(n)$ is modeled by a filtered white noise process. The filter is used to shape the spectrum of the output process. Unlike in non-parametric spectrum estimation, where the spectrum is estimated directly, here the parameters of the filter and the power of the noise have to be estimated, from which a spectrum estimator is obtained. The basic principle of parametric-spectrum estimation is illustrated in Figure 10.1. The corresponding linear system is shown in Figure 10.2.

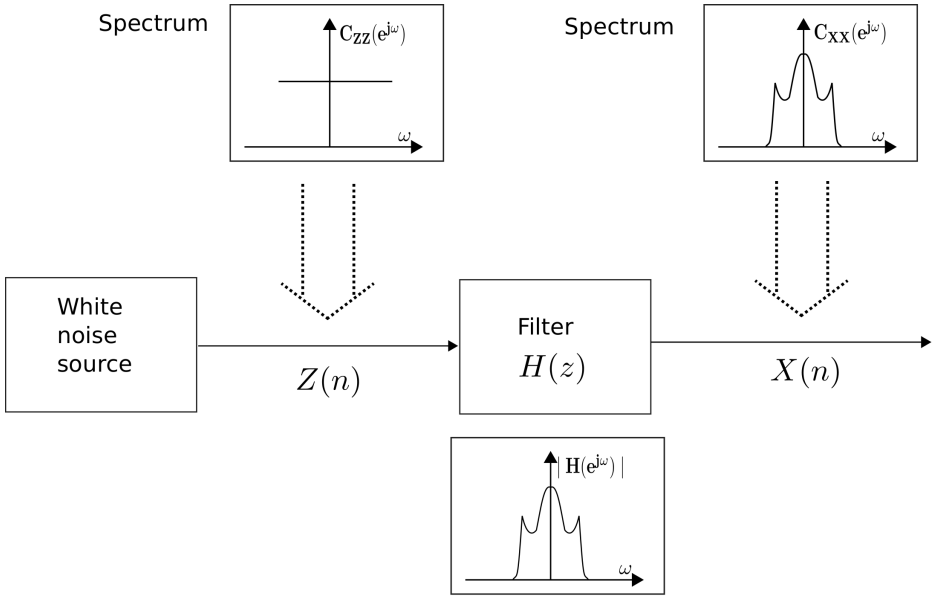

Figure 10.1.: Principle of parametric spectrum estimation.

Consider the system of Figure 10.2 with transfer function $H(e^{j\omega})$, input process $Z(n)$ and output process $X(n)$. It is assumed that the system is stable, causal and that the input process $Z(n)$ is a real-valued zero-mean white noise process with variance σ_Z^2. The system with transfer function $H(e^{j\omega})$ may be an all-pole system, an all-zero system or a system with poles and zeros, giving rise to an autoregressive (AR), moving average (MA) or autoregressive moving average (ARMA) process, respectively.

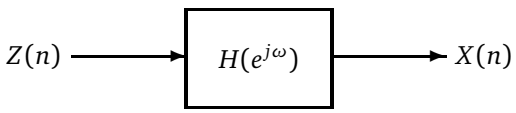

Figure 10.2.: Linear and time-invariant filtering of white noise.

In general, parametric spectrum estimation encompasses the following steps:

1. Select an appropriate model for the process, e.g. autoregressive (AR), moving average (MA) or autoregressive moving average (ARMA).
2. Estimate the model parameters from the observations.
3. Incorporate the estimated parameters into the spectrum model.

In this chapter, parametric estimators for different types of processes, namely AR, MA and ARMA, are discussed. Parametric estimators are also derived for the case, where the process of interest is disturbed by white noise.

10.1 Autoregressive Process

Consider the system in Figure 10.2. If the difference equation relating the output and the input signal is given by

$$X(n) + \sum_{k=1}^{p} a_k X(n-k) = Z(n),$$

the output process $X(n)$ is called an autoregressive (AR) process of order p, or in short notation AR(p). The parameters of the process, a_k, $k = 1, \ldots, p$, with $a_p \neq 0$, are the so-called AR parameters.

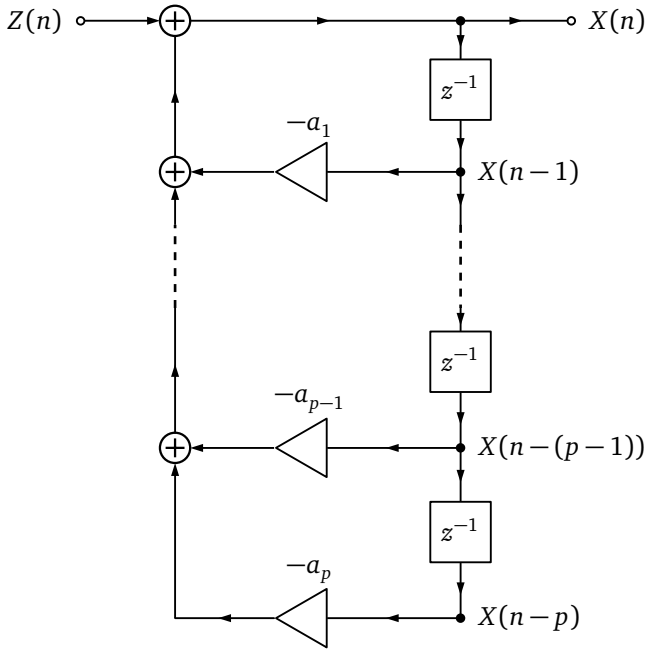

Figure 10.3.: Signal flow graph of a rational filter with order p.

The recursive filter possesses the following transfer function

$$H(e^{j\omega}) = \frac{1}{1 + \sum_{k=1}^{p} a_k e^{-j\omega k}}\,.$$

Because we have assumed the filter to be stable, the roots of the characteristic equation

$$z^p + \sum_{k=1}^{p} a_k z^{p-k} = 0, \quad z = e^{j\omega},$$

have to lie within the unit circle, i.e. $|z_l| < 1$ for all l roots of the above equation. The spectrum is given by

$$C_{XX}(e^{j\omega}) = \left|H(e^{j\omega})\right|^2 C_{ZZ}(e^{j\omega})\,.$$

Since the input process $Z(n)$ is a real-valued zero-mean white noise process, we have $\mathsf{E}[Z(n)] = 0$ and $\mathsf{E}[Z(n+\kappa)Z(n)] = \sigma_Z^2 \delta(\kappa)$. Thus, we have

$$C_{XX}(e^{j\omega}) = \frac{\sigma_Z^2}{\left|1 + \sum_{k=1}^{p} a_k e^{-j\omega k}\right|^2}$$

The objective is to estimate $C_{XX}(e^{j\omega})$ as given above, based on observations of the process $X(n)$ for $n = 0, \ldots, N-1$. This requires the estimation of the parameters a_k, $k = 1, \ldots, p$ and the noise power σ_Z^2.

Multiplying the difference equation

$$X(n) + \sum_{k=1}^{p} a_k X(n-k) = Z(n)$$

by $X(n-l)$ with $l \geq 0$, from the right and taking the expected value, leads to

$$\mathsf{E}[X(n)X(n-l)] + \sum_{k=1}^{p} a_k \mathsf{E}[X(n-k)X(n-l)] = \mathsf{E}[Z(n)X(n-l)].$$

Given that $\mathsf{E}[X(n)X(n-l)] = c_{XX}(l)$ and $\mathsf{E}[X(n-k)X(n-l)] = c_{XX}(l-k)$, we obtain

$$c_{XX}(l) + \sum_{k=1}^{p} a_k c_{XX}(l-k) = \mathsf{E}[Z(n)X(n-l)], \quad l \geq 0.$$

It remains to determine the term $\mathsf{E}[Z(n)X(n-l)]$. Assuming the recursive filter to be causal, i.e. $h(n) = 0$ for $n < 0$, leads to the relationship

$$X(n) = \sum_{k=0}^{\infty} h(k)Z(n-k) = h(0)Z(n) + \sum_{k=1}^{\infty} h(k)Z(n-k).$$

Thus, shifting $X(n)$ by l gives

$$X(n-l) = h(0)Z(n-l) + \sum_{k=1}^{\infty} h(k)Z(n-l-k)$$

Taking the expected value of the product $Z(n)X(n-l)$ yields

$$\mathsf{E}[Z(n)X(n-l)] = h(0)c_{ZZ}(l) + \sum_{k=1}^{\infty} h(k)c_{ZZ}(l+k).$$

Since $c_{ZZ}(k) = \sigma_Z^2 \delta(k)$ it holds that $\sum_{k=1}^{\infty} h(k)c_{ZZ}(l+k) = \sigma_Z^2 \sum_{k=1}^{\infty} h(k)\delta(l+k) = 0$ for $l \geq 0$ so that

$$\mathsf{E}[Z(n)X(n-l)] = h(0)c_{ZZ}(l) = \sigma_Z^2 h(0)\delta(l), \qquad l \geq 0.$$

Therefore, we obtain

$$c_{XX}(l) + \sum_{k=1}^{p} a_k c_{XX}(l-k) = \sigma_Z^2 h(0)\delta(l), \qquad l \geq 0.$$

To obtain the estimates of $p+1$ unknown parameters, i.e. $a_1, \ldots, a_p, \sigma_Z^2$, we require at least a set of $p+1$ linear equations of these unknown parameters. Assuming $h(0) = 1$, we choose the equations for $l = 0, \ldots, p$, resulting in the so called Yule-Walker equations

$$c_{XX}(l) + \sum_{k=1}^{p} a_k c_{XX}(l-k) = \begin{cases} \sigma_Z^2, & l = 0 \\ 0, & l = 1, \ldots, p. \end{cases}$$

Note that the difference equation in $c_{XX}(l)$ has a similar form to the system describing difference equation in $X(n)$.

Having observed $X(n)$, one can estimate $c_{XX}(n)$ as described in Section 9.6. This results in a linear system of equations with unknown parameters $a_1, \ldots, a_p$ and σ_Z^2. Using $\hat{c}_{XX}(0), \ldots, \hat{c}_{XX}(p)$, one would obtain a solution for $a_1, \ldots, a_p$. The solution is unique if the inverse of the matrix with the elements $\hat{c}_{XX}(l-k)$ exists, which is guaranteed if the filter is stable. Given estimates $\hat{a}_1, \ldots, \hat{a}_p$, one can use the Yule-Walker equations for $l = 0$ to get $\hat{\sigma}_Z^2$. Then it is straightforward to find an estimate for the spectrum $C_{XX}(e^{j\omega})$ given by

$$\hat{C}_{XX}(e^{j\omega}) = \frac{\hat{\sigma}_Z^2}{\left|1 + \sum_{k=1}^{p} \hat{a}_k e^{-j\omega k}\right|^2}.$$

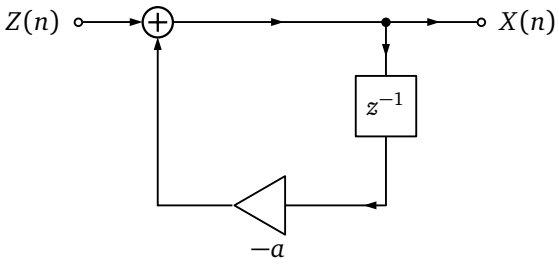

Figure 10.4.: Flow graph of an AR(1) process.

Example 10.1.1 *Consider the causal and linear time-invariant system as depicted in Figure 10.4, where $Z(n)$ represents a real-valued zero-mean white process with (unknown) variance σ_Z^2. We are interested in estimating the spectrum $C_{XX}(e^{j\omega})$ of the output process.*

First, we find the difference equation describing the relation between the output and the input, which is given by

$$X(n) + a \cdot X(n-1) = Z(n).$$

Then, we multiply from the right by $X(n-l)$ with $l \geq 0$ and take the expected value. This leads to

$$\mathsf{E}[X(n)X(n-l)] + a\mathsf{E}[X(n-1)X(n-l)] = \mathsf{E}[Z(n)X(n-l)],$$

which equals

$$c_{XX}(l) + ac_{XX}(l-1) = c_{ZX}(l).$$

We have a causal system with impulse response $h(n) = 0$ for $n < 0$. As above, the cross-covariance function $c_{ZX}(l)$ for $l \geq 0$ can be found to be $c_{ZX}(l) = h(0)c_{ZZ}(l)$. For $h(0) = 1$, we obtain the Yule-Walker equations as follows

$$\begin{aligned} c_{XX}(0) &+ ac_{XX}(1) = \sigma_Z^2 \\ c_{XX}(1) &+ ac_{XX}(0) = 0 \end{aligned}$$

We then solve the set of linear equations for σ_Z^2 and a, which yields

$$a = -\frac{c_{XX}(1)}{c_{XX}(0)}$$

and

$$\sigma_Z^2 = c_{XX}(0) - \frac{c_{XX}(1)^2}{c_{XX}(0)}.$$

Suppose now, that we observe a realization of the random process $X(n)$ for $n = 0, \ldots, N-1$ with $N = 512$, as depicted in Figure 10.5 (left). We want to estimate its AR parameters using the Yule-Walker equations. First, we obtain estimates for the covariance function $c_{XX}(l)$ at time lags $l = 0$ and 1, which can be performed through the estimator

$$\hat{c}_{XX}(m) = \begin{cases} \frac{1}{N}\sum_{n=0}^{N-1-|m|} \bar{X}(n)\bar{X}(n+|m|), & 0 \leq |m| \leq N-1 \\ 0, & \text{otherwise,} \end{cases}$$

where $\bar{X}(n)$ is a detrended version of $X(n)$. Then we use the formulae above to estimate $\hat{a}$ and $\hat{\sigma}_Z^2$. As a final step, we incorporate the parameter estimates into the spectrum model for an AR(1) process, which yields the spectrum estimate

$$\hat{C}_{XX}(e^{j\omega}) = \frac{\hat{\sigma}_Z^2}{|1 + \hat{a}e^{-j\omega}|^2}.$$

The estimated spectrum is shown in Figure 10.5 (right). For comparison, we also show the true spectrum and a non-parametric estimate which has been obtained using the Welch method.

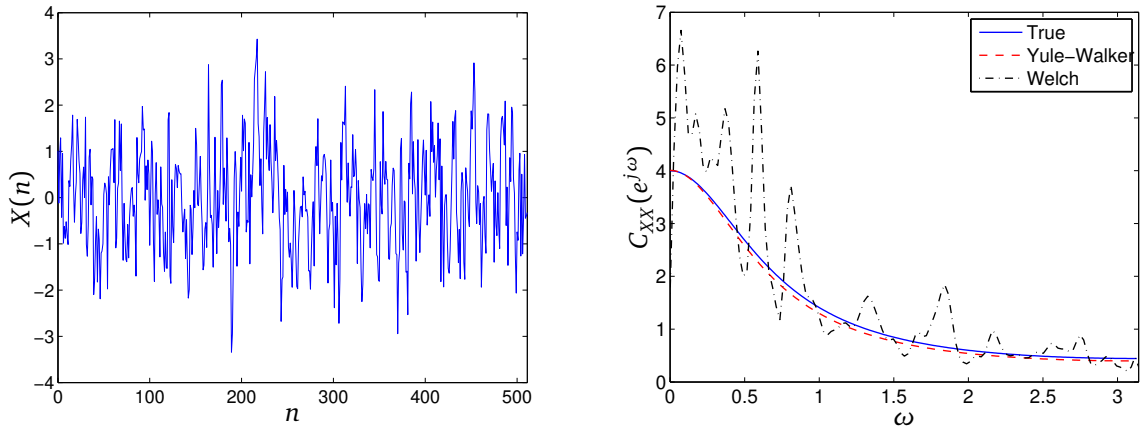

Figure 10.5.: Illustration of an AR(1) process (left), its true spectrum (solid line) and estimated spectra using the parametric method described above (dashed line) and the Welch method (dash-dotted line) (right).

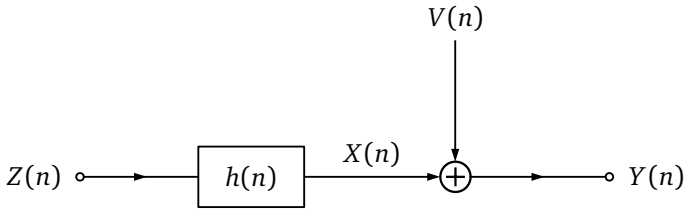

Figure 10.6.: Filtered white noise disturbed by additive noise

Extended Yule-Walker Equations

Suppose that an autoregressive process $X(n)$ is disturbed by an additive white noise process $V(n)$ with unknown variance σ_V^2. The additive noise process $V(n)$ and the white noise process $Z(n)$ are assumed to be uncorrelated. The flow graph of this problem is sketched in Figure 10.6. This model can be used when the process of interest is an AR process, but the available measurements are disturbed by white noise. The goal is to provide a parametric estimate of the spectrum $C_{XX}(e^{j\omega})$. Therefore, an extended version of the Yule-Walker equations has to be derived.

To obtain the extended Yule-Walker equations, we have to start with the difference equation relating $Z(n)$ and $Y(n)$. This equation can be obtained by writing down the difference equation of $X(n)$ and $Z(n)$

$$X(n)+\sum_{k=1}^{p} a_k X(n-k) = Z(k)$$

and then using $X(n) = Y(n) - V(n)$ to get

$$\begin{aligned} Y(n)-V(n)+\sum_{k=1}^{p} a_k (Y(n-k)-V(n-k)) &= Z(n) \\ Y(n)+\sum_{k=1}^{p} a_k Y(n-k) &= Z(n)+V(n)+\sum_{k=1}^{p} a_k V(n-k)\,. \end{aligned}$$

Following the same line of arguments as for the pure AR process, we multiply the previous equation by $Y(n-l)$ from the right for $l \geq 0$ and take the expected value. This leads to

$$c_{YY}(l)+\sum_{k=1}^{p} a_k c_{YY}(l-k) = c_{ZY}(l)+c_{VY}(l)+\sum_{k=1}^{p} a_k c_{VY}(l-k), \quad l \geq 0$$

In order to derive the extended Yule-Walker equations, the cross-covariance functions $c_{VY}(l)$ and $c_{ZY}(l)$ have to be obtained. The cross-covariance function $c_{VY}(l)$ is given by

$$\begin{aligned} c_{VY}(l) = \mathsf{E}[V(n)Y(n-l)] =& \mathsf{E}[V(n)(V(n-l) + \sum_{k=0}^{\infty} h(k)Z(n-l-k))] \\ =& c_{VV}(l) + \sum_{k=0}^{\infty} h(k)c_{VZ}(l+k)\,. \end{aligned}$$

As the processes $V(n)$ and $Z(n)$ are uncorrelated, the cross term in the previous equation vanishes and the equation can be simplified to

$$c_{VY}(l) = c_{VV}(l) = \sigma_V^2 \delta(l).$$

The cross-covariance $c_{ZY}(l)$ can be expressed as

$$\begin{aligned} c_{ZY}(l) = \mathsf{E}[Z(n)Y(n-l)] =& \mathsf{E}[Z(n)(V(n-l) + \sum_{k=0}^{\infty} h(k)Z(n-l-k))] \\ =& c_{ZV}(l) + \sum_{k=0}^{\infty} h(k)c_{zz}(l+k)\,. \end{aligned}$$

Again the cross-term vanishes and, according to the last section, $\sum_{k=0}^{\infty} h(k)c_{ZZ}(l+k) = \sigma_Z^2 h(0)\delta(l)$ for all $l \geq 0$ so that

$$c_{ZY}(l) = h(0)\sigma_Z^2 \delta(l), \qquad l \geq 0.$$

Using these results, the extended Yule-Walker equations are given by

$$c_{YY}(l) + \sum_{k=1}^{p} a_k c_{YY}(l-k) = \begin{cases} \sigma_Z^2 + \sigma_V^2, & l = 0 \\ a_l \sigma_V^2, & l = 1, \ldots, p \\ 0, & l > p. \end{cases}$$

The extended Yule-Walker equations can be used to estimate the necessary parameters, $a_1, \ldots, a_p$, σ_V^2 and σ_Z^2. If the covariance function $c_{XX}(l)$ is estimated by a consistent estimator, e.g. the sample covariance, the resulting estimators $\hat{a}_l$, $\hat{\sigma}_V^2$ and $\hat{\sigma}_Z^2$ are also consistent. Hence, we have consistent estimators for the spectra $C_{XX}(e^{j\omega})$ and $C_{YY}(e^{j\omega})$.

Suppose that an autoregressive process $X(n)$, e.g. the output of the system in Figure 10.4, is disturbed by a white noise process $V(n)$ of unknown variance σ_V^2 such that $Y(n) = X(n) + V(n)$, where $V(n)$ and the input process $Z(n)$ are uncorrelated. This results in the so-called extended Yule-Walker equations, and is considered in the following example with the goal of estimating the spectrum.

Example 10.1.2 *Consider the same system as in Example 10.1.1, but with $X(n)$ now being disturbed by a white noise process $V(n)$ with $c_{VV}(n) = \sigma_V^2 \delta(n)$. The noise $V(n)$ and input process $Z(n)$ are uncorrelated, i.e. $c_{VZ}(n) \equiv 0$. The new output process is given by $Y(n) = X(n) + V(n)$.*

The system transfer function $H(z)$ for the system depicted in Figure 10.4 is given by

$$H(z) = \frac{1}{1 + az^{-1}},$$

which leads to the difference equation

$$Y(n) + aY(n-1) = Z(n) + V(n) + aV(n-1)$$

describing the relation between $Y(n)$, the input $Z(n)$ and the additive noise source $V(n)$. Multiplying from the right by $Y(n-l)$ and taking the expected value. This leads to

$$c_{YY}(l) + ac_{YY}(l-1) = c_{ZY}(l) + c_{VY}(l) + ac_{VY}(l-1).$$

As before, the cross-covariance function $c_{ZY}(l)$ can be found to be $c_{ZX}(l) = h(0)c_{ZZ}(l)$ for $l \geq 0$. The cross-covariance function $c_{VY}(l)$ is given by

$$c_{VY}(l) = \mathsf{E}[V(n)Y(n-l)] = \mathsf{E}[V(n)\sum_{m=0}^{\infty} h(m)Z(n-l-m) + V(n-l)] = c_{VV}(l)$$

and consequently, $c_{VY}(l-1) = c_{VV}(l-1)$. Assuming $h(0) = 1$, we get the extended Yule-Walker equations for the signal plus noise scenario,

$$c_{YY}(l) + ac_{YY}(l-1) = \begin{cases} \sigma_Z^2 + \sigma_V^2, & l = 0 \\ a\sigma_V^2, & l = 1 \\ 0, & l > 1, \end{cases}$$

which can be used to estimate the parameters of interest.

10.2 Moving Average Process

Consider the case that the system in Figure 10.2 is a transversal filter with impulse response $h(n)$, input $Z(n)$ and output $X(n)$ as shown in Figure 10.7. The difference equation describing the relation between output and input is given by

$$X(n) = \sum_{k=0}^{q} h(k)Z(n-k) = Z(n) + \sum_{k=1}^{q} h(k)Z(n-k),$$

with $h(q) \neq 0$. In addition, $Z(n)$ is a white noise process, i.e. $\mathsf{E}[Z(n)] = 0$ and $c_{ZZ}(l) = \sigma_Z^2\delta(l)$. Then $X(n)$ is a moving average (MA) process of order q, or in short notation MA(q).

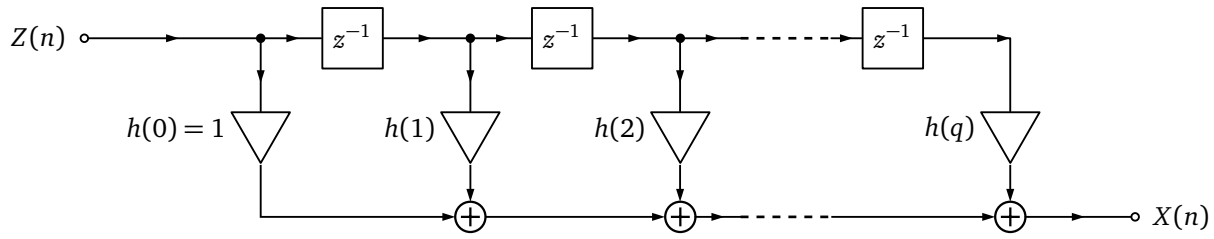

Figure 10.7.: Transversal filter of order q.

The spectrum of $X(n)$ can be calculated as

$$C_{XX}(e^{j\omega}) = \left|H(e^{j\omega})\right|^2 C_{ZZ}(e^{j\omega}) = \left|H(e^{j\omega})\right|^2 \sigma_Z^2 .$$

The covariance function $c_{XX}(l) = \mathsf{E}[X(n+l)X(n)]$ is

$$\begin{aligned} c_{XX}(l) &= \mathsf{E}\left[\left(\sum_{k=0}^{q} h(k)Z(n+l-k)\right)\left(\sum_{m=0}^{q} h(m)Z(n-m)\right)\right] \\ &= \sum_{k=0}^{q}\sum_{m=0}^{q} h(k)h(m)\sigma_Z^2\delta(l+m-k). \end{aligned}$$

Because $\delta(l+m-k)=1$ for $k=l+m$ and zero otherwise, we have

$$c_{XX}(l)=\sigma_Z^2\sum_{m=0}^{q}h(m+l)h(m).$$

Note that $h(n)$ is nonzero for $0\le n\le q$ and zero otherwise. The equation above can hence be rewritten as

$$c_{XX}(l)=\begin{cases}\sigma_Z^2\sum_{m=0}^{q-l}h(m+l)h(m), & 0\le l\le q\\ \sigma_Z^2\sum_{m=-l}^{q}h(m+l)h(m), & -q\le l\le 0\\ 0, & \text{otherwise.}\end{cases}$$

Substituting in the equation above the index m with $k-l$ for the case $-q\le l\le 0$, yields

$$c_{XX}(l)=\sigma_Z^2\sum_{k=0}^{q+l}h(k)h(k-l)\qquad -q\le l\le 0.$$

Therefore, the Yule-Walker equations are

$$c_{XX}(l)=\begin{cases}\sigma_Z^2\sum_{m=0}^{q-|l|}h(m)h(m+|l|), & 0\le |l|\le q\\ 0, & \text{otherwise.}\end{cases}$$

If we have estimates of $c_{XX}(0),\ldots,c_{XX}(q)$, we would need to solve a system of non-linear equations in $h(0),\ldots,h(q)$ and σ_Z^2, which might not have a unique solution. An alternative way of solving the Yule-Walker equations for MA processes is given below.

In the following, let $b(m)=\sigma_Z h(m)$ for $m=0,\ldots,q$ and $h(0)=1$, then

$$c_{XX}(l)=\begin{cases}\sum_{m=0}^{q-|l|}b(m)b(m+|l|), & 0\le |l|\le q\\ 0, & \text{otherwise.}\end{cases}$$

Let $\hat{c}_{XX}(0),\ldots,\hat{c}_{XX}(q)$ be (consistent) estimates for $c_{XX}(0),\ldots,c_{XX}(q)$. Then

$$\hat{c}_{XX}(l)=\sum_{m=0}^{q-l}\hat{b}(m)\hat{b}(m+l),\quad l=0,\ldots,q\,.$$

The estimates $\hat{b}(0),\ldots,\hat{b}(q)$ are consistent because of the consistency of $\hat{c}_{XX}(l)$, $l=0,\ldots,q$. The filter coefficients and therefore the moving average parameters can be estimated as $\hat{h}(1)=\hat{b}(1)/\hat{b}(0),\ldots,\hat{h}(q)=\hat{b}(q)/\hat{b}(0)$, and the variance of the input process as $\hat{\sigma}_Z^2=\hat{b}(0)^2$.

In general, we can find the parameters of a moving average process by applying spectral factorization. The principle of estimating moving average parameters will be shown in more detail to verify the solution given above.

The z-Transform of the impulse response $b(m)$ is

$$B(z)=\sum_{m=0}^{q}b(m)z^{-m}.$$

We already know from previous sections that the relationship between the spectra of the input and output signals can be expressed as

$$C_{XX}(e^{j\omega})=\sum_{l=-q}^{q}c_{XX}(l)e^{-j\omega l}=B(e^{j\omega})B(e^{-j\omega}).$$

By substituting $e^{j\omega}=z$, we obtain $C_{XX}(z)=B(z)B(z^{-1})$. We then:

1. Calculate $P(z)=z^qC_{XX}(z)$

2. Assign all roots z_i of $P(z)$ inside the unit circle to $B(z)$, i.e. $B(z) = b(0)\prod_{i=1}^{q}(1 - z_i z^{-1})$ with $b(0) > 0$ and $|z_i| \leq 1$.

3. Calculate $h(m) = b(m)/b(0)$ for $m = 1, \ldots, q$

As a final step, we apply the method of equating coefficients,

$$b(0) + b(1)z^{-1} + \ldots + b(q)z^{-q} = \sigma_Z \left(1 + h(1)z^{-1} + \ldots + h(q)z^{-q}\right)$$

and we obtain

$$\begin{aligned} b(0) &= \sigma_Z \\ b(1) &= \sigma_Z h(1) \Longleftrightarrow h(1) = b(1)/b(0) \\ &\vdots \\ b(q) &= \sigma_Z h(q) \Longleftrightarrow h(q) = b(q)/b(0). \end{aligned}$$

To get the power σ_Z^2 of $Z(n)$, we use

$$c_{XX}(l) = \sum_{m=0}^{q-l} b(m)b(m+l) \quad , \quad l = 0, 1, \ldots, q$$

and solve for $l = 0$

$$b(0)^2 = \frac{c_{XX}(0)}{1 + \sum_{m=1}^{q} h(m)^2}.$$

By replacing $c_{XX}(l)$ by its estimate $\hat{c}_{XX}(l)$, we obtain estimates of the parameters of the moving average process. Note that this procedure is only required if one is interested in the parameters of the moving average process. If there is only an interest in estimating the spectrum $C_{XX}(e^{j\omega})$ of $X(n)$, one simply uses the Wiener-Khintchine relation

$$\hat{C}_{XX}(e^{j\omega}) = \sum_{n=-q}^{q} \hat{c}_{XX}(n)e^{-j\omega n} = \hat{c}_{XX}(0) + 2\sum_{n=1}^{q} \hat{c}_{XX}(n)\cos\omega n\,.$$

Example 10.2.1 *AR and MA spectrum estimate of filtered white noise. Consider again the sequence from Example 9.2.2. Figure 10.8 (left) shows the estimated AR spectrum when we use $p = 6$ and the true spectrum. Figure 10.8 (right) shows the estimated MA spectrum when $q = 14$. Note that the MA spectrum estimate is equivalent to the Blackman-Tukey method in this case. It can be observed from Figure 10.8 that, when selecting good model orders p and q, both methods achieve better results than the non-parametric methods such as the periodogram and the Bartlett method in Figure 9.5. However, in this case the AR(6) spectrum estimate is most adequate since it perfectly fits the model from Example 9.2.2.*

10.3 Autoregressive Moving Average Process

Consider the case that the system in Figure 10.2 is a system with poles and zeros, as depicted in Figure 10.9. The system has a transfer function

$$H(e^{j\omega}) = \frac{1 + \sum_{k=1}^{q} b_k z^{-k}}{1 + \sum_{k=1}^{p} a_k z^{-k}},$$

with $a_p \neq 0$, $b_q \neq 0$. The system is stable and causal and the input process is a zero-mean white noise process. Note that the given transfer function differs from the general form of an IIR filter in that $b_0 = 1$, which avoids

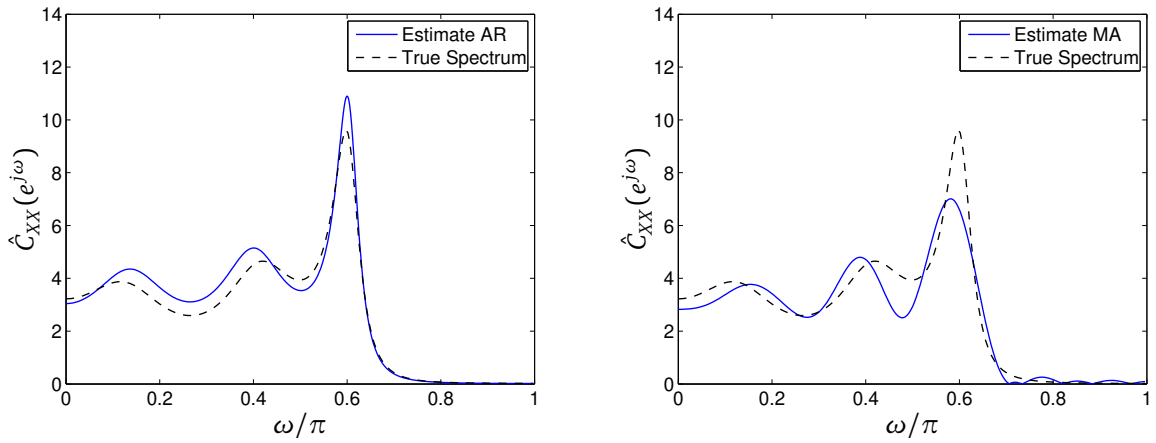

Figure 10.8.: AR(6) spectrum estimate (left) and MA(14) spectrum estimate (right) of the data sequence from Example 9.2.2.

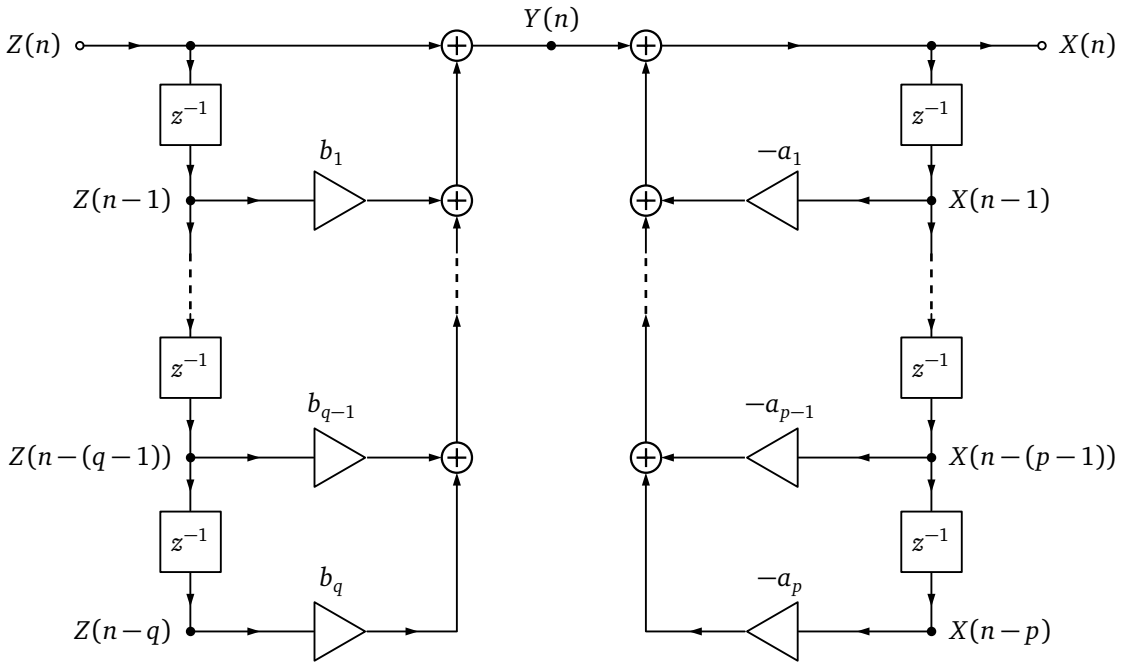

Figure 10.9.: Signal flow graph of a rational filter with orders p and q.

an over-parameterization of the numerator. Then, the output process $X(n)$ is said to be an autoregressive moving average process of orders p and q, or in short notation ARMA(p, q), whose difference equation is given by

$$X(n)+\sum_{k=1}^{p} a_k X(n-k) = Z(n)+\sum_{k=1}^{q} b_k Z(n-k).$$

An ARMA(p, q) process $X(n)$ can be understood as propagating a white noise process $Z(n)$ through a transversal filter and then a recursive filter, as shown in Figure 10.10.

In analogy to the autoregressive process, we multiply the difference equation from the right by $X(n-l)$ with $l \geq 0$ and take the expected value, yielding

$$\begin{aligned} c_{XX}(l)+\sum_{k=1}^{p} a_k c_{XX}(l-k) &= c_{ZX}(l)+\sum_{k=1}^{q} b_k c_{ZX}(l-k) \\ &= \sum_{k=0}^{q} b_k c_{ZX}(l-k), \end{aligned} \tag{10.1}$$

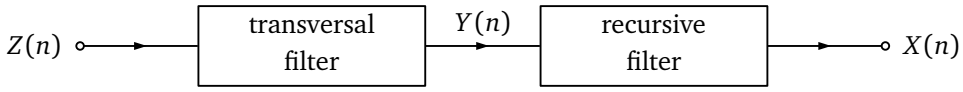

Figure 10.10.: A simplified low graph of an ARMA process.

since we have $b_0 = 1$. Since $X(n)$ is obtained by filtering the white noise process $Z(n)$ using a rational filter with unit sample response $h(n)$, the cross-covariance function $c_{ZX}(l-k)$ can be calculated as follows

$$\begin{aligned} c_{ZX}(l-k) =& \mathrm{E}[Z(n)X(n+k-l)] \\ =& \mathrm{E}\left[Z(n) \sum_{\kappa=0}^{\infty} h(\kappa) Z(n+k-l-\kappa) \right] \\ =& \sum_{\kappa=0}^{\infty} h(\kappa) c_{ZZ}(\kappa+l-k) \\ =& \sum_{\kappa=0}^{\infty} h(\kappa) \sigma_Z^2 \delta(\kappa+l-k). \end{aligned}$$

Because $\delta(\kappa+l-k) = 1$ for $\kappa = k-l$ and zero otherwise, we have

$$c_{ZX}(l-k) = h(k-l)\sigma_Z^2 \,.$$

Thus, the second term at the right-hand-side of Equation (10.1) can be written as

$$\sum_{k=0}^{q} b_k c_{ZX}(l-k) = \sigma_Z^2 \sum_{k=0}^{q} b_k h(k-l).$$

Since the system is causal, it holds that $h(k-l) = 0$ for $k-l < 0$, or equivalently, for $k < l$. Thus, for $0 \leq l \leq q$, we have

$$\sum_{k=0}^{q} b_k c_{ZX}(l-k) = \sigma_Z^2 \sum_{k=l}^{q} b_k h(k-l) \,.$$

and for $l \geq 0$

$$\sum_{k=0}^{q} b_k c_{ZX}(l-k) = 0 \,.$$

Therefore, we obtain the modified Yule-Walker equations

$$c_{XX}(l) + \sum_{k=1}^{p} a_k c_{XX}(l-k) = \begin{cases} \sigma_Z^2 \sum_{k=l}^{q} b_k h(k-l) & \text{for } l = 0, \ldots, q \\ 0 & l > q, \end{cases}$$

which can be used to estimate the parameters of an ARMA(p,q) model. For this, we first employ equations with $l = q+1, \ldots, q+p$ to solve for parameters $a_1, \ldots, a_p$. Then, we determine parameters $b_1, \ldots, b_q$ by using equations $l = 1, \ldots, q$ and the strategy described in Section 10.2.

From the above, one can estimate the coefficients $a_1, \ldots, a_p$ by solving

$$c_{XX}(l) + \sum_{k=1}^{p} a_k c_{XX}(l-k) = 0 \quad \text{for } l = q+1, \ldots, q+p \,.$$

It remains to solve the unknowns $\sigma_Z^2, b_1, \ldots, b_q$. From Figure 10.9, we can express $X(n)$ and $Y(n)$ in a difference equation

$$\sum_{k=0}^{p} a_k X(n-k) = Y(n),$$

with $a_0 = 1$. Thus,

$$\begin{aligned} c_{YY}(l) &= \mathsf{E}[Y(n+l)Y(n)] \\ &= \mathsf{E}\left[\sum_{k=0}^{p} a_k X(n+l-k) \sum_{m=0}^{p} a_m X(n-m)\right] \\ c_{YY}(l) &= \sum_{k=0}^{p}\sum_{m=0}^{p} a_k a_m c_{XX}(l-k+m) \end{aligned}$$

Because $Y(n)$ is an MA(q) process, $c_{YY}(l) = 0$ for $l > q$. Having consistent estimates $\hat{a}_1, \ldots, \hat{a}_p$ from the above equations, we can estimate the parameters $\sigma_Z b_k$ for $k = 0, \ldots, q$ as we did before for an MA(q) process. Instead of using the non-linear equations for the solution for the MA(q) parameters with $c_{XX}(l)$, we solve for $\gamma_k = \sigma_Z b_k$ ($k = 0, \ldots, q$) using

$$\hat{c}_{YY}(l) = \sum_{k=0}^{p}\sum_{m=0}^{p} \hat{a}_k \hat{a}_m \hat{c}_{XX}(l-k+n)$$

The estimators of $\gamma_k = \sigma_Z b_k$, $k = 0, \ldots, q$, are consistent. They lead to consistent estimators $\hat{\sigma}_Z^2 = \hat{\gamma}_0^2$, $\hat{b}_k = \hat{\gamma}_k / \hat{\gamma}_0$, $k = 1, \ldots, q$, for the parameters $\sigma_Z^2, b_1, \ldots, b_q$. Then, we have the consistent spectrum estimator

$$\hat{C}_{XX}(e^{j\omega}) = \hat{\sigma}_Z^2 \frac{|1 + \sum_{k=1}^{q} \hat{b}_k e^{j\omega k}|^2}{|1 + \sum_{k=1}^{p} \hat{a}_k e^{j\omega k}|^2}$$

for $C_{XX}(e^{j\omega})$.

Example 10.3.1 *In the following, we assume $p = 1$ and $q = 1$ such that we have an ARMA(1,1) process. Additionally, we assume the noise power to be $\sigma_Z = 1$. Using the general form of the transfer function of the system in Figure 10.9 for $p = 1$, $q = 1$, we get*

$$H(e^{j\omega}) = \frac{1 + b_1 e^{-j\omega}}{1 + a_1 e^{-j\omega}} = \frac{1}{1 + a_1 e^{-j\omega}} + \frac{b_1 e^{-j\omega}}{1 + a_1 e^{-j\omega}}$$

and consequently, the impulse response is given by

$$h(n) = (-a_1)^n u(n) + b_1 (-a_1)^{n-1} u(n-1).$$

In a next step, we use the modified Yule-Walker equations for $l = 0, 1, 2$

$$\begin{aligned} l = 0 \quad &: \quad c_{XX}(0) + a_1 c_{XX}(1) = h(0) + b_1 h(1) = 1 + b_1(-a_1 + b_1) \\ l = 1 \quad &: \quad c_{XX}(1) + a_1 c_{XX}(0) = b_1 h(0) = b_1 \\ l = 2 \quad &: \quad c_{XX}(2) + a_1 c_{XX}(1) = 0 \end{aligned}$$

to derive expressions for b_1 and a_1 in terms of $c_{XX}(0), c_{XX}(1)$ and $c_{XX}(2)$. First, we obtain for $l = 2$,

$$a_1 = -\frac{c_{XX}(2)}{c_{XX}(1)},$$

which can be used with the second equation ($l = 1$) to get

$$b_1 = c_{XX}(1) + a_1 c_{XX}(0).$$

Note that we would normally require the first Yule-Walker equation to find an expression for the noise power.

10.4 Model Order Selection

A problem arising with the parametric approach is that of estimating the number of coefficients required, e.g. p for the AR model. Having observed $X(0),\ldots,X(N-1)$ there are several techniques for doing this. Akaike's information criterion (AIC) suggests minimizing the following function with respect to m.

$$\mathrm{AIC}(m) = \log\hat{\sigma}^2_{Z,m} + m\frac{2}{N}, \quad m = 1,\ldots,M$$

The order estimate is the smallest m minimizing $\mathrm{AIC}(m)$. Another more accurate estimate is given by the minimum description length (MDL) criterion, obtained by taking the smallest m minimizing

$$\mathrm{MDL}(m) = \log\hat{\sigma}^2_{Z,m} + m\frac{\log N}{N}, \quad m = 1,\ldots,M$$

The term $\hat{\sigma}^2_{Z,m}$ is the estimated variance of the residuals. In case of an AR(m) model, the residuals can be estimated using

$$\hat{Z}(n) = X(n) + \sum_{k=1}^{m}\hat{a}_k X(n-k), \quad n = m+1,\ldots,N-1,$$

where $\hat{a}_1,\ldots,\hat{a}_m$ have been estimated using the Yule-Walker equations. Using all available samples of the estimated residual process, we can calculate its variance as follows

$$\hat{\sigma}^2_{Z,m} = \frac{1}{N-m}\sum_{n=m}^{N-1}\hat{Z}(n)^2.$$

Generally, as m increases, the variance of the residuals will decrease, that means fitting larger and larger models will usually lead to a smaller $\sigma^2_{Z,m}$, regardless of the true model order. In order to offset this, we add a penalty term $(2m/N)$ or $(m\log N)/N$ for AIC or MDL, respectively, which increases with m. The combined effect is that an order is chosen that has a small residual variance, while taking the order-complexity tradeoff into account.

Example 10.4.1 *Model order selection for filtered white noise. Consider again the sequence from Example 9.2.2, which is an AR(6) process. Figure 10.11 (left) shows the fitting term $\sigma^2_{Z,m}$ for orders* 1-10 *on the left ordinate and the AIC and MDL penalty functions on the right ordinate, respectively. The AIC and MDL cost functions are a combination of the fitting term (log) and the penalty function, and are shown in Figure 10.11 (right) for orders* 1-10. *We observe that both the AIC and MDL show a minimum at the true order $p = 6$.*

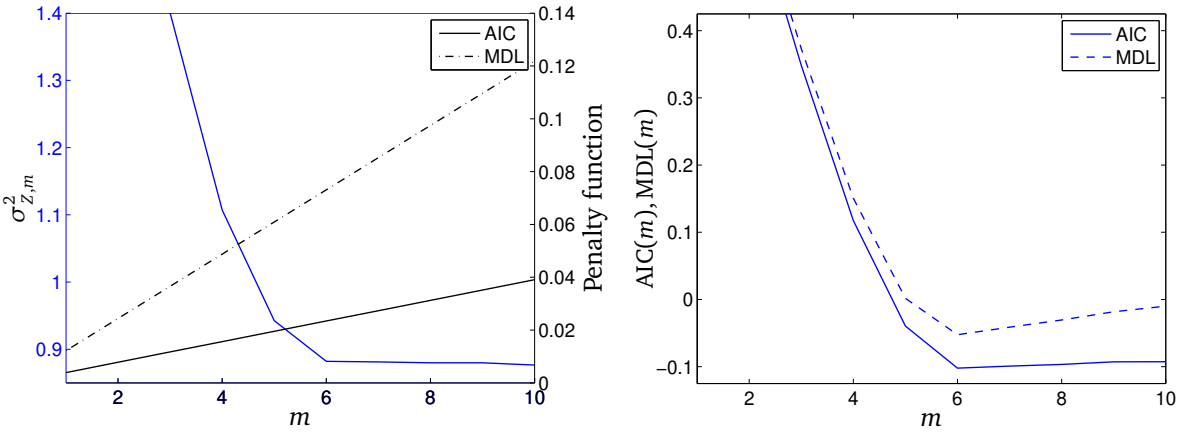

Figure 10.11.: Akaike and MDL information criteria for the AR(6) process for orders 1-10. The fitting term $\sigma^2_{Z,m}$ on the left ordinate and the penalty function on the right ordinate (left). The AIC and MDL cost function (right).

A Discrete-Time Fourier Transform

Sequence	Fourier Transform
$ax(n)+by(n)$	$aX(e^{j\omega})+bY(e^{j\omega})$
$x(n-n_d)$ (n_d integer)	$e^{-j\omega n_d}X(e^{j\omega})$
$e^{-j\omega_0 n}x(n)$	$X(e^{j(\omega+\omega_0)})$
$x(-n)$	$X(e^{-j\omega})$
	$X(e^{j\omega})^*$ if $x(n)$ real
$nx(n)$	$j\dfrac{dX(e^{j\omega})}{d\omega}$
$x(n)*y(n)$	$X(e^{j\omega})Y(e^{j\omega})$
$x(n)y(n)$	$\dfrac{1}{2\pi}\displaystyle\int_{-\pi}^{\pi} X(e^{j\theta})Y(e^{j(\omega-\theta)})d\theta$
$-jnx(n)$	$\dfrac{dX(e^{j\omega})}{d\omega}$
Symmetry properties:	
$x(n)^*$	$X(e^{-j\omega})^*$
$x(-n)^*$	$X(e^{j\omega})^*$
$x(n)$ real	$X(e^{j\omega})=X(e^{-j\omega})^*$
$x(n)$ real and even	$X(e^{j\omega})$ real and even
$x(n)$ real and odd	$X(e^{j\omega})$ pure imaginary and odd
Parseval's Theorem: $\displaystyle\sum_{n=-\infty}^{\infty}\lvert x(n)\rvert^2=\frac{1}{2\pi}\int_{-\pi}^{\pi}\lvert X(e^{j\omega})\rvert^2 d\omega$	
Special correspondences:	
$\delta(n)$	1
$\delta(n-n_0)$	$e^{-j\omega n_0}$
1, $(-\infty<n<\infty)$	$\displaystyle\sum_{k=-\infty}^{\infty}2\pi\delta(\omega+2\pi k)$
$a^n u(n)$, $(\lvert a\rvert<1)$	$\dfrac{1}{1-ae^{-j\omega}}$
$(n+1)a^n u(n)$ $(\lvert a\rvert<1)$	$\dfrac{1}{(1-ae^{-j\omega})^2}$
$u(n)$	$\dfrac{1}{1-e^{-j\omega}}+\displaystyle\sum_{k=-\infty}^{\infty}\pi\delta(\omega+2\pi k)$
$\dfrac{\sin(\omega_c n)}{\pi n}$	$X(e^{j\omega})=\begin{cases}1, & \lvert\omega\rvert<\omega_c\\ 0, & \omega_c<\lvert\omega\rvert\le\pi\end{cases}$
$x(n)=\begin{cases}1, & 0\le n\le M\\ 0, & \text{otherwise}\end{cases}$	$\dfrac{\sin[\omega(M+1)/2]}{\sin(\omega/2)}e^{-j\omega M/2}$
$e^{j\omega_0 n}$	$\displaystyle\sum_{k=-\infty}^{\infty}2\pi\delta(\omega-\omega_0+2\pi k)$
$\cos(\omega_0 n+\phi)$	$\displaystyle\sum_{k=-\infty}^{\infty}\pi\left[e^{j\phi}\delta(\omega-\omega_0+2\pi k)+e^{-j\phi}\delta(\omega+\omega_0+2\pi k)\right]$